Hydrology of a large unstable hillslope at Ebnit, Vorarlberg
Identifying dominating processes and structures

Dissertation
zur Erlangung des akademischen Grades
"doctor rerum naturalium"
(Dr. rer. nat.)
in der Wissenschaftsdisziplin "Geoökologie"

eingereicht an der
Mathematisch-Naturwissenschaftlichen Fakultät
der Universität Potsdam

von
Dipl. Geol. Falk Lindenmaier

Potsdam, August 2007

Nur wer sich ändert, bleibt sich treu (Biermann)

Acknowledgment

Abstract

The objective of the presented study is to improve the knowledge of control mechanisms of hydrological induced mass movements. To this end, detailed hydrological process studies and physically-based hydrological modelling were applied. The study site is a hillslope in the Dornbirn Ache valley near Bregenz, Austria. This so called Heumös slope features a deep-seated translational shear zone and surface near creep movements of up to 10 cm a year. The Cretaceous marlstones of the Austrian Helveticum have a high susceptibility for weathering and might form clay-rich cohesive sediments. In addition, glacial and post-glacial sedimentation contribute to unstable hillslopes in the Vorarlberg Alps. High yearly precipitation depths of about 2100 mm and rainstorms with both high intensities and precipitation depths govern surface and subsurface hydrological processes. Pressure propagation induced in hydrological active areas influences laterally the groundwater reactions of the moving mass. A complex three-dimensional subsurface pressure system is the cause for fast groundwater reactions despite low hydraulic conductivities.

Detailed hydrological process studies of landslides are not yet a common technique in landslide research. At first, the discussion will be directed towards the state of the art of hydrological process research. Then, a review of major studies concerning hydrological triggers, modelling and landslides will be given. The necessity to include scales in space and time is stressed in order to better identify the wide range of spatial patterns and to understand related processes in hydrology and, in particular, for unstable hillslopes. Finally, a scaling concept, which combines spatial and temporal scales of hydrological processes with landslide processes, will be proposed.

During almost 10 years of observation at the hillslope an exhaustive data set was gathered. Data mining and renewed post-processing as well as the implementation of meta-information enhanced the database. At last, an integration into a web-based information system (Molkenthin *et al.*, 2006) was achieved. This is nowadays an essential part for proper communication in large interdisciplinary studies. The data and methods section provides an overview of the database and the methods which were applied in this thesis.

Geological and pedological structures are closely related to hydrological processes. For the study site investigation, a top down approach was chosen. To understand hillslope scale variability, hydrotopes representing specific dominating processes were mapped using vegetation association distribution and soil core analysis. Detailed small-scale soil investigations followed to refine the understanding of these hydrotopes. A perceptional model was developed from the hydrotope distribution and was corroborated by these detailed investigations. The moving hillslope is dominated by surface-runoff generation. Infiltration and deep percolation of water is inhibited through clay-rich gleysols; the yearly average soil moisture is close to saturation. Steep slopes adjacent to the moving hillslope are far more active concerning infiltration, preferential flow and groundwater fluctuations. Spring discharge observations at the toe of the steep slopes are in close relation to groundwater table observations on the moving hillslope body. Evidence of pressure propagation from the steep slopes towards the hillslope body is gathered by comparison of dominating structures and processes. The application of the physically-based hydrological model CATFLOW (Maurer, 1997; Zehe *et al.*, 2001) substantiates the idea of pressure propagation as a key process for groundwater reactions and as a possible trigger for movement in the hillslope.

The approach of a detailed field-site investigation and the use of non-standard methods, for both landslide research and hydrology, in combination with physically-based hydrological modelling, resulted in a thorough understanding of dominant structures and processes of the hillslope (Lindenmaier *et al.*, 2005).

Zusammenfassung

Diese Arbeit soll die Zusammenhänge von hydrologischen Rahmenbedingungen von Massenbewegungen darstellen, damit eine Verbesserung des Verständnisses kontrollierender Mechanismen sowie die Bestimmung von hydrologischen Auslösern von Massenbewegungen ermöglicht wird.

Das Untersuchungsgebiet besteht aus einem ca. 2 km langen und 500 m breiten Hang mit einem maximalen Höhenunterschied von ca. 400 m. Das dort vorkommende Festgestein besteht im Wesentlichen aus Mergelstein. Die vergangenen Eiszeiten haben dieses Gestein überarbeitet und Grundmoränenablagerungen auf dem Hang zurückgelassen. Diese wurden in den letzen 10.000 Jahren von Hangschutt, der aus den benachbarten Steilhängen stammt, überlagert. Der Hangschutt ist sehr verwitterungsanfällig, die Kalkkristalle lösen sich und wandeln den Hangschutt in lehmiges Material. Bewegungsmessungen an der Oberfläche zeigen, dass sich der Hang mit ca. 10 cm im Jahr talabwärts bewegt. Diese Bewegungen werden sehr wahrscheinlich durch kleine ruckartige Ereignisse in ca. 8 m Tiefe ausgelöst. Ziel der Untersuchungen war, den Wasserhaushalt des Hanges so gut wie möglich zu erfassen und mit Computermodellen abzubilden. Dabei spielt die Heterogenität der pedologischen Eigenschaften einen wesentliche Rolle, als Eingangsparameter für die Modelle.

Grundwasserstandsmessungen in 5,5 m Tiefe auf dem Hang zeigen schnelle Reaktionen des Grundwasserspiegels nach Niederschlagsereignissen. Das Wasser dieser Ereignisse kann aber aufgrund des Lehms, der nur eine geringe Wasserdurchlässigkeit für Wasser besitzt, nicht in den tieferen Untergrund gelangen, sondern fließt fast vollständig an der Oberfläche ab. Dahingegen führt ein schnelles Versickern von Wasser in an den Hang anschließenden Steilhängen zu einem schnellen Grundwasseranstieg, der aufgrund eines gespannten Grundwasserleiters den Druck in die Hangrutschung weitergibt. Dort wird ein Überdruck aufgebaut, der sehr wahrscheinlich die Bewegungen auslöst. Die vorliegende Arbeit ist eine detaillierte Herangehensweise um Erkenntnisse aus der Hyrologie für die Bestimmung des Wasserhaushaltes von Massenbewegungen heranzuziehen.

Contents

1   Introduction

Landslides are one of the most dangerous natural hazards in mountainous regions that have a severe impact on the welfare of societies. Increasing settlement pressure, which is visible in the Alps since the 1950's, combined with a phase of less geomorphic activity in the past century is the reason for the loss of knowledge of the hazard of certain landslide or debris flow prone areas. It is only recently that with the help of new techniques and geotechnical risk mapping, hazard assessment for mass movement can be defined for certain areas (Ruff & Czurda, 2007) and thus are brought back to the public mind. A culmination of extreme precipitation events since the mid-nineties of the last century caused severe destruction of settlements through flooding and debris flows in the valleys of the Swiss and Austrian Alps. These precipitation events also initiated several large mass movements and lead to a phase of more intense denudation and geomorphological activity of mountainous hillslopes. For example, the precipitation events of May 1999 lead to the activation of the Rindberg mass movement in Austria (Schütz, 2000), featuring up to 160 cm movement per day of bedrock and debris material. The same precipitation events triggered the Rufi landslide in the Swiss Molasses (Eberhardt *et al.*, 2005). The event of August 2005 was even more extreme in means of damage to settlements in Switzerland (MeteoSchweiz, 2006) and Austria (Kanonier *et al.*, 2005).

The scientific community's efforts are multifarious with respect to predicting mass movements for both small slope failures and large landslides. These efforts are controlled by the problem statement of how to deal with the enormous scales in space and time encountered in the varied processes causing the failure of slopes. Aggravating the situation is the uncertainty about the localisation of subsurface geological structures that destabilise a hillslope. Similar restrictions apply to the determination of the occurrence of the necessary trigger in order to understand the hydrological controls of landslides. One has to account for the variability of precipitation as well as the uncertainty of processes, which might influence the water balance of a moving hillslope. Most often the scientists attention is brought to this specific site, only after a hydrological triggered landslide occurred. As a consequence, a lot of research deals with landslides which are already beyond their state of highest interest.

In shallow slope failures, infiltration and preferential flow in the unsaturated zone seem to be the major factors influencing stability (Rahardjo *et al.*, 2005). In more complex landslide types with deeper failure zones, a rising and falling groundwater table leads to changes in the stress field (van Asch *et al.*, 1999). But how are these subsurface stress variations linked to the climate variations observed in the atmosphere? What kind of thresholds need to be exceeded to trigger movement or even failure of a hillslope? It will not be possible to predict failures of complex mass movements, before the answers to these questions are better understood.

The site of interest investigated in this study is a deep-seated creep in cohesive sediments in the Vorarlberg Alps. The creep movements of this complex landslide are possibly triggered through the extreme hydrological setting of the region. Precipitation accounts to 2100 mm a year in average. Summer events are characterized with high intensities and high depths. This study focuses on spatial patterns that drive the dominant hydrological processes on this hillslope. The aim is to combine landslide research with process-based hydrology and physically-based hydrological modelling. The analysis of processes and structures on different scales and the establishment of connections between these scales provide sufficient evidence for the linkage of surface processes with deep-seated groundwater reactions.

1.1   A strategy for the investigation of hydrological processes on a landslide

Non-linear surface and subsurface processes that interact across a wide range of time scales influence the stability of large hillslopes. In addition, these processes are governed by a wide range of spatial patterns. These patterns constitute specific geological structures across several orders of magnitude. The process cascade starts with fast hydrological processes, such as rainfall and infiltration. These processes trigger subsurface water flow and pressure dynamics that in turn determine the interactions between the fluid and the solid phase up to the development of shear bands (Lindenmaier *et al.*, 2005). The latter consequently is a rather slow process. Grayson & Blöschl (2001) state that "observation and interpretation of spatial patterns are fundamental to many areas of the earth sciences such as geology and geomorphology, yet in catchment hydrology, our historic interest has been more related to temporal patterns and in particular that of stream flow". The integration of spatial patterns and structures into rainfall-runoff research has been and still is of primary interest in the hydrological community. In particular, since new computational advances aid in creating a better basis for spatially distributed modelling. New methods and the broader use of scientific approaches in related fields help to develop better tools to understand the relevant hydrological processes.

On the other hand, landslide research is located historically in the geomorphological or geological scientific community. Landslide research often lacks a deeper involvement of hydrological processes and their variability. Combining process-based hydrology with landslide research seems to be obvious but until recently both major involved scientific disciplines seemed to take only marginal interest in each other (Boogard, 2001; Malet *et al.*, 2005). Figure 1-1 sketches major processes and subsurface structures, which influence the trigger of a mass movement. The figure illustrates what range of scales is encountered in hydrological landslide research. The objective of this study is to narrow the gap between process-based hydrology and landslide research.
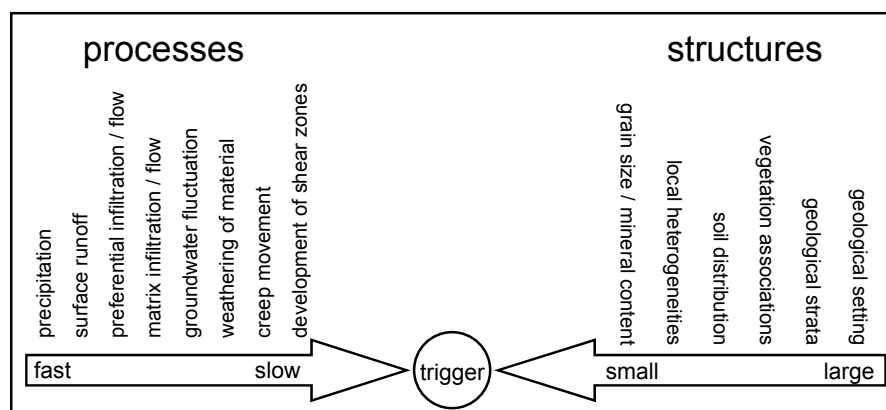
Figure 1-1: The range of scales of processes that influence the trigger of a mass movement from hydrological and geoscientific perspectives.

Process-based hydrology tries to link the point observation *precipitation* and *channel-discharge* through deepening the understanding of infiltration, subsurface water dynamics and runoff generation processes. To grasp the influence of hydrological processes on a moving hillslope one needs to deal with a two- if not three-dimensional distribution of structures and processes. In addition, the movement of the hillslope and high geomorphic activity induces a gradual change of structures. These structural changes are directly coupled back to hydrological processes.

The driving idea for this study was a top down approach in field investigations to identify spatial patterns of structures on different scales and understand their influence on hydrological processes. It seemed to be an advantage to use methods from vegetation ecology to define the spatial distribution of ecological moisture, which is a proxy for a dominating moisture regime and so for specific hydrological characteristics, too. These characteristics were used to define hydrotopes that are dominated by certain processes. More detailed investigations were directed towards these dominating processes. The following list will give an overview of what kind of methods, parameters and variables are needed to link hydrological process research, modelling and landslide research:

- Data characterising the forcing of processes: e.g. precipitation and climate.

- Catchment relevant observations: rain gauges, river gauges and spring discharge.

- Long and short term soil moisture variations: e.g. available as point observations by time domain reflectometry (TDR).

- Hydrogeological observations: groundwater table fluctuations and spring discharge.

- Spatial patterns which determine hydrological and geotechnical processes on the slope.

To determine these spatial patterns, a top down approach has been chosen:

- Use soil cores, vegetation association mapping and ecological wetness index for determination of patches with average long-term moisture characteristics.

- Combine patches with topographic factors for determination of hydrotopes with certain dominating processes.

- Identify processes in hydrotopes with a closer look at, e.g. macroporosity with dye staining experiments, determination of infiltration capacities or field hydraulic conductivity and laboratory determination of soil-specific parameters.

The soil investigation and the determination of an ecological wetness index were employed for the identification of dominant hydrological processes on the hillslope in 2001. The existing hydrological and climatological measurement network was enhanced, continuity of measurement was ensured and data quality was improved from 2001 on as well. A perceptional model was set-up with a first data analysis and interpretation (Lindenmaier *et al.*, 2005). A study on the impact of shrinking capabilities of regosols on runoff behaviour in a catchment in northeastern Baden-Württemberg (Lindenmaier *et al.*, 2006) was conducted between 2002 and 2005. Results from this study improved the process identification for the clay-rich soils of the hillslope study area in Vorarlberg. At the same time, the perceptional model's idea was used as the core idea for the proposal of a new research project. From 2006 on, in the frame of the new research group, detailed investigation followed for a thorough understanding of infiltration and lateral flow in the hydrotopes. Data of the field investigations as well as the hydrometeorological time series were implemented into the physically-based hydrological model CATFLOW (Maurer, 1997; Zehe, 2001). These model simulations corroborate the perceptional model.

1.2   A short history of interdisciplinary studies about the study site

This study is part of two interdisciplinary projects both financed by the Deutsche Forschungs-gemeinschaft (German Research Foundation, DFG). To bring together process-based hydrological approaches with landslide research and new monitoring methods, a research programme was initiated by scientists of the Universität Karlsruhe (TH) in 1997. The translated title of this programme is

"Hydrological and cinematic processes of large mass movements in cohesive sediments". In the beginning, there was a focus on geotechnical and geological investigation (Schneider, 1999; Schwenk, 1999; van den Ham & Czurda, 2002) as well as a surface movement survey (Depenthal & Schmitt, 2003; Howind & Schmitt, 1999) with the help of the Global Positioning System (GPS). From 2001 on, involvement to hydrological aspects was enhanced in the research area. The principal aim of the project to interrelate different scientific approaches to better understand movement of cohesive hillslopes has been mainly conducted through this thesis. This is why results and data from co-workers play an important part for understanding this thesis which is the synopsis of all research efforts to this point. Therefore, chapter 3 was specifically designed to comprise specific data and results from co-workers as well as local information from foregoing scientific work about this area.

Since 2006, a new DFG research group (For 581) is involved with the study site. The translated working title of this group is "Coupling of flow and deformation processes for modelling of large mass movements". Institutes from the Universität Karlsruhe (TH), Universität Potsdam, TU Berlin and the Universität Stuttgart are involved (Hinkelmann & Zehe, 2007). The goals are to improve subsurface hydraulic modelling of deep-seated landslides and to take a first step to combine hydrological and geomechanical process modelling.

Both research projects are associated with the "Integral Projekt", which is a cooperation of the Wildbach- und Lawinenverbauung, Austria and city of Dornbirn authorities in order to advance living conditions in the Dornbirn Ache valley.

1.3   Thesis outline

At first, it will be discussed how process hydrology can improve landslide research (Chapter 2). Therefore, advances and major topics will be emphasized. An overview of the state of the art of hydrological research on landslides will be given. There is an emphasize on the discussion about scales and scaling in hydrology. With this, the scaling issues in hydrology will be advanced to landslide research. The definition of spatial and temporal scales helps to define the dominant control mechanisms of landslides and improve quantification of observed phenomena.

The following chapter (Chapter 3) provides a general description of the study site and introduces the framework in which the perceptional model will be set up. The standing alone results of the affiliated partner projects of the first DFG research programme are presented as necessary prerequisite to this thesis' goal. The partners' work is interpreted more thoroughly in relation to hydrological and hydrogeological issues in this chapter. This is necessary to understand the approach and strategy of the thesis with its broad and integrating character. Results from some selected scientific publications not related to the DFG research programmes are included as well concerning the geological and glaciological development.

Chapter 4 describes the data and methods used in this work. Additionally, some methods used by co-workers are explained as well. In case that the reader is not familiar with these kind of methods. Hydrological investigation is mainly based on time series analysis. As data collection and documentation before 2001 was deficit-ridden, additional sources for measurements and time series were looked for and vast data mining was conducted of the first research groups' data. Meta information was established for this data and was integrated into a web based information system (Molkenthin *et al.*, 2006). Besides the information system, this chapter gives an overview of available data and time series coverage. Applied methods which were used to get additional information about the hillslope comprise field investigation,

measurements and mapping, laboratory analysis of collected samples as well as computer software application. The computer model CATFLOW is described in chapter eight then.

Chapter five to seven will present the results of field and laboratory work from 2001 and 2006 as well as the analyses of the collected time series data. This is the main part of the thesis which highlights the mechanisms that control the spatial patterns and processes. Chapter five concentrates on spatial patterns, chapter six on the process identification, and chapter seven integrates the results into a perceptional model of dominating processes and structures that lead to movement of the Heumös slope.

Chapter eight deals with the set up of the physically-based hydrological model CATFLOW and discusses the results of several model settings and simulations. The simulations underpin the perceptional model ideas for dominating hydrological processes on the slope.

Finally, chapter nine discusses the findings of observation and data investigation with the simulation results.

The appendix comprises important data from co-workers and own work as well as the model set-up for CATFLOW.

2 Hydrological processes and modelling in landslide research

Precipitation is a key factor for triggering mass movements. Consequently, a lot of landslide studies deal with rainfall induced landslides (Crosta, 2004). However, the advances in hydrological sciences only slowly gain acceptance in the scientific landslide community. Brundsen (1999) states this in his review paper, and Malet *et al.* (2005) still had the same opinion in 2005. Though the early years of the 21st century slowly brought more advanced hydrological studies, landslide hydrology research still lacks a thorough inclusion of process-based hydrological approaches. Process-based hydrological research is a complex and difficult issue in catchment hydrology. In addition, mass movement poses additional complexity for hydrological issues as the movement might constantly change surface and subsurface structures which again have an effect on hydrological processes. For example, accumulation of debris and strong erosion rates in mountainous areas strongly influence hydrological processes and the quality of observation. The state of the art in landslide hydrology as well as an overview on how hydrological process studies can be incorporated into landslide research is discussed here. In addition, aspects of structural scales will be discussed which need to be dealt with in landslide research, especially concerning marlstones. These should be considered as special landslide prone geological strata in classification schemes as Maquaire *et al.* (2003) point out.

2.1 How do hydrological sciences help in landslide investigation?

2.1.1 Runoff generation processes

Hydrological approaches with a process-based view on the water cycle developed slowly from the 1970's on (Anderson & Burt, 1990). It has been a large step coming from simple Unit Hydrograph calculations (Sherman, 1932) towards process-based hydrology nowadays. For a long time, infiltration excess overland flow (Horton, 1933) was regarded as the only runoff generation process (Anderson & Burt, 1990; Beven, 2004). The observed runoff hydrograph was seen as the integration of all processes of the catchment but further examinations of these processes leading to the hydrograph were rare. The ongoing field research of the past 30 years brought the identification of more runoff processes and complexity to hydrological sciences. Processes other than infiltration excess runoff do play a similar important, if not more important role for the runoff generation. Examples are saturation excess overland flow (Dunne & Black, 1970), preferential flow through macropores and interflow (Beven & Germann, 1982) or the influence of the displacement of water of different residence times, also called piston flow (Uhlenbrook & Leibundgut, 2002). Mass movements are influenced through the moisture content in the unsaturated zone and through groundwater fluctuations. To understand and to predict changes of local subsurface hydraulic systems in landslides one needs to link surface hydrological processes with subsurface processes. Hence, water fluxes through infiltration and deep percolation must be separated from processes like surface runoff generation or evapotranspiration. The closing of the water balance gives better ideas of the subsurface process reactions which might trigger mass movement.

2.1.2 Scale issues in hydrology

There are observable hydrological processes in nature but it is necessary to have methods to conclude from our *point* observations towards the runoff reaction of say, a larger catchment. With the forthcoming of ever better computational power, the use of numerical hydrological models becomes more detailed and sophisticated. Quantitative information is needed and has to be derived through observation and interpolation of data in the field. Blöschl & Sivapalan (1995) differentiate between a *process scale*, an

observation scale and a *model scale* and discuss methods to transfer information in between these scales. Certain hydrological processes play a dominant role in certain *spatial scales* but with a point of view, which is focused on a larger area, the importance of this process might be reduced and overshadowed by other processes. These processes might become more dominant or it becomes more and more difficult to describe the specific process with adequate and available data, which means that certain simplifications need to be taken. In the words of Blöschl (1996) "different processes become operative at different scales". Like for spatial scales, it is possible to determine processes on different scales in time as well. The definition of space and time scales of patterns and processes for a field research site helps to understand dominating processes and structures. This is necessary to develop tools, which help to interpret parameters or processes observed on one scale and then are supposed to influence the next larger or smaller scale.

2.1.3 Scales and scaling in landslide research

Spatial patterns of subsurface and surface characteristics have significant influence on hydrological processes (Schulz *et al.*, 2006) but also on mechanisms influencing mass movement. Especially the subsurface structures encountered in unstable hillslopes have a key role for these mechanisms. Geological and pedological subsurface structures evolve through long term processes over tens of thousands to millions of years and so they might be consequently observed as static units, e.g. a geologic strata or a soil. Hence, a more proper definition of subsurface structures and their interplay with both geo- and pedological processes, as well as hydrological processes should be defined. A changed "spatial scale", similar to Blöschl and Sivapalan (1995), with a focus on *structural scales* in mass movements is introduced (Figure 2-1).
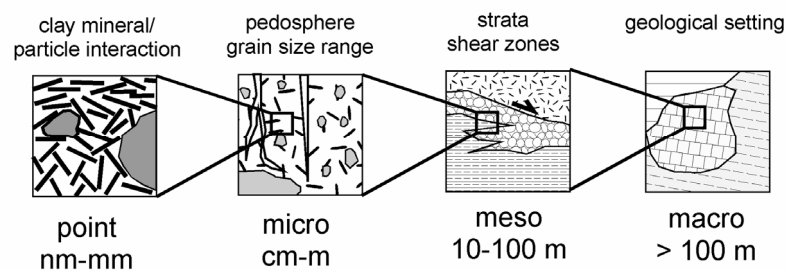
Figure 2-1: Important structural scales which both influence stability and hydrological processes of landslide prone areas, similar to Blöschl & Sivapalan (1995).

The *macro scale* would comprise the geological setting as a result of large-scale depositional environments, mountain development, the glaciation and post-glacial geomorphological development of an area. The *meso-scale* deals with the local hillslope strata and stability of the hillslope body, e.g. the definition of shear zones in the subsurface or the movement type. The *micro scale* defines the heterogeneities of the strata types and includes the pedosphere. Cracks, macropores and grain size distribution would be key factors in this scale. For example, mountainous hillslopes can feature a range of grain sizes from micrometers towards several tens of meters. The *point scale* would define heterogeneity of material properties, e.g. clay mineral content and types, weathering phenomena of material, its interaction with water and other particle sizes and its influence on stability.

Multiple different processes influence the water balance of a moving hillslope. The heterogeneity of spatial structures determine, which process might be dominating over others at a certain place or time. As observations are always limited and as it is not possible to describe the full heterogeneity of a study site,

methods for simplification or aggregation are needed to be able to integrate scarce observations into a perceptional model of a mass movement and finally into a numerical model to reproduce and predict the impact of dominating processes.

Interdisciplinarity in science can e.g. mean that theories or methods from one scientific field are transferred to other fields and vice versa. Discussions about scaling in geology are rare, as scales of space and time and scaling is just too common there. Geology is scaling for a lot of its aspects, e.g. when micro fossil associations in a sediment profile are used to explain climate conditions at the Cretaceous-Tertiary boundary about 65 million years ago (Stinnesbeck *et al.*, 2001). But on the other hand, to define different scales in landslide investigation can focus on dominating processes, which might be overseen otherwise. A more physically-based hydrological approach can better explain encountered and observed phenomena, as it will be discussed in the next chapter.

Space-time patterns of runoff generation in mountainous regions are more diverse as in lowland regions, refer to Kirnbauer *et al.* (Kirnbauer *et al.*, 2001). Knowledge about soils and interrelated hydrological processes helps to understand runoff generation and provides better data sets for modelling (Lin *et al.*, 2006). Sufficient soil maps or classifications of surface runoff generation in mountainous regions are yet in development in the Austrian Alps (Markart *et al.*, 2006). Markart *et al.* (2006) developed a soil type based decision support system for the Austrian Alps which helps in determining dominating runoff processes. With classification schemes like this and hazard mapping of failure prone areas (Ruff, 2005) an upscaling of hydrological processes combined with failure prone geological structures might become possible.

Threshold behaviour governs the predictability of hydrological processes (Zehe & Blöschl, 2004; Zehe *et al.*, 2007). For example, a certain soil moisture content is needed before macropores or shrinkage cracks contribute to the flow of water in the unsaturated soil zone. Thresholds also govern mass movements, e.g. certain groundwater levels are needed to exceed stability of a slide or certain soil moisture is needed to reduce the friction angle of a material below the factor of stability. To understand threshold reactions on a plot scale, it might help to better define possible landslide triggering climate conditions. Hence it is of utmost importance to understand the space-time patterns of hydrological processes of moving hillslopes (Lindenmaier *et al.*, 2005).

2.2 Why do we need process-based hydrology and physically-based models for landslide hydrology research?

2.2.1 Classification of landslides and its role for hydrological induced landslides

Landslides can be classified in different ways, e.g. a differentiation is made through their causes. Causes are normally preparatory, sustaining and triggering (Therzaghi, 1950) and can be from internal or external origin. Internal causes are mechanisms that reduce shear strength, whereas external causes are responsible for overcoming internal strengths, causing a failure (Bell, 2003). Landslides can also be determined through their failure mechanism. Failure mechanisms as defined in the EPOCH project (Casale *et al.*, 1994; Dikau *et al.*, 1996) are *fall, topple, rotational or translational slide, planar, lateral spreading* or *flow,* and as a combination of two or more types a *complex* failure mechanism is defined (Table 2-1). As explained in more detail in chapter 3.3.6, the investigated site consists of a deep-seated translational slide combined with several small scale, near surface failure structures.

Therzaghi (1950) states that precipitation and rises of piezometric levels are one of the major triggering causes for mass movements. Concerning precipitation as external cause, shallow landslides are often reported to be triggered by short high intensity-rainstorms (Jahns, 1978; van Asch *et al.*, 1999). Water finds its way directly into the unsaturated zone and causes failure through changing the friction or cohesion of the solid material there. Deep-seated large movement zones are readily linked to long continuous wet periods (Jahns, 1978). They are often reported to be triggered through positive pore pressures at shear zones which are caused through rising groundwater levels (Flageollet *et al.*, 1999; Schuster & Wieczorek, 2002; van Asch *et al.*, 1999). It is suggested that larger volumes of infiltrating water is needed which reaches the groundwater system. In addition, higher antecedent precipitation amounts are suggested to be necessary to establish a link between landslide movement and precipitation (Iverson, 2000). Consequently, van Asch *et al.* (1999) suggest that less detailed meteorological information, e.g. on a monthly base, is necessary.

Table 2-1: Classification of mass movements after Casale *et al.* (1994) and Dikau *et al.* (1996).

Type	Rock	Debris	Soil
Fall	Rockfall	Debris fall	Soil fall
Topple	Rock topple	Debris topple	Soil topple
Slide (rotational)	Single (slump) multiple successive	Single multiple successive	Single multiple successive
Slide (translational) Non-rotational	Block slide	Block slide	Slab slide
Planar	Rockslide	Debris slide	Slab slide
Lateral spreading	Rock spreading	Debris spread	Soil (debris) spreading
Flow	Rock flow (Sackung)	Debris flow	Soil flow
Complex (with run-out or change of behaviour downslope, note that nearly all forms develop complex behaviour)	e.g. rock avalanche	e.g. flow slide	e.g. slump-earthflow

Note: a compound landslide is one that consists of more than one type, e.g. a rotational-translational slide. This should be distinguished from a complex slide where one form of failure develops into a second form of movement, i.e. a change of behaviour downslope by the same material.

This might be true for a lot of systems but it has to be stated that observation of hydrological signals and movement of hillslopes used to be based on a long term signal observation in the past, e.g. most precipitation values are only available on an hourly, monthly or yearly time-step. Additionally, the precipitation gauge might not necessarily be located near the landslide itself so that a good time resolution of reacting hydrological processes is further hampered. The legitimate question is whether higher sampling intervals of hydrological and geotechnical measures would resolve „long term reaction behaviour" to be a short-term behaviour instead. It is the question, whether a *creep*, e.g. observed on a 3-month or yearly base, is not rather a succession or combination of small-scale local and jerky movements. For example, van Asch (2005) observed that local inhomogeneities in the shear zone can lead to a differentiated velocity pattern.

2.2.2 Stochastic approaches in landslide hydrology

In many hydrologically influenced landslide studies, precipitation thresholds are of major concern. Delmonaco & Margottini (2004) report that thresholds are calculated from cumulative precipitation for certain landslides on a time-step of two months up to yearly precipitation sums. Thresholds derived from hydrological events combined with landslide occurrence needs a profound database and are more or less

restricted to shallow landslides (Terlien, 1998). Measures for rainfall events are used to determine event types which lead to the failure of landslides or not. Such combinations of measures are actual precipitation depths and antecedent rainfall or rainfall intensity and duration. When databases are not sufficient for stochastic threshold approaches, deterministic approaches which include hydrologically advanced models become necessary (Terlien, 1998), especially concerning deep-seated landslides (shear zones greater than 5 m). Terlien (1998) states that understanding the spatial distribution of pore water pressures is necessary to be able to predict landslide behaviour. Stochastic approaches are useful to understand the spatial and temporal occurrence of landslides but the prediction of specific events that lead to failure is difficult.

2.2.3 Hydrological and stability models for shallow slope failures

Combined hydrological and slope stability models are readily defined and described in literature but a lot of projects on hydrologically driven landslides are focused on shallow landslide occurrence. These then often neglect preferential flow as one of the dominant subsurface flow processes. In the following, the focus is on some of the more advanced hydrological approaches in landslide investigation. Collison & Anderson (1996) and Wilkinson *et al.* (2000) use a combined hydrology - stability model called CHASM, which was designed by Anderson & Lloyd (1991). The model employs the Darcy law for saturated conditions and Richards' equation for unsaturated conditions. Unsaturated hydraulic conductivity is derived by the method of Millington & Quirk (1959) for porous media. For calculations of stability of vegetated slopes in the humid tropics a conceptual evaporation and canopy interception module was added. CHASM is designed to calculate different stability scenarios; a closer view on a closed water balance is not favoured.

Cho & Lee (2001) refer infiltration on a generalized Darcy's law for unsaturated conditions in porous media and state that low hydraulic conductivities lead to shallow landslides whereas high hydraulic conductivities lead to deeper landslides with longer initiation times after rainfall. In this study, neither preferential flow nor vegetation influence is incorporated into the hydrological model.

Tsaparas *et al.* (2002) state that extensive and detailed seepage analysis is needed to better understand slope stability conditions influenced by heavy rainfall and infiltration. A Richards' equation approach is used in this study but the inclusion of evapotranspiration could not be accomplished. This limits the analysis on single rainfall periods with the necessity of defining initial conditions for each calculation. Long-term water balances were not calculated. Rahardjo *et al.* (2005) state that the unsaturated soil mechanic principle should be used in slope failure studies. With more than 85% of saturation in a soil, saturated soil mechanics can be applied. In lower saturation states, unsaturated soil mechanics need to be applied. They use monitoring and simulation to derive pore water pressure profiles. The studied slopes are located in residual soils on granitic rocks in Singapore (Rahardjo *et al.*, 2004). Darcy's law is altered for unsaturated conditions and they use measured soil water characteristic curves (Rahardjo *et al.*, 2005). The pore water pressures distributions are used to calculate factor of safety values with a commercial limit equilibrium slope stability programme. Though the concept uses advanced hydrological approaches, heterogeneity and preferential flow paths were not considered for the slope pore water pressure calculations.

Shallow slope failures are wide spread as traffic line construction induces cutting and steepening of natural slopes and so trigger many mass movements. Shallow slope investigation has advantages as the studied settings pretend to be quite homogenous or not too complex. In addition, numerous slides are

available for investigation. Yet studies with hydrological approaches are often too simple as they only partly deal with the complexity of heterogeneous soils, hysteresis of soil hydraulic parameters and preferential flowpaths.

2.2.4   Process-based investigation of large mass movements

Large-scale landslides are more seldom than shallow slope failures. In addition, landslides usually occur in mountainous regions, a landscape type where hydrological observation is even less dense or sophisticated than in lowlands. A coarse net of precipitation stations hampers good quality of rainfall data. This limits the possibility of grasping the additional heterogeneity of precipitation which is induced through the rough mountainous terrain. Large landslides tend to be of a complex type (Dikau *et al.*, 1996) both for the movement as well as for the trigger mechanism. Many studies that deal with hydrologically triggered landslides are rather descriptive instead of focusing on understanding the hydrological processes associated with the failure, e.g. Eberhardt *et al.* (2005) or Hong *et al.* (2005). Only recently has this focus shifted to understanding the hydrology of complex landslides, e.g. during the TESLEC project (temporal stability and activity of landslides in Europe with respect to climatic change, Dikau & Schrott (1999)) and the EPOCH programme (temporal occurrence and forecasting landslides in the European Community, Casale *et al.* (1994)). Publications about research sites like the Alverà landslide (Italian Alps) and the Barcelonnette basin (southern French Alps) present those studies.

The Alverà landslide is situated in the Dolomitic Alps. Similar rock composition in the area lead to similar slope failure of several landslides. Angeli *et al.* (1998) decided to use a conceptual approach to the model subsurface hydraulics which should be applicably on adjacent landslides. They decided on an observational approach to understand major relations between precipitation, pore pressures and stability of the hillslope. With this they then decided to apply a linear storage model to simulate groundwater level combined with a visco plastic stability model. Clay soils and cracks govern subsurface hydraulics on the Alverà landslide which features low slope angles. Piezometer observations show rapid water fluctuations of a relatively short duration after precipitation events above a certain threshold level. During snowmelt conditions a different behaviour is observed. The piezometer responses are attributed to a system of interconnected cracks (Angeli *et al.*, 1998), this system corresponds to the observed threshold levels. Cracks are likely to be superficial shrinkage cracks as well as deeper reaching extension cracks. The hydrological model is on a conceptual basis but seems to reproduce groundwater levels fairly well. Swell-shrink behaviour and associated porosity changes are attributed to a sensitivity of model output to porosity values and inconsistencies of model output thereafter. A sufficient evapotranspiration module is missing in the model. Angeli *et al.* (1999) and Bonomi & Cavallin (1999) deepen the insight to the Alverà landslide through extended geotechnical and hydrogeological investigations. Soil property observation is enhanced, backing a two layered soil strata with a coarse debris clay including cracks on top and more consolidated fine clays below. New piezometer measurements show fast reactions of piezometric pressure signals in correlation to precipitation with a 5 h delay time. The water level is shallow in 0.5-1.7 m depth. Generally, piezometric fluctuations rise quickly within hours and, differing to this, with a pressure release lasting several days. Snowmelt has low influence on groundwater reactions. Low measured matrix hydraulic conductivities of 10^{-8} m/s do not correspond with the observation of sub-vertical crack systems. Zones with differing groundwater reactions were identified for a groundwater model application with MODFLOW. MODFLOW simulations are stated to give reasonable results, though calibration was restricted (Bonomi & Cavallin, 1999). The vertical influence of infiltrating water is calculated; lateral influence for groundwater reactions is considered but not further examined. It has to be stated that these

studies do not present spatially distributed data for hydraulic conductivities and that reliable surface runoff data is not existent. In addition, my own observation is that evapotranspiration implementation is generally poor in MODFLOW.

The Barcelonnette basin in southern France is subject to extended research for landslides and hydrological triggering of landslides (Antoine *et al.*, 1995; Flageollet *et al.*, 1999; Henry *et al.*, 2002; Malet *et al.*, 2003; Malet *et al.*, 2005; Maquaire *et al.*, 2003; Remaître *et al.*, 2005; Remaître *et al.*, 2005; Squarzoni *et al.*, 2003; van Asch, 2005; van Asch & Buma, 1997; van Asch *et al.*, 1999; van Asch *et al.*, 1996). Two different geological frameworks of varved clay rocks (van Asch *et al.*, 1996) and marly rocks make this region a landslide-prone area. Especially the marly environment makes it possible to find parallel conclusions to the investigated site in the Vorarlberg Alps so that research of the "Terres Noires" region will be discussed further in detail.

The Terres Noires is a region dominated by black marls which cover southeastern France. These rocks show a high susceptibility to weathering and are prone to erosion and slope failure (Antoine *et al.*, 1995). The relatively homogenous, smectite-poor marls disintegrate into platelets. With further deterioration, mainly through the dissolution of carbonates, these platelets disintegrate into clayey material (Antoine *et al.*, 1995) which weakly resemble the platelet structure. This weathered material is subject to easy erosion by water. Decalcification seems to be a major process; macropores and fissures are reported to play an important role in subsurface water dynamics. A special method for measuring average hydraulic conductivity in clay soils is used (Bouma & Dekker, 1981), showing considerable variations in saturated hydraulic conductivity values in general and in vertical and horizontal directions for each sample. Upper soils have high conductivities and are underlain by low permeability layers. The early hydrologically based studies in the Terres Noires region feature simple one-dimensional hydrogeological models with monthly and yearly time-steps (van Asch & Buma, 1997). Flageollet *et al.* (1999) try to establish a rainfall threshold for the Terres Noires region but fail as landslide occurrence and types are too diverse and do not always correspond to hydrological signals. On a multiple year basis, wet periods coincide with landslide activity but on the other hand dry periods do so as well. Systematic correlations on a monthly rainfall basis are not feasible, too. Malet *et al.* (2005) present a profound publication dealing with a hydrological model in the saturated and unsaturated flow zones featuring a 2.5 dimensionally distributed concept. The model features a core based on finite differences of a Darcy-generalised transient simulation, with an evapotranspiration module, a snow module and a simple conceptual module to simulate bypass flow through fissures of the uppermost layer. The model has an advanced concept but fails to simulate some peak groundwater heights. Recharge reactions are simulated with a significant delay. The model is based on a daily time-step and surface runoff is not included in the water balance.

2.2.5 Recommendation for studies in landslide hydrology

In my opinion an approach is needed which first defines dominating structures and processes in the field. This is a process of detailed investigation in different scientific fields. Besides geological structure knowledge, soil distribution and heterogeneity plays an important role. A close look at the vegetation on the hillslopes gives clues about the stability and moisture regimes. With expert knowledge dominating structures and processes can be defined and less dominant features can be checked for their sensitivity on the landslide behaviour. Then adequate models or simplifications can be chosen, the more physically-based they are the better the possibility is to redraw conclusions for the perceptional model one has of the landslide. It appeared to me that most of the hydrologically based landslide studies do not try to get closed water balances for their simulation, take Boogard & van Asch (2002) as an exception. Precipitation leads

to infiltration into the subsurface but without a knowledge about the quantities of water in surface runoff generation, infiltration and subsurface stormflow or deep percolation it is difficult to get a good idea of failure implicating rainfall thresholds.

2.3   Importance of subsurface structures at different scales

Hydrological models were often originally designed to be used in lowland agricultural environments (Zehe *et al.*, 2001). Malet *et al.* (2003) state that uncultivated mountainous landscapes are not readily or only recently considered in hydrological models. These environments are essential for the development of landslides and debris flows. It is not only the heterogeneity of mountainous soils and scree material that makes it difficult to grasp hydrological processes on landslides. The landslide-prone material is also subject to constant geomechanical changes which enhance the heterogeneity. The accumulation and erosion of talus slopes, development of residual soils and fast weathering processes of the material give additional stress on unstable hillslopes besides hydrological loading and unloading. Considering hydrologically induced landslides one should not forget the spatial variability of the geological strata, the soil column and the soil material. The influence of pore water on clay minerals or carbonate is of crucial importance for the stability of hillslopes. Especially clay soils are a challenge both from a mechanical and hydrological point of view due to their special mineralogical shape and *abnormal* behaviour concerning strength of the solid-fluid-gaseous material. Not to forget the strong influence of charging of clay minerals, near particle fluids and their influence on pore sizes and strength, see Xiang (1997) for example.

For the identification of dominant structures which influence the stability of hillslopes a broad range of scales need to be considered. Ideally, several scientific disciplines and point of views should be included. In the following the structural scales introduced in chapter 2.1.3 are used to discuss important subsurface structures. The focus is on structure types which are found on the investigated site combined with information from the literature.

2.3.1   Macro-scale or region-scale

The *macro*-scale comprises the geological and tectonic setting of a landslide prone area. Sedimentation, bury, diagenesis and tectonic evolution influences weathering conditions of a geological unit and therefore stability. The inclination of strata and fissure systems which are derived through tectonic evolution influence the stability of mountains and their hillslopes.

2.3.2   Meso-scale or hillslope-scale

The *meso*-scale is considered to be the catchment scale in hydrology. There, the local geological setting has to be considered, e.g. the type and layering of bedrock and sediments. Weathering and the influence of climatic boundary conditions also need to be considered on a long term temporal scale.

In the Austrian Alps many landslides are induced through geomorphological changes due to glaciation cycles. Glacial deposits are often subject to failure as they are often over-steepened. In addition, the broad range of grain size distribution enhances the instability.

Marlstones pose a special threat on stability considerations. The term *marls* is often used instead of the more precise term *marlstone* in the literature. Marls are also a notion for unconsolidated material of clay and carbonate. In the thesis, *marlstone* is used to significantly distinguish the rock type from unconsolidated material, unless any author using the term *marl* is cited. It is not always distinguishable from the text in which respect the author used this term. The denotation of a marlstone means that there is

a consolidated rock, composed of clay- and silt-sized particles. These consist mainly of clay minerals, quartz and carbonates. As a denotation for a mixed component rock, the composition can vary significantly. It is a rock type which combines stability characteristics both from limestone and mudstones to an unfortunate combination for stability reasons.

Frydman *et al.* (2007) found that residual friction angles strongly depend on the amount of clay sized carbonates in marls, as samples of investigated marl profiles in Israel show. Eberhardt *et al.* (2005) suggested the failure zone of the Rufi landslide in Switzerland lies in the transition of highly weathered to moderately weathered marls in contrast to observations in similar landslides. Maquaire *et al.* (2003) state that marls in the Barcelonnette basin are strongly affected by either mass movements or gully erosion. The reason is that these marls are highly susceptible to weathering. Maquaire *et al.* (2003) also state that there is "a general lack of awareness of the special nature of this clay bearing, silty rock *(= marlstones in the case of the Terres Noires; annotation of the author*), which can swell or disintegrate when exposed to atmospheric triggers (wetting-drying cycles and freeze-thaw cycles)". Antoine *et al.* (1995) and Maquaire *et al.* (2003) try to define the geomechanical properties of this marly material. Due to its heterogeneity and special character, they report difficulties in predicting the formation of mudflows, large earthflows and debris-flows.

The location and characteristics of shear zones and properties of movement should be investigated on the *meso*-scale as well. Baum & Johnson (1993) discusses the influence of shear zone surface roughness on the velocity of landslide movement. Surface roughness has been recognized as a source of sliding resistance in soil landslides. Basal and lateral slip surfaces are irregular and can retard a movement. Movement might be with a constant speed, which is interrupted by shorter, faster periods. Internal deformation and rotation of larger blocks need to be considered as well (Baum & Johnson, 1993). Van Asch (2005) discusses the role of excess pore pressure which influence the velocity pattern in earth flows. Earth flows cannot be considered as uniform, zones of compression and extension may develop and lead to excess pore pressures.

2.3.3   Micro-scale or pedo-scale

The *micro*-scale represents the upper soil and is the interconnection of the climatic influence to the landslide body. The soil might often be subject to movement through soil creep and small-scale earth flows.

Clay-rich soils bring a special characteristic on the soil heterogeneity and especially to the subsurface hydrological processes due to small grain sizes as well as the special shape of clay minerals and their chemo-mineralogical behaviour. For example, the swell-shrink characteristic of clay-rich soil influences geomechanical and hydraulic properties. Meisina (2004) reports on the importance of swelling-shrinking properties and its influence on shallow landsliding in the Apennines, Italy. The state of the soils is mostly near saturation. So they develop cracks easily during dry periods which feature fast preferential infiltration during rainstorms which can consecutively lead to slope failures. Shrinking and swelling of soils are important in hydrological aspects of agricultural sciences (Attenberger, 1989; Honisch *et al.*, 2002; Kohler *et al.*, 2001; Stamm *et al.*, 2002), especially on the micro-scale. A consideration of soil shrinkage in micro or meso-scale catchment hydrology has not been conducted too often so far (Harvey, 1971; Lindenmaier *et al.*, 2006). A profound representation of hydrological processes induced by shrinkage in hydrological models still needs to be examined further.

Other micro-scale structures might influence the water balance of a landslide. Malet *et al.* (2003) did a thorough examination of soil surface characteristics (e.g. crusting, vegetation, stone cover) and soil investigation on clay soils derived from marls to better understand the infiltration on a landslide. They generally found a high variability of hydraulic parameters in the Terres Noires. For the same landslide Maquaire *et al.* (2003) point out that the grain size distribution is usually determined in small, matrix dominated samples sizes. This leads to false interpretations of hydraulic properties and other soil-specific parameters. In hillslope scree material, large samples up to 100 kg need to be taken to get a proper grain size distribution. Steep hillslopes feature the development of soil pipes, which might additionally enhance the heterogeneity of soil water dynamics and influences the stability (Hardenbicker & Crozier, 2002; Uchida *et al.*, 2001).

2.3.4   Point-scale or material-scale

The *point*-scale describes the soil-specific properties both for geomechanical and hydrological aspects. This scale definitely interconnects with others, e.g. concerning shrinking and swelling processes. Internal shrinking and swelling of clay minerals like smectites or vermiculites due to exchangeable interlayer cations may influence the shrinkage characteristic of soils or clay pastes (Kariuki & Van der Meer, 2004; Olsen & Haugen, 1998). More likely, shrinkage behaviour of soils is not so much a function of the internal swelling capacity of specific clay minerals but of the volume fraction of particular components in the soils and especially the size and structure of the clay minerals (Wilding & Tessier, 1988). These influence interparticle porosity (Chertkov, 2000; Chertkov, 2003a). The volume change of the pores influences the hydraulic function of the matrix in non-rigid soils (Chertkov, 2003b; Kim *et al.*, 1999; Peng & Horn, 2005). This might as well lead to the development of cracks - even in saturated conditions. This then allows preferential infiltration into lower soil horizons (Bronswijk, 1988; Novák *et al.*, 2000; Šimůnek *et al.*, 2003). If the soil wets up above a certain threshold, the cracks successively close and surface runoff generation will dominate as for example found in vertisols of northern Mexico by Návar *et al.* (2002).

The variability of soil-specific parameters for hydraulic, as well as stability investigations are of concern for the scientific community. Hicks & Samy (2002) investigated the impact of the variability of the undrained shear strength on failure zone development, shear strength parameters are even more seldom to be measured in quantitative amounts for single hillslopes. Reid (1997) points out that even small variations in hydraulic conductivity of one order of magnitude in soil slopes influence effective stress fields and slope stability. He also states that variability in several orders of magnitudes of hydraulic conductivity might impose slope failure, e.g. when blocks of very low conductivity occur in higher conductivity layers (Haneberg, 1995). A lot of studies are performed in sandy soil types (Cho & Lee, 2001; Iverson *et al.*, 2000) as parameters are more easy to obtain. It is necessary to describe heterogeneities in clay soils as differences of hydraulic conductivity are more enhanced through larger differences of matrix conductivity and macropores than it is for sandy soil.

3 The study site and its geological setting

This chapter introduces the study site (Figure 3-1) and comprises information dealing with the geological investigation and measurements of the movement of the investigated slope. These were conducted within the frame of the first research project. Additional information about the glaciations of the area is provided to develop a perceptional model of the geological structures on the slope. These prerequisites will later help to understand the structures that were found at different scales on the hillslope body. Through the history of geological development, the sparse information of the subsurface can be enhanced and a link to hydrogeological processes can be developed. Chapter 4.1 provides further information about maps, the digital resources, boreholes and movement measurements including data and measurement methods from the research partners.
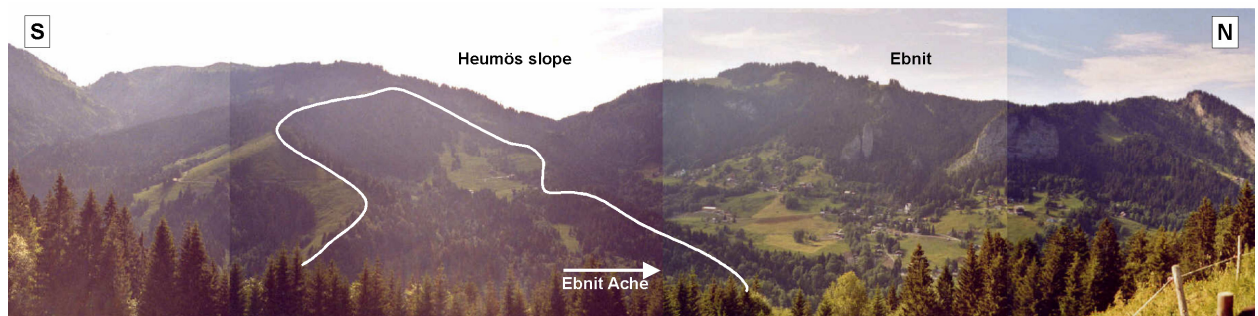
Figure 3-1: View on the village Ebnit and the adjacent Heumös slope, the white line represents the catchment boundaries, the meadow on the right site is the moving hillslope body. The view is towards the west, the drainage is towards the north.

3.1 Geographical setting, topography and hydrography

The study area, called the Heumös slope, is located in the eastern Vorarlberg Alps in Austria, 10 km southeast of the city of Dornbirn, the economic centre of the state of Vorarlberg (Figure 3-2). The Heumös slope is located 0.5 km south of the village of Ebnit at the end of a paved road. Both the village and the surrounding area belong to Dornbirn in an administrative sense. Dornbirn has an elevation of about 429 m above Adria (a A), whereas the church of Ebnit is located at 1075 m a A.

The river network is composed of the Gunzen Ache (river of Gunzen) in the northeast and the Ebnit Ache (river of Ebnit) in the southwest, at the Schanerloch canyon the Ebnit Ache changes its name to Dornbirn Ache (river of Dornbirn), which drains directly into the Bodensee (Lake Constance), parallel to the Rhein (river Rhine) at 400 m a A. The springs of the Ebnit Ache lie beneath the Hoher Freschen (2004 m a A), the highest mountain surrounding the valley. Further mountains around the valley anti-clockwise from the Hoher Freschen are Alpkopf (1788 m a A), Mörzelspitze (1830 m a A), First (1765 m a A), Hochälpele (1464 m a A), Karren (971 m a A), Staufen (1465 m a A), Schöner Mann (1532 m a A), Hohe Kugel (1645 m a A) and Vorderhörnle (1656 m a A). The landscape of the Ebnit, Gunzen and Dornbirn Ache watershed can be parted into three sections: 1) the upper part of the valley is characterised by mountainous but gentle slopes formed by glaciers in soft sedimentary rocks, grey marlstones respectively. 2) The middle section is very steep, here the river cuts into calcareous rocks forming the Schanerloch, Schaufel, Alploch and Rappenloch canyons. 3) The foreland or lower section comprises the alluvial fan, where the city of Dornbirn is located as well as the Rhein plain. As the main focus is on the first two

landscape types, this system will be referred to as the Dornbirn Ache valley. The third landscape is rather dominated by the geomorphological influence of the Bodensee and the Rhein.

Dornbirn is the economic centre of Vorarlberg with tourism playing only a secondary role, for the village Ebnit tourism is the major local business. Founded in 1351 AD by Walser settlers it has been an enclosed settlement and was difficult to reach until a spectacular road was build alongside the canyons in 1921. Since then tourism thrived with a boom in the 60's, which lead to the construction of numerous holiday homes in Ebnit and a holiday village on the Heumös slope run by the "Kolpingwerk". Tourism declined with the rising mobility of tourists and day tourism is more important nowadays. Most inhabitants work outside the village and use the road to commute so it has major importance for the village.
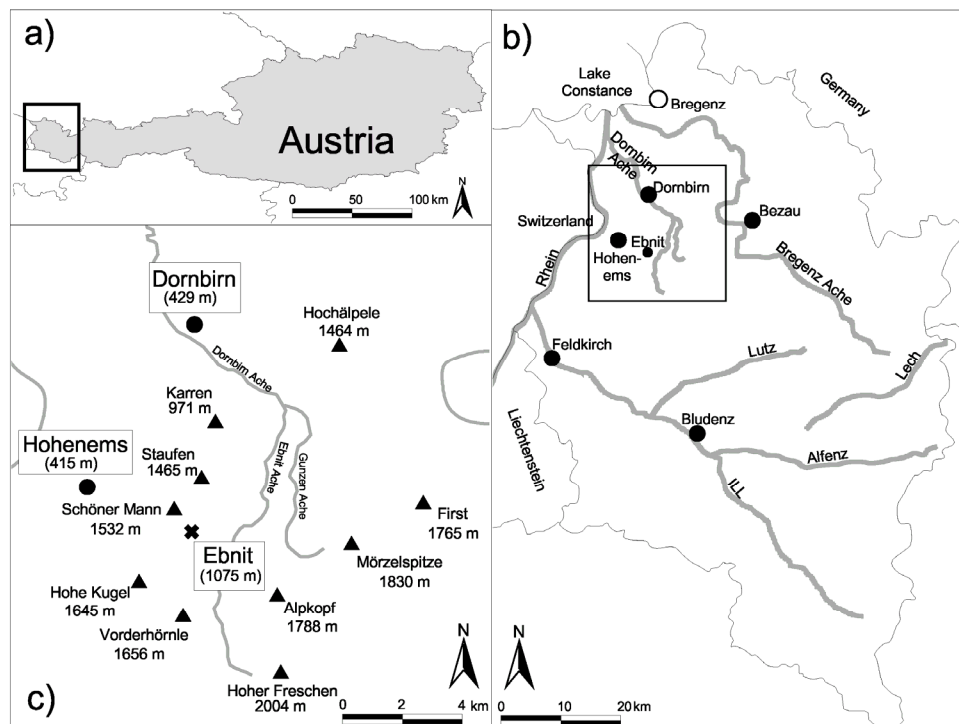
Figure 3-2: a) Location of the study area in Austria; b) Vorarlberg with major cities and rivers; c) the upper Dornbirn Ache area. Heights are given for the settlements and major peaks surrounding the Dornbirn Ache catchment. The GIS data is from Ruff (2005).

The Heumös slope is separated from Ebnit in the north by the so-called Bruder creek (Bruderbach; Figure 3-3), which has deeply cut into the soft marlstones. It is the second largest western tributary to the Ebnit Ache. The Heumös slope itself is surrounded by marlstones, it stretches from 940 to 1360 m a A, slope angles of more than 60 % can be observed as well as almost flat areas (Figure 3-4). The shape of the Heumös slope can be described as a tilted bathtub; half open to the north and east. It has a concave shape from the highest parts from the south towards the north and a convex shape from the highest point in the west towards the east. In the south and the north steep slopes rim an eastwards directed middle slope. The extension is about 2000 m in west to east direction and about 500 m at its widest extent in north to south direction. The toe of the hillslope is bordered by the Ebnit Ache. There, erosion by the river has lead to over-steepened slope angles. Two small slides occurred in the over-steepened slope, the larger one must have occurred before 1965 (Smit Sibinga-Lokker, 1965).

A paved and gravelled road cuts the slope at the middle of its west to east extension, which gave the possibility to install three weirs for discharge gauges. These were installed at the creeks crossing the road (Figure 3-3). From north to south, creek 3 is encountered first, also called the Heumös creek. Its spring area are wetlands and scars of small slides in the northeast of the slope; it quickly cuts 2-3 m deep into the slope, crosses the road and then leaves the Heumös slope flowing towards the Bruder creek in a northeasterly direction. All other creeks flow from west to east and drain directly into the Ebnit Ache. Creek 1 has two source areas: one lies in the northwest in wetlands above the ones of the creek 3. The second source area lies in the southern slope. This same goes for creek 2 which joins creek 1 below the road. The southern slope is characterised by numerous deeply cut gullies. For stabilisation of the upper part of the mid-slope, which is used for skiing in winter, several surface drainage channels were dug and tile drains were installed. Creek 4 runs from the height of the sewage plant of the holiday village towards the toe at the Ebnit River. In the lower part of the mid slope, both creek 1 and creek 2 produced also deeply cut gullies with depths up to 30 m.
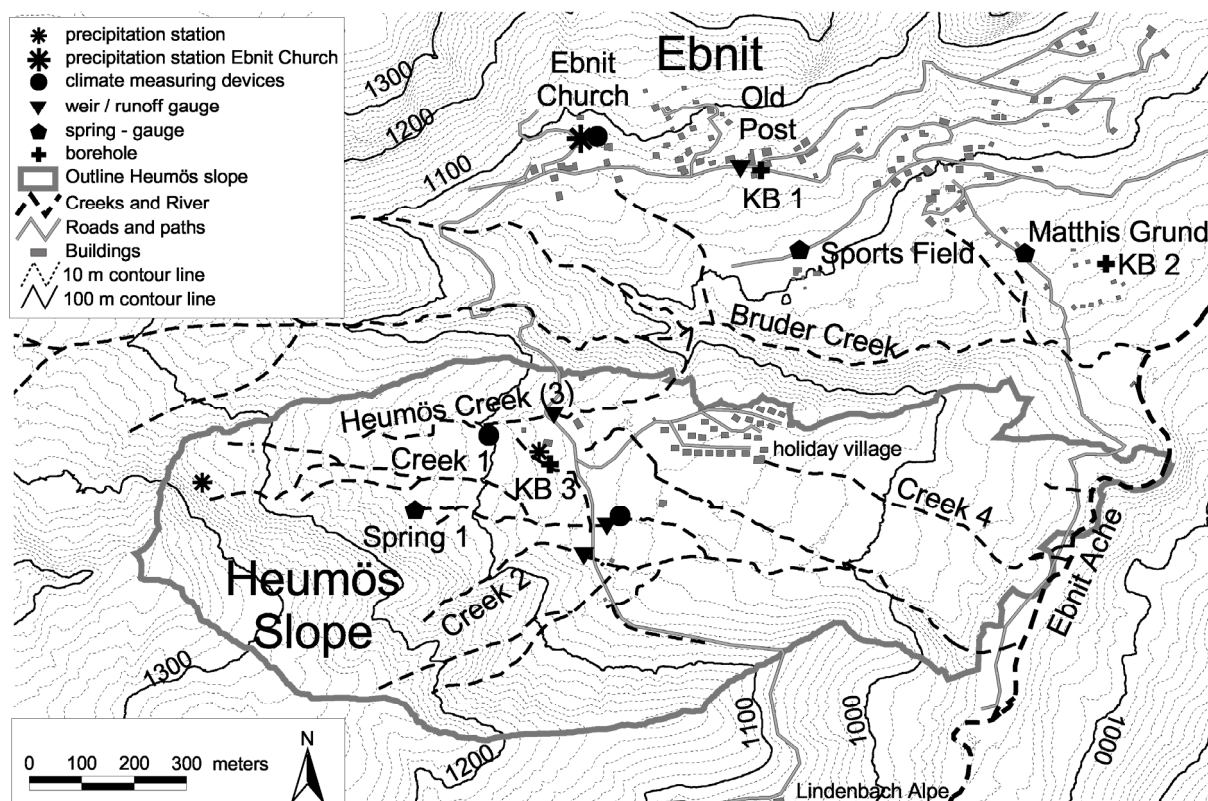
Figure 3-3: Map of the village Ebnit and the Heumös slope showing the borehole locations, the location of the measurement equipment and the settlements (Lindenmaier *et al.*, 2005).

For a better orientation on the Heumös slope and identification of important areas some terms will be introduced describing the geological and hydrological boundaries of the slope. The outer boundary in figure 3-4b encompasses the total hydrological catchment area of all four creeks (Figure 3-3). The *southern slope* (Figure 3-4b) is a lot steeper than the rest of the catchment and contributes significantly to surface runoff as well as it is the major source area for scree accumulated north of it. The *hillslope body* is the part which shows creep movement and surface runoff drainage towards the east, it has the highest sediment accumulation. Geologically, the *northern slope* is more similar to the hillslope body but is steeper and dominantly drains towards the south or southeast.

18
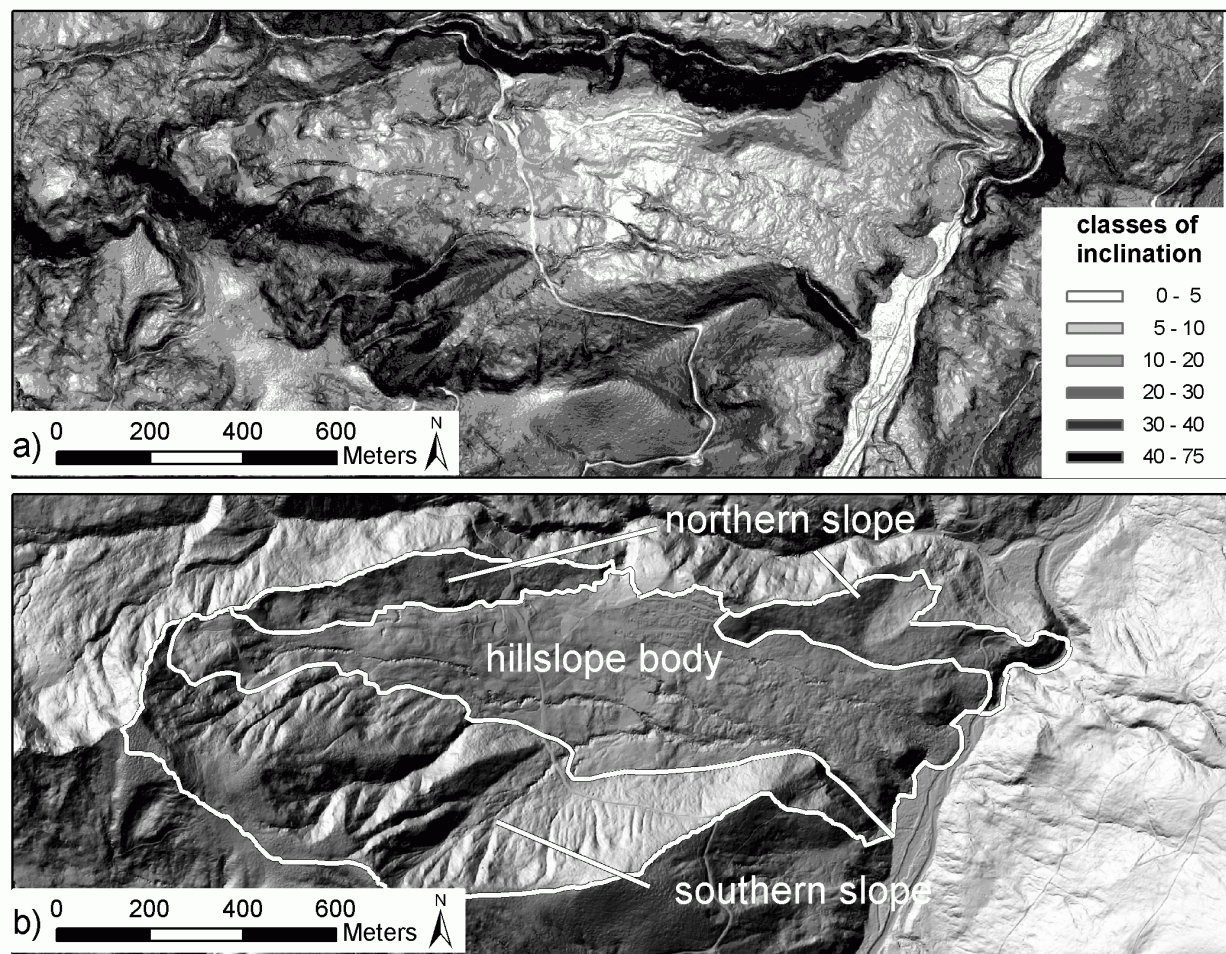
Figure 3-4: a) Classified slope angle of the study site, note the flat areas in the middle and the periodic bulging in the east (flat areas alternate with steeper ones). b) The shading of the airborne laser scan digital elevation model (ALS DEM) shows the small-scale topography which is especially shaped by the deeply cut creeks in the south and east. Also note the two small rotational slides in the over-steepened slope towards the Ebnit Ache. The slides changed to earthflows at the toe and left a distinct morphological shape.

3.2   Geological setting

Mass movements are determined by subsurface properties which in turn are the result of the geological development and genesis of recent structures on a hillslope. Hence, it is important to get an idea about the long-term time scales of the very slow processes like the sedimentation of primary rocks, mountain evolvement as well as the post-glacial development. Geological strata can imply failure zones; texture and chemical-mineralogical composition of the primary rock might lead to specific weathering and to the genesis of critical geomechanical material. A short description of the geological setting of the Dornbirn Ache watershed will follow, focusing on the area of the investigated slopes with the aspect on the material and hydrogeological attributes.

The Dornbirn Ache watershed is built up of Cretaceous and Tertiary marine sediments – dominating calcareous and marlstone formations of the Helveticum and with minor importance of the Penninicum, these hard rocks will be named *bedrock*. In the post-marine time of mountain evolvement, denudation prevailed but the Pleistocene glaciations as well as post-glacial mountain forming left patches of unconstrained or partly constrained sediments, named *glacial* or *post-glacial sediments*.

19

The sedimentation of the primary rocks took place in different coastal, marine or shelf environments, which are named throughout the Alps with specific terms: e.g. Helveticum or Penninicum. The rocks of the Vorarlberg Helveticum of the Dornbirn Ache watershed are part of the northern shelf sediments of the Cretaceous Pennin Ocean. Sedimentation was influenced by transgression and regression phases, leading to a pronounced interbedded strata. Besides carbonate platforms and reefs, sediments with lower carbonate and a higher clay fraction are found of a shelf to deep sea margin with approximate water depths of 100 m (Wyssling, 1986). The sediments of the Penninicum are deposited in a lower shelf to basin environment but also feature some horsts (a horst is a raised fault block bounded by normal faults). The major sediment type is a Flysch which is a sediment transported from the shelf margins into the deep sea. Limestones and marlstones are also found on the horsts (Oberhauser, 1998).

A nappe is a sheet-like allochthonous rock unit that has moved in a predominantly horizontal surface (Bates & Jackson, 1984). Formerly neighbouring sedimentary units are tectonically overthrust so that rock units, which were separated spatially and temporal, might be neighbours nowadays. The sedimentary environment of the Helveticum is represented by the Säntis nappe (Figure 3-5), which shows a development of a more carbonaceous facies at Dornbirn towards a more marly facies at the Hoher Freschen (Oberhauser *et al.*, 1991). A transition can be seen at the height of Ebnit, which is surrounded by limestones, whereas the southern slope of the valley is dominated by marlstones. The Säntis nappe lies below the nappes of Penninicum and Ostalpin but has been thrust over the Alpine Molasses (Figure 3-5). As the higher nappes are eroded in northeastern Vorarlberg, the Säntis nappe dominates (Oberhauser, 1998), leaving only small remnants of the Liebenstein nappe (Ultrahelveticum) and the Feuerstätte nappe as well as the Vorarlberg Flysch (both Penninicum) at the Hohe Kugel and Hochälpele peaks, both mountains are located at the rim of the Dornbirn Ache watershed.

The geologic layers are tectonically bent and twisted; they show several anticlinal and synclinal folds with stronger forming in the limestones in the north. It is more difficult to detect the folds in the marlstones towards the Hoher Freschen. The folds have evolved through a distinct compression of the nappes in approximate north to south direction (Figure 3-5a, Figure 3-6). The fold axes have a general west to east direction (Oberhauser *et al.*, 1991) and dip in southwest and northeast direction. The north facing axial planes are steeper so that a north vergence is observable. The limestones exhibit stronger and larger folds whereas the marlstones show smaller folds, which are less pronounced in the outcrops.

The Leimern formation on the southeastern Heumös slope belongs to the overthrusted Liebenstein nappe and, therefore, shows a tectonic boundary towards the Wang formation (Figure 3-5b). The compression and folding in southwest to northeast direction is the reason for a fissure system in the bedrock. Four major fissure systems are defined by Schwenk (1999), both of them are perpendicular. The more dominant system is in east to west and north to south direction, respectively in 100 and 175 degrees; the second system has angles of 65 and 145 degrees. The layering is aligned against the major scarps and has a strike of 60 to 80 degrees and a normal dip of 30 to 60 degrees around and on the Heumös slope (Schwenk, 1999).

3.3 Local geology

The local geology as well as the development of the hillslopes during glaciation and afterwards are important for the understanding of the perceptional model of the mass movement. Information from earlier scientific work is presented here before a discussion of the perceptional model follows in chapter 7.1.

3.3.1   Cretaceous bedrock

The rocks surrounding Ebnit and the Heumös slope date from Lower Cretaceous up to the Lower Tertiary, mostly from the Säntis nappe but locally also from the Liebenstein nappe (Figure 3-5b). On shelf plains and also on shelf-deep sea margins (shelf slopes) calcareous and marly sediments but also calcareous sandstone were accumulated. The facies of a rock is determined by the sedimentary environment, e.g. whether it has been deposited on a carbonate platform or at a shelf slope. This also depends on the climatic condition. This means that similar rock units can both be located spatially besides each other as well as temporal on top of each other. Rock outcrops from the Valanginian, Drusberg, Schratten, Garschella and Seewer formations surround Ebnit, whereas rocks from Amden, Wang and Leimern formations margin the Heumös slope. These sedimentary rocks and their weathering products chiefly influence the recent geological material on the hillslopes and so also of the mass movements. Figure 3-7 shows the distribution of geologic strata of the Ebnit area.
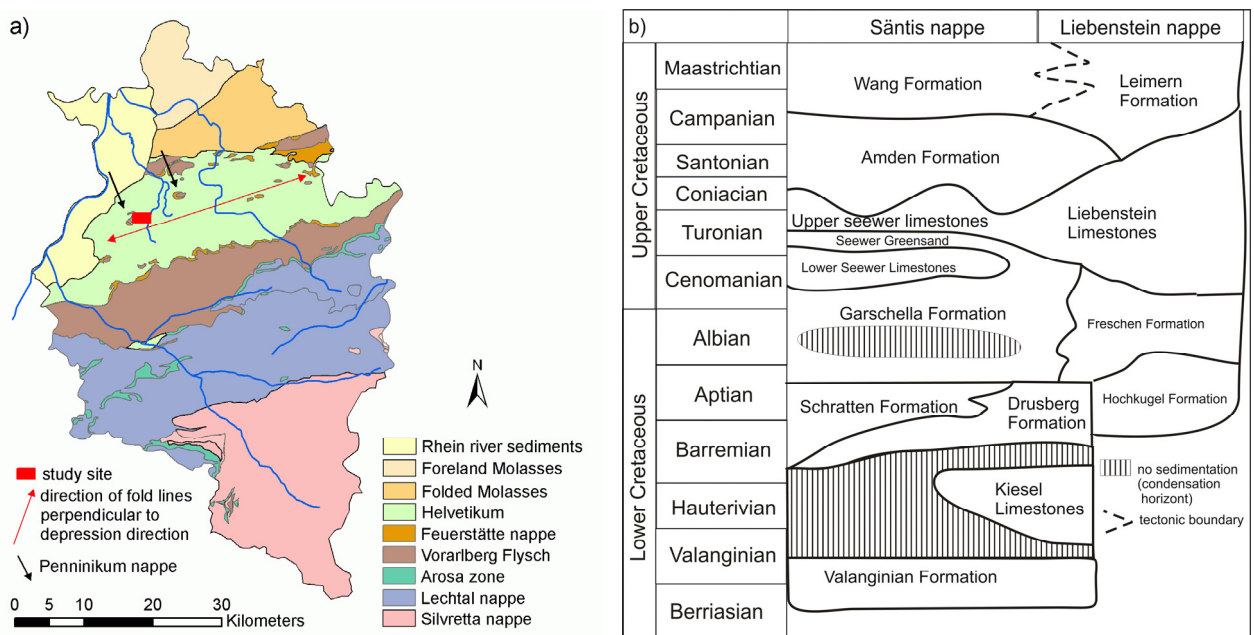
Figure 3-5 a) The geological overview of Vorarlberg including the direction of major fold axes in the Säntis nappe of the Helveticum; small black arrows indicate the nappes with Penninicum rocks of Hohe Kugel and Hochälpele surrounding the Dornbirn Ache watershed. Data changed after Ruff (2005). b) Simplified timetable of the Cretaceous with major rock formations in the Säntis nappe and Liebenstein nappe, changed after Oberhauser (1991).

The *Valanginian formation* consists of fossil- and carbonate-rich, well-banked limestones as well as siliceous limestones interbedded with minor marlstone layers. The *Kiesel Limestone* is a pronounced layered siliceous limestone interlayered with shales; its appearance is minor in the Ebnit area. The next younger formation is the *Drusberg formation*, interbedded strata from thin limestone layers, clayey marlstones and marly limestones, representing a deep-sea facies. Thickness and appearance of the carbonate layers increase upwards. The *Schratten formation* is geographically located besides the Drusberg formation as well as chronologically on top representing limestones from shallow carbonate platforms (Figure 3-5b). It is interlocked with the Drusberg formation in a complex manner (Oberhauser *et al.*, 1991). The rock cliffs above Ebnit are made out of this Schratten formation. A regression of the ocean lead to erosion of the Schratten formation in the northern Helveticum, leaving a hiatus in the

sedimentation history. The *Garschella formation* is accompanied along with a transgression phase with a higher contribution of quartz sand, leaving glauconitic rich sandstones, which locally alternate with the Drusberg formation. Sedimentation rates were low then. Besides the greenish (glauconite) sandstones there are also marlstones, carbonate layers and condensation horizons containing phosphorites. The *Seewer formation* was deposited in a hemipelagic to pelagic environment, representing deep-sea limestones from a deep helvetic through. A new regression phase starts with sedimentation of the clay-rich silty to sandy detrital sediments along with carbonate: the *Amden formation.* Around the Heumös slope these are sandy to clayey grey marlstones which are finely shattered (often also called "Leist marlstones"). Brown fissure planes and the absence of calcareous interbedded layers are characteristic. The *Wang formation* follows the Amden formation representing marly strata but which also feature layers with higher carbonate content. The rocks show a distinct layered facies. Sandy marlstones up to banked limestones can be found especially to the west of the Heumös slope. The Wang layers tend to be stiffer than the Amden layers and they also include thin greenish, glauconite-containing sand layers.
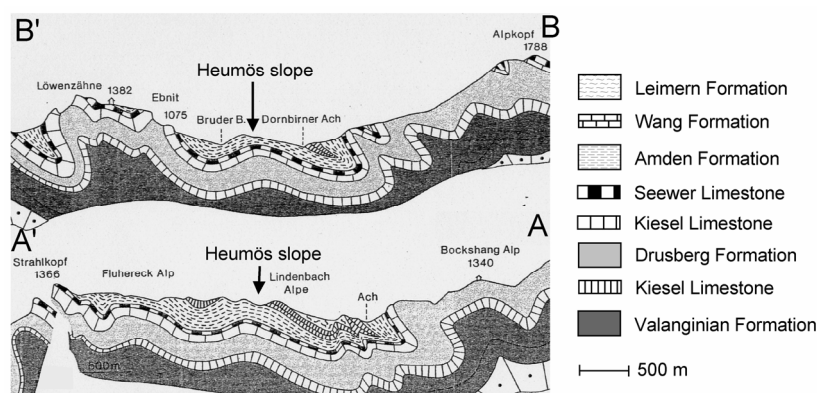
Figure 3-6: Section of profiles drawn by Oberhauser *et al.* (1991) crossing the Heumös slope. Note the over-steepened northern fold planes. For the location of profiles see Figure 3-7.

The *Leimern formation* is chronologically identical with the Wang formation but tectonically belongs to the Liebenstein nappe. The Leimern formation is found in the south and west of the Heumös slope. White or green to grey marlstones with dark spots are characteristical but also red components are found. Schwenk (1999) suggests that the Leimern layers south of the Heumös slope were popped up through tectonic folding of the Helveticum as they show a normal layering (out-of-the-syncline thrust) and differ from the Leimern layers around the Hohe Kugel as they are less tectonically reworked. Maps from Oberhauser 1998 and Oberhauser *et al.* (1991) suggest that the Wang layers surround the Leimern layers south of the Heumös slope (Figure 3-7).

Oberhauser *et al.* (1991) describes the Wang layers as a possible aquifer due to fissures in the more calcareous and sandy rocks, whereas the Leimern and Amden layers function as aquitard even though the fissuring is profound, the aperture is too fine to feature water flow. On the southern slope the Wang layers are easily distinguishable because the harder rock is more stable and so morphology shows an edge towards the Amden layers. These follow below and are much steeper than the relatively flat Wang layers. The steepest slopes are located in the Amden layers there. The boundary between the Wang and the Leimern layers is less profound and hard to distinguish, the reason for different views in Schwenk (1999), Oberhauser (1998) and the newest digital map of Oberhauser as displayed in Walter (2006). Schwenk's (1999) mapping is the most specific on the Heumös slope so that his interpretation is thought to be best in this area. His map has been altered locally during field trips for this thesis (Figure 3-7).
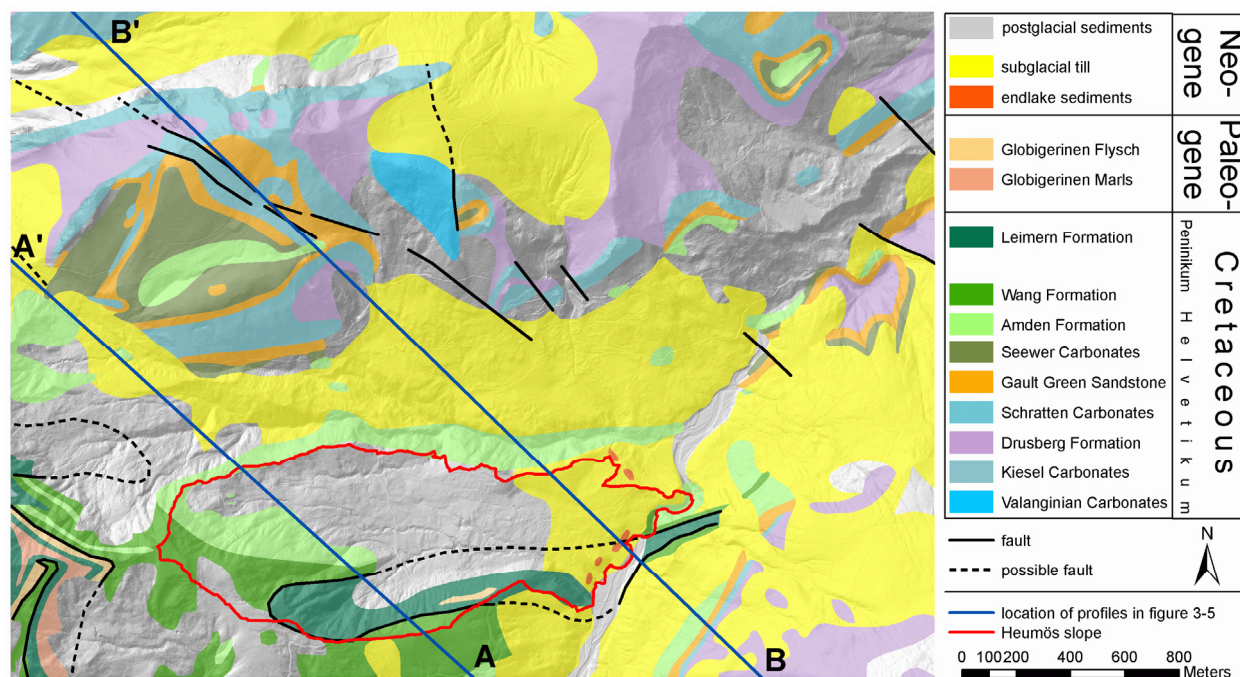
Figure 3-7: The geological map of Ebnit and the Heumös slope, which is displayed with a red border. The map is derived from maps of Oberhauser *et al.* (1991), Schwenk (1999) and personal observations. It is combined with the hillslope shade of the digital elevation model, the blue lines are profiles from figure 3-5.

3.3.2   Glacial development

The Dornbirn Ache valley has been heavily shaped by glaciers, namely from the Würm glaciation (115.000-10.000 BC). Former glacial periods are hard to distinguish as the Würm glacial maximum reworked their remnants. At the Würm glacial maximum the combined Rhein glacier (Rhine glacier) and Ill glacier flew from the west and south over the mountain ridges into the Dornbirn Ache valley and only some hilltops were left ice-free as nunataks, for example the Hohe Kugel and Schöner Mann (Figure 3-8a). The Bregenz Forest glacier overflowed the eastern ridges and made a minor contribution to the Dornbirn valley system (Smit Sibinga-Lokker, 1965). The Bruder creek valley and the Heumös slope were covered by a side arm of the Ill glacier flowing over a pass north of the Hohe Kugel peak (Fluhereck-pass). The height of the glacier on top of the Heumös slope was about 1450 m, which is approximately 150-300 m of ice above today's surface. Smit Sibinga-Lokker (1965) mentions glacial erratic blocks from gneiss, amphibolites, sandstones from the Buntsandstein (Lower Triassic) and Red Lias limestones found near the Heumös slope. Granite boulders are rather an indication for the Bregenz Ache glacier and were not found nearby. During the glacial maximum an older Ebnit Ache glacier was overflowed, which means that existing subglacial till was additionally compacted and further material was added on top. Older ice remnants reduced erosion forces through the overflowing glacier, which might be important for stability considerations.

After the Würm maximum, the glaciation receded until the surrounding glaciers did not overflow the rim of the Dornbirn Ache valley any more. The glaciation in the valley receded after it was not fed by the incoming glaciers any more so that an ice-free area developed with a Rhein glacier side arm intruding from north to south (Figure 3-8b), in the opposite direction of the fluvial system of the valley (Smit Sibinga-Lokker, 1965). This led to several end lake formations, also at the height of Ebnit. Remnants of these glacial lake sediments can be found below Ebnit and at the toe of the Heumös slope. Former

surfaces of the glacier base are the terraces of Ebnit and are found near the Lindenbach Alpe directly south of the Heumös slope.
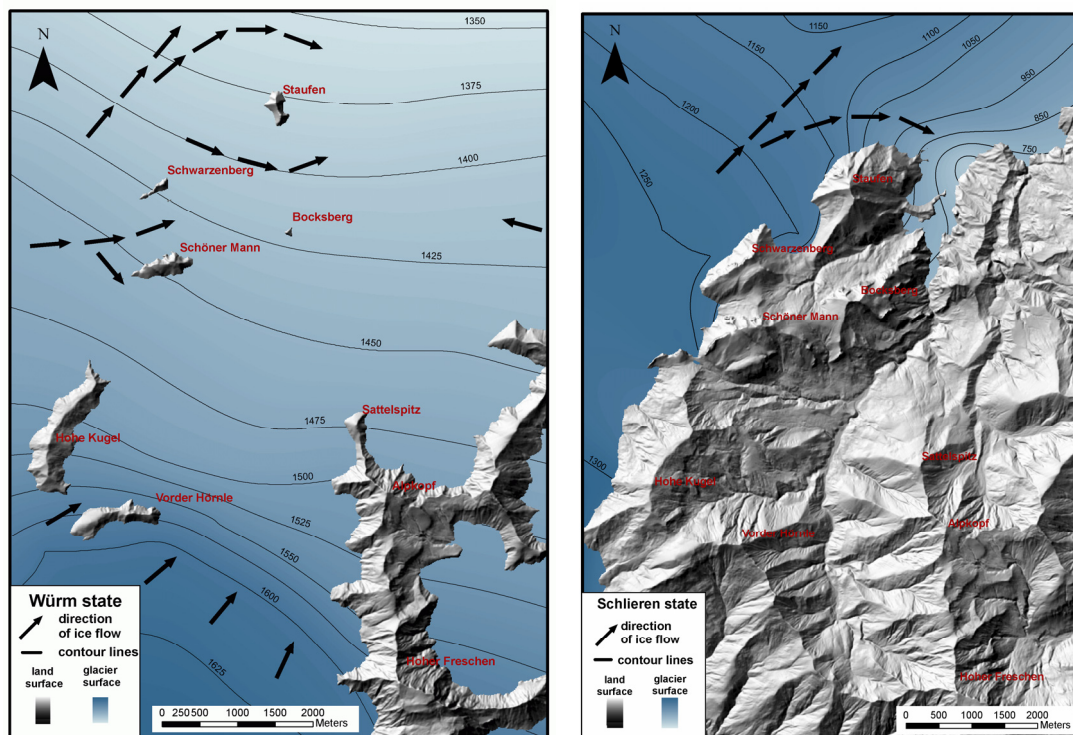
Figure 3-8: Approximate ice coverage during the Würm glacial maximum a) and the Schlieren state b). Maps are recalculated after sketches of Smit Sibinga-Lokker (1965). Black arrows indicate major ice flow directions.

3.3.3   Post-glacial development

Before the Würm glaciation the bottom of the Rhein valley was located about 400 m higher than today. The high former surface and then the glaciers greatly influenced the course of draining water in post-glacial times. The receding glaciers subsequently opened the Dornbirn Ache valley towards the Bodensee; the rivers removed large parts of the glacial sediments and end lake sediments (Smit Sibinga-Lokker, 1965). Preformed canyons could be deepened, forming the Rappenloch and other canyons. At the height of Ebnit, the Ebnit Ache cut all the way down to the bedrock, probably removing at least 30 or more meters of glacial sediment. Rock outcrops in the bed of the Ache are from the Amden-, Wang- and interbedded Leimern formations. Consecutively, the river removes the counter bearing of the Ebnit and Heumös hillslopes, though local authorities try to keep the river flowing east of the steep slopes, which form the toe of the Heumös slope.

While glacial material and end lake sediments were removed from the Ebnit Ache, debris material was accumulated on the slopes on top of the subglacial till. Material properties of post-glacial sediments and facies are discussed in chapters 5.1.2 and 7.1.4.

3.3.4   Strata from borehole KB 3

Borehole KB 3 was drilled on top of the Heumös slope figure 3-9 (Schneider, 1999), besides the Heumös Alpe (Figure 3-3) down to 24 m below the surface. From the soil surface there are 9.8 m of sedimentary strata consisting of debris material from adjacent bedrock, which are the post-glacial sediments. This

strata is differentiated as layers of *coarse scree* and *loamy scree*. Following the borehole description in Schneider (1999) the upper 7.3 m are dominated by loamy to sandy material with rock fragments (loamy scree) or rock fragments with minor matrix content (coarse scree). Coarse scree is of less extent and is found in a layer from 1.7 to 2.4 m with rock fragments as a more dominant component. A loamy scree layer contains wood in 5.9 to 7.3 m. Below this, a layer with coarse scree material is found with more rocks and less loamy matrix. From 9.1 to 9.8 m the debris material is suggested to be loosely deposited. The consistency of the loamy material is dominantly described as soft and soft to firm (Chapter 4.1.4).
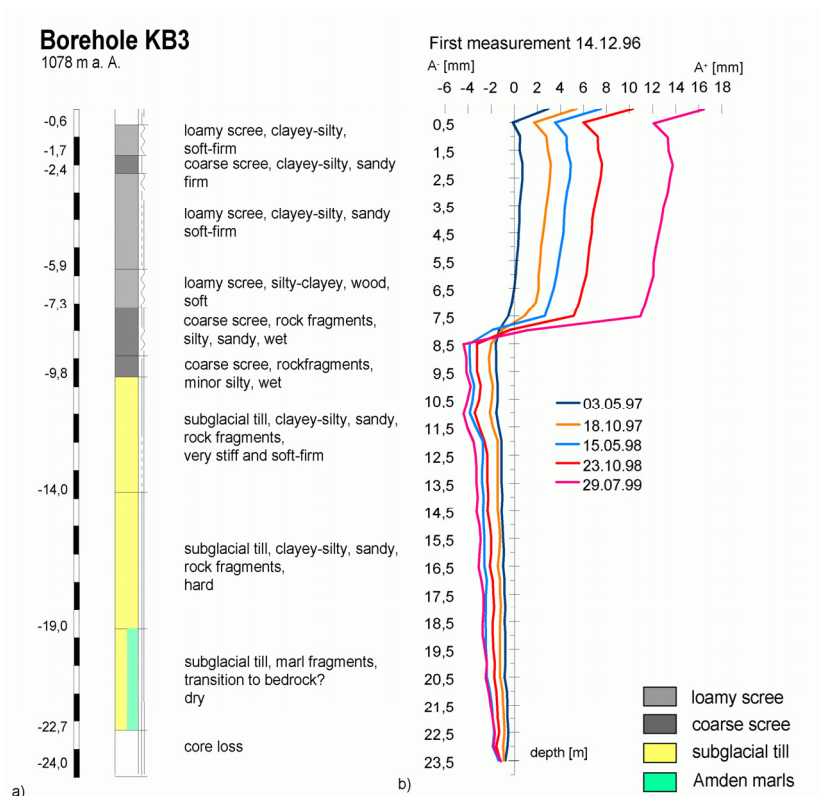
Figure 3-9: a) The geological profile of borehole KB 3. Carbonate contents of samples in certain depths are found in Appendix B-1. b) Movement profiles from measurements with an inclinometer, a weak shear zone is seen between 7.5 and 8.5 m. Creeping is indicated above the shear zone, negative values below indicate the missing anchor in the bedrock. Both figures are changed after original data of Schneider (1999).

Below the scree, down to 19.0 m depth, subglacial till is found with rock fragments of marlstone, limestone and sandstone, the matrix is described as silty-clayey and sandy. Layering is less pronounced than in the debris material. From 19.0 to 22.7 m a mixed layer of subglacial till and weathered Amden marlstone was found, the material was dry. From 22.7 to 24.0 m material was lost in the borehole. Technical reasons prevented that the borehole could be drilled into the bedrock. This is essential for measurement of movements in with inclinometer devices. Boreholes are equipped with inclinometer-pipes with rills to ensure a precise measurement of inclination changes that can be caused by movement. For convenience of the reader the method is described in more detail in chapter 4.2.3.

3.3.5 Bedrock identification by hammer blow seismic

Walter (2006) conducted three seismic profiles with the hammer blow method at the rim of the hillslope body. Two profiles are located parallel to the road at the southern slope. There, the thickness of the sediment layer increases from around 1.1 m towards 7.5 m. Further uphill on the southern slope, a

constant sediment thickness of 1.0 m was detected. At the northern rim, northwest of the holiday village, a third profile shows results of a thickness of 1.8 m to 2.0 m. This information will add to the discussion of the sediment-bedrock interface in chapter 7.1.3.

3.3.6   Geotechnical aspects

The mass movement of the Heumös slope is considered to be of a complex and compound type (Dikau *et al.*, 1996). On the 1 km² sized slope different movement types contribute to the overall shape depending on the inclination. This chapter is based on the interpretation of Schwenk's (1999) findings (Figure 3-10). It is thought to help understanding the hydrological characteristics as well, since these are influenced by the movement through changing structural patterns. Surface movement and creep might not necessarily correlate and compare directly with movement at deep seated shear zones, as material properties might differ. The borehole log shows layers with different consistencies. Soft layers rather exhibit rheological behaviour and are influenced by changing water content, which decreases the cohesion. Rigid layers rather show shear zone development and so translational behaviour. Forces and triggers must not be similar for small and large scale movements but similar movement patterns could reveal relations. The discussion and presentation of geotechnical features gives clues of heterogeneity on the hillslope scale.

Deep seated translational movement at shear zones

Deep-seated translational shear planes are expected between the bedrock – subglacial till transition, and are partly proved between the subglacial till – post-glacial sediment transition in the borehole KB 3. Shear plane existence and localisation will be further discussed in chapter 7.1.5.

Scarps, gullies and rock fall in the southern slope

The bedrock's fissure systems (Chapter 3.2) can produce rock falls in the Amden marlstones. These are expressed through deep scarps in the southern slope but also north of the slope boundary in the Bruder creek valley (Figure 3-10). The layering is aligned against the major scarps and has a strike of 60-80° and a normal dip of 30-60° so that these rather have a stabilising function. Gullies can easily develop in the bedrock of the Leimern and Amden marlstones in combination with the two major fissure zones. In contrast, the Wang layers are more stable which is expressed through less steep slopes and higher accumulation of weathered material. The upper end of the north exposed scarps often correspond with the transition between Amden marlstones and the Wang layers. The southern slope is dominated by scarps from rock fall and deep gullies from perennial creeks with adjacent small rotational slides. Debris flows can go down along the gullies, leading to accumulation of material in the hillslope body as debris fans, this is observable in the airborne laser scan digital elevation model (ALS DEM, Figure 3-4).

Deep and shallow rotational slides on the upper hillslope body

On top of the deep-seated translational movement, multifarious smaller movements are identifiable through marks on the surface like shallow and deep rotational slides, debris flows, gullying with adjacent rotational slides and soil creep and earth flows. The northern slope features deep rotational slides in the west. The western mid slope functions as place for debris material to accumulate. The upper subsurface moves towards the east, chiefly showing shallow rotational slides and small bulging earth flows also recognizable in the vegetation pattern. Notable are huge steps in the topography of the western mid-slope (Figure 3-10). On the height of the holiday village the slope angle smoothes, earth flows and soil creep are the most important surface marks here.

Deep rotational slides, earth- and debris flows on and at the toe of the hillslope body

The eastern-slope is dominated by subglacial till which shows deep rotational slides. These develop towards mud flows at the toe towards the Ebnit Ache and the toe of creek 1, which both drive the mass movement through erosion.
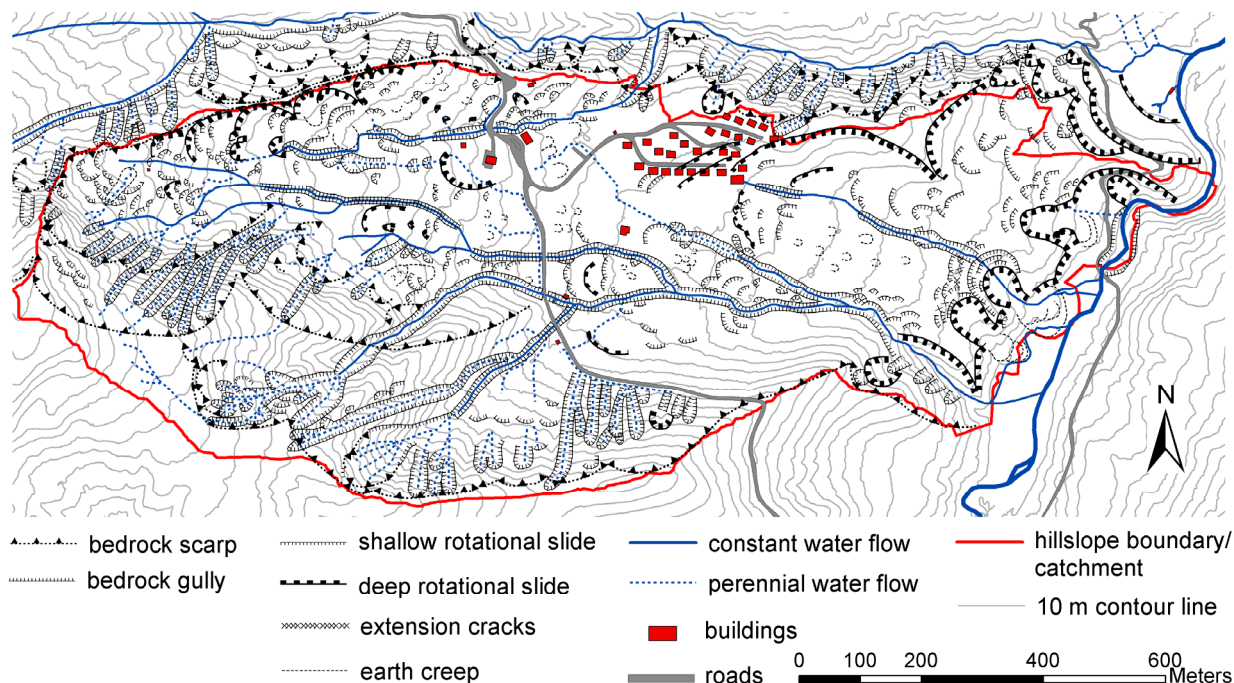
Figure 3-10: The geotechnical map after Schwenk (1999), deep rotational slides in sediment material dominate the northwestern and eastern part. Bedrock scarps and gullies dominate the southern slope. Soil creep and shallow slides dominate the hillslope body.

3.3.7   Properties of bedrock and sediments

Rock types of Heumös slope

Bedrock and sediment properties are essential for understanding the causes of mass movement and the interaction of water with the geological material. This is why a description of major rock material as well as former investigations are presented here. Bedrock contributes to the glacial and post-glacial sediments and so influence their composition and properties. The presented data is comprised in appendix D, further information about soil properties from a pedological viewpoint will be presented in chapter 5.

The rock types surrounding the Heumös hillslope body are marlstones, marly limestones and, with minor importance, sandstones. The *Amden marlstones* are more tectonically strained due to their incompetent material properties than e.g. the marly limestones from the *Wang formation*. As a consequence, the marlstones are shattered into very fine fragments. The rock usually has a light grey colour, figure 3-11a displays shattered marlstones besides the road. A single marlstone fragment still has a brittle and strong material property but on a larger scale the marlstones are considered to have a high susceptibility to weathering. As most dominant source rocks, they also contribute to the most rock clasts in the debris sediments. Again, these fragments (cm to m in size) are susceptible for different conditions of alteration, some break into fragments, some even break into very small chips. In some areas, e.g. in the northwest corner of the northern slope, the in-situ marlstones are strongly altered in a different way: The in-situ rock

27

is leached of carbonate and a clay-rich material is encountered which still has the structure of the shattered rock fragments but a reddish-brown or white colour (Figure 3-11b). The Amden marlstones are not considered to have qualities of an aquifer (Oberhauser *et al.* 1991). The rock outcrops of the Amden marlstones do not show seeping groundwater or wet regions of fissured rock. This would be observable when these rocks would be a fissured groundwater containing rock. The fissures aperture is too fine to transport water.

The rocks of the *Wang formation* are marlstones with higher carbonate content, their clasts are usually harder and more compact; they have a grey to dark grey colour. Wang sandstones might be greenish but usually they consist of thin layers so that they have only a minor contribution to clasts in the sediments. The Wang layers can be a good aquifer due to fissures, as Oberhauser *et al.* (1991) reports.

The *subglacial till* seldom crops out on the Heumös slope. It is relatively finely grained as a large portion of the matrix is derived from weathered limestones and marlstones. Rounded clasts of various materials and sources can also be found; observed sizes are up to half a meter. Single, larger clasts are more distinct on the surface. These clasts are not only derived from the adjacent marlstones and limestones but are also sandstones, quartz pebbles and even some magmatic or metamorphic clasts. The finely grained subglacial till matrix is hard to distinguish from the post-glacial sediments. The stability is fairly good as long as the subglacial till is not saturated with water, then it can develop into a very unstable mass as was observed by Smit Sibinga-Lokker (1965). The *glacial endlake sediments* and *riverbed sediments* (Figure 3-11c) are sandy to silty but with loose bearing and so quite mobile as the rotational slides show this at the toe of the hillslope.

The composition of the *post-glacial sediments* is best described as composite material with two end members: One end member is an almost matrix-free material of coarse rock fragments from hazelnut grain upwards to meter-sized blocks. This end member is e.g. found at the base of some scarps of the Amden marlstones and will be named *coarse scree* (Figure 3-11d). The other end member is a silty clay without any larger grain sizes and with varying carbonate content (Figure 3-11e). A most dominant post-glacial sediment type is likely a material full of marly rock fragments in a clayey to silty matrix, in other words a *loamy scree*. The deep gullies of the creeks are best to identify the coarse debris material: runoff events wash out the fine matrix and coarse grains are left behind.

Mineral composition

Clay mineral content is a good indicator of the state of weathered material. It is assumed that the sedimentation environment leads to a material with a more or less similar mineral composition. Different exposure of the material towards oxygen, water and vegetation over time might influence the weathering state and so the mineral composition of the debris material. Some major processes which also influence Heumös slope material are carbonate solution and leaching, the border expansion of illites and the change of non-swelling clays to smectites.

Schneider (1999) examined rock and soil samples up to a depth of 2 m for their mineralogical content with x-ray diffractometry, a standard technique in mineralogy. Each three samples of Amden marlstones, subglacial till, endlake sediments and debris loam from the mid slope and eastern slope were examined on a semi-quantitative mineral content: Feldspar is rare in all samples (< 3 %); the content of quartz is more or less equal for both source rock and weathered material (28-35 %). Major changes are therefore found in the carbonate and clay mineral fractions. The carbonate content is reduced in the weathered soil samples: 5 % and 30 % against ~40 % in less weathered samples. The clay content shows a shift from

illite and kaolinite towards swelling clay minerals like smectites. The content of smectite in the Amden marlstone sample is about 10 %, the two debris loam samples show contents of 15 % and 50 % (Appendix B-2).

a)

b)

c)

d)

e)

Figure 3-11: Photographs of encountered rocks and sediments on the Heumös slope: a) and b) Amden marlstones in altered and strongly altered condition; c) subglacial till, lake or river sediments near the Ebnit Ache, d) coarse scree, e) loamy scree, here as a stagnic gleysol.

In addition, qualitative x-ray diffractometer samples (Schneider, 1999) in the borehole log showed that material is weathered increasingly from bottom to top. Illite peaks broaden due to border expansion towards the surface; smectite peaks enlarge and indicate more pronounced weathering. Increasing kaolinite peaks indicate a general increase of clay minerals in the sediment matrix towards the surface. Clay minerals feature higher plasticity when they are able to shrink and swell due to incorporation of water into interlayers. This is essential for the development of failure zones in clayey slopes (van den Ham, 2006).

The carbonate content was measured in the strata of the KB 3 borehole. The material seems to be depleted of carbonate with approximately 30 % carbonate content at the top. Deeper samples then rise to 42-47 % of carbonate content, before they drop at the transition from the post-glacial sediments to the subglacial till. The coarse scree layer there has 36 % of carbonate content. This might indicate stronger weathering in this layer. The subglacial till then shows high carbonate contents of more than 50 % (Appendix B-1).

3.4   Movement characteristics

Movement characteristics were recorded in the borehole with a measurement in the soil column at borehole KB 3 and with the help of the Global Positioning System (GPS) on the soil surface. Measurements were not recorded as time continuous data but by events conducted during measuring

campaigns. Data and results are derived from research partners (Depenthal & Schmitt, 2003; Howind & Schmitt, 1999; Schneider, 1999; Schwenk, 1999). For convenience of the reader, the measurement methods are described in more detail in chapter 4.

3.4.1   Subsurface movement

The inclinometer measurements at borehole KB 3 indicate a weak but clear deformation zone in 7.5 m to 8.5 m depth which is equivalent to a coarse scree layer at the post-glacial sediment - subglacial till transition (Figure 3-9). The observed movement rate has been 12 mm in the A-direction and about 7 mm in the B-direction in 1.5 years (Schneider, 1999). As the inclinometer pipe was not properly anchored in the bedrock the movement in the coarse scree material needs to be seen relative compared to an assumed movement in the whole sediment body. The movement at the shear zone might be larger, too, compared to the stable bedrock layers. A backward sloping is observed below the deformation zone in 7.5 m to 8.5 m depth and a forward sloping is observed above (Figure 3-9). It is not possible to determine whether this is due to soil creep or whether it is a measurement artefact in a non-anchored casing. The upper, downward sloping is probably more realistic, as GPS measurements of KB 3 suggest a lateral downslope translation of the surface of about 2 cm in two years (Appendix C-1).

Further understanding of possible shear zones can be gained with results from the boreholes KB 1 and KB 2 (Schneider, 1999), located in Ebnit (Figure 3-3). The geologic strata is more distinct due to defined sediment thickness and anchoring in the bedrock of the inclinometer casing. The surrounding carbonaceous rocks deliver more resistant clasts than the marlstones do at the Heumös slope.

Borehole KB 1 in the centre of the village shows 7.0 m of post-glacial scree below the surface. It is dominated by marlstone clasts. Below this, subglacial till follows from 7.0 to 12.0 m. This material is coarser and with harder clasts than the appropriate material in KB 3, according to Schneider (1999). From 12.0 to 17.5 m Amden marlstone follows. A distinct shear zone was detected at the subglacial till – Amden marlstones transition.

Borehole KB 2 is located at the bottom of Ebnit. There are about 5.5 m of post-glacial scree and loamy scree, before subglacial till is encountered. A subglacial till – Amden marlstone transition then follows at 13.9 m depth. A shear zone lies at the post-glacial sediment – subglacial till transition (Schneider, 1999).

3.4.2   Surface movement

Surface movement was measured with geodetic equipment (Depenthal & Schmitt, 2003; Howind & Schmitt, 1999). The original eleven object points are chosen in a manner that they represent all tree-free parts of the Heumös slope from west to east in the main moving direction. They were observed for a total of 75 months. After an irregular spacing of measurements, a 3 to 6 months-spacing was used between 1999 and 2001. Measurement epochs are conducted in May, August and November. The traverse points are only linked to the lowest object point (GPS 1) near the holiday village, which increases the uncertainty of the traverse point measurements. The additional object points (GPS 50-62) enhance the movement characteristic of the initial object points GPS 1-11. Identified movement direction for all points is generally downslope, which means towards the east. A prevailing direction does not exist, it is rather a range of directions. Vertical movement was more irregular and often below detection limits (Depenthal & Schmitt, 2003; Howind & Schmitt, 1999), an artefact of the measuring system as GPS is less accurate in height measurements.
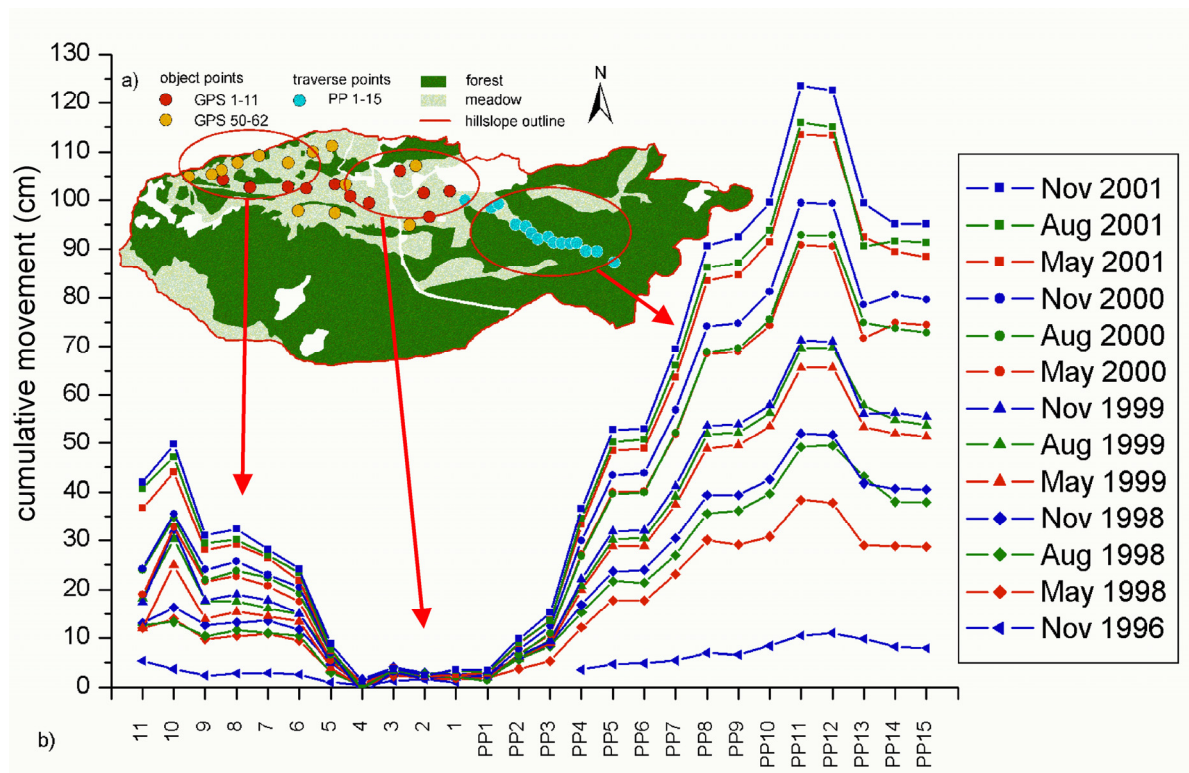
Figure 3-12: a) Map of GPS points with zones of similar movement behaviour on the Heumös slope. b) Absolute deformation distance of GPS and terrestrial points for each epoch, after Depenthal and Schmitt (2003).

In figure 3-12 the planar motion is presented, three movement categories can be identified from west to east:

1) Average displacements per year of 5.5 to 11 cm are found in the steep upper part of the hillslope body, these are the object points GPS 6-11.

2) Object points GPS 1-5 are located west of the holiday village in a plain area, they do not show significant movement with average displacement per year of 1.5 cm, movement of point 5 is interjacent to the faster points upslope.

3) The lowest group, the traverse points (PP) measured with terrestrial survey, have increasing movement rates towards the east, some points with more than 10 cm/a. Traverse points PP 8-12 have an average displacement of up to 23 cm per year. The movement vectors show an interesting behaviour in relation to the observation periods (Figure 3-13): From May to July there is a movement in the southern direction, from August to November there is a movement in a northeasterly direction and in winter (December to April) the movement direction is southeast. There is an exception for the last measurement period where the directions are switched. No definite reason for this seasonality could be found so far (Depenthal & Schmitt, 2003). Possible explanations could be the influence of the erosion from either creek 1 in the south or Ebnit Ache in the east. Solifluction or seeping water could also be a possible reason. It is probable that several processes lead to the movement with the most dominant determining the direction during a specific period.

The movement behaviour of the additional object points (GPS 50-62) presents additional information: object points GPS 52-59 are located near the rim of the northern slope. High inclination of slopes and low

sediment thickness characterise the rim. This is reflected in the low movement rates of these points. Object points GPS 51, 60, 61 are interjacent to group 1 and 2. Object points GPS 50 and GPS 62 are related to group 2 with low displacements.
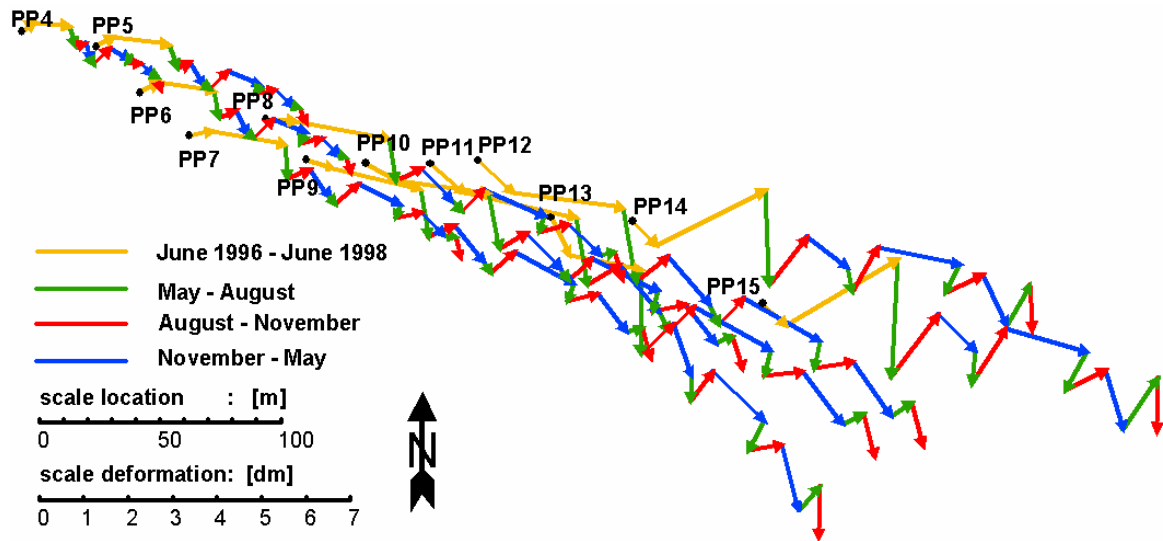
Figure 3-13: The movement vectors of selected terrestrial points which show a measurement period – dependent direction. Note that the last measurement in November is directed in the May-August direction, data and drawing altered after Depenthal and Schmitt (2003).

4 Data and methods

Physically-based modelling requires good and exhaustive data sets. Field studies and measurement of hydrometeorological parameters are supposed to deliver those. Often, not enough importance is devoted to data gathering, data quality and its presentation to associated partners. For this study and the co-projects of the new DFG-research group the old existing data has been proofed, reworked and given a new order. Most of these data sets are now available in the information system of the DFG-research group (Molkenthin *et al.*, 2006). Specifications of the measurement devices and data can be found in the appendix E and the research projects website (http://www.grosshang.de).

Landslides likely occur in mountainous areas which present extreme environments in a certain sense. Heterogeneity and spatial variability is often stronger than it might occur in lowlands in similar scales. This requires a more intense analysis of applied methods in a field research including their constraints. The most dominant restriction found during the research was the debris transport and the related change of the rating curve due to accumulation of debris in the weirs so that closed water balances were difficult to establish. Similar observations explain that a lot of landslide studies do not try to close the water balance. Stronger geomorphological forces such as weathering, debris accumulation and denudation also lead to enhanced heterogeneity in spatial patterns. This chapter will summarise data sources, availability and quality as well as methods applied in the field, laboratory and at the desktop. To enhance the idea of spatial and temporal scales, methods and data are comprised in chapter 4.1 dealing with spatial information. Chapter 4.2 then deals with data and processes, which were captured by time series measurement.

4.1 Spatial information

Spatial information can be derived e.g. from printed maps, digital maps, through space or airborne observation techniques but also through field work like point sampling, mapping and laboratory examinations. The following list provides the spatial data sources used in this thesis from large to small scales:

- Airborne data and digitised maps: aerial photographs and airborne laser scan digital elevation models (ALS DEM); digitised features from official, printed maps, e.g. topolines.

- Mapping of geology, soils and vegetation patterns in the field and with the help of maps and airborne data. Mapping is conducted on the catchment scale.

- Geophysical methods: to derive subsurface information in profiles on a hillslope scale.

- Point sampling on the plot scale: borehole drilling, dynamic push methods with hollow core sampling, infiltration and hydraulic conductivity measurements in the field, soil cores and profile determination, dye tracer experiments, sample taking for laboratory analysis.

- Laboratory investigations on the micro scale: grain size distribution, soil parameters and hydraulic conductivity, mineral composition and consistency limits.

4.1.1   Digital data

Digital elevation data and aerial photographs

Digital elevation data is available from three sources: 1) as digital 20 m topolines in CAD exchange format (Computer Aided Design) for the whole Dornbirn catchment area; 2) as a digitised ArcInfo coverage from Schwenk (1999) which was refined through a GPS measurement campaign including 600 points (Pret, 2001). GPS measurements can only be taken in tree free areas. Most of the creeks are in forest patches. This is why deep gullies were not incorporated into the DEM from Pret (2001). A digital elevation model (DEM) in raster format was derived through combining both data sources and was improved by the implementation of depth contours. This DEM is mainly used for the model studies of this thesis. 3) Recently, Vorarlberg was overflown with airborne laser scan altimetry equipment. A new digital elevation model (ALS DEM) was derived from this raw data with 1 m resolution in planar direction and 10 cm averaged resolution in height (Figure 3-4). The Wildbach- und Lawinenverbauung kindly ceded this excellent digital data of the upper Dornbirn Ache catchment for this thesis.

Digital aerial photographs are available for the 1992 flying date as well as digitised paper prints of data for the 2001 flying date.

Digital topographic data

Most of the digital topographic data is from raw data sources of Schwenk (1999). He digitised hydrological and geotechnical features, a geological map, landuse as well as buildings, streets and other features, implemented into a Geographic Information System (GIS). Some of this data was advanced with own observations. Schneider (1999) and Schwenk (1999) provided the digital base for the geological map in this thesis. Own spatial information like the ecological wetness index map or point measurement locations are also in digital format.

Data quality

Digital maps were compiled with ArcInfo, ArcView, ArcGis, AML and AutoCad software. The digital elevation data from the old sources is too coarse to represent the fine scale topography on the moving hillslopes. The airborne laser scan data is excellent of the Heumös slope therefore but soil creep, small slides and human activity constantly change the surface. Therefore, a field documentation of the human activities has been conducted but needs further attention. Human impact changes the hydrological system with the most severe impact. These are e.g. soil exchange, subsurface drainage implementation and remodelling of the ski run.

A drawback in quality of GIS data is the fact that some data was probably projected in the Austrian reference system (Bundesamt für Eich- und Vermessungswesen, Austria) while for other data a reference system of the Landesvermessungsamt Baden-Württemberg (Germany) was taken. Meta information for digital data is sparse for all sources. Discrepancies which occurred during projection of both data sets into one reference system could not be eliminated due to this.

4.1.2   Data from mapping

Geological and geotechnical maps

Schwenk (1999) mapped the Heumös slope and the southern Ebnit Ache valley in great detail both geologically and geotechnically. Publications from Oberhauser (1998), Oberhauser *et al.* (1991) and

Schneider (1999) are also used for geological interpretations (Chapter 3). The new map, to be published in 2007 from the Austrian Geological Survey (Geologische Bundesanstalt, Austria) gives a differing view on local geology. This new interpretation needs to be proofed thoroughly yet. The detailed geological maps can still be refined in detail as own observations indicate. This is especially important for a better understanding of the sediment – bedrock transition as discussed in chapter 7.1.

Soil mapping, vegetation distribution mapping and ecological wetness index

A strategy to identify hydrological processes on a moving hillslope is needed to better understand the possible triggers of movement as well as to further close the water balance. Mountainous environments bring additional uncertainty for hydrological measurements like discharge or precipitation so that it is necessary to gather more information to understand average long-term hydrological behaviour of the subsurface and to define dominating hydrological processes. Vegetation distribution is a helpful indicator for average soil moisture conditions. In addition, detailed soil description helps to understand flow patterns.

Ellenberg (1992; 1996) uses characteristical needs of plant species and categorises these properties. For example, the preferred water conditions of a soil, nutrients availability or soil acidity define what kind of plant species dominantly prosper in a certain area. Or the other way round, specific conditions of the water balance of a soil, nutrient availability or simply the grain size distribution define the border conditions for plants prospering on a certain soil patch. Not to forget human impact and time as an influencing factor. Species which have a narrow range of variable properties can be used as habitat indicator species. Several indicator species on a soil patch can be used for a spatial interpretation of the living conditions. After Ellenberg (1992) these indicator species are a short description of the ecological behaviour of a vegetation association. This helps to carefully draw conclusions towards the environmental factors, which define the competition of plants and a spatial distribution of specific factors can be derived. The ecological moisture index is derived through averaging the moisture index of all indicator plants found of a vegetation association at a specific site. It is a useful tool to estimate soil moisture conditions on a seasonal scale to a multiple year scale. A translation for German moisture types expressions and vegetation types of some typical patches are listed in Appendix D-1 and D-2. The term *ecological moisture* describes moisture on an ordinal scale and is derived from plant properties. On the other hand *soil moisture* describes both qualitative information, e.g. when used in defining the moisture of a soil (AG Boden, 1996), or quantitatively when water content is measured by laboratory methods or with in situ measuring devices as time domain reflectometry.

On the Heumös slope, several complete vegetation associations were identified in the field after a method of Wilmanns (1993). The purpose was to find leading indicator species but anthropogenic influence and the similar soil types encountered during soil description complicated this specific approach (Dittfurth, 2002). Limits using complete vegetation association were for example the use of the forest free areas as pastures for summer grazing of cattle and horses, or for skiing in winter. Another example is the former extensive use of local wood, leading to an unnatural forest stand. This is why the method was altered and a combination of soil core recording and a reduced but yet detailed vegetation association definition was used (Dittfurth, 2002). In forested parts, the dominating tree type is the leading species but for calculation of the ecological moisture index, the tree species have been neglected. The steep forested parts are not easily accessible which means that a more general mapping of these areas was conducted. These patches are mapped with a larger extent and aerial photographs were included into the mapping procedure. Alders and fir trees are easily distinguishable there. On pastures and meadows, dominant grass species were used

for indication. For example, all dominant species with more than 5 % coverage in an area were specified. Soil identification was combined with the vegetation analysis around the soil core location (Dittfurth, 2002). The extent of the occurrence of similar plant types around the soil core location defines the patch size of a similar ecological wetness indicator, which is derived by the average of the single index of all major plant types. The ecological moisture index is categorized for display in the maps. In a second step, the patches were combined with information about topography, slope angle, geological structures and material to derive hydrotopes, which help understanding activity of specific units on the Heumös slope.

4.1.3   Geoelectrical and electromagnetical depth investigations

Investigations with geoelectrical devices were conducted in July 2001 (Hannich, 2001) for additional vertical information to define the bedrock – sediment transition. A geoelectrical depth measurement was conducted at borehole KB 3 to correlate the apparent geoelectrical resistivity to geologic units. With varying distances of the electrodes, which are arranged in a profile away from the borehole, it is possible to link the apparent geoelectrical resistivity of these measurements with the geologic strata as found in the borehole. The depth measurement was conducted with a SYSCAL R2 from IRIS Instruments (France); the calculations were conducted with a programme from Zohdy (1989). A Schlumberger arrangement was used (Reynolds, 2005). The maximum distance was 250 m in the profile which corresponds to a maximum depth of around 42 m.

Electromagnetical measurements were taken in four profiles to get information on the electrical conductivity in the subsurface. Three parallel profiles in north to south direction (GEP 1-3) are located west of the holiday village, across the borehole and at the height of spring 1 (Figure 4-1). A west to east profile (GEP 4) cuts the other profiles perpendicular. The conductivity of the subsurface material depends on the mass of minerals which feature electrical conductivity. For example, quartz is not conductive whereas clay minerals are highly conductive. The specific conductivity of a geologic strata also depends on the electrical conductivity of the porewater.
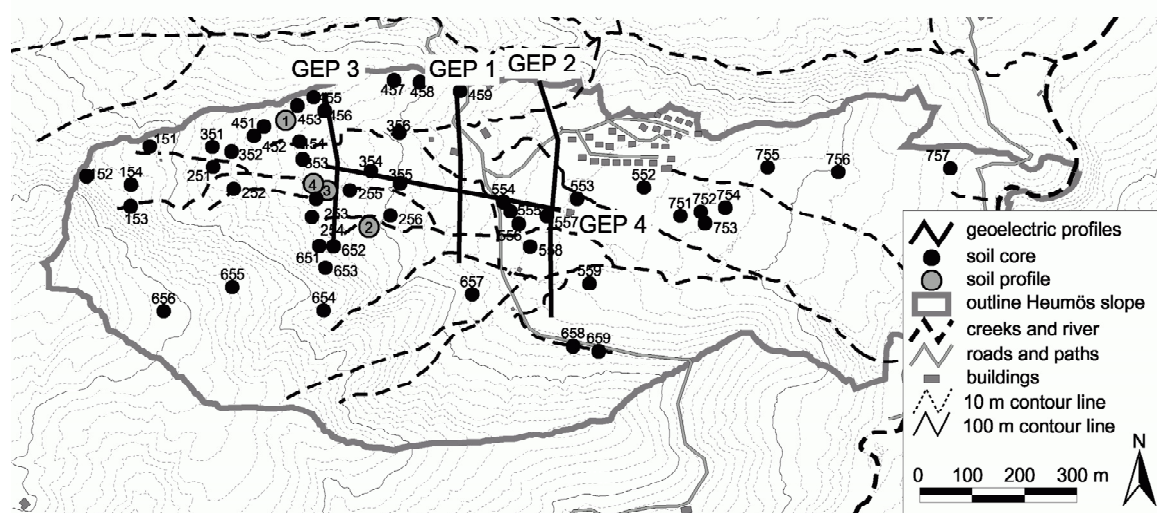
Figure 4-1: The distribution of soil cores, soil profiles and electromagnetical profiles (GEP) from the field campaigns in 2001.

The electromagnetical measurements are conducted inductively with a magnetic dipole field. Induced electrical currents lead to a secondary magnetic field which is measured with an overlaying first field. The proportion of the two fields can be related to the electrical conductivity of the subsurface material. The

geoelectrical depth measurements are used to relate the geologic strata with the electrical resistivity. Measurements were conducted with an EM34-3 from GEONICS Ltd. (Canada). With different arrangements of the electromagnetical coils (horizontal and vertical coplane) in different distances (10 m, 20 m and 40 m) and different frequencies (6400 Hz, 1600 Hz or 400 Hz) measurements in six different depths were taken. The measured profile is located in between the two coils.

4.1.4   Point sampling

Boreholes

In December 1996, three boreholes were drilled (Schneider, 1999), two at the village of Ebnit (KB 1 and 2) and one at the Heumös slope (KB 3). For the location of the boreholes please refer to figure 3-3. The depth of the boreholes is between 18 and 24 m, KB 1 and 2 could be drilled well into the bedrock, whereas KB 3 could not reach the bedrock due to technical reasons. In May 2001 two additional boreholes were drilled down to 20.5 m in preparation for a sewage treatment plant east of Ebnit and were equipped as groundwater and inclinometer gauge. The German grain size and consistency classification (DIN 4022-1, 1987) was used to describe the borehole logs. It has been translated into English with the help of the British code of practice for site investigation (BS 5930, 1999), see Table 4-1.

Table 4-1: Translation of consistency values for borehole KB 3 and dynamic push log description.

Classification altered after BS 5930 (1999)	Classification after DIN 4022-1
very soft	breiig
soft	weich
firm	steif
stiff	halbfest
hard	fest

Sediment cores derived with percussion probing and hollow core sampling

An enforced hollow steel pile, which is sharpened at its open end, is rammed into the ground with a pneumatic hammer (percussion probing). This method is a standard method in applied geological investigation and often used in combination with dynamic probing (Rammsondierung). For its German expression "Rammkernsondierung" (RKS), several English synonyms were found for the method itself, the sampling devices and the machines which are used to drive the hollow steel pile into the subsurface. The machines are either direct push rigs or pneumatic hammers, also called percussion hammers. The sampling device (the hollow steel pile) is either called a hollow core sampler, a window sampler or a percussion gouge. The method could be described as dynamic probing or percussion probing. In this work, the words "hollow core sampler" and "percussion probing" are used. To have a clear distinction between boreholes made by a rotation drilling rig and the boreholes of the percussion probing, the latter ones are just called holes, soil profiles taken with small diameter hollow core samplers (Puerckhauer) are called soil cores.

The hollow core sampler are 1 or 2 m long and opened on a fifth of its side so that the soil material can be examined and removed. Massive steel piles are used as extension to drive the hollow core sampler further into the sediment with the pneumatic hammer. The used hollow core sampler has an inner diameter of 60 mm and was driven between 1.5 m and 5.0 m into depth.

In June 2006, 11 holes (RKS 1 – RKS 11) were driven into the upper horizons to determine geological material and consistency values in a north to south profile at the height of spring 1 (Figure 4-2). Some

disturbed samples were taken for water content measurement in the laboratory (Appendix D-4), though a systematic sampling could not be conducted as water in the boreholes often disturbed original water content. Percussion probing with direct push rigs or pneumatic hammers is a fairly easy and cheap method to gather subsurface information. A drawback is that, while hammering, the pore water is pressed out of the sample so that porosity and water content might be altered. Strata thickness might change through compression of the sample. It is also a fact that hollow core sampling limits the view into the subsurface through the small diameter of the casing. Penetration into the subsurface was mostly stopped because the pneumatic hammer could not penetrate the marly rock clasts in the underground. At some points the marlstones were penetrated and were then recovered as dry gravel. The small hollow core sampler diameter additionally hinders a clear distinction of bedrock and gravel.

Average soil hydraulic conductivity by slug test method

Four of the hollow core sampler holes were build into temporary groundwater wells (Figure 4-2, Appendix D-7), a 2-3 m long, 50 mm diameter HDPE-pipe was installed in the hole. The lower pipe has a 0.9 m filter leg. Fine gravel (5-8 mm) was arranged in the slot between pipe and hole. Above the filtered pipe, swelling Bentonite clay was used to seal the hole. Ten litres of water were poured into the pipe at once. A pressure data device logged the recession of the water table height, while the water seeped into the ground. This data as well as the borehole parameters (diameter, depth, filter length) were used to calculate an average hydraulic conductivity (K_{sat}) for the material. The data was used to calculate saturated conductivity after a method for pipes in unconfined and unsaturated soils suggested by Knoedel *et al.* (1998) as well as DIN 18130-2 (2003). Both methods yielded results which did not differ more than half an order of magnitude for each sample. Slug tests are an easy and cheap method to obtain hydraulic conductivity of the subsurface. The method of hole drilling, the diameter of the hole and the build up of the well, as well as pore size differences between filled gravel and the surrounding soil can make this a quite rough method (Bouwer, 1989; Butler, 1998). Nevertheless, the results give a useful estimation on the order of magnitude of hydraulic conductivity.
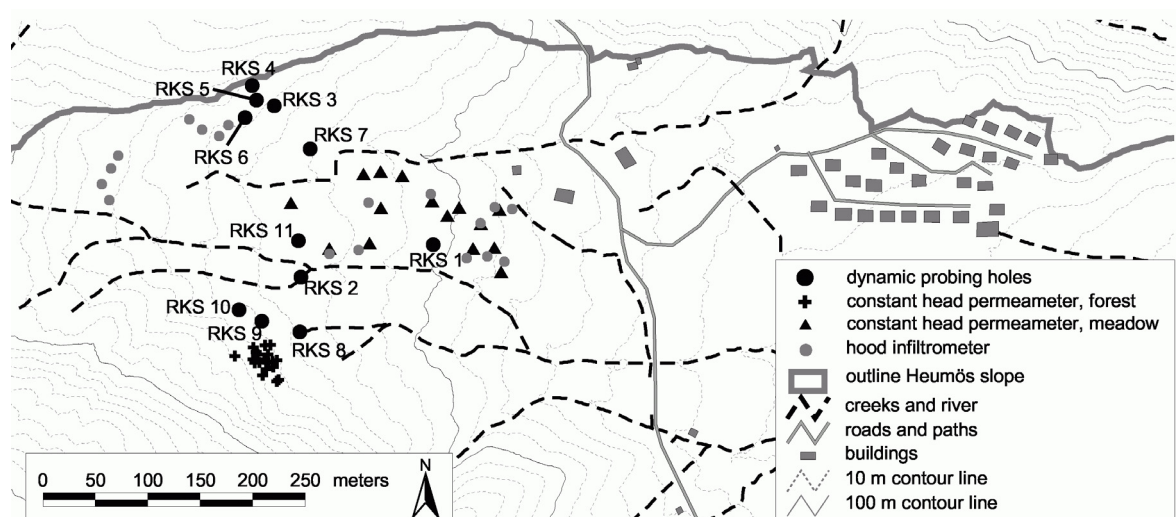
Figure 4-2: Distribution of percussion probing locations, approximate location of constant head hydraulic permeameter tests and hood infiltrometer tests from the field campaigns in 2006.

Soil profiles and soil cores derived by the Purckhauer method

Forty-nine soil core samples were taken with the Purckhauer method up to depths of 1 or 2 m and four soil profiles were digged (Figure 4-1), each combined with an analysis of the surrounding vegetation type to derive patches with similar ecological moisture properties. The soil description was done after the soil mapping manual of AG Boden (1996) and DIN 4220 (1998), specifying several soil properties as soil colour after the Munsell Soil Colour Chart (2000), soil type, soil density, carbonate content, skeleton content, humus content, root content and soil moisture.

The soil matrix grain size is almost similar in all soil profiles, as the parent material is derived from weathered marlstones and limestones on the whole entity. This is why a clear distinction of soil horizons was often difficult. The Geologisches Landesamt Baden-Württemberg (1995) suggests to include the colour, marbling and texture of a soil to define soil horizons. These properties are indications for oxidising or reducing conditions.

Constant head permeameter measurements

In a field course and during fieldwork in June and August 2006, 68 measurements with a compact constant head permeameter device after Amoozegar (1989) and Ksat Inc. (USA) were conducted (Appendix D-7). A hole with the radius r is augered into the soil to the desired depth, a cylindrical filter is put into the hole and water is poured with a constant head H, such that $H/r \geq 5$ until a steady state flow rate is attained. At this point the saturated hydraulic conductivity (K_{sat}) can be calculated via the Glover solution (Amoozegar, 1989), which considers only the saturated flow component from the auger hole.

Based on the hydrotope definition (Chapter 5.3) it was decided to closely sample two areas: the meadow at the height of spring 1 to represent wet ecological wetness indices and the forest of the spring 1 catchment, to represent dry ecological wetness indices. Standard depths of 12, 20 and 50 cm were tested, though in 50 cm depth only a few measurements were made due to very low hydraulic conductivities.

Infiltrability measurements

On plane parts of the meadow (wet ecological wetness indices), 19 hood infiltrometer measurements were conducted (Appendix D-7). The hood infiltrometer device (UGT, Germany) is designed to allow infiltration on the undisturbed soil surface with zero tension (Zimmermann *et al.*, 2006), saturated hydraulic conductivities are measured. This instrument involves a circular source of standing water whose positive pressure potential can be overcome by applying a corresponding vacuum with a Mariotte device underneath a small plexiglas dome (the ''hood''). This dome is put in good contact with the soil surface over the source of water so that infiltration is achieved at zero tension. Since there is no need of any contact material, measurements with the hood infiltrometer reflect particular properties of the soil surface as compaction or silting. While the hydraulic head in the water column underneath the hood may be adjusted to values between zero and the air entry value, flow at zero tension to measure infiltrability was preferred, which can be calculated directly from steady-state flow according to Wooding (1968).

Dye tracer experiments

In August 2006 a further detailed investigation was conducted with a tracer experiment. The fairly mobile dye tracer Vitasyn Blue AE 85 (BB) was used on a one square meter large plot that was selected in the forest besides the catchment boundaries of spring 1, where slope angles of 30-40 degrees prevail. The retardation factor for brilliant blue relative to a conservative tracer such as Bromid ranges from 1.1 (Flury & Flühler, 1995) up to 20 (Allaire-Leung *et al.*, 1999). The use of BB for the identification of the

susceptibility of loamy, sandy and loess soils for preferential flow was proved by Flury *et al.* (1994) and Zehe (2001a).

On the Heumös slope the heavy clay soils with shrink-swell behaviour, including shrinkage cracks and a steep environment, made it necessary to use a simplified test method (Zehe & Flühler, 2001a). Twenty litres of water were stained with brilliant blue to get a solution with approximately 4 g/l of dye. This solution was carefully applied with a standard watering can to the plot. The steepness of the slope (approx. 40 degrees) lead to the leaking of a small amount of surface runoff through the sealed frame but most of the applied dye infiltrated. The plot was left overnight and was then excavated in 5-10 cm steps to document macroporosity. Vertical profiles are usually excavated to document infiltration. Shrinkage cracks have a more horizontal distribution and connectivity so that a planar view parallel to the soil surface was used instead. The profile was dug 50 cm deep before bedrock was reached.

4.1.5   Laboratory investigations

Grain size distribution

Grain size distribution was determined for all horizons of the four soil profiles on each two samples. One sample was sieved after DIN ISO 11277 (2002), the second was treated with sodium pyrophosphate after DIN ISO 11277 (2002) and then the fine grain size content was determined.

Soil density, porosity and water content

Soil density was determined with at 32 undisturbed soil cores (100 cm³) after DIN 18125-1 (1997). Porosity values were calculated for these undisturbed samples as well as for several other samples, taken in 2006 (Appendix D). Gravimetric water content was determined on undisturbed soil cores and disturbed samples, e.g. derived from window sampling after DIN 18121-1 (1998).

Soil hydraulic conductivity

The 32 undisturbed soil cores were also used for measuring the soil hydraulic conductivity with an ICW laboratory permeameter from Eijkelkamp Agrisearch Equipment (The Netherlands). Saturated undisturbed samples in steel sample cylinders are exposed to a gradient of water level. Water that seeps through the sample is caught in a burette where the amount of water in a certain time can be determined (Appendix D-7). The AG Boden (1996) and DIN 10381-4 (2004) suggest 5 or 7 undisturbed samples for laboratory hydraulic conductivity measurement. Eijkelkamp Agrisearch Equipment suggests for 20 to 30 samples in case of clay soils to account for heterogeneity. Soil heterogeneity is enhanced in clay soils due to expansion and contraction of the material. This high amount of samples could not be achieved at one single soil profile, so that it was decided to take a maximum of 4 samples at each location and use results in combination with soil type classification to enlarge the number of samples in each group.

Liquid-, plastic- and shrinkage-limit

Five soil samples were taken to determine the liquid-, plastic- and shrinkage limits with the Atterberg method after DIN 18122-1 (1997), DIN 18122-2 (2000) and DIN 18124 (1997) to show the principal influence of shrinkage on hydraulic properties. A clay paste at the liquid limit was used for the determination of the shrinkage limit. The ring form determines the volume of the wet sample; the volume of the sample at the shrinkage limit is determined by the radius and height measurement.

Soil shrinkage characteristic curve

The soil shrinkage characteristic curve (SSCC) describes the volume change of soils in relation to the specific water content (Braudeau *et al.*, 1999; McGarry & Malafant K.W.J., 1987). Four zones of volume change are usually distinguished: *zero*, *residual*, *normal* and *structural* shrinkage (Braudeau *et al.*, 1999). The *normal* shrinkage zone is usually the most important for the volume change in soils (Peng & Horn, 2005); volume loss is proportional to water loss. A deformation of pores occurs instead of a penetration or displacement of air in the pores (Bronswijk, 1988; Chertkov, 2000).

The SSCC was calculated after a model from Chertkov (2000; 2003a), the model is based on the principal shape of clay particles and the respective pore volume which results out of the shape of the clay particles. With the assumption that the volume of all pores changes proportionally during swelling or shrinking procedure to the total volume of the clay matrix, the microparameters describing the pore volume can be scaled to macroparameters, which are derived through the Atterberg limits and volume definition (Appendix 2.A). Clays belong to deformable soils which stands in relation to the water content. The liquid limit describes the maximum water content, additionally it should be noted that "the liquid limit is empirically understood to be the water content at which the shear strength approaches that of a liquid" (Fam & Dusseault, 1999). The shrinkage limit describes the soil volume state when no water is left in the minimum possible pores. The air entry point is the moisture content from which on all pores are filled with water, for clay soils this is not the maximum water content as pores do increase the volume as they take up water to the liquid limit. Chertkov (2003a) considers this to be a linear progression. A model which describes the volume change behaviour, the soil shrinkage characteristic curve respectively, can be described (Chertkov, 2000; Chertkov, 2003a).
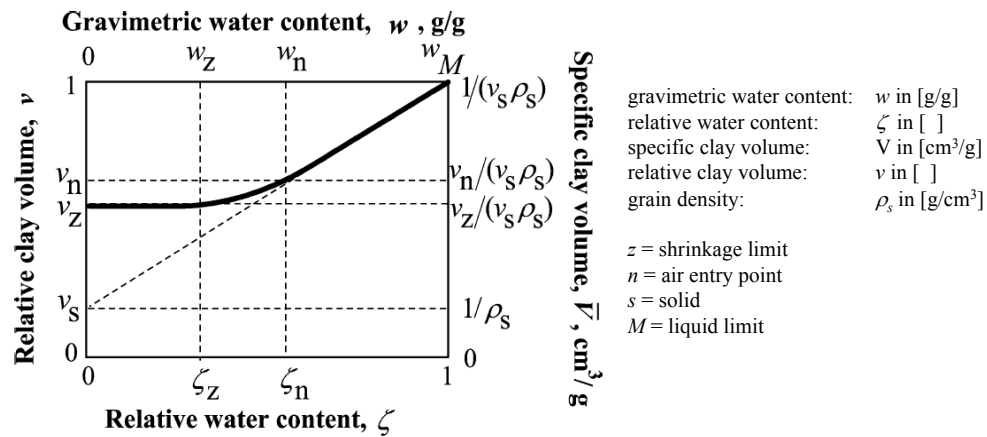
Figure 4-3: Soil shrinkage characteristic curve after Chertkov (2000). The fourth, structural shrinkage relation is not included, as it is not found in clay pastes but in undisturbed soil samples.

A dimensionless relative water content ζ of the clay paste is defined as a ratio of gravimetric water content to its maximum (at the liquid limit) as

$$\zeta \equiv w / w_M; \ 0 \leq \zeta \leq 1 \tag{1}$$

A dimensionless relative volume of the clay (v) is defined as

$$v \equiv V / V_M; \ v_z \leq v \leq 1 \tag{2}$$

These values can be converted to the gravimetric water content (w) and the specific clay volume (V) with following equations:

$$w = w_M \cdot \zeta; \qquad \overline{V} = \frac{v}{v_s \cdot \rho_s} \tag{3,4}$$

In the following, the gravimetric water content (w) and the specific clay volume (V) are used to describe the shrinkage characteristic curve as it might be more convenient for the reader. The pore volume remains constant from zero water content to the water content at the shrinkage limit. The gravimetric water content volume relation is

$$\overline{V} = V_z; \ \ 0 \leq w \leq w_z \tag{5}$$

with $\overline{V}$ being the specific clay volume in [cm/g]; V_z the specific clay volume at the shrinkage limit, w the gravimetric water content in [weight-%] and w_z the water content at the shrinkage limit.

From the relative water content w_z to the air entry point w_n the relation is

$$\overline{V} = V_z + \overline{a} \cdot (w - w_z)^2; \ \ w_z \leq w \leq w_n \tag{6}$$

with $\overline{a}$ being a constant derived out of microparameters, see also appendix A.

From the air entry point w_n to the maximum water content w_M the relation is

$$\overline{V} = \frac{1}{\rho_s} + \frac{w}{\rho_w}; \ \ w_n \leq w \leq w_M \tag{7}$$

with ρ_s and ρ_w being the density of the solid material and the density of water respectively. These equations can be used to calculate the soil shrinkage characteristic curve (SSCC) after Chertkov (2003a). Though it is relevant for clay pastes and not the whole soil, it is a good and fairly easy way to get an approximation of the swelling behaviour and extent which is useful e.g. to understand the volume change of soils and preferential flow in shrinkage cracks of clay-rich soils.

4.2   Time-dependent information

Time dependent information are basically precipitation, runoff and meteorological variables. Automation of measuring these variables with a high time resolution is possible, when the financial budget is in accordance with the failure frequency of the devices. To gain exhaustive data sets of the movement requires a substantial investment, especially for the automation of measurements. The time resolution of movement measurement might be lower than necessary if measurement are not automated.

The characterisation of hydrological processes is the primary object which is based on time series investigation for understanding the movement behaviour of the Heumös slope. Additionally, for physically-based hydrological modelling it is essential to have sufficient high resolution time series data of precipitation, evapotranspiration, runoff and groundwater storage recharge.

4.2.1 Hydrometeorological data

Precipitation measurements

The government of Vorarlberg runs six precipitation stations adjacent to or in the catchment area of the Dornbirn watershed. The official stations are around the Dornbirn Ache valley: these are the Dornbirn, Gütle, Bödele, Meschach and Hohenems stations of the Hydrographischer Dienst Vorarlberg (Austria) and the Hochälpele station of the Vorarlberger Kraftwerke AG (Austria). One of these is the Ebnit precipitation station which is being run since 1894 at an altitude of 1080 m near the church of Ebnit, which is also called 'Ebnit church I' rain gauge. By courtesy of the Hydrographischer Dienst Vorarlberg, monthly paper strips from this rain gauge could be digitised from 01/01/1998 until 25/04/2001. The old device broke on 25/04/2001 and a new digital rain gauge was installed on 15/05/2001. Corrected data from this rain gauge is available from 01/01/1998 until June 2004, only missing August 2000 and the period from 25/04/2001 to 15/05/2001 (Figure 4-4). A part of the same data is also provided by means of the city of Dornbirn devices, it is referred to as 'Ebnit church II' rain gauge because the sampling strategy and interval is different to the Ebnit church I rain gauge. Sometimes this is reflected in diverging observations for single events in the data sets, as the sampling interval is different for both data loggers. It should also be noted that there are differences in the digitised data and the digital recorded data. Very small events are neglected during digitising. Also monthly sums of precipitation are available since 1894 and a storm event selection from 1950 to 1993 (Hydrographischer Dienst Vorarlberg, Austria).

A meteorological station was installed from IMKO GmbH (Germany) at the Heumös slope in the autumn of 1998 (elevation: 1095 m, Figure 3-3). The station records precipitation, wind direction, average wind speed, global radiation, relative air humidity and temperature, six time domain reflectometry devices (TDR-rods) were originally installed, too. The station failed after it had run 2 months, broken and submerged TDR-rods, unstable power supply for the rain gauge and no adequate maintenance has lead to constant failure since then and no data was gathered. In August 2001 the station was overhauled and brought to function again. Since then, the power supply failed several times, e.g. through a broken battery and recharge device in the summer of 2002, in January to February 2004 and in January 2005 through a broken fuse. Mice which bit the cables as well as moisture in some devices also lead to gaps in the data records. Maintenance intervals were chosen to be three months from 2001 on, which was a good compromise between financial restrictions and time restrictions and the danger of too much data loss. The precipitation data at the Heumös slope weather station experienced more data loss than the other devices there, as the rain gauge clogged or froze and could only be cleaned during maintenance, so this data should be used critically and with precaution.

Two additional continuously recording rain gauges ran on the Heumös slope in autumn of 1998 beside the Heumös Alpe and the borehole KB 3 (1075 m, 22.06.1998 – 15.08.1998) and at the most western end of the slope near the uppermost western rock scarp (1240 m, 17.08.1998-15.10.1998, Figure 3-3).
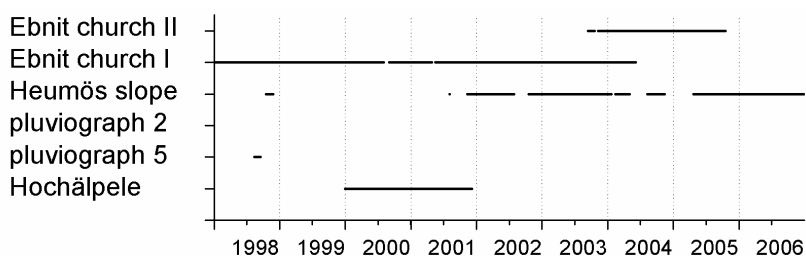
Figure 4-4: An overview of operation periods and available data of precipitation gauges.

Additional meteorological time series

The Heumös weather station has been providing reliable climatological data sets since 2001 (Figure 4-5). Additional climatological and precipitation data from the nearest station in a similar height to the Heumös slope has been provided by the Vorarlberger Kraftwerke from the Hochälpele station for 2000 to 2001, no specifications are known here. The data comprises precipitation, air temperature, wind speed and radiation in a 90° and 60° angle.

In 2003 the city of Dornbirn installed climatological and several runoff devices at four locations in Ebnit and at the Heumös slope. All equipment is connected by radio to a central data logger. The installation and devices are made by Sommer Messtechnik (Austria). Specifications of the devices are found in appendix E. Additional devices from Dornbirn are movement monitoring of the Breitenberg cliff above Dornbirn, the water height and geophone observation at Staufer Lake, a small water power plant in the canyons of Dornbirn Ache, the water height of Dornbirn Ache at the Furt location (Dornbirn) and together with the Hydrographischer Dienst (Austria) a gauge at Dornbirn Enz at the point where the Dornbirn Ache enters the city.
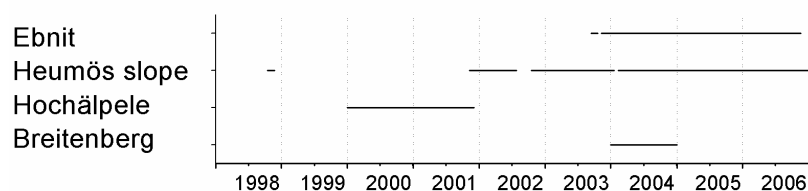
Figure 4-5: An overview of operation periods and available data of the climatological time series.

4.2.2   Discharge, groundwater and soil moisture measurements

Catchments, gauged sub-catchments and discharge data

The outlets of three sub-catchments have been observed since 1998 on the Heumös slope (Figure 3-3). Weirs were installed near the gravel road which crosses the slope in north to south direction. The weirs catch the discharge of creek 1, 2 and 3 (also called Heumös creek) from the upper half of the slope. The weirs are designed as triangular weirs with a 90° angle for smaller runoff events and are topped with a rectangular weir after 0.5 m height in creek 1 and creek 3 (Schwenk, 1999). The Wildbach- und Lawinenverbauung built the weirs out of wooden logs (diameter: 10 cm). The wooden construction is mantled by a metal and sealed with a plastic cover which means that the weir is not a sharp-crested weir. Mechanical paper-strip loggers from Ott Messtechnik GmbH & Co. Kg (Germany) were installed in a vertical concrete pipe which is connected to the weir-body with a plastic pipe. A local volunteer changed the paper strips each week. The water level at the weir was recorded as well. In 2003 creek 1 was equipped with a digital supersonic device of City of Dornbirn (Chapter 4.2.1), in 2006 a second supersonic device was installed in the concrete pipe tunnelling the adjacent road. Creek 3 was equipped with a pressure probe from Aquitronic Umweltmesstechnik GmbH (Germany) in January 2004. At the same time, discharge data recording was stopped in creek 2. The idealised water height-discharge relation and measurements are found in appendix E.

Several factors lead to limited data quality of the time series data: 1) the broad-crested weir leads to a distortion of the discharge. The rating curves needed to be calculated for sharp-crested weirs as discharge measurements could not be made for maximum water heights and interpolation was necessary. 2) The plastic pipe is not necessarily located in sufficient distance from the notch of the weir. From the notch

backwards to the pipe location the water surface is not even so there are discrepancies in the water height recorded on the paper strips and the water height recorded by the volunteer. 3) Additional uncertainty of the runoff data comes from the mechanical data loggers. Time resolution is approximately on a half hour basis for these paper strips though digitising was conducted for 6 min time-steps. The time resolution was improved significantly with the digital devices. 4) Debris transport in the creeks, especially in early summer, leads to gravel deposition in the weirs and a clogging of the plastic pipes. The Wildbach- und Lawinenverbauung and city of Dornbirn authorities try to clean up the weirs each summer but this is usually not be done straight after clogging. Gravel in the weir often lead to an observation of an artificial groundwater body rather than a discharge observation, which resulted in constant changes in the rating curves.

Table 4-2 displays catchment sizes for the observed parts of the catchments as well as the total size of the catchments located on the Heumös slope. Figure 4-6a shows the location of the weirs and the areas assigned to them in a closer look, combined with a display of topography and vegetation. The three gauged sub-catchments are significantly different from each other concerning topography and vegetation (Figure 4-6b). Creek 1 sub-catchment has the largest catchment area comprising both parts of the hillslope body as well as the steep slopes and is either forested or used as meadow. Creek 2, south of creek 1, is completely within the southern slope area and exhibits steep gradients and is totally forested. Creek 3 is dominantly covered with meadows and is not connected to the southern slope.

Table 4-2: The size of creek catchments on the Heumös slope, as well as gauged sub-catchment sizes calculated out of the ALS DEM.

	Catchment sizes on Heumös slope [m²]	Catchment sizes of gauged catchments [m²]
Creek 3	102500	67330
Creek 1 and 2	630070	Creek 1: 209330 Creek 2: 90142
Creek 4	99470	
Rest	25530	
Total	857570	

The shape of the catchments is also reflected in the amount of debris transport, creeks 1 and 2 have a high debris transport rate, the Heumös creek transports smaller and less debris material. Therefore, the Heumös creek delivers the best runoff data. Debris transport and clogging of the weirs is the worst factor influencing the quality of the data. An example for a "yearly" clogging cycle: in autumn of 2001 the debris in the weir basin was removed, during the winter and spring no debris material was transported in the creek, which indicates that the runoff in winter and early spring is less intense. Good observation was possible in May 2002. In June, creek 1 was already clogged with debris material; the other two weirs were clogged later on that year, creek 2 in August and Heumös creek probably in October. Figure 6-4b shows the discrepancy of a clogged and debris-free weir in August 2004. Strong summer events often lead to debris transport and clogging. A good indication for clogging is a constantly higher baseflow after a storm event. The clogging and repeated dredging of the weirs constantly influence the water stage – discharge relation.

In addition to the upgrade of creek 1 measurements, the city of Dornbirn installed three additional weirs for spring discharge and surface discharge measurements in Ebnit. A time series coverage of discharge is displayed in figure 4-7.
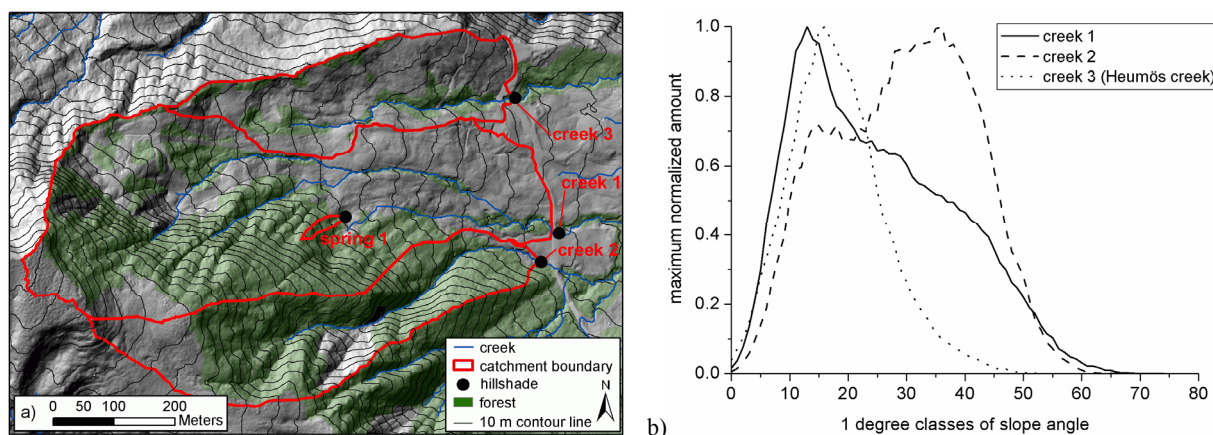
Figure 4-6: a) A hillshade view of the western Heumös slope with approximate catchment boundaries of creeks and spring 1. The road borders the catchments in the west, water flows through concrete pipes below. In plane areas between creek 3 and creek 1 catchment the definition of "real" catchment boundaries is difficult. Forested areas are held in dark green. b) The display of observed angles of the 1 m² airborne laser scan DEM. The different morphology with creek 1 as interjacent type is clarified. The small peak in low angles of creek 2 belongs to plane areas at the head of the catchment.

Spring 1 catchment and spring discharge data

Similarly to the creeks, spring 1 which lies at the transition of the southern slope and the hillslope body was equipped with a horizontal paper stripe logger from SEBA Hydrometrie GmbH (Germany, build in 1954) in vertical concrete pipes (Figure 3-3, Figure 4-6). Three small outlets were drilled into the concrete pipe to let the spring water out, producing a complicated stage-discharge relation (see appendix E). Spring 1 was equipped with a piezometer device logger from Aquitronic Umweltmesstechnik GmbH (Germany) usually used for groundwater level logging in early 2005. The new data has a better time resolution and quality but features a more diverse reaction; maximum amplitudes are greater than with the mechanical device, probably due to the technical set-up of the mechanical gauge.

Schneider (pers. communication), who tapped the spring in 1998, told that she had inserted a PVC pipe into a naturally existing soil pipe which then guides the water into the vertical concrete pipes. These are used as collecting pot for the water and measurement equipment. Observations show that not all spring water is caught and that a substantial amount is lost to parallel pipes or seeps out besides the spring, especially during heavy rainstorms or snowmelt.
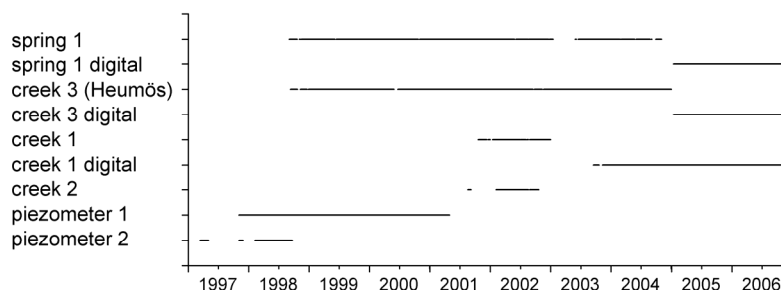
Figure 4-7: An overview of operation periods and available data of discharge measurements at weirs, springs and piezometers.

Soil moisture

Long term soil moisture changes were measured with the time domain reflectometry method (TDR) included into the meteorological station on the Heumös slope. The manufacturer of the TDR-rods is IMKO GmbH (Germany). The measuring principle is based on the propagation of guided electromagnetical waves along an electrical transmission line. Soil moisture values are derived from the measured electrical signals (Becker, 2004), this functions well with sandy soils and good calibration of the probes. In clay soils, there are distortion of measured signals, due to the high porosity, charged clay mineral content and water contents which exceed the measurement range of the probes (Blonquist *et al.*, 2006; Blonquist *et al.*, 2005; Jones *et al.*, 2005). Influence of soil temperature on measured signals is recorded, too (Wraith & Or, 1999).

Until August 2001, six rods were installed in an open soil pit. The reinitialisation of the meteorological station included the build up of a new TDR-rod profile in a soil pit properly closed after installation. The rods were installed in following depths: 20 cm, 35 cm, 50 cm and 60 cm, the profile is located three metres upslope of the meteorological station in a rather wet soil patch. The soil type is silty to clayey with rock fragments. During installation of the rods in September 2001 seeping water was observed in the lower part of the ditch at 60 cm depth. During a check in November 2006, water quickly accumulated at about 30 cm depth. The measured volumetric water contents of the TDR rods are high, which can indicate influence by charged clay minerals. This is why undisturbed soil samples were taken in November 2006 and analysed for their porosity and water content to determine the bias of the measurements (see also chapter 5.2.2). All samples were near saturation when taken, porosity lied at an average of 0.58, the volumetric water content calculates to a similar average. A comparison of gravimetric water content, calculated volumetric water content and the TDR-signals in table 4-3 indicates that TDR signals are in accordance with the water content. Only the TDR rod in 50 cm depth seems to overestimate the values.

Table 4-3: Comparison of TDR-measurements with water content from undisturbed soil samples. Porosity and water content are high; saturation of soil is reached for all samples.

Sample/ depth	Gravimetric water content [weight-%]	Volumetric water content [vol.-%]	Porosity n [ ]	Degree of saturation [ ]	Volumetric water content of TDR rod [vol.-%]
20A	67	60	0.61	0.96	65.5 (20 cm)
20B	55	54	0.55	0.96	
30A	49	54	0.57	0.90	60.8 (30 cm)
30B	87	66	0.67	0.95	
50A	60	57	0.55	1.10	72.2 (50 cm)
50B	56	58	0.56	1.10	58.2 (60 cm)

Piezometer head measurements

Three piezometer devices as well as temperature devices were installed in separate boreholes of KB 2 in the lower part of Ebnit in 5.5 m, 10.0 m and 13.7 m depth. The devices worked quite well but failed after a while through clogging of the devices or breaking of cables. Data is available in the period from 03/11/1997 until 30/04/2001 for device 1, until 26/10/2001 for device 2 and until 26/09/2001 for device 3. The devices are built into sand (0.6 – 1.2 mm), the borehole was filled with Compactonit pellets (clay) and additionally with a Tixoton Concrete suspension to seal the piezometer devices from the surface.

One of the two boreholes of KB 3 near the Heumös Alpe was equipped with two piezometer devices in 12.0 and 5.5 m depth as well as a temperature device. The devices are set up similarly to borehole KB 2. The temperature device never worked. The piezometers were installed in December 1996 and failed on

29/11/1997. They were able to be reactivated on 07/02/1998 and ran continuously until final failure on 23/09/1998. No reactivation was possible afterwards.

4.2.3   Mass movement data

Inclinometer measurements

Subsurface movement can be detected with inclinometer devices: the borehole is equipped with a casing which has two perpendicular sets of rills, one of those is oriented to main movement direction. The inclinometer pipes must reach several meters into the bedrock which supposedly does not show movement so that measured movements are not in a relative manner. The inclinometer itself is a device to measure tilting angles of the casing; it uses very fine inclination readings in the casing in defined distances. Combined inclination readings in depth, which are subtracted from the null-measurement, give deflections and disturbances in the inclinometer casing. Defined directions, which are perpendicular to each other, ensure comparable readings. Small perpendicular rails in the casing guide the inclinometer device, the directions are defined as A+/A– and B+/B– directions.

Inclinometer measurements were conducted by Schneider (1999) from 1996 to 1998 (Figure 4-8) in Kb 1 to KB 3. KB 1 and KB 2 are located in Ebnit, whereas KB 3 lies besides the Heumös Alpe. Measuring campaigns were not in equal time steps throughout the whole observation period. An investigation of the inclinometer measurement in regard to hydrological signals was not possible, the raw data did not include all measurements which were recorded in the graphs and measurement campaigns were not regular enough.

GPS and terrestrial surveying

The Institute of Geodesy in Karlsruhe conducted measurement campaigns with GPS equipment and terrestrial surveying to determine the soil surface movement (Depenthal & Schmitt, 2002; Depenthal & Schmitt, 2003; Howind & Schmitt, 1999; Schneider, 1999) from 1995-2001 (Figure 4-8). Campaigns with varying time lags were changed to fixed time lags in 1998 with three campaigns in the snow-free period, with 3 and 6 months in between. One measuring campaign usually lasted a week.

The GPS measurements on moving grounds required a very precise network of fixed points. A frame of five stable reference points were determined at the beginning of the measuring periods in 1995 on surrounding hilltops with the help of existing measuring points of the Austrian state survey, the Bundesamt für Eich- und Vermessungswesen (Austria), see Howind & Schmitt (1999). On several slopes so called object points were marked in either large rocks or inserted concrete blocks with special centering devices. On the Heumös slope 11 object points were marked in 1995. In 1996 the net was expanded with a traverse of 16 points (called traverse points) used for measurements with ground survey techniques as they were conducted in wooded areas. The traverse points were marked and fixed by tubes. In 1998 another 13 GPS object points were added on the Heumös slope. The reference network was observed in a static mode and the object points in a stop and go mode with at least 3 readings (Howind & Schmitt, 1999). Measurements were taken in three-dimensional WGS84-coordinates, these were transformed over geographic coordinates into two-dimensional conform coordinates and ellipsoidal heights (Howind & Schmitt, 1999). Data was distributed in the projection system of the Landesvermessungsamt Baden-Württemberg (Germany), see appendix C. The point coordinates were calculated for the different measurement periods by least-squares adjustments (Mierlo & Illner, 1998). In all periods the achieved accuracies for the object point coordinates are approximately 6 mm in the plane

component and 10 mm in the height component. The achieved accuracies for the traverse point coordinates ranged from 8 mm to 30 mm for both components. These differences in quality were caused by the unfortunate soil conditions, as the wooded area around the traverse was very moist most time of the year (Depenthal & Schmitt, 2003).
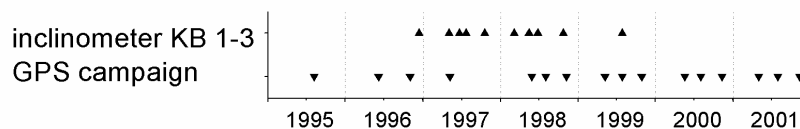
Figure 4-8: An overview of measuring campaigns for inclinometer and GPS measurements.

The comparison of surface movement characteristics with hydrological signals was conducted with final data sets of Depenthal & Schmitt (2002). Only lateral movements were used, these show more clarified reactions. Most of the height measurements are too near to the measurement errors and so the uncertainty is increased. For this thesis, data sets are referred to a null-observation point which is June 1998. Measurement errors are subtracted, this means that with large errors movement from one campaign to the next might be negative. In a first attempt these data should be discarded. Instead, the data has been included as e.g. not all points show negative values for the same campaign and the negative points enhance the overall trend. In appendix C, data with high errors are marked in grey.

4.3   Analysis of rainfall-runoff data

4.3.1   Estimation of runoff coefficients for selected rainfall-runoff events

Periods with qualitatively good rainfall-runoff time series were used to determine runoff coefficients. Periods were selected from the summers of 2002, 2004 and 2006. These are mostly periods when gravel was removed out of the gauges and before the gauges were refilled with gravel again in the following autumn. Events were selected and cut out for further use with the programme NQEDIT (2005). The rainfall-discharge events were selected manually. With the programme UH (for unit hydrograph) selected events are analysed using single ordinates and the unit hydrograph is adjusted with the method of least squares (Ihringer, 2005). The calculated unit hydrographs were not expressive at all, so that solely the achieved event-based rainfall sum, direct runoff sum and the runoff coefficient was used for catchment characterisation. Data uncertainty and a hydrograph reaction which shows a very low retention behaviour inhibited more sophisticated methods. Baseflow separation was conducted with a straight line approach; recession events were cupped at a maximum of 4 l/s.

4.3.2   Recession analysis for creeks, spring discharge and piezometer

The recession curve of a groundwater gauge, spring or river tells about the natural storages *S* feeding surface runoff in a general way. This is valuable information concerning storage properties and aquifer characteristics (Tallaksen, 1995). On the Heumös slope it was helpful to investigate the storage behaviour, because important time series of surface runoff, spring discharge and piezometer heights do not always overlap. Physically meaningful methods based on the Boussinesq equation and linearisation assumptions (Rupp *et al.*, 2004) did not yield feasible results for the piezometer and springs, as necessary assumptions for the use of these models were not fulfilled. A linear single storage method (Dyck & Peschke, 1995) has been applied to creek discharge, spring discharge and the groundwater height decline with the assumption of $S = K*Q$ with Q = discharge or water height and the depletion of the storage with

$$\ln Q(t) = \ln Q(t_0) - (t - t_0)/K \qquad\qquad (4)$$

using a semi-log plot for the recession curve and fitting a linear equation to the data. Whereas *t* is time and *t_o* is the following time step. A specific constant *K'* can be distinguished for different recession episodes. *K* is the negative reciprocal value to *K'* with the relation of *K=-1/K'* and expresses the time span needed to deplete the storage. Conclusions about the dimension of the aquifer are not possible but with the K factor an idea of storage in the aquifer can be gathered. This allows a comparison of the different storages featured in creek discharge, spring discharge and piezometer.

4.3.3   Automated precipitation event selection for event characteristic evaluation

An automated selection of events from the hydrological years of 1998 to 2006 was conducted for the evaluation of precipitation behaviour. Data sets for this selection procedure are the digitised Ebnit church precipitation data from paper strips and digital data from the new rain gauge at Ebnit church, this should be noted as the creation of these datasets includes differences in the outcome as digital data differs from digitised data in some manner. In the text, the automated event selection is also referred to as "selected events". Time series with 10 min time-steps with accumulated precipitation data was used. A selected event begins with a first precipitation value, it finishes is when there was no precipitation for more than six hours. A time span of 6 hours without precipitation selects favourably long events and might combine several short rainstorms but seemed to be a feasible compromise. The runoff response time lies between 12 and 36 hours (Chapter 6.2.3), six hours as ending criterion should therefore not cut out too many successive events. To reduce the total data set and clean out very small events, the time-steps without precipitation were set in relation to the total time span, events with more than 99 % of "precipitation free time" steps were excluded, events with more than 79 % "precipitation free time" were excluded when the precipitation depth was smaller than 3 mm leading to a reduced data set with 690 events. Precipitation depth, total time span, average intensity, maximum intensity and start time were calculated and compared (Appendix F-2).

4.3.4   Efficiency criteria for model output

A comparison of a calculated and measured discharge and a soil moisture time series was done using several efficiency criteria. *O* refers to observed data, *P* to predicted data by the model, the bar above *O* or *P* means the mean of this parameter, *n* is the number of values.

The *correlation coefficient* is a normalised measure of the strength of the linear relationship between two variables. It is the ratio of the covariance of two variables to the product of their standard deviations (Davis, 2002). It is an unitless ratio, when there are only two stochastic variables, the empiric correlation coefficient can be calculated after

$$r_{OP} = \frac{1}{n-1}\sum_{i=1}^{n}\left(O_i - \overline{O}\right)\cdot\left(P_i - \overline{P}\right) \Bigg/ \left(\sqrt{\frac{1}{n-1}\sum_{i=1}^{n}\left(O_i - \overline{O}\right)^2} \cdot \sqrt{\frac{1}{n-1}\sum_{i=1}^{n}\left(P_i - \overline{P}\right)^2}\right) \qquad (5)$$

A high correlation coefficient in a discharge time series analysis means that the calculated discharge and the measured discharge have a similar reaction time, e.g. the maximum of an discharge event is at the same time-step. A low correlation coefficient is achieved when calculated data does not have the same reaction behaviour, e.g. calculated peaks are not at the same time stamp than measured peaks or when peak discharge does not have similar values. The gradient and intercept of the regression on which r is based gives additional information about its performance (Krause *et al.*, 2005).

$$r_{OP}^2 = \left(\sum_{i=1}^{n} (O_i - \overline{O}) \cdot (P_i - \overline{P}) \middle/ \sqrt{\sum_{i=1}^{n} (O_i - \overline{O})^2} \cdot \sqrt{\sum_{i=1}^{n} (P_i - \overline{P})^2} \right)^2 \qquad (5)$$

The *Nash-Sutcliffe efficiency* (Nash & Sutcliffe, 1970) is a measure to compare discharge time series with calculated time series. The efficiency E_{ns} is defined as one minus the sum of the absolute squared differences between the predicted and observed values normalised by the variance of the observed values during the period under investigation (Krause *et al.*, 2005). A large disadvantage is the fact that the differences between the observed and predicted values are calculated as squared values. As a result larger values in a time series are strongly overestimated whereas lower values are neglected (Legates & McCabe Jr., 1999). This means an overestimation of the model performance during peak flows and under-estimation of low flows.

$$E_{ns} = 1 - \left(\sum_{i=1}^{n} (O_i - P_i)^2 \middle/ \sum_{i=1}^{n} (O_i - \overline{P_i})^2 \right) \qquad (6)$$

The *balanced volume* is a simple comparison of the sums of the values of time series which are measured and calculated. It is a measure to get an information about the quality of a model to grasp the water balance. The sum of measured values per time-step is divided by the sum of calculated values per time-step for the volume balance,.

$$C_{rec} = \left(\sum_{i=1}^{n} (O_i) \middle/ \sum_{i=1}^{n} (P_i) \right) \qquad (7)$$

The nearer the value is to 1, the better the recovery of surface runoff from the model. The overall water balance would be in good accordance even though the performance of the model might be not so good in calculating a single event because the adequate process is not exactly represented by the model.

5 Structures and patterns identified at the Heumös slope

This chapter advances the introduction to the geological setting of chapter 3. It also presents pedological and vegetation information of the Heumös slope. It provides more details on structural information, including patterns from the surface and the unsaturated zone. This information will help to develop a perceptional model to understand the characteristics of the hillslope in chapter 7.1, to better understand the patterns, structures and processes that control runoff and movement. Hence, the interfaces of strata are of importance e.g. as potential failure zones. In addition, the encountered clay-rich material has to be investigated for their material properties (Boogard *et al.*, 2002; Maquaire *et al.*, 2003; van den Ham, 2006). This has partly been done by the work of Schneider (1999) and Schwenk (1999) but still needs further refinement. Finally, the distribution of landscape units and vegetation types is analysed, which helps to understand the spatial patterns of average soil moisture conditions.

5.1 Subsurface structures and properties

Through the work of Schneider (1999) who drilled borehole KB 3 as well as Schwenk (1999) who refined the geological map of Oberhauser *et al.* (1991) and mapped the geotechnical features (Figure 3-7), there is a good but not excessive knowledge about the geological surface and subsurface (Chapter 3.2 and 3.3). However, this knowledge lacks more precise information about the thickness distribution of the post-glacial sediments, the subglacial till and about the position of the sediment-bedrock transition. Furthermore, hydrogeological characteristics need to be refined. Especially hydraulic conductivity parameters and their spatial variability are of interest.

5.1.1 Depth of bedrock estimation with geoelectrical methods

The interpretation of electromagnetical conductivity profiles (Figure 5-1a) requires an association of the geoelectrical depth profile (Figure 5-1b) with the borehole log of KB 3. The interpretation of the geoelectrical depth profile is generally hampered by a clear detection of Amden marlstones in KB 3. This is essential to know as a relation between bedrock properties needs to be set up with the apparent specific geoelectrical resistivity values (electrical resistivity). Table 5-1 assigns the electrical resistivity to the layers found in the borehole (Figure 5-1b). It must be noted that the differences of electrical resistivity of strata of 20 to 65 Ω*m are too small to determine sharp boundaries in the electromagnetical profiles. For example, Reynolds (2005) reports electrical resistivity values for dry marlstones of 30-70 Ω*m, for limestones 50-10^7 Ω*m, clays 1-100 Ω*m, dry clays 50-150 Ω*m and for clayey sand 30-215 Ω*m. No information for saturated clays was found in the literature. The similar electrical resistivity ranges mean that the observed electrical resistivity is within the same range of expectable electrical resistivity for all rock types in the borehole. This hampers a clear determination and association.

The coarse scree and loamy scree are generally difficult to differ in means of the material composition, which is due to a broad range of compositional variability of the material (Chapter 3.3.3, 3.3.7 and 5.1.2) Only small electrical resistivity differences from 48 Ω*m (loamy scree) to 55 Ω*m (coarse scree) were determined. However, the increase of electrical resistivity in figure 5-1 could reflect a decrease of porosity in the post-glacial sediments (Table 5-1). The shift between the scree and the subglacial till is a bit more distinct, the electrical resistivity step is from 55 Ω*m (coarse scree) to more than 60 Ω*m (subglacial till). The facies change between the coarse scree and the highly compacted subglacial till should be more distinct than in between the coarse and loamy scree. A careful re-interpretation of the lower borehole log recordings from Schneider (1999) was made. Schneider (1999) did not have the

possibility to interpret the borehole log combined with the geoelectrical depth profile. Schneider describes the lowest layer as a transition of subglacial till to Amden marlstone (19.0 to 22.7 m), which is not a clear determination (Figure 3-9a) of material properties. Hence geoelectrical interpretation is not feasible. The core loss below this layer up to 24 m depth was then ascribed to dry Amden marlstone rock without cohesion that fell out of the drill stem during recovery.

Table 5-1: Comparison of geoelectrical depth profile with the borehole log of KB 3, see also Figure 5-1b.

Apparent electrical resistivity [Ω*m]	Depth of layer in KB 3 [m]	Material definition in borehole log	Interpretation of apparent electrical resistivity in relation to geologic material
20-48	0-8.5	loamy scree	Continuous rise of electrical resistivity with depth, related to increasing density and decreasing liquid content, decreasing smectite content leads to decreasing charge of clay minerals
50-55	8.5-10	coarse scree	Slightly higher but constant electrical resistivity than in loamy scree
55-65	10-19	subglacial till	electrical resistivity values could mean high compaction of subglacial till and low water content
53	19-30	subglacial till and Amden marlstones	Constant and slightly lower electrical resistivity than in the subglacial till above: still subglacial till, weathered Amden marlstones or already unweathered Amden marlstones?
37	30-42	core loss	Sharp decrease in 30 m depth: Amden marlstones or other rock type encountered?

Consequently, two possible interpretations could be considered when the information of the borehole log is combined with the geoelectrical depth profile:

The first interpretation after Hannich (2001) suggests similar material compositions for the subglacial till - marlstone transition layer (19.0 to 22.7 m) and in the subglacial till layer above figure 3-9a. The Amden marlstones are considered to be deeper (~30 m) with electrical resistivity values of around 37 Ω*m, which is distinctly lower than the electrical resistivity of the post-glacial and glacial sediments. This interpretation suggests that the Amden marlstones would not begin above a depth of 30 m. Consequently, a high water content would be necessary for such low electrical resistivity values (Figure 5-1b). This would mean that Amden marlstones are encountered on the hillslope in a great depth of more than 60 m, according to the electromagnetical conductivity profiles. Amden marlstones would be encountered in lower depths (30 m) of the GEP-1 profile near the borehole KB 3. As stated in chapter 3.3.7, Amden marlstones are considered to have a low water content and is rather in dry condition so that resistivity values should be higher than 37 Ω*m.

The second interpretation is a revised view on the borehole log. This would mean that the subglacial till - weathered marlstone transition (19.0 to 22.7 m) is in fact just a weathered Amden marlstone. Unweathered marlstones would be encountered below. This is backed by the "core loss layer" in Figure 3-9, because only a double casing drill stem would inhibit dry rock material to fall out of the drill head. A double casing drill head was not used for borehole KB 3. For the interpretation of electrical resistivity in the depth profile this would mean that both the subglacial till and the Amden marlstones have similar values of about 53 Ω*m, a distinguish of single layers would not be feasible. The low resistivity at 30 m (Figure 5-1b) would then consequently be another rock type or a water-containing layer.

For the general interpretation of the electromagnetical profiles (Figure 5-1a and Appendix D-3) this would mean that a transition between the subglacial till and the Amden marlstones is not detectable as the differences in material properties are too low. However, the curved shape of the southern part of the profile is remarkable. It might resemble the shape of the bedrock surface nevertheless.

a)

b)
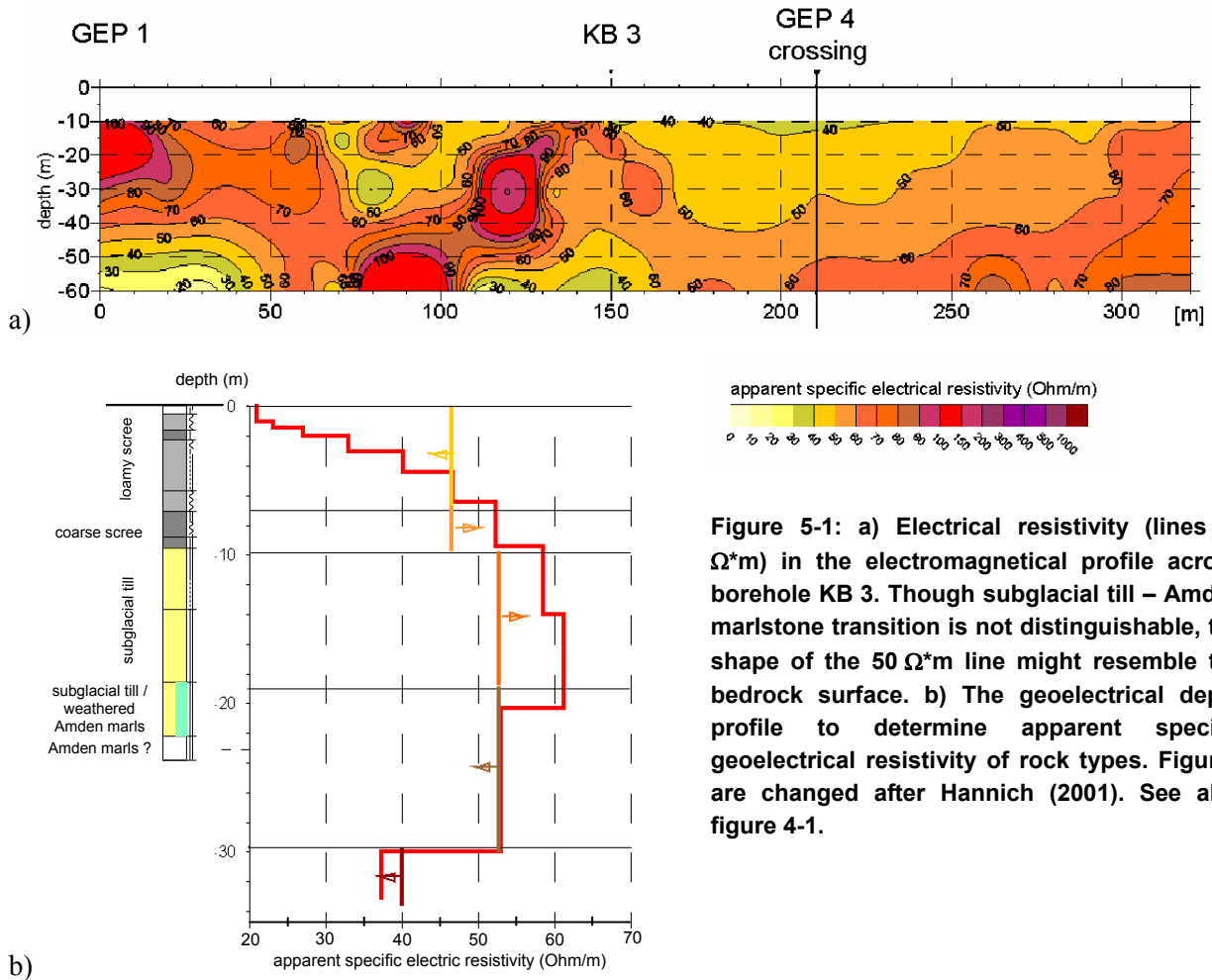
Figure 5-1: a) Electrical resistivity (lines in Ω*m) in the electromagnetical profile across borehole KB 3. Though subglacial till – Amden marlstone transition is not distinguishable, the shape of the 50 Ω*m line might resemble the bedrock surface. b) The geoelectrical depth profile to determine apparent specific geoelectrical resistivity of rock types. Figures are changed after Hannich (2001). See also figure 4-1.

5.1.2 Post-glacial sediments on the hillslope body

Additional information about subsurface properties of the postglacial sediments was achieved by hollow sampler logs conducted through percussion probing across a north to south profile on the hillslope body (RKS 1-11). The location of the hollow core sampler holes is displayed in figure 4-2. In general, material from the hollow core sampler logs ranged from silty clay without gravel sized marlstone fragments (*loamy scree*) to gravel sized marlstone fragments with a minor matrix component of silty clay (*coarse scree*). The gravel consisted exclusively of marlstone or carbonaceous marlstone fragments, all have an angular shape. As the result of the high heterogeneity of material properties of the post-glacial and glacial sediments, recorded water content and especially description of consistency are more important to classify the material.

At the northern slope, all boreholes reached down to a depth of 3.2 m. Silty clay with gravel was found in all four hollow core sampler logs (RKS 3, 4, 5 and 6; for the location see figure 4-2). The consistency of the matrix was firm for most of the material. In RKS 3 and 6 a silty clay layer with a soft consistency was encountered at the very top. In RKS 6 the hollow core sample hole filled with water that seeped out of this soft horizon. The lowest bit of recovered material was a brownish clay in the logs which was considered to be strongly weathered Amden marlstone. To summarise the post-glacial sediment composition on the northern slope: a shallow soft silty clay layer is followed by up to 3 m of firm loamy scree with gravel before Amden marlstones are reached at a depth of 3.2 m. Sampling was conducted in

June 2006 shortly after snowmelt. The upper soil column, the soft silty clay, was still water saturated from 3 days of being covered with snow. The stiff material below suggested that there is no deep matrix infiltration even after snowy winter periods.

RKS 7 was placed at the bottom of the northern slope; RKS 1 and 11 were placed near creek 1. Retrieved material in the logs was mostly a silty clay with gravel but also gravel-free clays were encountered (Figure 5-2). The consistencies in RKS 7 were generally described as softer than on the northern slope, soft to firm respectively. RKS 7 was placed at the foot of a small slide. Soft to very soft material was found here in a depth of 2.3-3.4 m. This shows that clay with a critical consistency can be found even in greater depths. The latter layer also contained wood. Possibly, humus-rich layers indicate paleo-surfaces in greater depths.

A more heterogeneous build up of the subsurface is found at the foot of the southern slope (Figure 4-2 and Figure 5-2). The hollow core sampler holes were penetrated at different kinds of locations there. Near spring 1 RKS 8b showed a silty clay with increasing stiffness from soft to stiff. Boreholes above the spring could only be conducted no further than 0.5-1.0 m and did not yield any layering. RKS 10 is located near a small-scale slide and yielded soft to very soft, gravel poor silty clay down to 4.8 m, wet gravel and a brownish red clay followed, which possibly indicates bedrock at 5.2 m depth.
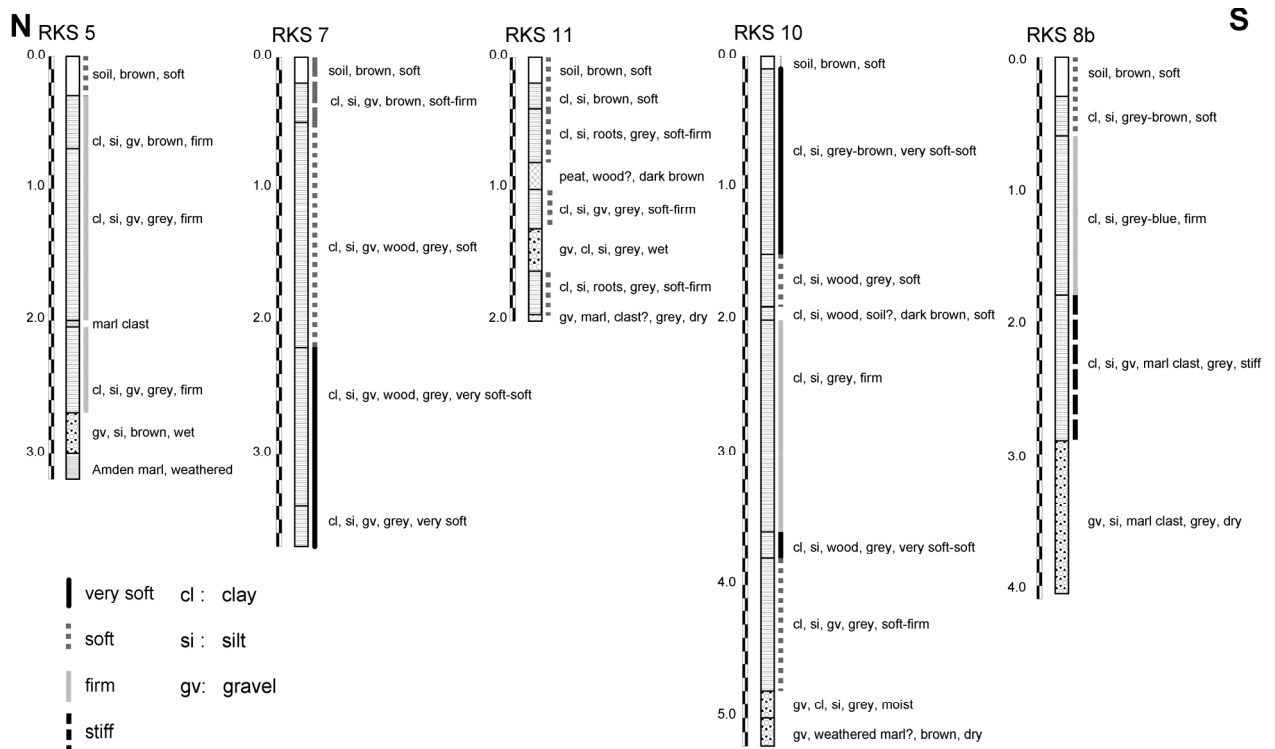
Figure 5-2: Selected hollow core sampler logs, from north to south across the hillslope body. The material consistency is quite similar, showing compositions of both scree and loamy scree. Consistency is a more appropriate parameter for the distinction of different horizons than grain size or material composition.

The build up of the scree and loamy scree in the hollow core sampler logs depends on the position of sampling: soil patches with damp to wet ecological moisture values also yielded deeply weathered material which can be described as a gravel-free silty clay (= *loamy scree*). This loamy scree shows that water greatly influences the composition of the material. Areas with drier soil moisture regimes show more gravel in the logs, which is a *coarse scree* respectively. This is especially true for the northern slope

where the bedrock surface was reached at a depth of about 3 m. The layering of material with different consistencies can be due to small scale rotational slides or debris flow sediments interbedded with soil horizons. A consistent layering in the post-glacial sediments cannot be determined so that the identification of consistent spatial subsurface patterns in the post-glacial sediments is restricted. It is suggested that composition of the post-glacial sediment is in accordance to small scale sedimentation and erosional events and that the sampling density of the hollow core sampler holes is not dense enough to resolve this variability. Wood even in deep layers means that reworking and burying of former vegetation or soils is a possible explanation.

Samples were taken in several borehole logs for a gravimetric water content determination. The consistency of these samples was often determined as very soft. In contrast, the water content determination showed lower values than expected if compared to samples taken near the surface: e.g. 40 vol.-% of a soft sample compared to 60 vol.-% for sample taken near the surface (Appendix D-4).

5.2 Soils, vegetation and ecological moisture index

5.2.1 Vegetation associations and map of ecological moisture index

Elevation-related vegetation zones after Ellenberg (1996) were the potential original vegetation cover before settlement started in the Ebnit Ache valley. This would have been mixed forests with beech trees on the lower Heumös slope and mixed forests with silver firs on the upper hillslope. After settling began in 1351 AD, the original deeply rooting silver firs (*Abies alba*) were chopped down to allow more pastures for livestock on the slopes and also for wood supply. In a later reforestation the deeply rooting silver firs were replaced by common spruce (*Picea abies*) and grey alders (*Alnus incana*) with shallow roots. Common spruce is rather found on steep slopes and in generally drier areas, whereas the grey alders are found in wet and flatter areas. The shallow roots of the common spruce might add to instability of the upper soil column, if compared to the original deep-rooted silver firs. A potential for subsurface pipe development in former shallow root holes might be enhanced as well (Uchida *et al.*, 2001). In recent years the very moist pastures on the eastern slope were abandoned, a mixed forest with common spruce and grey alders developed there slowly. About a third of the Heumös slope is not forested: a marginal part is covered with buildings or roads, and the remaining area is covered with meadows.

The forest-free area, when not sealed or close to settlements, is dominantly used for cattle and horse grazing from June to September. In winter the meadows are often covered in snow and used for skiing. The animals are fenced off in certain areas so that the meadows can regrow for a while in other places. Not all meadows are used intensively as some are too wet for grazing. These are especially the meadows east of the street and the holiday village. The grazing certainly leads to some preference or denial of specific plants. For example, peppermint (*Mentha longifolia*) thrives in some areas, this plant is not eaten by the cattle. The hooves of the cattle leave significant marks in the moist soil; small puddles in the hooves marks are abundant.

Three vegetation association sub-types are defined in the unforested meadows (Waldenmeyer, 2000): 1) *Scirpus sub-type* derived from a *Calthion type* (Ellenberg, 1996), which is a meadow with wet ecological moisture conditions due to a distinct gleyic evolution. It is influenced by grazing; a higher soil nutrient value is also suggested. 2) *Molinia sub-type*, derived from the *Molinia-Arrhenathereatea type,* is described to be quite similar to the *Calthion type* (Ellenberg, 1996). Waldenmeyer (2000) associates soil conditions with less gleyic influence and more variable moisture conditions, although Ellenberg (1996) suggested that this is not necessarily a criterion for differentiation. 3) The *Ononis sub-type* is derived from

the *Meso-Bromion type*, a carbonaceous dry meadow (Ellenberg, 1996), showing drier moisture conditions (alternating dryness to alternating wetness).

Figure 5-3 displays classified patches of ecological plant moisture derived by the detailed mapping of indicator plants as explained in chapter 4.1.2. A translated classification scheme after Ellenberg (Hill *et al.*, 1999) and a selection of indicator plants with their ecological indices is listed in Appendix D-1 and D-2. Considering the goal of the soil mapping analysis, which focuses on the ecological moisture distribution, the specific types of vegetation associations are of minor importance than the actual moisture values. The average ecological moisture regime suggests which process dominates runoff generation or infiltration at the specific vegetation association patch. The ecological moisture index deduces a seasonal or long-term behaviour of the soil moisture regime.

The inclination of each patch is also related to the ecological moisture (Figure 5-3); flat areas collect water and can even develop into swampy areas, see e.g. the middle of the hillslope body. Steeper regions generally have drier ecological moisture values assigned to, these are especially the southern and northern slopes. Patchy moisture distribution on the hillslope body reflects the small-scale topography due to shallow soil creep there.
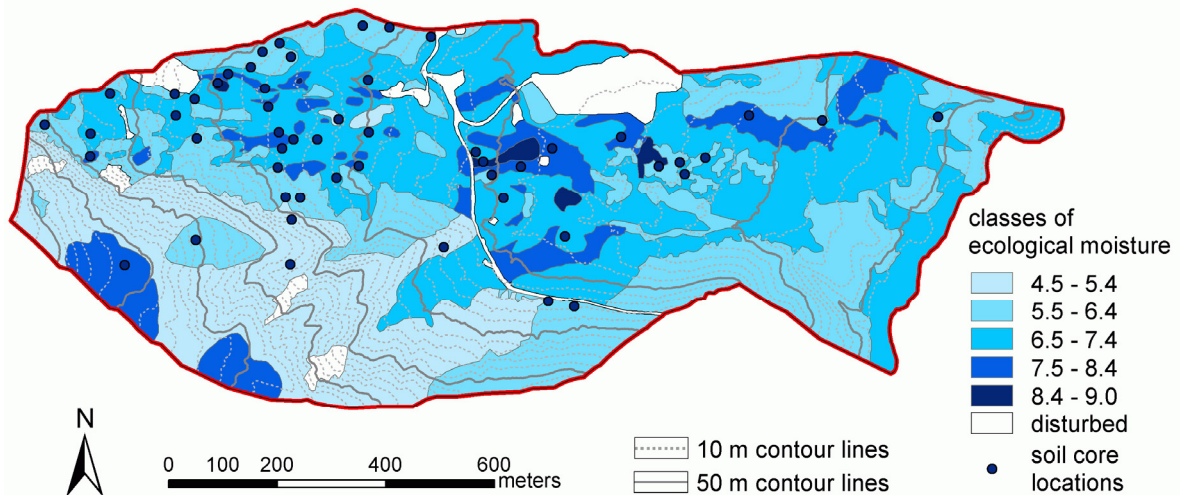
Figure 5-3: Patches of similar ecological moisture derived by soil core investigation and vegetation association mapping. Map changed after Dittfurth (2002).

5.2.2   Distribution of soils and soil-specific parameters

Soils and soil structure

The soil description was conducted with the German soil classification system (1996) and then was translated into the FAO system (Kuntze *et al.*, 1994). *Gleysols* dominate on the hillslope body. These are mostly *stagnic gleysols* influenced by surface water but *gleyic gleysols* with local groundwater influence are also determined. Groundwater influence occurs near the creek gullies, in swampy regions and especially in the east, at the toe of the hillslope body. Water seeping out of the soils can be observed there. Patches of an ecological moisture class of *wet to open water* show swamp-like properties with high humus contents in the soil matrix. Soil depth varies greatly; it is rather influenced by geomorphic processes on the hillslope than by soil development processes. Earth flows and slides bury soils and so stop soil development. In contrast, erosion reduces the height of the soil column. Gleyic characteristics of

deeper horizons are not easy to distinguish from source rocks, as these are originally grey. The carbonate content can be used to distinguish soil development. For example, the area between the southern slope and creek 1 is depleted of carbonate content to a considerable depth, which is attributed to higher accumulation rates of sediments. The area between creek 1 and creek 3 to the west shows a low carbonate depletion. Here, erosion likely prevails.

Residual soils are dominant on the southern slope and on parts of the northern slope; these soils can be determined with caution as *vertic leptosols* in the FAO classification. *Vertic* usually is a characteristic for soils with strong shrinkage and swelling characteristic in the humid tropics which can show slickensides. This is not feasible for the Vorarlberg Alps but shrinkage and swelling is a dominant characteristic of these residual soils. The soil thickness is often no more than 1 m on top of the bedrock on the southern slope. Young talus cones in some regions consist of rock clasts – no soil development is found there. Near some deep gullies in the southern slope there are remnant talus terraces, which feature deeper sediment and soil covers. Patches of bare rock are abundant.

Soil structure is the arrangement of soil particles into aggregates. A gleyic colour pattern in the soil profile shows an accumulation of iron and manganese oxides in the upper soil column (reddish, brownish) and a leaching in lower horizons (greyish colour). Soils on steeper slopes and with more variable moisture conditions have more distinct soil peds distribution than soils from flat areas and wetter moisture conditions. The horizons show a high variability of soil structure in spite of a very similar texture: gleying and leaching features, different humus content, colours and an overall similar grain size distribution suggest this. It is an indication on the heterogeneous soil development which is closely linked to the geomorphological activity of the slope. A long-term soil moisture condition is also expressed by the characteristic of the soil structure as well.

Soil pipes and macropores

Macropores play a dominant role in the soils of the Heumös slope, enhancing the heterogeneity of the soil and influencing the subsurface hydraulics. Former root holes from marsh plants are the most dominant circular macropores found in the soils. These macropores have diameters of around 0.3 to 1.0 cm and show a higher occurrence in swampy areas. These root holes can be opened to the surface in the gullies of the creeks and on steep slopes in the forest and so function as small springs.

In the 2006 field campaign, soil pipes were found in the southern and northern slopes, in both locations with a diameter of around 10 cm: Besides spring 1 a shallow pipe transported water about 10 cm below the soil surface during a long lasting precipitation event. The pipe on the northern slope feeds and leaves a small sinkhole near auger hole RKS 5. It is not known whether the pipes end in the soil or return to the surface again.

Shrinkage cracks are a second dominant type of macropores in the area, especially at the southern slope. The shrinking capability of the soils shows a significant possible volume change (Figure 5-4 and following text). Clays with high moisture contents, especially in swampy areas, are susceptible for shrinkage crack development during dry periods: In June and July 2006 precipitation was below average: 96 mm in June (30-year average is 260 mm) and 147 mm in July (30-year average is 247 mm). Fieldwork started on July 24th when shrinkage cracks were observable even in usually swampy areas. The surface aperture of these cracks exceeded 2.5 cm in diameter. The cracks were rather observed in areas which were not covered with grass. Grass seems to stabilise the water balance in dry periods, probably because roots might balance the moisture distribution in the soil column. The observation of cracks in a newly dug

ditch near the holiday village showed that the swelling is a slow process, the cracks reduced their diameter only by half after 7 days and 110 mm of precipitation. In spring time and after long periods of moist climate conditions, observations showed that cracks close further then (Wienhöfer, pers. communication).
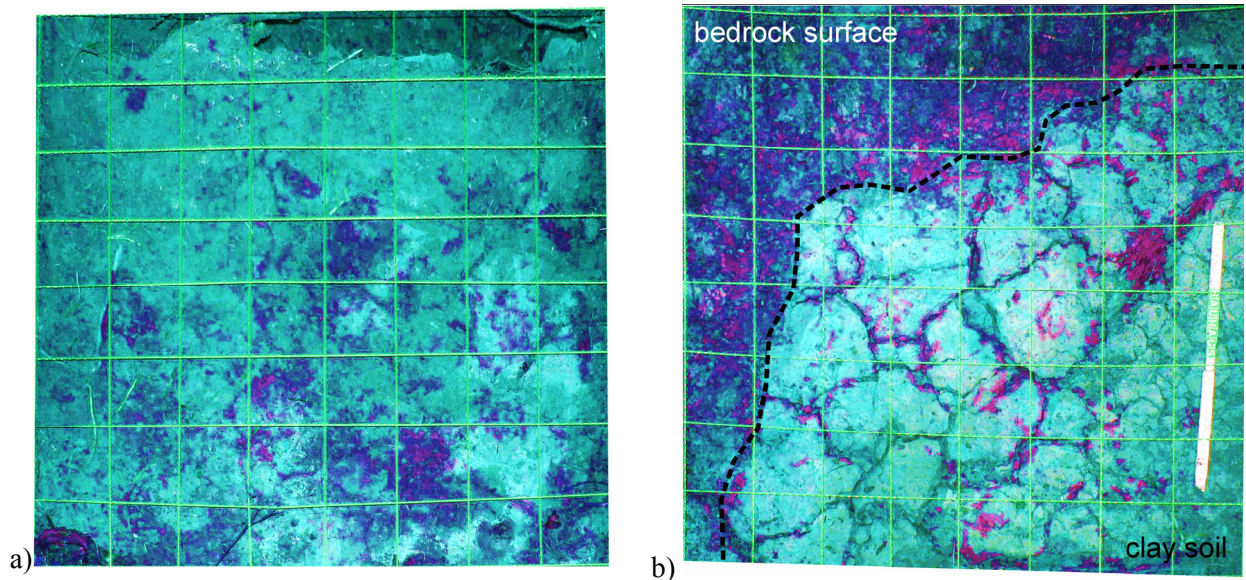
Figure 5-4: False coloured photographs of the brilliant blue profile. The view is parallel to the soil surface in downslope direction, a square represents 10 cm; light blue = no stain; violet = weakly stained; pink = intensively stained; a) in 5 cm depth, just below the humus horizon (A_h); b) in 25 cm depth, the upper left corner is removed down to bedrock (Amden marlstones). The dye seeped downslope between bedrock surface and soil. Hence the dark violet colouring.

The plot stained with brilliant blue was located near the catchment of spring 1 on the southern slope. The soil profile of this plot had a thin humus horizon and vegetation cover of about 5 cm. An uneven surface of a beige to grey clay-horizon appeared below this horizon which meant that the humus overlay has little exchange with the clay. Below this massive clay, bedrock was reached in 50 cm depth, a weathered Amden marlstone. The stained soil was removed in layers of 2, 5, 10, 15 and 25 cm before a vertical profile was dug; a selection of photographs is shown in figure 5-4.

A spatially unspecific stained patch was revealed at a depth 5 cm depth where about 40 % was strongly stained and 27 % was lightly stained. The dye intensity corresponds with the humus content of this horizon. Macropores were not yet stained or visible in this layer. In the next lower horizon (10 cm) the unspecific dye patches were strongly reduced. In following depths (15 and 25 cm) an unspecific staining was not visible any more. Only macropores, roots and shrinkage cracks and their margins were stained. The stained macropores have an aperture of below 1 mm up to several centimetres. The shrinkage cracks show a similar range of aperture, increasing in width and number towards the depth. The surfaces of the cracks show soil development, so it is likely that the shrinkage cracks remain over a long period and that they reopen during dry periods. Soil crumbs in the cracks and weathered crack surfaces were the better stained material in depth but the clay showed colouring in some areas as well. Dye seeped approximately 5 mm into the clay at some crack surfaces. Roots were also stained around their skin, which means that preferential flow also exists alongside of roots. The dye was stopped by the bedrock surface and flowed between the clay-bedrock transition which can be seen in the upper part of Figure 5-4. The profile was re-

examined on 23/11/2006; the cracks had closed further but were still observable and the clay was less stiff.

The observed shrinkage cracks of soils of the southern slope indicate that despite high yearly precipitation depths, swelling and shrinkage of soils dominates the subsurface hydraulics. The matrix hydraulic conductivity only seems to have marginal impact in relation to the fast subsurface flow processes even though the shrinkage crack development is strongly coupled to the soil moisture conditions and so to antecedent climate conditions. Shrinkage cracks are probably always hydraulically active, even in almost closed conditions.

Soil texture and porosity

The German texture classification is more diverse than the US soil texture classification scheme (Scheffer & Schachtschabel, 1998). Table 5-2 gives an overview of classified German soil types related to the SCS classification scheme for the Heumös slope horizons. The soil texture is finely grained, the determination and classification of 226 soil horizons yielded silty clays to be most dominant, followed by silty loams. Sandy soils only have a marginal occurrence (Figure 5-5a, Table 5-2). Figure 5-5b shows the grain size distribution for the four soil profiles with an average clay, silt and sand content of 52.1 %, 37.9 % and 10.0 % respectively. Minimum and maximum values vary with some respect but the median lies close to the average in the box plot. The soils of the Heumös slope reflect the source material which is found in the surrounding rock outcrops. The fast weathering Amden and Leimern marlstones seem to contribute to the soils dominantly, the leaching of carbonate leaves clay-sized and silt-sized grains. The more sandy or more carbonaceous fragments of the Wang formation are less abundant in the soils. Due to their high silt content it is supposed that the soils have a high field capacity.

Table 5-2: Defined soil types of soil horizons: The German taxonomy (DIN 4220, 1998) and the US Soil Survey Division Staff (1993) soil classification and the frequency of occurrence.

Soil type after AG Boden classification	Translation to US soil taxonomy	Frequency of occurrence in a total of 226 soil horizons [%]
Tt	clay	1
Tu3	silty clay	69
Tu2	silty clay	9
Lu	silt loam	14
Ls2	loam	7

The examined soil profiles and undisturbed soil cores were free of larger clasts, which is a matter of sample selection but, of course, influences the hydraulic conductivity estimation. When the material which lies in the gullies is checked out, it gets obvious that a far wider range of grain size distribution prevails on the Heumös slope than any laboratory grain size distribution measurement method can show (Figure 3-11). Grain size distribution curves of Schneider (1999) and Schwenk (1999) as well as Dittfurth (2002) represent a matrix grain size distribution. Larger volumes of material would be necessary for sieving, up to 100 kg as Maquaire *et al.* (2003) suggest.
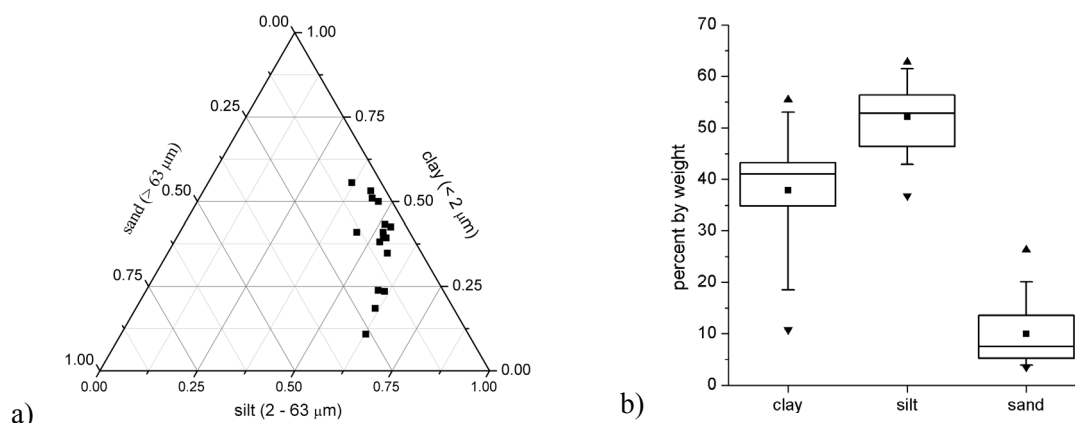
Figure 5-5: The grain size distribution of 16 soil profile horizons of profiles 1-4 a) composition diagram; b) box plots to show the variability of grain size classes. Box plots are a useful presentation of essential aspects of a sample distribution (Davis, 2002). The box shows the spread of the central 50 % of a distribution, whose lower limit is set at the first quartile and its upper limit at the third quartile. The bar in the middle of the box represents the median. The square represents the average of the sample distribution. The whiskers represent the 5 and 95 percentiles. Box plots used in this thesis also show maximum and minimum values (small bars) when they are located significantly outside the sample distribution, as well as the 1 and 99 percentile, represented by triangles.

Table 5-3: Porosity values derived from undisturbed soil cores from soil profiles of 2001 and from the TDR profile of 2006.

	Profile and soil horizon after AG-Boden (1996)	Soil type after AG-Boden (1996)	Depth of sample taken [cm]	Porosity [-]
undisturbed samples from soil profiles	G1 - Sd	Tu3	10-35	0.54
	G1 - Sw	Tu3	35-65	0.50
	G1 - eCv	Tu3	65-85	0.29
	G2 - Srw	Tu3	15-25	0.53
	G2 - Srw-eCv	Lu	25-120	0.60
	G3 - Ah-Srw	Tu2	30-50	0.76
	G3 - Srw	Tu2	50-90	0.63
	G3 - eCv	Lu	90-160	0.55
undisturbed samples from TDR profile	Srd	Tu3	20	0.61
	Srd	Tu3	20	0.55
	Srd	Tu3	30	0.57
	Srd	Tu3	30	0.67
	Sw	Tu3	50	0.55

The porosity values of soil types were determined in 2001 and 2006. A high porosity is anticipated in the wet patches as high water contents lead to a porosity increase in clay soils. Values of the 2006 samples near the TDR-rods give an average of n = 0.58. Samples from 2001 are undisturbed soil samples from the permeameter measurements from each horizon of 3 soil profiles with porosity values ranging from n = 0.29 to n = 0.76, the average and median are at n = 0.55. The n = 0.29 sample is derived from a C-soil horizon in a depth of 65 cm on the northern slope (profile 1, see also chapter 4.1.4) which exhibits low hydraulic conductivities. This low porosity is not suggested to be an outlier. It indicates that in dry, residual and lower horizons, porosity decreases due to a self loading of the soil column and consequently a shrinkage of pore volumes.

Soil shrinkage characteristic curve

One sample taken near spring 1 in a depth of 50 cm depth has been used to derive plasticity limits and to calculate swelling capacity after the model from Chertkov (2000; 2003a). It was taken out of a ditch, digged while drainage pipes were implemented. The encountered soil type is a stagnic gleysol with a very high water content (60 weight-%) and no gravel content. Atterberg limits, density and water content are listed in Figure 5-6. The high water content and the Atterberg limits indicate that the material is close to critical stability and can be determined as a plastic clay with high plasticity. It has a plasticity range of intermediate to high plasticity conditions according to the water content, similar to the findings of Dittfurth (2002), Schneider (1999) and Schwenk (1999). The calculated characteristic shrinkage curve (Chertkov, 2000; Chertkov, 2003a) in figure 5-6 shows that a distinct volume change can be expected when soils get drier or wetter. Clays tend to enlarge their pores further when initial porosity is air-free and filled completely with water. So the swelling of clay means that there is a normal relation between volume increase and water uptake. The calculated soil shrinkage characteristic curve in figure 5-6 shows that the volume can still increase by about 35 % when the pores are water saturated. The actual soil moisture ranges of the soils do not reach shrinkage water contents on the Heumös slope but lower water contents still mean that shrinkage can be significant.
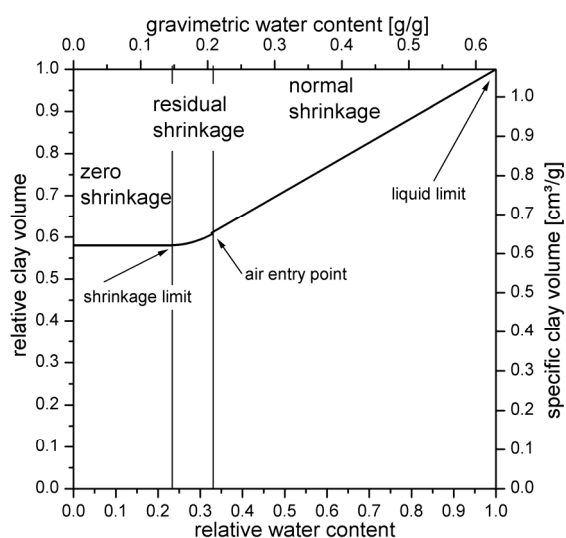
water content	0.60	[weight-%]
liquid limit	0.63	[weight-%]
plastic limit	0.28	[weight-%]
shrinkage limit	0.22	[weight-%]
shrinkage volume	0.33	[weight-%]
grain density	2.25	[g/cm³]
dry density	1.60	[g/cm³]
wet density	1.00	[g/cm³]

Figure 5-6: Atterberg limits, density and shrinkage character-istics for soil sample from a depth of 50 cm.

5.3 Spatial and local estimation of soil hydraulic conductivity and infiltration capacity

This chapter is supposed to give an overview of the infiltrability capacity and values of saturated hydraulic conductivity (K_{sat}) from tests on the Heumös slope as well as on the undisturbed soil cores in the laboratory. The high variability and overall low conductivity values makes interpreting data a challenging task. Very low conductivities mean long sampling intervals whereas macropores and shrinkage cracks lead to infiltrabilities much larger than sampling device limits allow to measure. Yet data is essential and sufficient to define dominating patterns of K_{sat}. Specific patches were selected for investigation so that the ecological moisture distribution mapping can help to scale the results of K_{sat} towards larger units.

Compact constant head permeameter

One compact constant head permeameter test location was located on the meadow at the height of spring 1, to define conductivities on the upper soil column of the moving hillslope body (Chapter 4.1.4, Figure 4-1). A second test site was placed near spring 1 in the forest to find out about contrasting behaviour on the southern slope. The high variability of measured values dominated the results on each test site.

- Forest: the upper two sampling depths showed similar results, the median is $2.4*10^{-5}$ m/s in a depth of 12 cm with an asymmetric distribution and a shift to higher conductivities (Figure 5-7a). In a depth of 20 cm the median lies at $1.6*10^{-5}$ m/s, again the focus of distribution is on higher conductivities in the box plot. A considerable amount of measurements without results was due to the high macroporosity of the soils in the forest. The upper high conductivity layers are quickly followed by less permeable soils in a depth of 50 cm. The three measurements there show an average of $1.5*10^{-7}$ m/s.

- Meadow: the range of observed conductivities in a depth of 12 cm is lower than in the forest, the median lies at $6.4*10^{-7}$ m/s and the distribution is more centred in the box plot (Figure 5-7b). The range of the box plot triangles in a depth of 20 cm is similar to the same range in the forest. The distribution is more centred as well and has a median of $1.9*10^{-6}$ m/s. The soil types of both measurement clusters are similar so that differences can be accounted to less macroporosity on the meadow. The three samples in a depth of 50 cm on the meadow have similar values than in the forest; the average hydraulic conductivity is $1.7*10^{-7}$ m/s. It indicates a lower permeability towards the depth.

The range of different K_{sat} values of the specific depths is significant. This range is not based on differences in soil matrix but on macropore distribution. The hillslope body features less macropores and less shrinkage cracks due to a higher moisture regime in general. This is also observable in the ecological moisture distribution. The forest has a higher distribution of macropores and shrinkage cracks. Not all cracks feature such large apertures as observed in the summer of 2006 but the conductivity of the cracks dominates infiltration and subsurface flow even in closed conditions. The low K_{sat} values in a depth of 50 cm on the meadow reflect the stagnic soil properties in lower depths.

Infiltrability

The hood infiltrometer tests need plane areas so measurements were only conducted on the meadow of the hillslope body (Figure 4-1). The infiltrability features high capacities in contrast to the K_{sat}-values of the constant head permeameter tests. The median of the 19 hood infiltrometer tests lies at $1.0*10^{-4}$ m/s and is therefore 2.5 magnitudes higher than K_{sat}-values in a depth of 12 cm (Figure 5-7c). Observations during precipitation events on the hillslope body also suggest that the very upper soil column, including the grass vegetation must be capable of taking up water in high quantities (Wienhöfer, pers. communication).

Slug tests in temporary groundwater gauges

Four slug tests in hollow core sampler holes on the northern slope and the hillslope body were conducted in an approximate depth of 1-2 m (Figure 4-2), in RKS 3, 6 and 9 respectively and in a depth of 2-3 m for RKS 1. Calculated conductivities for the shallow tests are in between $1.7*10^{-9}$ to $5.0*10^{-9}$ m/s (Figure 5-7c). The deeper test in RKS 1 showed slightly higher conductivities with $1.3*10^{-8}$ m/s but this is due to

not sufficient fixing of the bentonite seal and does not present higher conductivities in further depth. This value should be ignored. The slug tests generally show that very low hydraulic conductivities are encountered in greater depths in the hillslope body and strengthen the idea of an impermeable subsurface there.
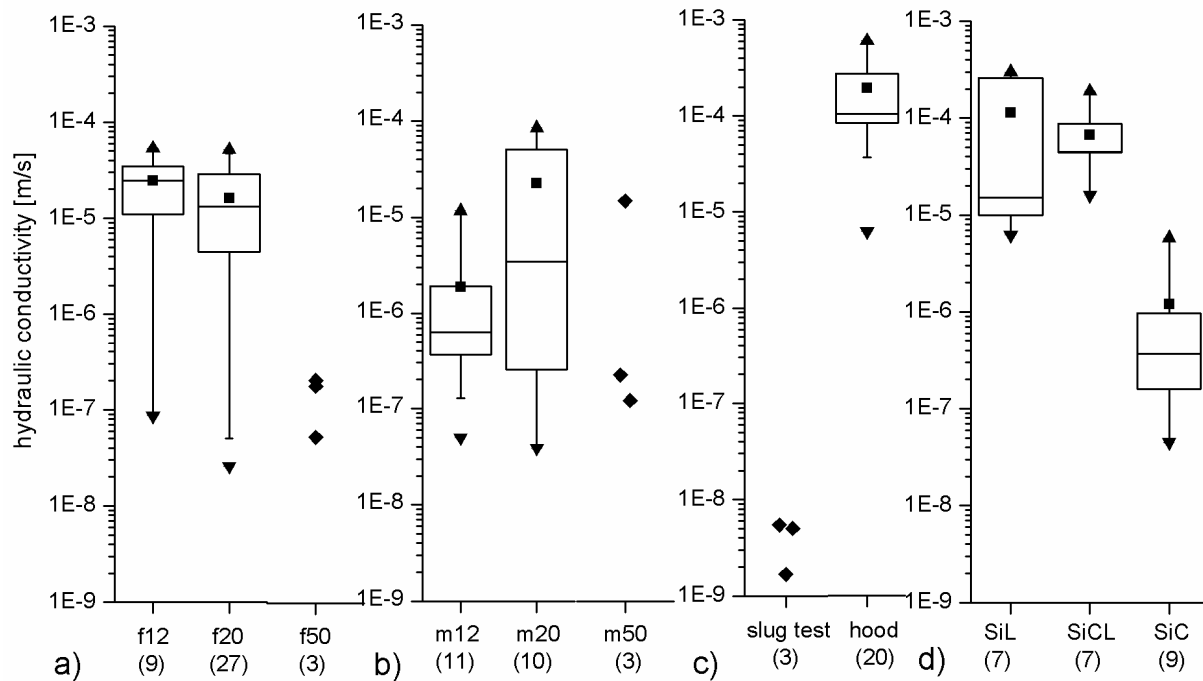
Figure 5-7: Soil hydraulic conductivity (K_{sat}) and infiltrability in a box plot display; a) K_{sat} of constant head measurements in the forest in a depth of 12, 20 and 50 cm; b) K_{sat} of constant head measurements on the meadow in a depth of 12, 20 and 50 cm; c) K_{sat} of slug tests in a depth of about 1-2 m and hood infiltrability values at the soil surface; d) K_{sat} of undisturbed soil cores, sorted by soil type. For explanation of box plots please refer to figure 5-5.

Undisturbed soil cores from soil profiles

The results from hydraulic conductivity determination in undisturbed soil cores (Figure 4-1) give a similarly differentiated picture of the measured soil hydraulic conductivity like the constant head permeameter measurements. The soil profiles were selected according to their ecological moisture regime, the box plots in figure 5-7d visualise the comprised sample distribution of the undisturbed soil cores according to their soil type.

- Profile 1 (Figure 4-1) was located on an area with relatively dry moisture conditions (ecological moisture: 5.5-6.4) on the northern slope. During sampling the soil material itself was dry and stiff. The lower two horizons showed a high number of samples (five out of eight) which did not react in the permeameter at all or so slow that evaporation could not be excluded in relation to water flow. Hydraulic conductivity in the uppermost horizon lies at an average of $1*10^{-5}$ m/s, for the lower horizons at $9*10^{-7}$ m/s, when non-reacting samples are excluded.

- Profile 2 was located in a wet, swampy area at the foot of the southern slope (Figure 4-1); ecological moisture class: 6.5-7.4). The consistency of the material was soft to very soft, roots of marsh plants hampered taking undisturbed samples. Hydraulic conductivity is in a range from $4*10^{-5}$-$2*10^{-7}$ m/s; the median is $1*10^{-5}$ m/s (average $2*10^{-5}$ m/s) for 7 samples of two horizons. However, the K_{sat} is

suggested to be very low in the lower horizons as the soil definition and the long-term moisture conditions suggest a stagnic soil layer.

- Profile 3 (ecological moisture: 7.5-8.4) was adjacent to an erosion gully of creek 1, approximately 0.5 m were dug away from the surface cut of the creek, yet some disturbances from horizontal leaching or erosion were suspected. The hydraulic conductivity of all three horizons (10 samples) show a wide range of K_{sat} from $3*10^{-4}$ m/s to $2*10^{-7}$ m/s, the average is $9*10^{-5}$ m/s; the median is $4*10^{-5}$ m/s.

Table 5-4: Horizon wise measured soil hydraulic conductivity for undisturbed soil cores; *macropore* and *no reaction* means that hydraulic conductivity is outside the measurement range of the laboratory permeameter device.

profile – horizon after AG-Boden (1999)	soil type	sample 1 [m/s]	sample 2 [m/s]	sample 3 [m/s]	sample 4 [m/s]	moisture during sampling
G1 – Sd	Tu3	macropore	2.6E-04	1.5E-05	6.2E-06	dry
G1 – Sw	Tu3	2.0E-07	4.5E-08	no reaction	no reaction	dry
G1 – eCv	Tu3	2.5E-06	no reaction	no reaction	no reaction	dry
G2 – Srw	Tu3	macropore	4.5E-05	1.0E-05	9.6E-07	wet
G2 – Srw-eCv	Lu	4.5E-05	2.8E-05	9.3E-06	1.6E-07	wet
G3 – Ah-Srw	Tu2	macropore	1.9E-04	5.8E-05	1.6E-05	moist
G3 – Srw	Tu2	3.0E-04	2.0E-04	5.6E-07	3.7E-07	moist
G3 - eCv	Lu	macropore	8.8E-05	5.8E-06	1.6E-07	moist

macropore: sample with conductivity above detection limit
no reaction: sample with no flow reaction in 12 hours

The estimation of saturated hydraulic conductivity with undisturbed soil cores is a relatively simple method, yet it has the drawback that the device is designed rather to measure matrix hydraulic conductivity in silty to sandy samples than a combined hydraulic conductivity of matrix and macropores in clay samples. The wide range of hydraulic conductivity measured in single horizons with differences of up to three orders of magnitude in the three profiles (Table 5-4) indicates that both samples with a clear matrix dominated hydraulic conductivity as well as samples with preferential flow paths are found in the soil horizons, even though cracks and macropores were not visible during taking the samples. This is backed by the amount of samples which either showed no reaction at all or fast reactions outside the measurement range. It also means that matrix hydraulic conductivity is not in favour for water infiltration in contrast to preferential flow paths referring to the laboratory permeameter tests.

6 Climate and hydrological process identification

The following chapter comprises the results from the analysis of gathered hydrometeorological measurements. Special focus is on precipitation and runoff time series investigation. Precipitation is the most variable factor influencing the hydrological system. Runoff generation is a reaction on rain- and snowmelt events. Its close investigation gives an idea on what processes dominate the water balance of the hydrological system of the Heumös slope.

6.1 Precipitation and meteorological setting of the upper Dornbirn Ache catchment

The shape of the state of Vorarlberg has an elongated north to south alignment, which mirrors the mountain ranges of the Vorarlberg Alps. These open towards the west to the Bodensee and the upper Rhein valley. Dominant wind directions from the west unload their water masses at the edge of the mountains, leading to higher precipitation rates in the west than the east of Vorarlberg (Werner & Auer, 2001). Additionally, orographic and land-sea effects from the Bodensee influence the precipitation regime in the Dornbirn Ache valley, enhancing convectional rainstorms in the summer.
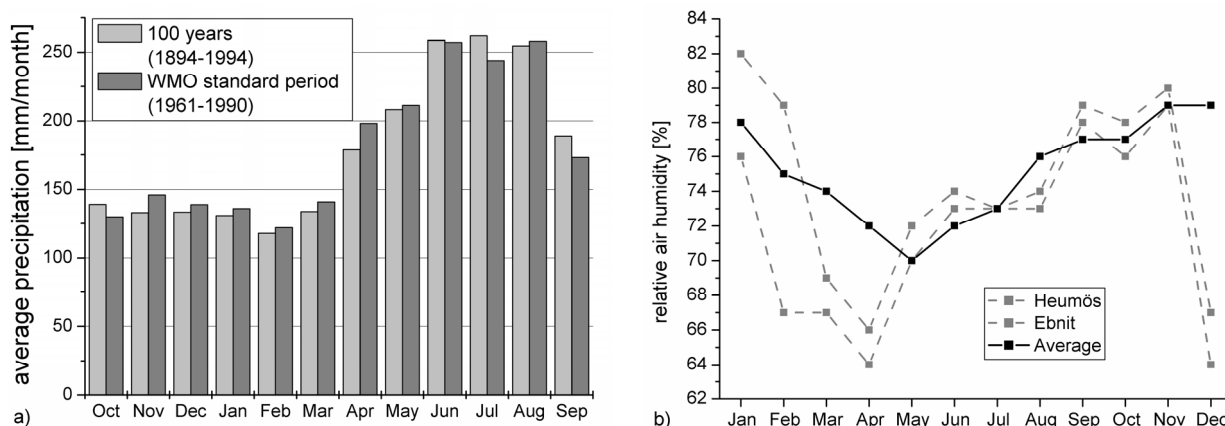
6.1.1 Precipitation

The hydrological year is defined through the separation of months with high precipitation depths from months with lower precipitation depths, it spreads from October of the previous year to September of the regarded year. The average yearly precipitation depth for the Ebnit church rain gauge is 2155 mm for the WMO standard period from 1961 to 1990 and 2139 mm for the years from 1898 to 1998. The record yields values typical for orographical heights of 1000 to 1100 m a A in the Vorarlberg Alps (Werner & Auer, 2001). The "rainy" season includes six months, April to September respectively. These months have average precipitation depths of more than 150 mm and up to 250 mm per month; they are referred to as "summer" in the text. The "dry" season has lower monthly precipitation depths. Less than an average of 150 mm usually fall in October to March; these months are referred to as the "winter" season.

In the winter months, precipitation might fall as snow but May, June and September may feature some snow events, too. The snow cover normally becomes permanent around end of December and stays until March. Some of the observed years from 1998-2006 showed rather abnormal behaviour of late snow fall with first snow fall in February or March and a snow cover until April. Snow coverage was below average in the observed years except for 1999 and 2006. The soil usually is water saturated before snow accumulation and does not freeze. So that it is unlikely that snow cover has a large impact on soil moisture during snow coverage. It is considered that snow accumulation and melt do not influence greatly the water balance of summer periods, as the baseflow of the creeks is quickly reduced to very low values after snowmelt. The existing database is not sufficient yet for a detailed investigation of the influence of snow cover, more specific observation devices are needed therefore and were recently installed.

It is an important question of how to identify critical precipitation events which might influence the mass movement. The recorded precipitation regime of the Ebnit church rain gauge is extreme, compared to non-alpine situations in Central Europe but is likely found in similar alpine regions and orographic heights. The Heumös weather station rain gauge yields results which are in close accordance to the Ebnit church rain gauge but data gaps are more abundant and larger for the Heumös rain gauge (Chapter 4.2.1). This is why Ebnit church is used for the investigations. The variability of precipitation is generally high as it is coupled to the general weather regime of Central Europe. The measured precipitation time series

need to be investigated in regard to precipitation patterns, despite the assumption that precipitation occurrence, intensity and duration might be coincidental. The definition of dominating precipitation patterns will help to identify events, event types, succession of events or certain thresholds which need to be exceeded to trigger movement in the hillslope body of the Heumös slope. Two different types of precipitation events are identified and discussed in the following.

Figure 6-1: a) Average precipitation per month for the Ebnit church rain gauge for a 100 year period and for the WMO standard period. April to September average more than 150 mm; June to August have maximum average sums. October to March have average precipitation depths below 150 mm. b) The average monthly air humidity for 2004 and the calculated long term average air humidity by Werner & Auer (2001). The shift between the Heumös and Ebnit gauge is about 3 % and of technical origin. Each half a month are missed in January and February 2004 in the Heumös station data, which results in lower average values.

Long lasting events with high precipitation depths

Long lasting precipitation events with large depths occurred regularly in the recent years and could have been the cause for small-scale and shallow landslides through the saturation and mobilisation of the clayey unsaturated soil zone. Wetting might have been so extreme that the upper soils developed into small-scale earth flows. Two extreme precipitation events occurred in May 1999, inducing several landslides in the area, see also Keusen (2000), Schütz (2000) and Eberhardt (2005). In the Ebnit Ache valley several small-scale slides were observed but no large movements. Events in August 2000 and August 2005 also exhibited extreme precipitation depths which were critical for shallow landslide development and produced damage across the region. Table 6-1 gives an overview of events larger than 100 mm which occurred between 1998 and 2006. The events were extracted with the automated event selection method (= selected events) described in chapter 4.3. The criteria of ending an event after six hours of no precipitation split some of the largest events. They were merged again manually. Additionally, days with maximum precipitation are listed in table 6-1.

The event of 22-23/08/2005 was so far the most extreme in precipitation depth and damage since recording begun 100 years ago (Kanonier *et al.*, 2005). Together with the events in May 1999 and August 2000, which also brought high damage, a culmination of extreme events has been observed since the 1990's. Kanonier *et al.* (2005) estimated a return period of 75 to 150 years for the daily precipitation depth in August 2005. The extreme event from 22-23/08/2005 shows discrepancies in the database: the Heumös station reported 248 mm for both days, whereas Kanonier *et al.* (Kanonier *et al.*, 2005) reported

a daily precipitation depth of 220 mm for the 22nd alone. The time series from Ebnit church rain gauge features precipitation depths which are too low. Especially precipitation signals are missing on the 23rd so that data from the Heumös station is preferred for the evaluation of this event.

This long lasting event type is characterised by a prolonged duration of more than 24 hours with almost constant precipitation and only small precipitation-free periods. The average intensity during such an event is often larger than 1 mm (Table 6-1).

Table 6-1: a) Selected large precipitation events with a sum greater than 100 mm for the period of 1998 to 2006. b) Maximum daily precipitation depths. Gaps in the Ebnit church rain gauge database are completed by literature data and rain gauge data from the Heumös station.

a) date of event	precipitation depth [mm]	duration [h]	average intensity [mm/h]	b) day	daily precipitation depth [mm]
Summer				22.08.2005**	155.2
10.06.1998	144.5	66.0	2.19	11.08.2002	142.2
10.05.1999	210.1	110.7	1.90	21.05.1999	122.8
20.05.1999	209.9	74.0	2.84	06.08.2000***	120.0
21.06.1999	108.7	38.5	2.82	05.10.2003	116.9
07.07.2000	118.7	123.2	0.96	12.05.1999	98.8
08.06.2001	102.6	83.7	1.23	23.08.2005**	97.1
17.06.2001	103.8	47.8	2.17	12.06.1998	87.5
04.09.2001	107.4	48.2	2.23	17.07.2002	81.5
10.08.2002	205.1	68.3	3.00	28.04.2006**	78.3
22.09.2004*	147.2	101.5	1.45	07.06.2002	73.7
22.08.2005**	248.2	37.7	6.95	03.06.2004	73.0
28.05.2006*	123.3	77.2	1.60	21.09.2000	68.4
Winter				22.05.1999	67.0
14.03.1998	107.7	66.7	1.62	28.11.2003	66.2
16.02.1999	202.3	177.0	1.14	21.06.1999	66.1
14.03.2000	192.1	137.7	1.40	09.10.2003**	64.6
08.04.2001	107.0	146.8	0.73	05.09.2001	64.4

*   City of Dornbirn database from the Ebnit church rain gauge
**   database from the Heumös rain gauge
***   data from Kanonier (2005);
All other data from the Ebnit church time series (digitised and digital data from Hydrographischer Dienst Vorarlberg, Austria)

High intensity summer storm events

Average precipitation intensity rises in the summer months, indicating more convectional types of precipitation events (Figure 6-2a). The average intensity of events more than triples from January (0.83) to July (2.64). Outliers are more frequent in the summer months, the average is also oblique towards higher intensities. A trend towards events that are accentuated in the beginning is observed in the summer. The histogramme in figure 6-2b is derived from the selected events (Chapter 4.3). The average intensity of each event is calculated and plotted for summer and winter events. Events with an average of more than 3 mm/h indicate summer events, these have an explicitly higher occurrence than winter events. In table 6-2 a selection of summer events is displayed, which is also displayed in forthcoming discharge or model investigations. The average and maximum intensities are high, precipitation depths are at least 25 mm or more.

A shift towards the dominance of convective events is also expressed in the dominating beginning times of precipitation events. In winter there is no dominant beginning time. In summer a majority of events begins around 5 p.m., which indicates a favourite time for convectional events in the late afternoon. A storm event statistic including the years from 1950 to 1993 (Hydrographischer Dienst Vorarlberg, Austria) shows the same characteristical features. Interestingly, a second peak was found at 6 a.m. in the

digital data set. This is an effect of dew precipitation in the morning recorded by the more precise digital precipitation gauge with the digitised paper strips do not show this effect.
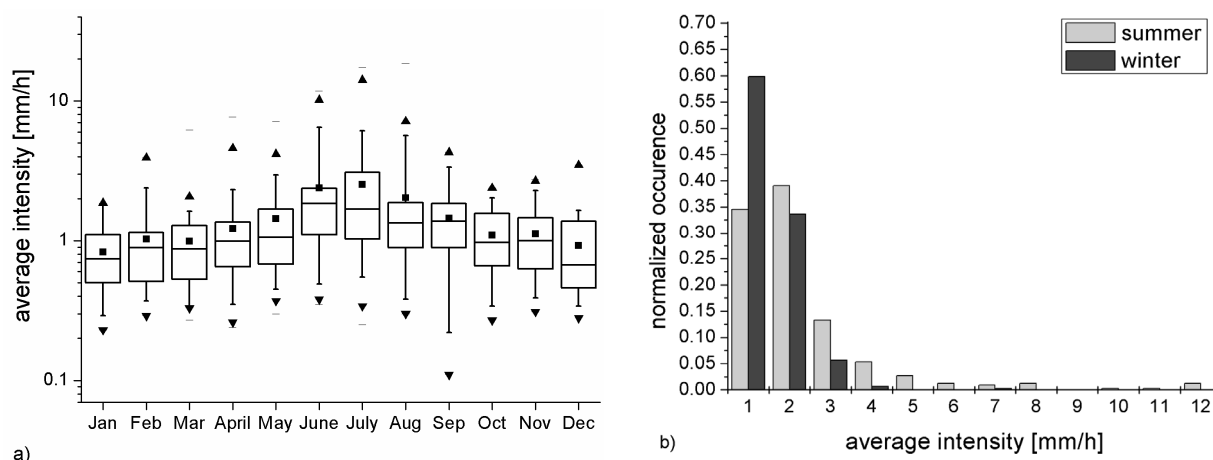
Figure 6-2: a) Box plot of average precipitation intensities from January to December for all selected events (1998-2006). Events include precipitation free time intervals. For explanation of box plots please refer to figure 5-5. b) occurrence of average precipitation intensities in winter and summer, intensities of 3 mm or more characterise summer events.

Table 6-2: Selected typical precipitation events in the summer with a maximum duration of 24 hours.

| event begin	precipitation depth [mm]	precipitation duration [h]	average intensity [mm/h]	maximum intensity [mm/10min]
20.09.2000 15:50	95.4	24.2	3.95	3.3
11.05.2002 14:20	32.6	16.7	1.95	5.0
18.05.2002 17:00	42.4	14.3	2.96	3.2
19.06.2002 15:50	25.4	2.5	10.16	12.8
03.07.2002 17:10	40.1	13.5	2.17	2.7
12.08.2004 17:40	32.2	4.5	7.16	7.2

6.1.2   Temperature, air humidity, wind and global radiation

The following chapter compares values from the year 2004 (Figure 6-3). This is an exemplary year with fairly complete records from the Heumös weather station as well as from the Ebnit weather station. The average measured temperature on the Heumös slope and in Ebnit in 2004 is about 7° centigrade. This is slightly higher than calculations from Werner & Auer (2001) with 6.2° centigrade for the topographic height of 1000 m. Werner & Auer (2001) also state that the average temperature is more influenced by the orographic height of the station than by the exposition of the area.

The relative air humidity is rather moist. The distribution of hourly values shows a maximum at 80 to 90 % relative air humidity content for Ebnit and for the Heumös slope in 2004. In Figure 6-1b the average monthly air humidity for both stations is plotted with the calculated values for 1000 m a A from Werner & Auer (2001). Despite temporal variations the calculated average monthly air humidity is resembled in the 2004 curves.

The dominant wind direction is influenced by the exposition of the valley. The surrounding mountain ridges lead to low wind conditions in the valley. The maximum average wind speed in Ebnit was 5.6 m/s in 2004, it is measured in 10 min time intervals by the device. On the Heumös slope it was 5.0 m/s. The absolute maximum wind speed in a gust of wind was 15.7 m/s measured with a specific device. Rising and falling winds are recognised on the Heumös slope and in Ebnit at most times of the year. Rising

wints at night (18:00-5:00) and the early morning dominate the wind direction in an angle of 280° from the north (west wind), parallel to the west – east direction of the slope and adjacent ridges (Table 6-3 and Figure 6-3). During the day (6:00-17:00) falling winds dominate with an angle of 90°-100° (east wind). The occurrence of falling wind directions is yet less than for rising wind directions. During precipitation episodes, wind direction shows the same maxima than for no precipitation episodes but the variability is greater. In frost periods the device can freeze; this happened for example in the months of January and December 2004 (Figure 6-3).
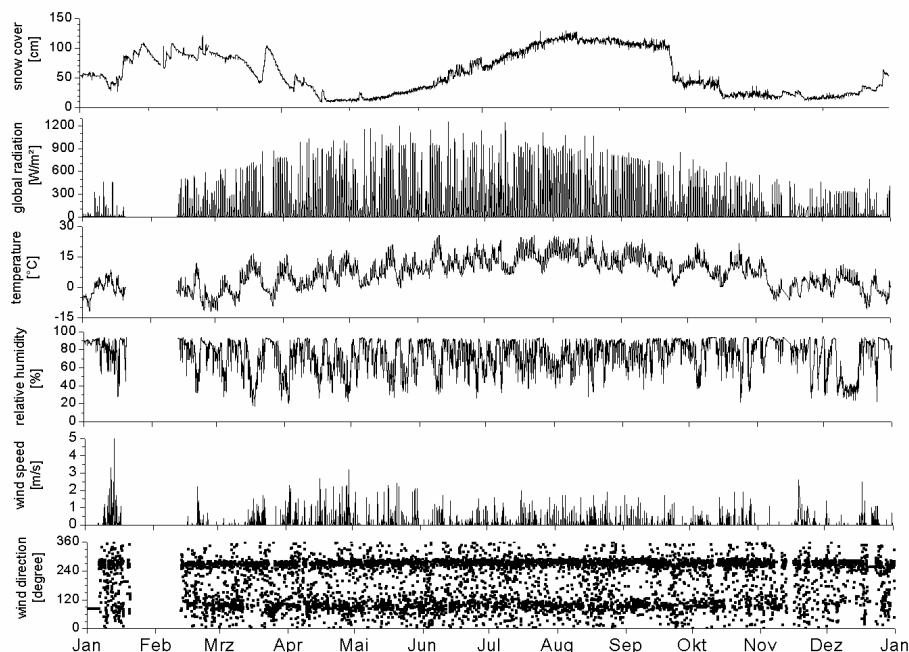
Figure 6-3: Climate data for the year 2004 for the Heumös station: 2004 can be taken as a typical year for climate variability and has a good data coverage. From the top: snow height in cm (data is corrected with temperature, the summer section of the curve displays vegetation growth); global radiation in W/m²; temperature in °C; relative humidity in %; wind speed in 2 m height in m/s and wind direction in 360° displayed as time series with hourly values. Dominating wind directions are less pronounced during precipitation events.

6.1.3 Evapotranspiration

Ebnit has a moderate mountainous climate regime. A good estimation of the evapotranspiration depths is valuable because it is a part of the long-term water balance of the hillslope and helps to reduce the uncertainty of discharge time series. Several approaches and comparisons were used to estimate evapotranspiration. Werner & Auer (2001) classified the potential evapotranspiration depth in steps for the Vorarlberg Alps to be 500-600 mm/year for heights of more than 1000 m a A and 600-700 mm/year for an orographic heights of up to 1000 m a A. The Partenen weather station, Vorarlberg, which lies on a similar orographic height (1028 m) than Ebnit (1050 m), has a calculated yearly evapotranspiration depth of 556 mm. The standard equation for the calculation of the potential evapotranspiration in Austria (Werner & Auer, 2001) is *ETP = 690,6 – 0.068Z-1.581*10-8*Z³* (mm/year), with *Z* being the height above Adria in metres. This would calculate a yearly evapotranspiration depth for Ebnit church of 600 mm.

Table 6-3: A comparison of values of temperature, relative air humidity and global radiation from the Heumös weather station and city of Dornbirn meteorological devices for 2004; Figure: Wind rose of hourly values for the weather station on the Heumös slope, parted into day (6 am – 5 pm) and night (6 pm – 5 am).

	Temp. Heumös [°C]	Temp. Ebnit [°C]	Air humidity Heumös [%]	Air humidity Ebnit [%]	Global radiation [W/m²]
average	7.2	6.7	73.8	71.6	123.9
median	7.6	7.0	78.6	76.1	1.00
minimum	-12.1	-11.5	17.3	13.4	0.00
maximum	25.8	26.0	94.4	95.0	1256.0
standard deviation	7.5	7.6	17.6	16.5	226.85
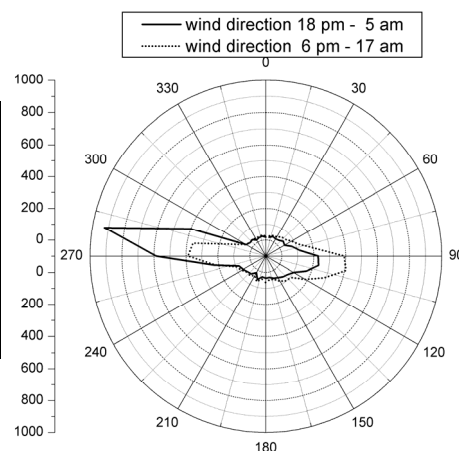
The available data from the Heumös weather station and Ebnit weather station were used to calculate annual evapotranspiration depths after Haude (1955) using a Haude-factor for grass vegetation after Löpmeier (2001). Missing data for the Heumös weather station adds up to 16-84 days for each year (Chapter 4.2.1, Figure 4-5) so that yearly values are too low and can only be used as a rough estimation. The coverage for Ebnit in the years 2004-2006 is better in this respect. The years 2002 and 2004 to 2006 are within the regional range for evapotranspiration depth (Table 6-4). The year 2003 was an extremely hot and dry year and therefore shows an extraordinarily high value. Calculations of evapotranspiration after Haude is valid only for daily sums smaller than 7 mm/day. In the summer of 2003 these values are topped for several months. The Haude values are generally lower compared to regression data from Werner & Auer (2001).

Table 6-4: Evapotranspiration depths for several years with good data coverage.

Year	Evapotranspiration depth after Haude on the Heumös slope (1.10. – 31.09.) (amount of missing days in brackets) [mm]	Evapotranspiration depth after Haude in Ebnit (1.10. – 31.09.) [mm]	Evapotranspiration depth after Penman-Monteith, calculated with CATFLOW on a single grass covered slope. [mm]
2002	443 (84)	n.a.	665
2003	615 (17)	n.a.	683
2004	453 (23)	475 (0)	584
2005	432 (16)	424 (0)	n.a.

The model CATFLOW uses a Penman – Monteith approach after Kolle (1996) for calculating evapotranspiration, including specific plant properties and soil hydraulic conditions (Chapter 8.1). For the CATFLOW calculations a single grass-covered slope exposed to the north was used. A detailed description of the slope is given in chapter 8.3. Gaps in the time series for the calculations were filled with periods of either the Ebnit time series or adjacent years, unless the gaps were situated at the beginning or end of the respective hydrological year (Chapter 8.2.5). The results of the CATFLOW evapotranspiration calculation are closer to the average values of Werner & Auer (2001) than the Haude values (Table 6-4). The detailed Penman – Monteith approach after Kolle (1996) calculates the most reliable yearly evapotranspiration depth for the Ebnit region despite of the lack of a snow accumulation and related sublimation in CATFLOW.

6.2   Results from creek discharge observation

Channel runoff is one of the most important and most traditional evaluation factors in hydrological sciences. It helps to understand the water balance of a catchment area. It is the product of runoff-generating processes combined with sinks like deep infiltration and evapotranspiration. In classical hydrology it is the standard variable for comparison. This works relatively well in large or in lowland headwater catchments. In mountainous areas precise observation becomes more difficult and the runoff volume as calibrating variable for studies or numerical models looses its advantages, e.g. through the clogging of the weirs by debris. Considering such restrictions, it is no surprise that hydrological studies of landslides seldom include discharge observations (Chapter 2.2.5). Catchment studies in mountainous regions show that runoff-generating processes are more diverse and not fully understood so far (Casper, 2002; Gräff, 2004; Gräff *et al.*, 2007; Kirnbauer *et al.*, 2001). This chapter will provide results of the observation and investigation of discharge time series on the Heumös slope. A synopsis of the runoff generation processes and dominating spatial patterns will be made in chapter 7.2.

6.2.1   Comparable time spans, short term budgets and data quality

The periods from May to August 2002, May to July 2004 and July to September 2006 were chosen for further analysis. In these time spans the weirs were almost debris-free. Despite good recording conditions during these time spans the data might still contain errors.

In figure 6-4a the precipitation depth and the discharge sum are plotted for May 2002. Field observation show that the recession is quick, the baseflow is generally very low for all catchments and that the baseflow is adjusted to low levels quickly after snowmelt or rainfall events. These observations are helpful to set up water balances for shorter periods than a year: snowmelt discharge ceded on 22/04/2002 and was followed by a rainfall event for the plotted month in figure 6-4a. On May 1st the recession of this event ended and baseflow was at its minimum. Hence, a closed monthly based water balance should be expected. Creek 1 plots below the precipitation line in figure 6-4, this seems to be the best observation for this time span. Creek 2 overestimates the last event. This could be either due to a diverse precipitation on the southern slope where creek 2 catchment is located, or the rating curve relation changed during this event. Creek 3 plots too high for all events (solid green line, figure 6-4a). A baseflow adjustment of the measured water height shows more likely results. The water height was reduced by two centimetres (dashed green line) and the discharge was recalculated with the rating curve again.

In 2004, creek 3 was filled with gravel faster than creek 1, usually this is the other way round. Figure 6-4b shows the influence of the gravel clogged weir on creek 3 discharge measurement. The peaks are less sharp and an artificial retention is observed. The 2006 data is from digital devices and debris clogging could be recorded well. Debris was removed on July 28th, 2006 in creek 1 and creek 3. The creek 3 gauge stayed debris-free all summer and autumn, whereas creek 1 was partly clogged in September.

Short-term water balances and precipitation depths allow conclusions about the specific data quality in the investigated period. It is possible to close the balances for specific summer periods when weirs are debris-free. Retention of water in the catchments is low. The pre-event water level is reached shortly after precipitation ceased. This means that the unsaturated zone and groundwater storage is of minor importance for reaction on the catchment scale. This will be discussed in further detail in the following text. It simplifies a comparison of measured time series with the model performance in chapter 8.4. The mentioned, good quality snowmelt-free summer periods were taken for comparison to suit this demand.
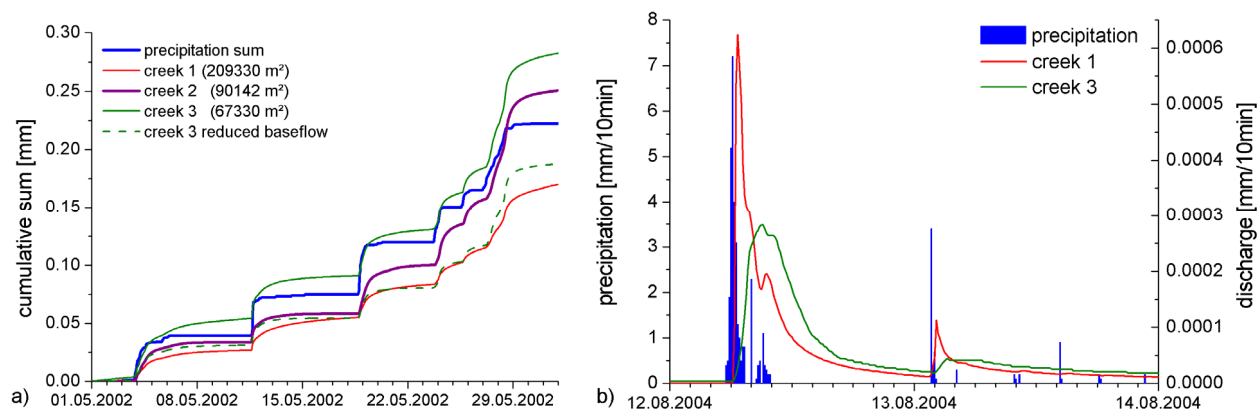
Figure 6-4: a) Precipitation and runoff sums for May 2002. Creek 3 (Heumös creek) plots too high. Two centimetres were subtracted from the water height and discharge was recalculated, 2 cm water height correspond to 0.8 mm on the paper strip. b) Influence of gravel in the weir: creek 1 is gravel-free; creek 3 is filled with gravel. Peak height is reduced, reaction time is extended and the shape is damped.

6.2.2 Discharge reaction and runoff coefficients

The recession curves and reaction times show differences for all three catchments. These are influenced by different translation and retention factors but a consistent pattern is difficult to determine due to the data uncertainty. The small catchment sizes and the steepness make it difficult to determine between errors and differences derived due to topography or different hydrological processes. It is noteworthy that a correlation of the creek 3 time series and time series of the Enz gauge of the Dornbirn Ache catchment (50 km²) has a correlation coefficient of 0.96 with a time lag of approximately 1 h. This means that translational forces dominate before retention in the catchments, even for the Ebnit Ache catchment.

The investigation of the precipitation – discharge relation shows a quick reaction on precipitation or snowmelt. The runoff response often begins with onset of precipitation, the maximum being 1-2 hours after the maximum precipitation intensity. This is observable for the 2004 and 2006 events, which feature digital data precisely in temporal resolution. The quickness of a reaction is dependent on antecedent climate conditions and precipitation. Moist conditions and a rainfall event accentuated in the beginning show a reaction of the discharge in between the first 15-30 minutes of the event. With drier antecedent conditions an initial loss and delayed reaction is observable.

A simple comparison of the rainfall-discharge sums and calculation of runoff coefficients is most applicable for a comparison of the catchments. As events are often successive, baseflow separation is often hampered: baseflow in dry condition is below 1 l/s, maximum discharge runs up to more than 200 l/s for creek 3 and more than 350 l/s for creek 1 (see Appendix F-1). Generally, baseflow is only slightly higher in winter than in summer but there is no long enough observation with digital devices and without debris clogging so far for the summer and winter to determine more exact values. Snowmelt leads to typical, temperature driven discharge curves.
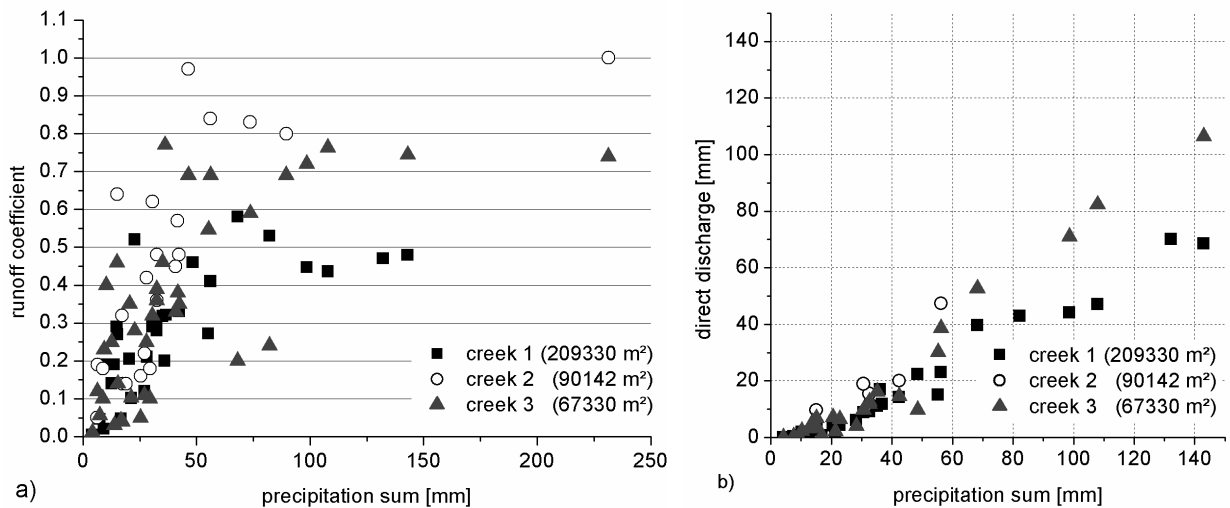
Figure 6-5: a) Plot of precipitation sum versus runoff coefficient for all creeks, high precipitation sum lead to runoff coefficients near 1.0, b) plot of precipitation sum versus direct discharge. The average loss seems to get constant with higher precipitation sums.

In figure 6-5a the relation of the calculated runoff coefficients to the total precipitation is plotted. The plot shows that small precipitation depths, also lead to significant high runoff coefficients. With increasing precipitation depths, the runoff coefficient tend towards one. The spread of runoff coefficients for the same events of different creeks is rather due to data uncertainty.

Figure 6-5b plots direct discharge versus total precipitation showing a weak exponential course at the beginning and a straight line from 20 mm of precipitation on. This means that the initial loss for small events is high but changes to a constant initial loss from a certain threshold on, approximately 20 mm or more.
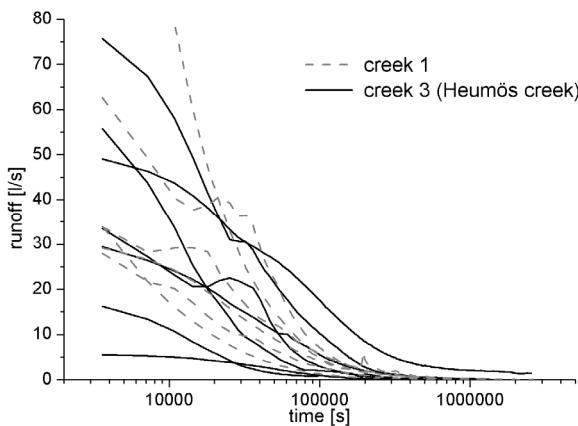
Event	creek 1		creek 3	
	late time [d]	early time [d]	late time [d]	early time [d]
22.05.2004	2.13	0.64	2.08	0.54
24.07.2004	2.15		2.61	0.26
30.08.2004	3.24		1.18	0.67
12.09.2004	0.77		0.79	0.20
23.11.2004	3.16		3.53	0.91

Figure 6-6 and table: Comparison of selected recession events for creek 1 and creek 3 in summer 2004. *K*-factors show similar recession behaviour, differences due to steepness of sub-catchment or channel length are not distinguishable.

Runoff coefficients are high in general, small events like the 06/08/2002 event with 6.41 mm of precipitation still has a runoff coefficient of about 0.12-0.19 for creek 2 and 3. Runoff coefficients of the 48 investigated events show a median at 0.34 and an average of 0.39. It is stated that in summer months more than a third of the precipitation is directly removed from the catchments. A relative high initial loss can be observed after longer periods without precipitation.

6.2.3   Recession analysis

A recession analysis (Chapter 4.3) was conducted for five events of creek 1 and 3 in summer 2004. Both creeks have similar time factors for recession. Two response times were distinguishable. The first and fast response time lies at about 0.2 to 1 day; the longer recession lasts for 2 to 3 days. The discharge declines fast and is supposedly only governed by surface runoff generation and return flow. The recession factors can be compared to recession factors of the spring and the piezometer devices (Chapters 6.4.3 and 6.4.3), differences or similarities of recession factors can be used as proxies of similar storage for the different compartments of creek discharge, spring discharge and groundwater table changes. A discussion in more detail will follow in chapter 6.5.1.

6.3   Soil moisture

The Heumös slope weather station is equipped with four Time Domain Reflectometry (TDR) rods to continuously measure soil moisture in a profile. Two rods are installed in 20 and 35 cm below the surface, two rods are installed in a depth of 50 and 60 cm. Dittfurth (2002) defined the ecological moisture with a wetness index of 7.5-8.4 for this area (Figure 3-9). This means that the area around the Heumös slope weather station can be considered moist to wet throughout the year. The soil is defined as a stagnic gleysol (Chapter 5.2.2). Two different points of view will be taken on the TDR signals: first an overview of the long-term variability on a yearly basis is discussed. Secondly, a closer look on times with event-based reactions will be taken. The rods at a depth of 35 and 55 cm show the most similar behaviour. The other two rods each show differing or even opposing behaviour in general but also have similarities.
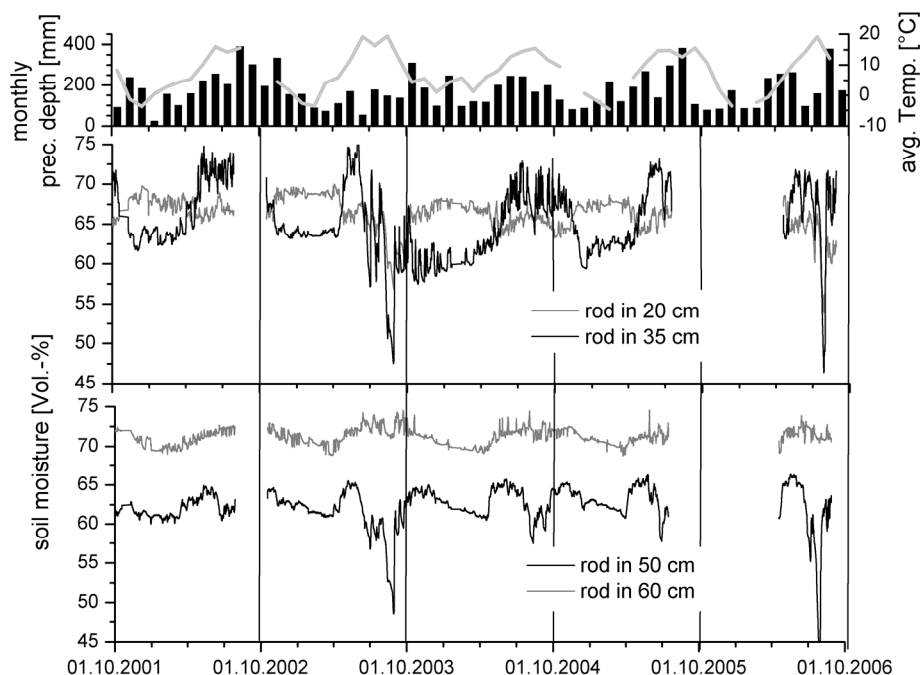
Figure 6-7: Monthly sums of precipitation for observation period of signals of the TDR-rods. All four rods are plotted, data is smoothed and rounded. The winter - summer periodicity is influenced by soil temperature and does not show lower soil moisture content in winter. Reactions of the 35 and 50 cm rod are notable. The other two rods seem to be shielded or defect.

6.3.1   Seasonal soil moisture variation

All TDR rods, except the one in a depth of 20 cm show a signal with higher values in summer and lower ones in winter (Figure 6-7). This is a rather odd observation: less evapotranspiration would imply higher moisture contents despite lower precipitation values in winter. The subsurface does not seem to be frozen when snow covers the soil surface, too. The lower values in winter account for a temperature effect in the rods as observed by Wraith & Or (1999). Values should be ignored in winter principally. Value changes during the winter period are very likely not accounted for real moisture changes but for bias of the rods. The opposing long-term signal of the 20 cm rod is attributed to a technical defect. This rod signal should not be considered further in the investigation of seasonal variation.

It must be noted that the maximum range of volumetric moisture values is very small for all rods despite the long-term temperature effect. Only long precipitation-free periods lead to a significant drop of the moisture signal. This is most pronounced in the 35 and 50 cm rods. The range of moisture for the 35 cm rod is between 47 and 77 vol.-%. The 50 cm rod has a range from 48 to 67 vol.-%. The very small values are only reached twice in 2003 and 2006 as it is shown in figure 6-7, usually the values do not drop significantly lower than the average. The 60 cm rod seems to be installed in a shielded location as the moisture value change ranges in between 68 and 75 vol.-%. This range is not considered to be of significance.

The 35 cm rod shows a continuously high value in wet summers. The volumetric water content can only drop significantly during extended warm periods e.g. in the summer 2003, from July to August 2004 and in July 2006. The 50 cm rod shows a similar behaviour. This means that the soil moisture variation is near or at saturation during an annual period. Only extreme dry periods lead to a reduction of soil moisture. Hence the variation of the soil moisture is solely due to evapotranspiration, deep infiltration is not a dominating process in the stagnic soils of the Heumös slope.

6.3.2   Event-based soil moisture variation

To understand the event-based behaviour one has to consider the overall soil moisture state which depends on seasonal fluctuations but also to a significant extent on the fact of how much precipitation fell during the preceding weeks or days. The 35 cm rod shows fast and pronounced reactions when the soil moisture state is dry. This is also observable in the 50 cm rod but with a less significant signal (Figure 6-8a). In 2004 monthly precipitation depths were close to the long-term average, please also compare chapter 6.1. The upper soil column showed drying and wetting cycles in relation with precipitation events in figure 6-8a. The 50 cm rod was in a saturated condition until the dry period at the end of July. After then, damped reactions are observable as well in this rod.

A similar behaviour was seen in 2006 (Figure 6-8b): snow until early June means a wet moisture state with no event-related soil moisture reactions for the rods. The unusually dry July then lead to reaction of both rods. The intense precipitation in August stands in contrast to high evapotranspiration rates. This means reduced but still visible reactions of the 35 cm rod. The 50 cm rod showed no or damped event related reactions. This means that the soil moisture changes in the soil column is dominantly driven by evapotranspiration and not by drainage into deeper soil columns. In autumn and winter event related soil moisture changes were usually not observable, even in the upper soil column.

The fast and pronounced reactions of both rods are ascribed to shrinkage crack development in dry periods which enhances a local drying of lower soil layers. The low matrix conductivities observed in lower horizons do not support the process of matrix infiltration to be the reason for these quick reactions.
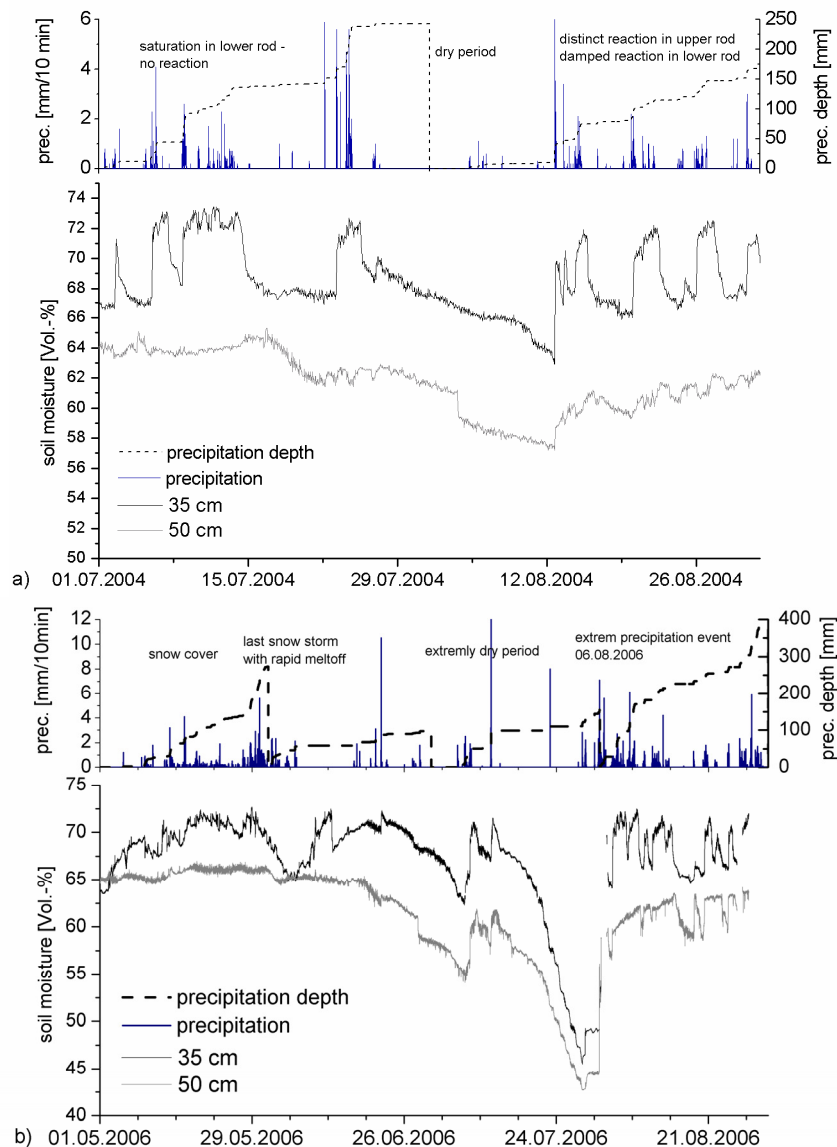
Figure 6-8: Soil moisture reaction due to evapotranspiration in the summer of a) 2004, a moderate wet year and b) 2006, with an unusually wet May and dry July in a moist patch near the Heumös weather station. Please note that moisture changes are small, e.g. compared to sandy soils: the lowest rod features maximum range of 7 vol.-%, single events feature changes of 1 vol.-%. Cumulative monthly precipitation and 10 min precipitation time intervals are also plotted.

6.4 Groundwater

The groundwater observation on the Heumös slope was conducted with piezometer devices in the clay-rich subsurface and through spring discharge reaction observation (Chapter 3.1). The spring is located at the transition of the southern slope and the hillslope body. The distance from the piezometer location to the spring is 280 m upslope (Figure 3-3). Unfortunately, the piezometer equipment failed in September 1998, the same month when the surface and spring discharge observation started. Therefore, overlapping time series of the piezometer and spring are rare for the quantification of groundwater fluctuation and recharge on the Heumös slope. The overlapping time series in figure 6-9 show that the spring discharge is

similar to the piezometer reactions and that surface runoff is not related to piezometer reactions. Certainly, two observed events are not enough to quantify what kind of precipitation event leads to groundwater reaction, or to see weather all spring reactions are related to a groundwater fluctuation.
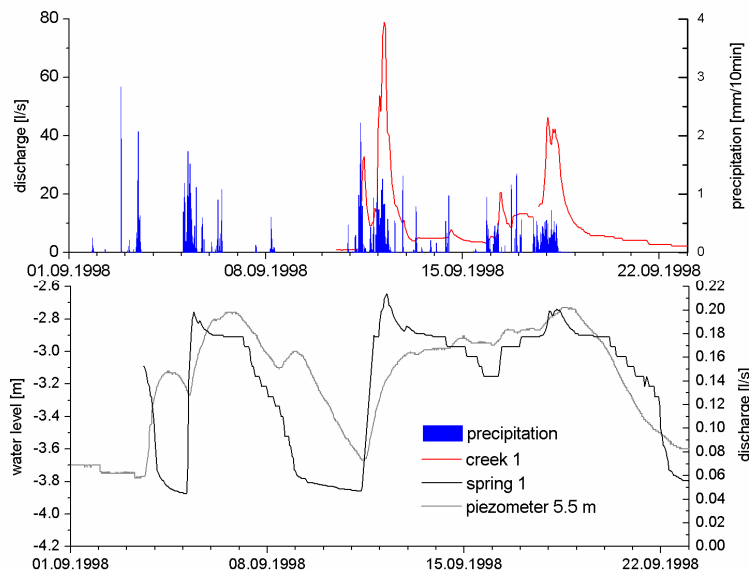
Figure 6-9: First creek and spring discharge time series and piezometer reaction in 5.5 m depth before the device failed. Note the fast reaction and elongated spring discharge and piezometer rise after certain events. The fast decline of the surface runoff stands in contrast to this.

6.4.1 Pressure reactions of piezometer devices

The piezometer observation in a depth of 5.5 m (Figure 6-10) starts with a rise of the groundwater table to an enduring high level in February 1998. Please refer to chapter 3.3.4 and 3.3.7 for location and technical information about the measurement devices. The high groundwater table from the winter time declines in a long recession period from early May to early June. The month May features a period of low precipitation (80 mm) in 1998. During the high groundwater table at a maximum of 2.6 m below surface, a precipitation event-related reaction is observable but less pronounced than in summer. A pronounced reaction is observable from early June on: the rise of the groundwater table after certain events can add up to changes of 1.2 meters. A dry period in August with a precipitation depth of 136 mm means that the groundwater table drops to its lowest value of 4.2 m below surface. The high groundwater table in winter and a capped rise of the consecutive summer events point to a finite subsurface storage reservoir.

A clear time lag between the beginning of precipitation events and a corresponding rise of the groundwater table can be observed: it takes between 5 and 36 hours to see a reaction on the piezometer, the average for 18 events is 14.4 hours. This is still considered to be quite a fast reaction. Direct deep infiltration is unlikely as the average conductivities lie at about 10^{-7} m/s to 10^{-9} m/s for the deeper soil column on the hillslope body (Chapter 5.3). This would mean that infiltrating water needs 3000 to 30000 hours to reach the piezometer device at a depth of 5.5 m. A temporal connection of groundwater bodies of saturated stagnic gleysols near the borehole and the pressure-inducing layer in a depth of 5.5 m is excluded. The borehole log (Figure 3-9) describes soft-firm and firm material in a depth of 1.5 to 5 m, which is a material condition unlikely to be water saturated during single precipitation events in summer.

The piezometer observation at a depth of 12.0 m, in the subglacial till, shows a much more damped reaction but behaves similar to the upper piezometer with an elongated high level from February to May. The long recession periods during the precipitation-free time in May and August and more pronounced pressure rises during certain summer events suggest that more precipitation is needed before a reaction

occurs and it consecutively leads to smaller rises. The reaction time between the first precipitation and the piezometer rising is between 30-100 hours for 5 events.
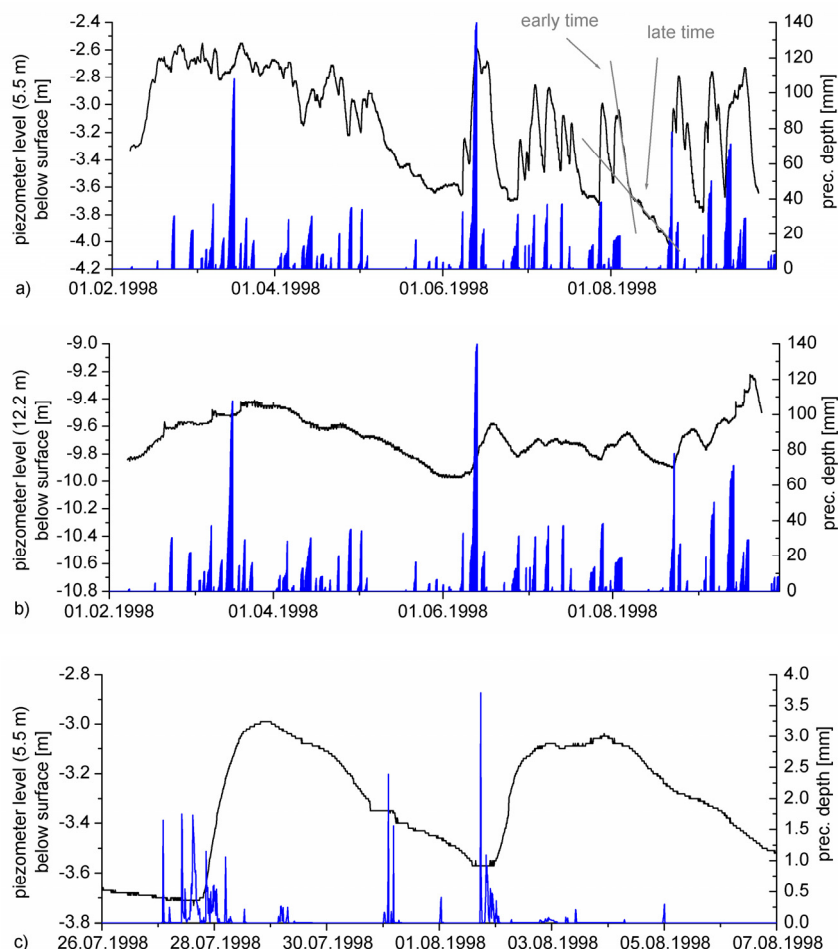
Figure 6-10: Piezometer reaction in 1998 combined with cumulative precipitation from selected events for a) a device in 5.5 m and b) a device in 12.0 m, c) a close up look on upper piezometer in August to display the delayed reaction, 10 mm precipitation intervals are plotted here.

6.4.2 Recession analysis

The recession analysis show that the recessions for both piezometers can each be parted into two reservoirs (Figure 6-10a and b). Most events only show a first inclination (early time), only very long recessions in May, July and August show a second inclination (late time) for the upper piezometer.

Eleven events are taken for the recession time analysis (Table 6-5), three of those were from winter and spring. The *K*-factor of the early time events in summer and winter are in a similar range and average at 13 days. The spring recession event (*K* = 41 days) and the late time events (*K* = 57-165 days) show a wider variability which accounts for more distortion, e.g. through small precipitation events.

It was possible to use four early time recessions and two late time recessions (May and August) for the *K*-factor determination for the lower piezometer device (12.2 m). An early time recession yielded an average *K*-factor of 72 days (three events). Late time analysis yields results with 272 and 280 days (two events). A comparison of piezometer recession factors of creek discharge (Chapter 6.2.3) and spring discharge (Chapter 6.4.3) will follow in chapter 6.5.1.

Table 6-5: A comparison of the recession time analysis. Results are separated into winter (elongated high groundwater table) and summer (high amplitudes on generally low groundwater tables). *Early time data* **refers to a first recession after event-based maximum.** *Late time data* **recession follows after the high winter readings and in long precipitation free periods.**

type	date when recession event starts (1998)	K-factor [days]	statistical parameters for K-factor evaluation		
			R²	95 % confidence bounds	
winter and spring recession in 5.5 m depth	08.04.	**16**	0.98	15	16
	25.04.	**11**	1.00	11	11
	08.05.	**41**	0.97	39	43
summer recession in 5.5 m depth, early time data	17.06.	**10**	0.98	9	11
	04.07.	**10**	0.99	10	11
	09.07.	**14**	0.97	13	15
	17.07.	**15**	0.97	14	15
	03.08.	**13**	0.99	13	14
	28.08.	**9**	0.99	8	10
	18.09.	**10**	0.97	9	11
summer recession in 5.5 m depth, late time data	17.06.	**71**	0.79	71	106
	17.07.	**165**	0.74	144	192
	03.08.	**57**	0.97	54	60
summer recession in 12.0 m depth, early time data	19.06.	**72**	0.99	70	74
	08.08.	**82**	0.96	79	85
	30.08.	**61**	0.98	56	66
spring and summer recession in 12.0 m depth, late time data	08.05.	**166**	0.98	161	170
	17.07.	**159**	0.92	151	167
	08.08.	**280**	0.91	280	318

6.4.3 Springs on upper Heumös slope
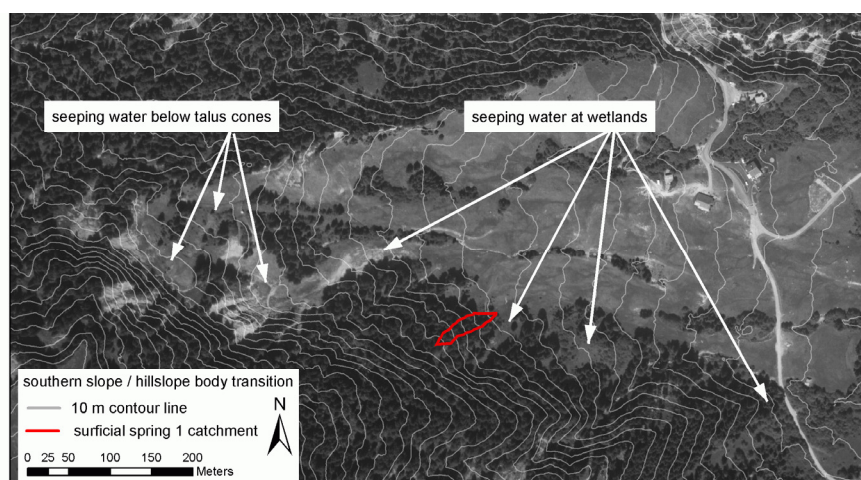
Springs at the southern slope - hillslope body transition

Springs or wetlands where water seeps out of the subsurface are abundant on the hillslope body. Wetlands can develop at the transition of steep inclinations to more shallow inclinations and often at former rotational slides. For example, the spring of creek 3 is located below the scarp of one of these slides. At the transition of the southern slope towards the hillslope body a series of small springs and wetlands indicate a more pronounced seepage of subsurface water (Figure 6-11). In the upper western part these wetlands are located at the foot of distinct talus cones. They are coarse enough to directly infiltrate water which flows from the adjacent bare rocks and which then feeds the wetlands down below. Further downslope to the east, these debris cones are covered with soil and vegetation so that these are harder to distinguish.

Catchment properties and discharge reaction of spring 1

The surficial area of the catchment of spring 1 does not reach up the total height of the southern slope. The total length of the southern slope is 330 m, the catchment of spring 1 reaches up about 80 m of the total hillslope length and is about 22 m wide at its maximum width (Figure 6-11). Hence the size of the surficial catchment is about 1128 m², derived out of the ALS DEM.

The soil cover is shallow, in some parts it is less than 1 m before Amden marlstones are encountered, these are considered to be impermeable. This means that a major part of the spring's groundwater body is contained in the shallow soil body. The Wang marlstones might hold a fissured groundwater body but they are situated well above the surficial catchment of spring 1. The soil thickness increases towards the spring. A typical shape of a flat debris cone is observed which could contain a larger groundwater body. Percussion probing holes could not reach to greater depths than 1 m, as the material is too gravely (Chapter 5.1.2).

Figure 6-11: Aerial photo with surficial catchment of spring 1 and locations, where water seeps out at the southern slope - hillslope transition.

The soil column is composed of a thin organic layer and dense residual clay. Shrinkage cracks were observed with wide apertures in July 2006 and decreased but still observable apertures in November 2006, for further details see the macropore section in chapter 5.2.2. Macropores originating from roots with diameters of 0.5–1.0 cm were observed, as well as pipes with diameters of 10 cm in shallow zones, maybe enhanced through shallow rooting trees (*Picea abies*).

For the mechanical device, the minimum average discharge lies at 0.033 l/s, the absolute minimum was reached in 2003 (0.022 l/s), absolute maximum is at 0.23 l/s (1998-2004). The new digital device records different values whose minimum is as low as 0.020 l/s (2005) the maximum is at 0.33 l/s (2006).

Table 6-6: Comparison of recession time analysis, the results are separated in early and late time data of spring events.

| date when recession event starts | early time | | | late time | | |
| | *K*-factor (days) | statistical parameters | | *K*-factor (days) | statistical parameters | |
		R^2	95 % confidence bounds		R^2	95 % confidence bounds
10.05.1999	**5**	0.98	4	5	**65**	0.96	60	70
29.08.1999	**3**	0.96	2	4	**61**	0.92	56	68
05.01.2000	**16**	0.98	14	18	**141**	0.88	125	162
07.09.2000	**5**	0.96	4	5	**37**	0.92	32	44
20.08.2000	**-**	-	-	-	**54**	0.82	43	72
08.02.2001	**-**	-	-	-	**67**	0.97	63	72
29.04.2001	**6**	0.95	5	7	**54**	0.94	48	61
20.07.2001	**-**	-	-	-	**25**	0.98	25	30
10.08.2001	**-**	-	-	-	**46**	0.99	46	51
17.09.2001	**-**	-	-	-	**22**	0.97	20	24
06.12.2001	**6**	0.92	5	8	**36**	0.93	31	42
28.07.2003	**4**	0.92	3	9	**30**	0.98	42	47
31.08.2003	**4**	0.90	3	6	**31**	0.97	28	36
11.09.2003	**8**	0.91	5	20	**24**	0.97	22	27
01.11.2003	**3**	0.92	1	26	**23**	0.95	21	26

Recession analysis

The linear storage approach (Dyck & Peschke, 1995) for recession investigation is applied to 11 events picked from the discharge time series from September 1998 to 2003 (Table 6-6, Chapter 4.3). The early time *K*- factor yields an average of 4 days for 10 events. The late time *K*-factor is spread from 22 to 67 days; the median is at 37; the average at 41 days. The late time recession from 01/05/2000 is 141 days respectively and is excluded from the other events as it lies in a long precipitation free period in winter.

6.5   Comparison of measured signals

6.5.1   Recession time analysis

The recession curve in a precipitation-free period provides information of storage behaviour. There are multiple ways to analyse recession behaviour (Tallaksen, 1995; Troch *et al.*, 1993). One restriction is the high variability encountered in the recession behaviour (Tallaksen, 1995). Data uncertainty and missing overlapping data are the reason for deciding to use a simple recession analysis (Dyck & Peschke, 1995) to determine possible storage systems on the Heumös slope. If it is presumed that storage systems, which influence channel discharge, spring discharge or groundwater table decline operate on similar processes, the *K*-factors can give a clue on these similarities. It should be noted that the recession analysis is on an event scale. Figure 6-9 shows similarities of spring discharge and piezometer decline and a differing behaviour of the creek discharge. The recession times back this observation and give a wider database for similarities between creek discharge and piezometer decline. Creek recession times are short, 2-3 days of late recession are comparable to the fast recession in the spring but not to early or late recession of the piezometer. Hence the groundwater body has no influence on the channel discharge on an event scale. On the other hand, late time recession values of the spring discharge are resembled in the average recession values for the groundwater body. Although the progression of spring and piezometer in figure 6-9 is slightly different: the spring shows a concave progression of the recession curve, the piezometer a convex progression. Different processes might be responsible for this, yet the very late time recession values hint similar storage depletion, 141 days for the spring; 165 day for the piezometer which is a very slow decline and can be attributed to slow seepage e.g. at the middle part of the slope where the post-glacial sediments decline.

Similar recession behaviour of the upper piezometer and the spring show that spring discharge at the rim of the moving body and the piezometer reaction on the other side of the moving body in 280 m distance is based on comparable processes. Early time recession is quick for the piezometer, with about 10 days it is only double the time than for the spring. Late time recession of the spring comes close to the one of the upper piezometer.

6.5.2   Comparison of spring and creek discharge

A connection of creek and spring discharge is visualised in figure 6-12a on a long-term scale: The average monthly spring discharge reflects the development of the average monthly discharge of creek 3. The average discharge rises until April and then declines until August, spring discharge is damped in relation to creek 3 discharge. The months August to December feature a similar average discharge for both systems. This indicates that snowmelt and pronounced precipitation events in summer influence surface runoff production as well as the fast reactions of the spring. Snowmelt does not lead to a longer average spring discharge. So it can be concluded that subsurface storage is not influenced by snowmelt longer than surface runoff. In autumn and winter precipitation is less pronounced and average spring discharge and creek discharge are on a similar level. There are several indications that the spring is governed by a threshold system:

1)   Not all precipitation events which lead to creek discharge, also lead to spring discharge. About 10 mm of precipitation is needed to trigger a reaction in the spring as was observed for the months of May to September 2006. The measurement of the electrical conductivity shows that the spring water is dominated by rainwater during strong precipitation events (Figure 6-14).

2) The spring discharge is twofold: a quick and intense spring reaction parallel to the creek reaction. And a prolonged tailing is in contrast to the quick recession in the creeks. Baseflow is constantly higher for the spring discharge than for the creeks on an event time scale (Figure 6-12b). A strong retention factor in the spring aquifer is in contrast to the fast reactions seen for a lot of precipitation events. The fast reactions are attributed to the intensely cracked soils. A connection to a second storage system with a constant contribution and stronger retention than for the soil storage system is a plausible explanation for the pronounced tailing. A possible aquifer could be the fissured Wang layers but these are not geologically connected to the surficial spring catchment (Chapter 3.3.1).

3) The reaction onset of the spring on a certain event varies in relation to the soil moisture: that onset is faster during dry conditions and slower during wet conditions. The 2006 time series of creek 1, creek 3 and spring 1 have a good quality in temporal resolution so that they can be used to compare the onset of events. The onset of discharge is explained as the time interval needed between the first precipitation interval and the rise of the discharge curve. Initial loss of precipitation before discharge begins hampers the identification of specific onset lags but differences of onset in-between the discharge curves are distinguishable. Creek 1 and creek 2 have almost identical onsets throughout 2006. The variations of the onsets of spring 1 and creek 1 are dependent on the antecedent conditions which means they are dependent on the soil moisture and shrinkage crack aperture (Figure 6-12c).
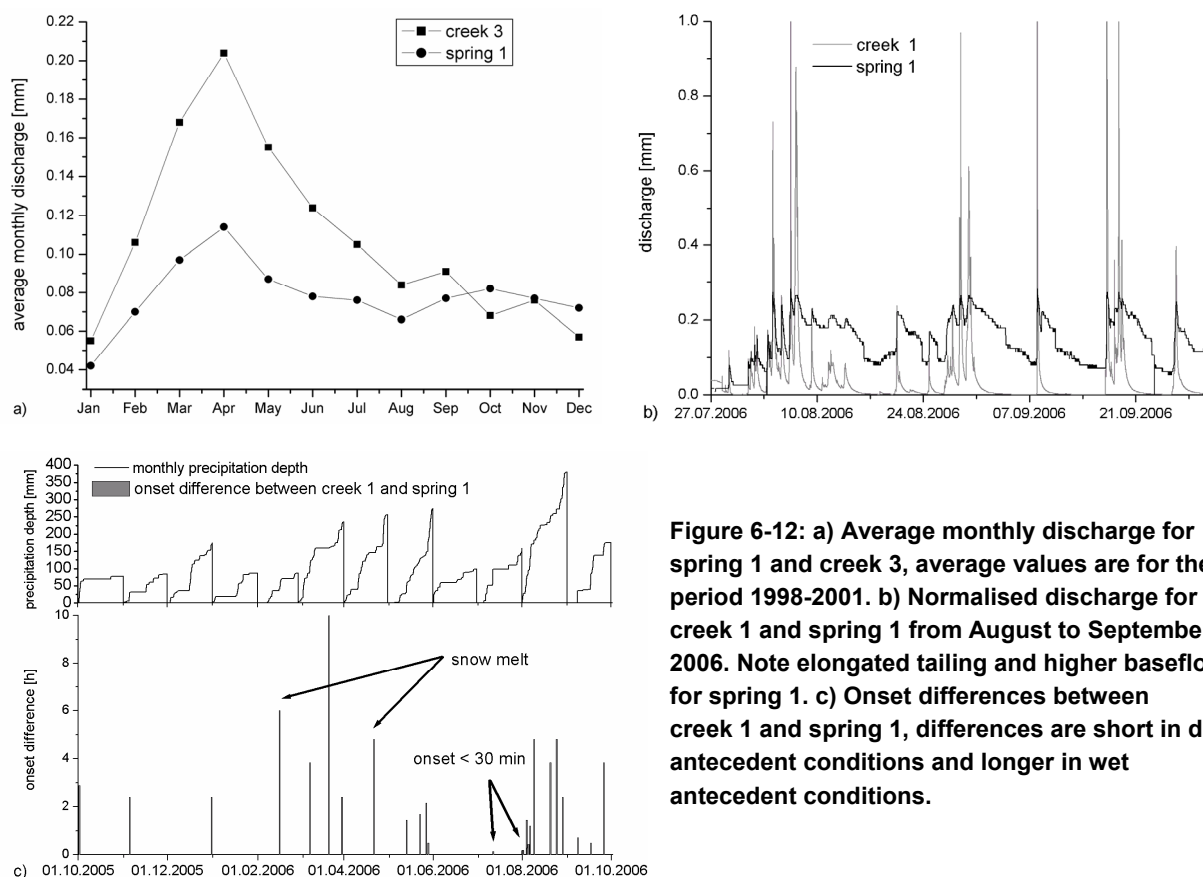

Figure 6-12: a) Average monthly discharge for spring 1 and creek 3, average values are for the period 1998-2001. b) Normalised discharge for creek 1 and spring 1 from August to September 2006. Note elongated tailing and higher baseflow for spring 1. c) Onset differences between creek 1 and spring 1, differences are short in dry antecedent conditions and longer in wet antecedent conditions.

6.5.3   Event reaction explained with multiple signal observation

Two events are selected and discussed in the following to show the general reaction behaviour of creeks and springs during certain governing global conditions like soil moisture states or precipitation event

succession. In figure 6-13 and figure 6-14 cumulative sums for creeks and springs are plotted as well as specific discharge to show the course of the hydrographs.

In figure 6-13a springtime precipitation event from May 2002 is displayed. The soil moisture state is wet, the main precipitation event cumulates to 32 mm in 28 hours, all events cumulate to 38 mm in 40 hours. The weirs were gravel free and so observation quality is good. The reaction of surface discharge is immediate for all three creeks, though peak height and recession differ. Especially, creek 3 shows the highest specific discharge peaks, its catchment has the highest proportion of meadows. A delayed reaction of the spring is observable, the elevated discharge and tailing after the creek recession also differs. The TDR-rods show now changes which mean that saturation is at its maximum.
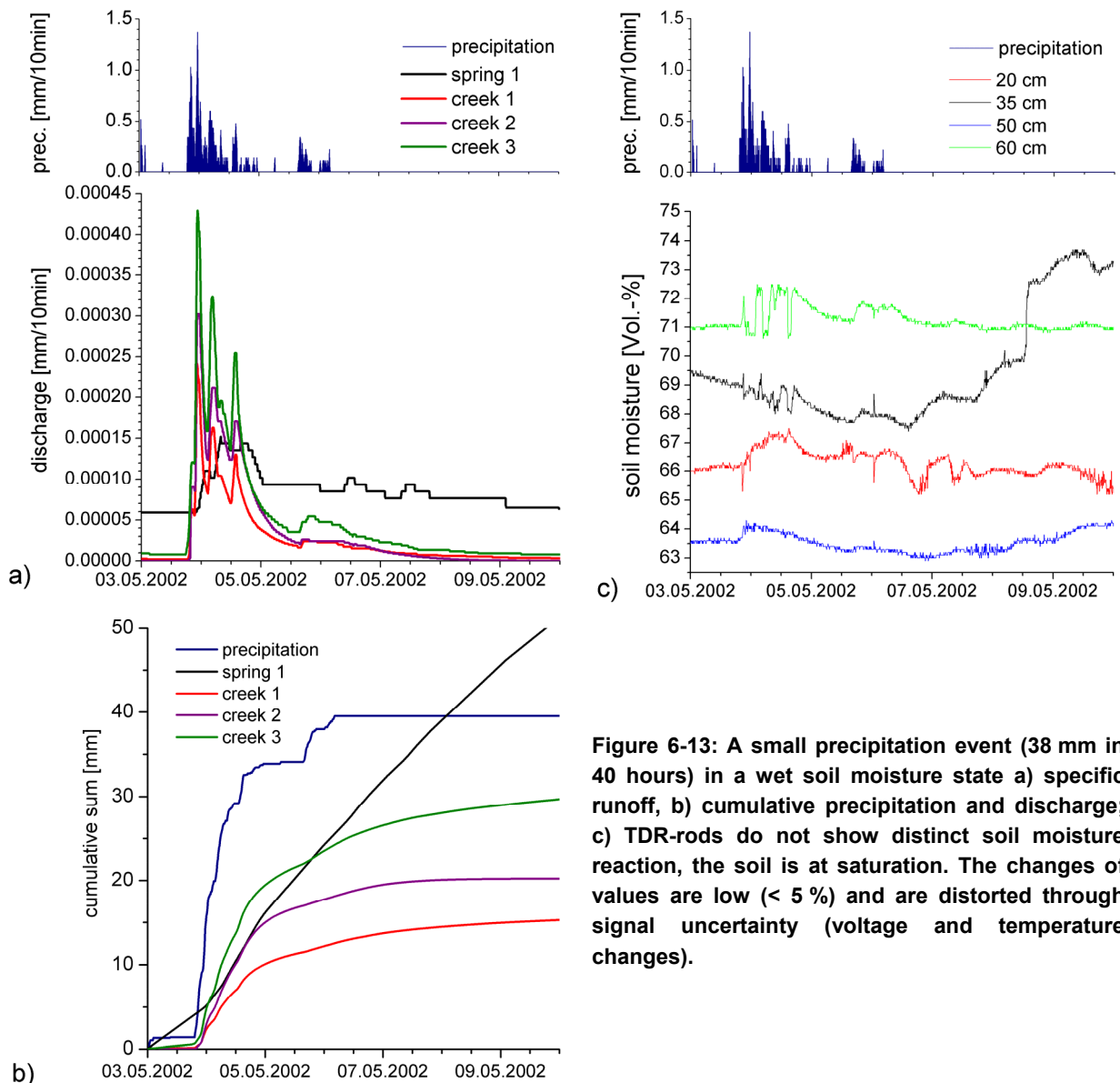
Figure 6-13: A small precipitation event (38 mm in 40 hours) in a wet soil moisture state a) specific runoff, b) cumulative precipitation and discharge; c) TDR-rods do not show distinct soil moisture reaction, the soil is at saturation. The changes of values are low (< 5 %) and are distorted through signal uncertainty (voltage and temperature changes).

In figure 6-14 a typical convective summer event is displayed. In August 2004, 32 mm of precipitation fell in 4.5 hours in dry antecedent conditions. Fourteen millimetres of precipitation fell in the preceding 18 days. Creek 3 reaction is delayed and too low due to gravel clogging of the weir, compared to reaction of creek 1. Though the cumulative sum is similar in both creeks. The dry soil moisture state leads to

initial loss and so to reduced discharge in the creeks, the spring tailing leads to an enhanced discharge. The TDR-rods show a distinct soil moisture rise, especially in the 35 cm rod. The electrical conductivity measurements during the event show that water is diluted as fast as reaction occurs in spring 1. This means that a shallow aquifer shows very fast water transport despite a clayey soil matrix. Fast preferential flow due to shrinkage cracks and soil pipes are the reason for this.
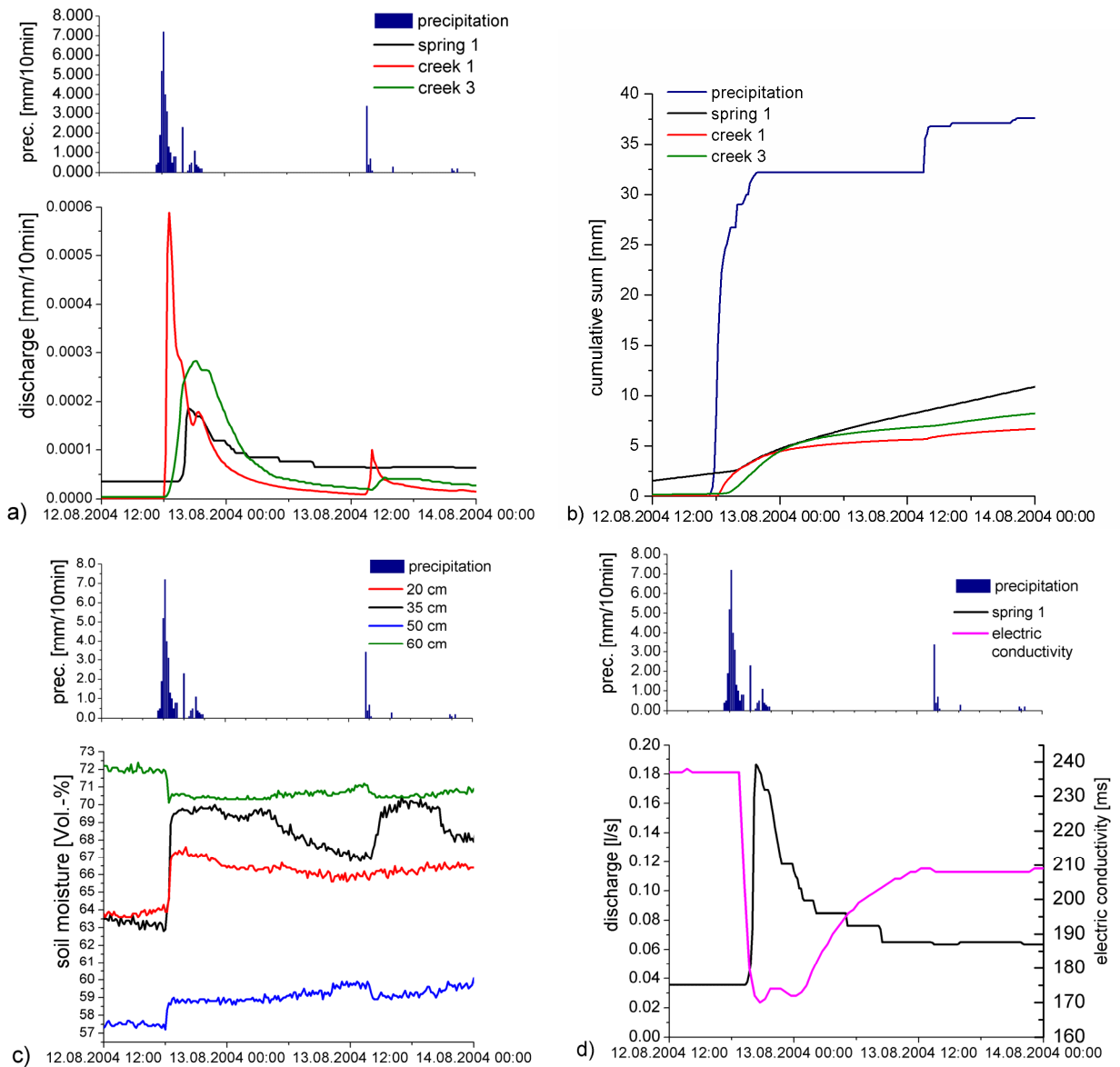
Figure 6-14: A convective precipitation event with dry antecedent conditions in August 2004. a) specific discharge of creek 1 and 3, creek 3 is clogged with gravel. b) the cumulative sums show similar results, c) signal of TDR-rods show a distinct soil moisture rise; d) electrical conductivity measurements during the event.

7 Synopsis of dominating processes and structures

The investigation of hydrological processes of a hillslope movement addresses multiple scientific disciplines. This chapter is supposed to have an integrating and interpreting character of the observed structures and processes on the Heumös slope. The goal is to combine dominating structures with relating dominating processes. As measurement and observation data sets are never exhaustive, which is especially true for subsurface information, a discussion of patterns across several spatial and temporal scales is required. Processes with large wavelengths and large-scale structures, which are presumably the base on which movement is initiated, are an issue for geological determination. Slow processes, like deep matrix infiltration, groundwater table changes and a possible relation to the creep movements, are strongly governed through these geological structures. On the Heumös slope, the observed fast reactions of the groundwater table are influenced by fast hydrological processes. Features influencing the water balance on a smaller scale are structures found in the biosphere and pedosphere. These are soil or vegetation type distributions as well as indicators for a variability of the soil hydraulic conductivity. The reaction on precipitation due to vegetation- and soil-distribution is rather dealt with hydrology and soil physics. The very upper soil horizon pushes quick processes, especially on the Heumös slope.

7.1 A geological model for the Heumös slope

A major drawback in geology is that a thorough understanding of the subsurface is difficult and costly to achieve. For this reason this scientific discipline is strong in interpreting the sparse information gathered without investing a lot of money into drilling or other ground surveying methods. A perceptional model will be developed and discussed to understand the complex processes leading to a movement on the hillslope. For the advance of numerical-hydrological and -geomechanical models it is important to quantify the subsurface properties better.

7.1.1 Is there a groundwater system in the bedrock?

The hillslope is rimmed by Amden marlstones and probably most of the bedrock below the sediments is also built of these tectonically stressed highly shattered marly rocks. Despite of the tectonic stress on the material it does not necessarily belong to any good and highly conductive groundwater bearing rock. Water saturation in the Amden marlstones is unlikely as Schneider (1999) found dry Amden marlstones in boreholes (KB 1 + KB 2) in Ebnit. The borehole loss in KB 3 also indicates dry, not cohesive material. This means that the local groundwater system likely ends at the transition of the sediments towards the Amden marlstones. This is an important assumption needed to understand the hillslope hydraulic system. One open question is left: what kind of geologic strata is the low resistivity zone in a depth of 30 m in the geoelectrical depth-profile? This can only be answered through additional drilling or more precise geophysical investigation.

In the case of the properties of Wang and Leimern rocks, it is more difficult to draw a conclusion on their influence on the groundwater system. Especially the fissured marlstones of the Wang formation are thought to have a facies which might contain a groundwater system. The groundwater characteristics of the Leimern marlstones are more difficult to judge as they have rock characteristics which either can be similar to the Amden or to the Wang layers (Chapter 3.3.7). On the other hand, these formations only partly underlie the hillslope body. Outcrops of the layers are found on the upper part of the southern slope. This means that a possible groundwater body in these rocks could only indirectly influence the

groundwater system of the hillslope body. A connection to the sediments body could be possible but has not been found so far.

7.1.2   How is the shape of the bedrock shape below the sediments?

The Bruder creek north of the Heumös slope has an asymmetric shape with a steeper inclination in the south and a more shallow inclination in the north. There could have been a similar pre-glacial runoff system on the Heumös slope. This would indicate a higher sediment thickness near the southern slope (Figure 7-1a, on the left). Similar to the Bruder creek valley, asymmetric v-shaped valley systems are reflected in the general morphology of the upper Ebnit Ache valley, which is induced by the regional tectonic: The fold planes of the Helveticum facing the north are steeper than the opposite planes. This leads to a number of west to east aligned valleys with steeper slopes facing the north. It is the question whether the folding is also reflected in such a small entity as sketched in figure 7-1b or whether there is a system with general constant dipping as measurements indicate (Chapter 3.3). The dip of layer boundaries is towards the south, as the geological investigations show. If there is an asymmetric bedrock folding it could be suggested that the bedrock morphology is asymmetric as well. Erosion might preferably take place in the core of a syncline and a higher sediment thickness in the south would be the consequence.

A second possible bedrock shape might be a more or less constant thickness of the sediments (Figure 7-1a, middle and right) which is also underlined by boundary shapes in the electromagnetical profiles. The resistivity lines show a shallow u-shaped subsurface (Figure 5-1a). A restriction for interpreting the electromagnetical profiles is the meagre relation of the apparent specific geoelectrical resistivity, especially concerning the sediment - bedrock transition (Figure 5-1b).
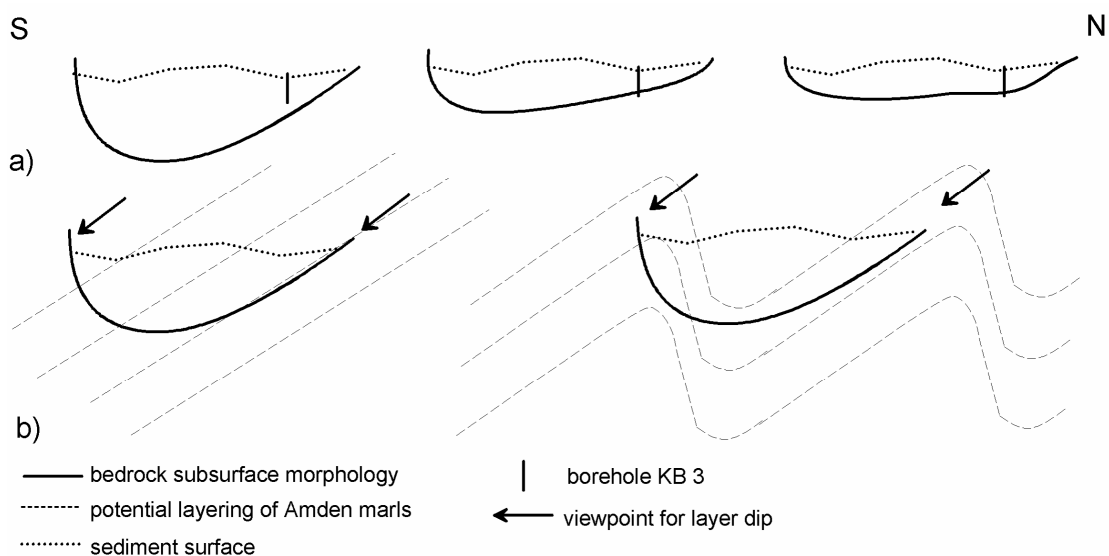

Figure 7-1: Sketches of possible bedrock shape and layering of Amden marlstones; a) possible buried bedrock shape, indicating higher sediment thickness in the south (left) or similar sediment thickness (right); b) possible influence of folding on bedrock shape.

7.1.3   Estimation of sediment thickness

It is essential to have a thorough idea of the sediment thickness for future drilling and for modelling purposes. Geological and geomorphological interpretation can give additional information on the sediment thickness on the slope: Small outcrops of rocks are found alongside the northern rim of the

Heumös slope and in some parts of the creeks, e.g. at the outlet of creek 1 towards the Ebnit Ache. Bedrock outcrops are observable at the southern slope – hillslope transition, too. In figure 7-2b the known bedrock outcrops are extrapolated in a north to south profile across KB 3. Either a v-shaped or a u-shaped bedrock surface is suggested. The profile indicates that the steep northern and southern slopes are covered only with thin sediment layers. Whereas the sediment thickness could accumulate to either ~30 m or ~50 m in the central hillslope body. An ~30 m boundary is shown in the profile in figure 7-2c. Creek 1 has removed all sediments and flows on bedrock. This suggests that the maximum thickness of sediments cannot exceed more than 30 m on the hillslope body.
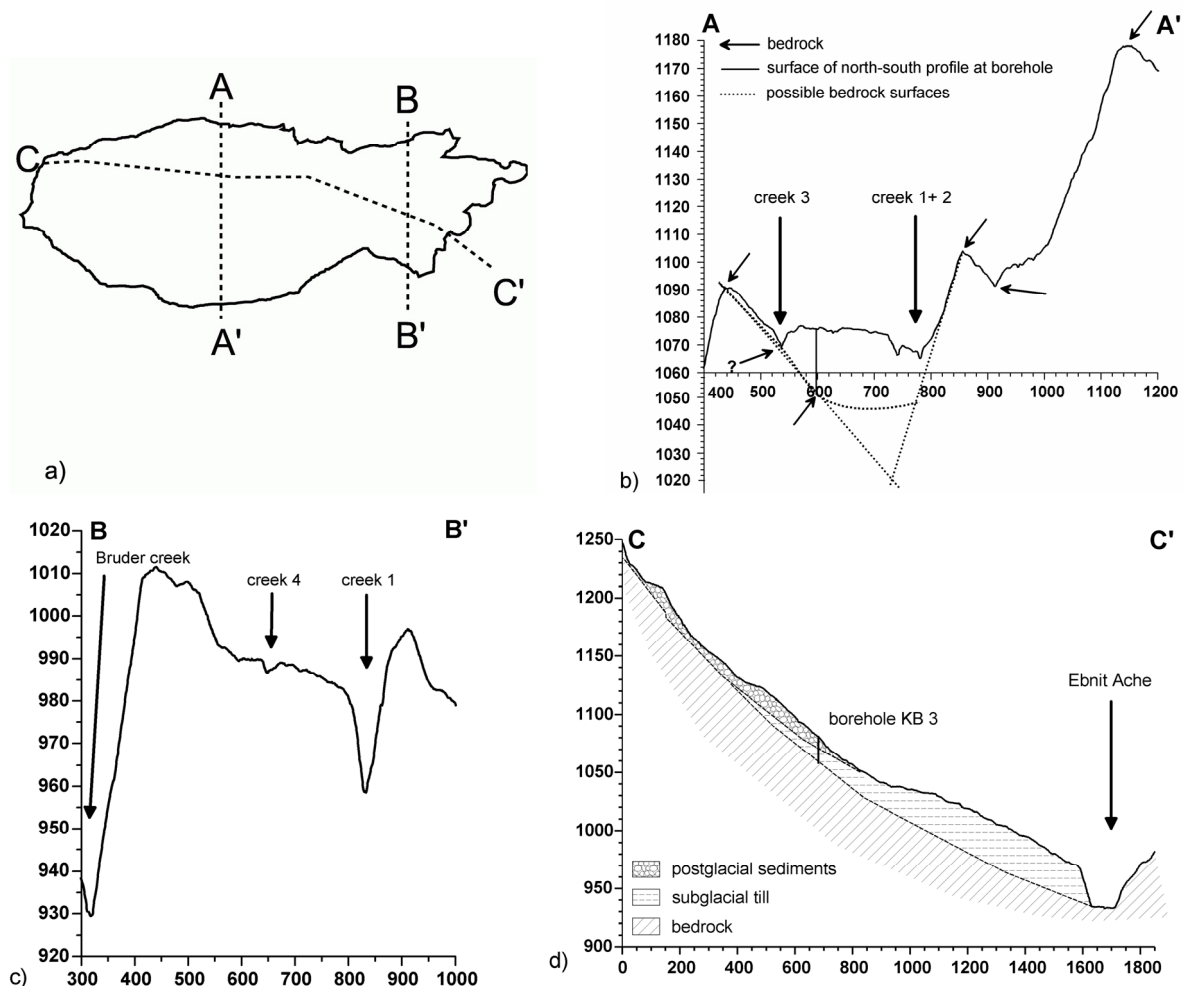
Figure 7-2: Model of subsurface distribution of geologic units of the Heumös slope. The height is scaled by the factor 2. Distribution and height of strata only relies on the KB 3 log, otherwise on geological interpretation; a) location of profiles; b) a north to south profile at the height of the KB 3, c) a north to south profile in the east, d) an east to west profile in direction of the maximum inclination. Profile data is derived from the airborne laser scan DEM. Lateral and vertical extension in metres.

The subglacial till thickness is approximately 14 m or more in borehole KB 3, in figure 7-2c and d the maximum thickness would add to 30 m. The texture and properties of the subglacial till are not well known. Smit Sibinga-Lokker (1965) states that the Rhein glacier overrun an older Ebnit valley glacier which probably enhanced the initial density of the material. This probably means a conservation of a pre-glaciation bedrock surface. Please note the steps in the postglacial sediments which indicate movement

and the uneven surface on top of the subglacial till which is due to bulging on the surface through soil creep (Figure7-2d).

Most of the southern slope features a very thin sediment or soil cover, bare rock in scarps dominates this area. In the western uppermost part a typical scarp – debris cone situation is found: rocks from the scarps accumulate in a coarse scree body which develops into a small north-directed rotational slide then. Similar debris cone accumulation is suggested for the rest of the southern slope – hillslope body transition, though mostly covered by vegetation and more weathered than at this location. Where the surface inclination from the southern slope drops below 30° degrees intensified debris accumulation is suggested, compare figure 3-4. The thickness of the post-glacial sediments is about 10 m on the hillslope body (Figure 3-9). Towards the southern and northern rims the thickness decreases: the window sampling revealed the bedrock depth at the northern rim to be about 3 m. Hammer blow seismic from Walter (Walter, 2006, chapter 3.3.5) revealed depths of 2 m at the north and 1 to 7 m in the south. This indicates increasing depths towards the middle of the hillslope body. This means that the post-glacial sediments on the western hillslope body taper out towards the rims and feature a maximum thickness of about 10 m.

7.1.4   Post-glacial sedimentation – a perceptional model

The climate was probably harsher and more severe directly after the ice receded than it is nowadays. This would infer both high erosion rates of the bedrock and accumulation of coarse scree on top of the subglacial till. This would explain the coarse scree layer in the KB 3 borehole log. It is likely that the whole area was covered with coarse material before more moderate climate helped to develop preliminary soils and a vegetation cover. Common sense would suggest a sedimentation rate which would have been higher than erosion in the beginning. Physical weathering through freezing and thawing would have prevailed. This balance later shifted towards lower sedimentation rates and stronger chemical weathering, the development of a vegetation cover might have supported clay mineral accumulation.

The soft material of the Amden and Leimern marlstones are easily weathered to small shattered rocks exposing a large surface to surrounding water which then dissolves carbonate. This leaves clay minerals dominating the material composition in the post-glacial sediments, including a large portion of smectites. Both subglacial till and debris material are dominated by high clay contents which can build up critical material for movement in combination with abundant water. The consistency of the loamy scree is soft even in larger depths which means that stiffer material can overlay soft material leading to instability of the soil column. Changes in water content and consistency of the layers as found in the hollow core logs (Chapter 5.1.2) indicate that complex processes govern weathering and with that the stability in the post-glacial sediments. It is a matter of water availability, flux and small-scale movements which influence the consistency and gravel content of the encountered material. A small scale spatial pattern is the cause of these developments. An exact definition of soil hydraulic conductivities to specific depths or subsurface volumes (layers) is especially restricted through this. However ablation and sedimentation is governed through the southern slope so that a wedging of layers towards the north is more pronounced.

7.1.5   Is there a second shear zone between subglacial till and bedrock?

The geologic situation on the Heumös slope is somewhat different to the situation in Ebnit 1) the weathering product of geological material is finer. In Ebnit there are more limestones, which produce a coarser debris that is less susceptible to weathering. 2) In Ebnit the sediment column is shallower. Nevertheless, the shear zones in boreholes KB 1 and KB 2 suggest that the existence of a second shear zone on the Heumös slope is possible. In KB 1 and KB 2 shear zones are either located in the debris –

subglacial till or in the subglacial till – Amden marlstones transition. This suggests that there is at least one additional shear zone at the subglacial till – Amden marlstones transition on the Heumös slope as well. There could be a shear zone located in the Amden marlstones itself as well. The post-glacial sediment layer ends at the height of the road and the holiday village (Figure 3-7). The upper shear zone should consequently end in this area if it is consistent and does not shift into the subglacial till (Figure 7-2d).

7.2   Hydrotope delineation to understand the pattern of runoff responses

The water balance of the Heumös slope plays a major part in generating movement by influencing the cohesion of the clay material as well as changing the hydraulic load of the hillslope body. Hence, it is interesting to develop a concept for the spatial pattern of dominating hydrological processes both on the surface and the subsurface. Leptosols dominate the southern slope with a small thickness of Ah and Bc horizons. Gleysols on the post-glacial sediments of the hillslope body show greater depths and strong stagnic or gleyic properties. The topography influences the soil water conditions: flat areas develop swampy zones whereas steep areas are exposed to changing soil moisture conditions and consequently to swelling and shrinking. The topography features a high dynamic with slides, earth flows as well as gully erosion governing soil development. The soil description did not reveal significant differences in soil types which would be the best parameter to scale point observation of soil hydraulic conductivity towards the catchment scale. The matrix hydraulic conductivity is low in general making soil structures like shrinkage cracks or macropores to the first order control of the subsurface water flow. Macropores as root holes are abundant and soil pipes seem to be important as well. These were found on the meadows as well as in the forests so far. Shrinkage cracks are a dominant structure which influence preferential flow in wet and dry soil conditions.

The measurement of hydraulic conductivity is conducted on a point scale. The high variability of results shows that matrix and macropore hydraulic conductivities are combined during these measurements. It is necessary to scale the point observations towards patterns where matrix infiltration dominates over preferential infiltration and vice versa. This will be determined with the help of the ecological-moisture-distribution map. This map proved to be useful for understanding the dominating water fluxes of the Heumös slope. Local information about the soil profile and ecological moisture, derived from vegetation association definition, are combined with topography, slope and geological structures to identify hydrotopes on the catchment scale (Figure 7-3).

- Hydrotope #1: The southern slope is steep with an inclination of up to 60 degrees. The soil cover is patchy and it exhibits thin debris or residual soils quickly followed by bedrock in some parts. Other parts show exposed bedrock and sparse vegetation. Finally, there are parts that show an accumulation of several metres of debris as can be seen in some gullies near the road. The ecological moisture regime is dominantly fresh to moist. The area is predominantly covered with common spruce with shallow roots. The infiltration capacity in this area is considerably higher than at the rest of the slope due to the presence of coarse scree, large macropores, pipes and shrinkage cracks. In addition, shrinkage cracks and their contribution to a general hydraulic conductivity is governed by the soil moisture state. Consequently, a threshold process governs the capacity of preferential infiltration as observed in the spring. Fast preferential infiltration and lateral subsurface flow are the dominating processes. A small-scale change of infiltration and seeping of water can be observed. Though the high precipitation depths lead to substantial surface runoff generation, the amount of water which infiltrates is large enough to influence the local groundwater system significantly on the

southern slope. The observation of spring 1 is a proxy for the hydrotope 1 behaviour: the reaction of subsurface water on precipitation events is always fast but reaction onset is soil moisture dependent. Additionally, a soil moisture dependent threshold governs whether a precipitation event leads to a reaction in the spring or not. The long tailing of the spring hydrograph after events shows that a groundwater storage is filled which then needs sufficient time to be depleted again.
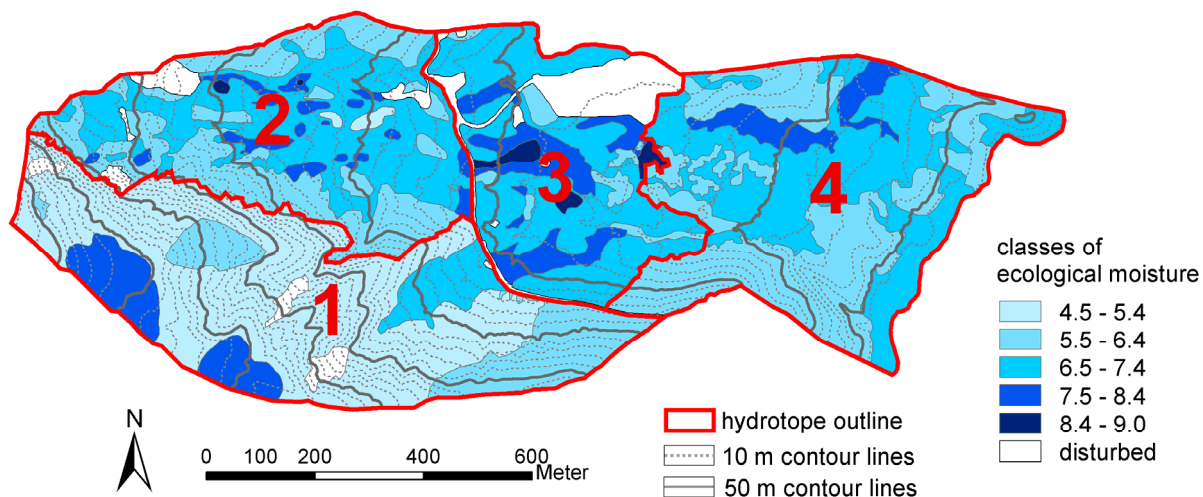
Figure 7-3: Hydrotope delineation on the Heumös slope: soil type and ecologic moisture pattern is scaled up including slope inclination and geologic information to define areas with dominating hydrological processes.

- Hydrotope #2: The north and mid part of the Heumös slope is dominantly covered with meadows and shows a highly variable topography with small scale topography features that are attributed to soil creep and small scale slides. The northern slope exhibits moist to damp ecological moisture conditions and so is proportionally drier through a thinner sediment thickness and a higher inclination. The hillslope body has a predominant damp to wet ecological moisture regime, bulging areas are drier and plane areas are usually very wet as indicated by the vegetation. The creeks develop deep gullies, eroding the soft material and leaving large boulders. Soil profiles show significant stagnic and gleyic properties indicating low infiltration capacities. The water balance is governed by surface runoff generation through saturation excess in wet parts. The soil features decreasing hydraulic conductivities into the depth (Chapter 5.3) which is shown by stagnic properties. Wet patches enlarge during precipitation events and lead to an increase of surface runoff contributing areas. The hydraulic conductivity is twofold: constant head permeameter tests and laboratory measurements show higher conductivities in the upper horizons and lower conductivities in the lower horizons. In addition, hood infiltrometer measurements show an increased infiltration capacity for the very uppermost soil layer. Consequently, infiltration excess runoff generation does not occur. A very shallow return flow on steeper parts of the hillslope is observable. For example, water flows downslope in the grass and root zone in the uppermost 10 cm of the soil column on the northern slope. Wet soil moisture states lead to very fast reactions in the creeks and a quick response following maximum precipitation intensities. In a dry soil moisture state it takes more time for a discharge reaction to occur but this reaction is still considered to be quick. Runoff coefficients are generally high. From a certain precipitation depth on direct runoff is governed through a constant loss factor. Fast recession of the runoff curves show that retention is low and that subsurface water contributes to creek discharge in a small extent during peak discharge but to a large extent during

baseflow. The piezometer reactions do not seem to be related to the fast surface runoff reactions observed in the creek discharge.

- Hydrotope #3: The central area shows wet ecological moisture conditions, besides common spruce and grey alder islands there are meadows and small moors with open water. This hydrotope differs from hydrotope #2 through the decline of post-glacial sediments and prevailing subglacial till as uppermost sediment as well as a lower inclination. Infiltration is low into the highly stagnic and gleyic gleysols; thus saturation excess runoff generation dominates in this hydrotope in case of rainfall. This area comprises the most anthropogenic changes through buildings, like the holiday village, the ski station and roads. Recently installed subsurface drainage and soil exchange will influence the runoff generation in future.

- Hydrotope #4: The eastern, lower part of the slope adjacent to hydrotope #3 shows a small-scale relief due to soil creep. This leads to a small-scale landscape pattern of dry, spruce covered ridges and wet depressions covered by alders. Some moors enhance the prevailing wet ecological moisture conditions. This area is also governed by saturation excess overland flow. The over-steepened sharp decline towards the Ebnit Ache is covered with extension cracks and features water seeping in large patches. This can lead to rotational slides, two of which are in figure 3-4. These slides developed into earth flows which still consist of very soft clay-rich material at the Ebnit Ache valley. The gullies of creek 1 are cut all the way down to bedrock, as the Ebnit Ache is. Both rivers destabilise the counter-bearing of the hillslope body through erosion, this might be the reason for changing directions of the traverse points (Chapter 3.4.2).

The ecological moisture distribution and hydrotope definition as well as the rainfall-runoff relation show that the hillslope body is a wet surface runoff-dominated system. Any deficit of water in the uppermost unsaturated zone is quickly filled without too much loss of precipitation. The TDR-signals show an overall wet system which seldom dries out significantly and into greater depths. Saturated conditions prevail most of the year and at most of the area except the southern and northern slopes. These patterns indicate that direct infiltration on the hillslope body is not a favourable process and in contradiction to the relatively fast groundwater reactions which is seen in the piezometer. Though long time balances are not calculable with the existing data, high runoff coefficients and low evapotranspiration values in relation to the precipitation show that high fluxes into the subsurface and high fluxes in the groundwater system do not exist on the hillslope body.

7.3 Pressure propagation from hydrological active regions towards inactive regions as a hypothesis for fast groundwater reactions

The subsurface reaction in the southern slope is represented by spring 1. Shrinkage cracks and macropores in shallow residual clay soils, as well as scree cones, imply preferential infiltration into the sediments of the southern slope. Because of the small thickness of the strata, the preferential infiltration and a high hydraulic conductivity triggers a quick filling of the groundwater storages. The steepness and specific strata thickness might be the reason for a substantial pressure rise uphill of the toe of the southern slope. A constantly filled confined aquifer in the hillslope body, which is laterally connected to the shallow aquifer in the southern slope, is an explanation for the similar behaviour of the piezometer and spring 1 reactions. The quick rise of both spring discharge and the groundwater tables as reaction on a precipitation event is followed by a long tailing in both cases. The tailing is caused by following features. 1) the confined aquifer of the hillslope body has almost no possibility to release stress through increased fluxes, as the confining strata is thick and has a very low conductivity (see slug test results in chapter 5.3).

Stress release is conducted through slow seeping at the surface. The margin where the post-glacial sediments diminish in favour of the subglacial till, at the height of the holiday village, is a very moist area indeed and therefore serves as a stress release zone. The swampy hydrotope #3 and the eastern margin of hydrotope #2 might be stress release zones of the confined aquifers as well. 2) Another possibility for stress release would be local movement in the aquifer, the coarse scree layer at the post-glacial sediment – subglacial till transition, which contains the detected shear zone.
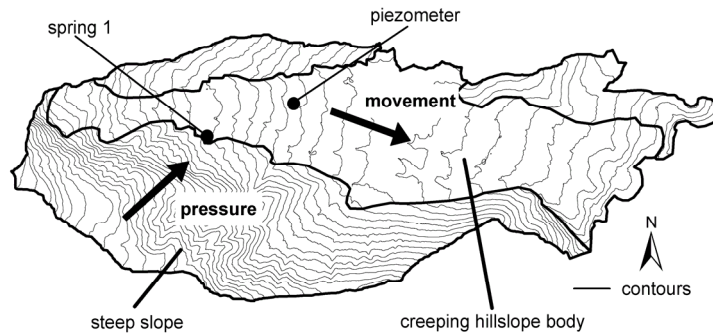
Figure 7-4: Pressure propagation from shallow aquifers in the southern slope towards the confined aquifers on the hillslope body. Fast preferential infiltration in the southern slope (residual soils and scree cones) trigger the filling of aquifers which influence lateral pressure, rises in the confining layers.

7.4   Observed movement compared to hydrological signals

The Global Positioning System (GPS) was a new possibility for a high-precision measurement of movement during the time when research started on the Heumös slope in 1995. High precision data was not available from the US Government before the mid nineties (Wunderlich, 1995). In addition, inclinometer measurements were still the classic observation type for movement in the subsurface. Both systems are hampered by high initial costs and also high running costs in the case of GPS observations. This makes both systems inapplicable when a high temporal resolution of movement measurements is needed.

Deep-seated mass movements are supposed to react on long term groundwater signals (Schuster & Wieczorek, 2002; van Asch *et al.*, 1999) and are supposed to be of a delayed type and not event-based. This is not the case on the Heumös slope. Walter (2006) used nanoseismic monitoring (Wust-Bloch & Joswig, 2006) to detect very small rupture events in the subsurface of the Heumös hillslope body. Most events were detected during a precipitation event with a depth of 37 mm in September 2005. The existence of micro-earthquakes means that a selective and impulsive stress release occurs during precipitation events. This is an indication that small jerky movements occur during precipitation events and that a continuous creep of the hillslope body is a less likely movement process. This means that observed "creep movements" on a long temporal scale of e.g. several months could likely be a succession of small jerky movements. An influence of uneven shear zone surfaces on the movement speed is discussed by Baum & Johnson (1993). A hysteresis of movement patterns due to these uneven surfaces is explained by small scale pressure build up and release due to movement before and behind shear zone heterogeneities (van Asch, 2005). These observation underpin the existence of jerky movements even in clay-rich sediments, where creep is observed most often. The chosen temporal measurement scale of GPS and inclinometer measurements is probably not the right scale to detect precipitation event-based reactions of the subsurface movement. Observations in the field and through locals are not quantitative

but also indicate a relation between single precipitation events and movement. However, a comparison of precipitation proxies and GPS measurements will be made to see whether there might be a relationship.

Movement in different locations can be the product of different stress release processes. A creep in the upper soil column must not necessarily be based on the same process than movement at the shear zone in a depth of 8 m. There, material properties are different due to higher loads or different pore properties. This is why a comparison of precipitation proxies with inclinometer measurements would have been interesting as well. This could not be conducted as a complete raw data set for the inclinometer measurements is not available any more (Schneider, pers. communication) and the measurement intervals are neither periodic nor at the same reference dates for GPS measurements.

7.4.1 Movement characteristic of object and traverse points

It makes most sense to divide the lateral measured distance between two measuring campaigns by the number of elapsed days to get a proxy for movement behaviour in equal time intervals (Table 7-1). This gives a comparable value of an average movement rate per day for each observation period, which then will be compared to different precipitation proxies. Several groups both in terms of location and movement behaviour can be separated (Figure 7-5).

Table 7-1: Reference dates of movement measurements with related precipitation depth and average daily precipitation.

reference date for measurement period	time span [days]	average movement group 1 per day per time span [mm]	average movement group 2 per day per time span [mm]	average movement group 3 per day per time span [mm]	precipitation sum [mm]	average precipitation per day per time span [mm]
04/06/1998	zero reference date for measurements					
06/11/1998	155	0.013	0.014	0.111	1073	6.93
07/05/1999	182	0.005	0.006	0.046	959	5.27
08/08/1999	93	0.031	0.015	0.034	1074	11.54
09/11/1999	93	0.019	0.023	0.074	491	5.28
10/05/2000	183	0.010	0.007	0.063	1045	5.71
11/08/2000*	93	0.019	0.016	0.043	1000	10.75
12/11/2000	93	0.030	0.032	0.064	456	4.91
13/05/2001*	182	0.019	0.005	0.032	933	5.12
14/08/2001	93	0.028	0.012	0.045	726	7.81
15/11/2001	93	0.017	0.030	0.067	606	6.52

* missing data in Ebnit church time series, August 2000 was taken from Kanonier (2005) , for April-May 2001 Heumös weather station data was used

Group 1 is located on the uppermost western hillslope body and includes object points 10, 11, 55, 56, 59 (Figure 7-5). Group 2 is located on the central hillslope body, east of group 1 and west of the road. Group 2 includes object points 5-9, 51, 60, 61. The object points at the height of the holiday village did not show significant movement so that they were not included into the comparison. Group 3 is comprised out of the eastern traverse points PP01 to PP15.
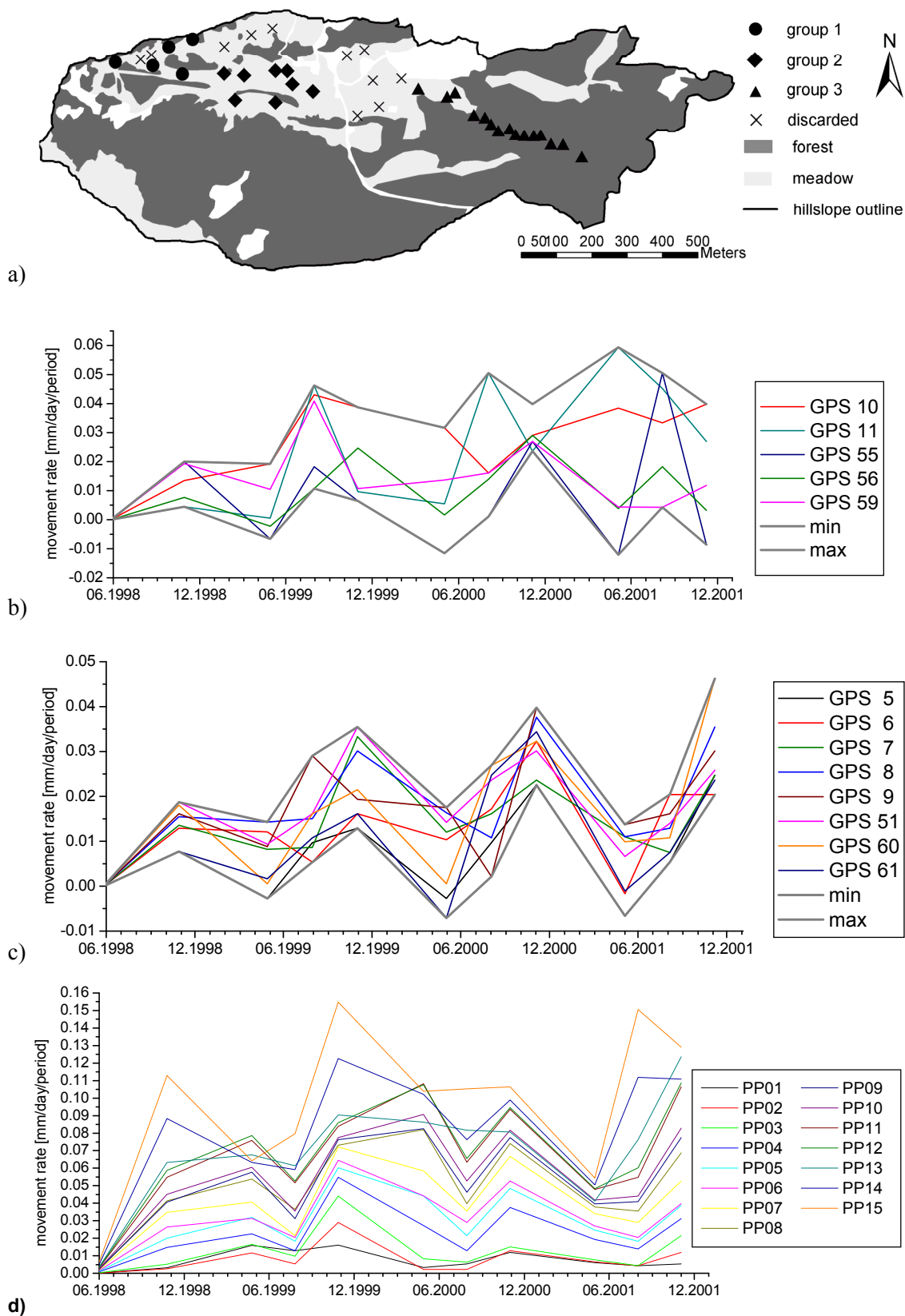
Figure 7-5: a) Overview of selected groups and discarded measurement points for the comparison with precipitation proxies; b) Group 1 in the uppermost steep area of the Heumös slope; c) Group 2 consists of GPS points in the middle part of the slope; d) Group 3 are the traverse points from the terrestrial survey.

Considering the average movement rates per day, group 1 and 2 show comparable behaviour (Figure 7-5). Group 2 points have a more uniform movement rate per measurement period than the ones of group 1 but similarities within group 1 can be distinguished as well. Group 2 has maximum daily movement rates for a reference date in November and minimum movement rates for a reference date in May, which is the 6 months winter period. GPS object points from group 2 show the best conformity, a seasonality can be depicted: lowest movement rate occurs in the 6-months winter period from November to May, increasing movement rates in the spring period from May to August and maximum movement rate occurs in the August to November period. Other groups have no or less distinct periodicities. The uniformity of movement can be drawn to the translational movement at the shear zone. Group 1 is influenced by more shallow rotational movement of single points.

Group 1 shows a more disperse signal: one maximum is in August 1999, a second maximum is shared by the August and November 2000 reference date, point 56 rather shows a behaviour similar to group 2. Group 3 shows similar behaviour for points with lower movement rates to group 2 movement and a little more diverse behaviour for points with higher movement rates. These points are only linked to object point 1 so that a successive error might influence results.

7.4.2   Precipitation proxies and periodic movement

Examining data sets that are characterised by their position along a line is a common tool in geology. (Davis, 2002). A sequence analysis of sample points of e.g. in a borehole log requires the comparison of different data sets which can be obtained even if they might not be directly related to each other. It is a method to discuss possible scenarios on a basis of scarce information. This sequence analysis will be used to investigate whether specific proxies of precipitation in different temporal scales are comparable to the observed movement rates or not. Several precipitation proxies were plotted against average movement per day values: average daily precipitation rate, monthly precipitation sums, daily precipitation sums exceeding 30 mm and finally against a time series of cumulative precipitation events from the automated precipitation event selection. Selected results are plotted in figure 7-6 for group 2 as it shows the most periodic movement behaviour from all groups. The graphs show the average movement per day and measurement period as a horizontal line, the dot displays the date of the measurement campaign. The most interesting precipitation signals are displayed as well. In appendix F-3 additional graphs for other groups and precipitation characteristics are plotted. Similar movement patterns can be predicted, if similar relations of precipitation proxies and movement rates were found for more than one group or period.

Average daily precipitation rate per GPS measurement period

First, the average daily precipitation rate is compared to movement rates. The average daily precipitation represents the same time scale than there is for the GPS measurements. The graph in figure 7-6a shows that periods with high average daily precipitation plot in a similar periodicity to high average movement for group 2. Highest average precipitation plot with low movement rates but correspond to highest movement rates in the following period. On these comparable time scales a periodicity and delayed reaction for the movement can be predicted.

Monthly precipitation sums

Monthly precipitation sums show no clear relations to movement rates. For example, group 2 has both high and low precipitation months during periods of high and low movement rates (Appendix F-3).

Daily precipitation sums

Days with precipitation depths larger than 30 mm cumulate between May to July of each year (Figure 7-6b), these months are related to low to medium movement rates for group 2. Maximum daily precipitation in May 1999 and August 2000 are not reflected in the movement rates directly. A shifted reaction of maximum precipitation days and following movement period could be suggested similar to the daily precipitation rate.

Cumulative precipitation events

Considering impulsive movement as has been detected with nanoseismic monitoring, single precipitation events with specific antecedent soil moisture states as well as with specific triggering conditions most likely govern movement processes. The selected precipitation events are plotted as cumulative sums against group 2 movements in figure 7-6c

Long lasting events with high precipitation depths occurred in February and May 1999 as well as in March 2000, August 2000 and in September 2001, please compare table 6-1. Some of these events lead to surficial small-scale slides in the upper Dornbirn Ache valley (May 1999, August 2000). The February 1999 and March 2000 events occurred in low-speed movement periods in the winter period respectively. Which means that large precipitation depths might not trigger movement in wet antecedent conditions. The May 1999 events occurred directly after a measurement campaign, medium movement rates in May-August period could be the reaction to this. The August 2000 and September 2001 events occurred during the "fast" August-November period. A relation of large events with a specific movement speed is not recognisable.

The high movement rates of all three observed years relate to periods with low precipitation. The question might arise whether a simple precipitation proxy is really useful to relate climate conditions to movement rates. It is rather suggested that certain conditions of the subsurface, combined with high intensity precipitation events which occur in summer, are the dominant mechanisms for triggering movement. Subsurface conditions are, among others, a combination of the soil moisture state which influences both shrinkage crack development and cohesion. The hydrological trigger would be a precipitation event which can contribute quickly to changes of the soil moisture state or groundwater table. The fast spring discharge reaction and long tailing, the shrinkage crack state during wet and dry periods as well as the pressure propagation from the southern slope towards the piezometer gauges are most dominant during the summer and early autumn months. When impulsive movements, as detected by Walter (2006) are considered, a periodicity on a 3 to 6 month temporal scale must not necessarily reflect a continuous creep with changing speeds. It is rather suggested that certain soil moisture states and coupled preferential infiltration trigger fast pressure rises in the groundwater body and so trigger stress release in specific locations. A higher movement speed on a 3 to 6 month scale would rather be a culmination of small pressure releases than a high-speed continuous creep. It has to be stated that the 3 to 6 month temporal scale of movement measurement is too coarse to reflect real movement behaviour. The periodicity of average daily movement rates and average daily precipitations rates is true on this scale but does not sham the important mechanisms for movement.
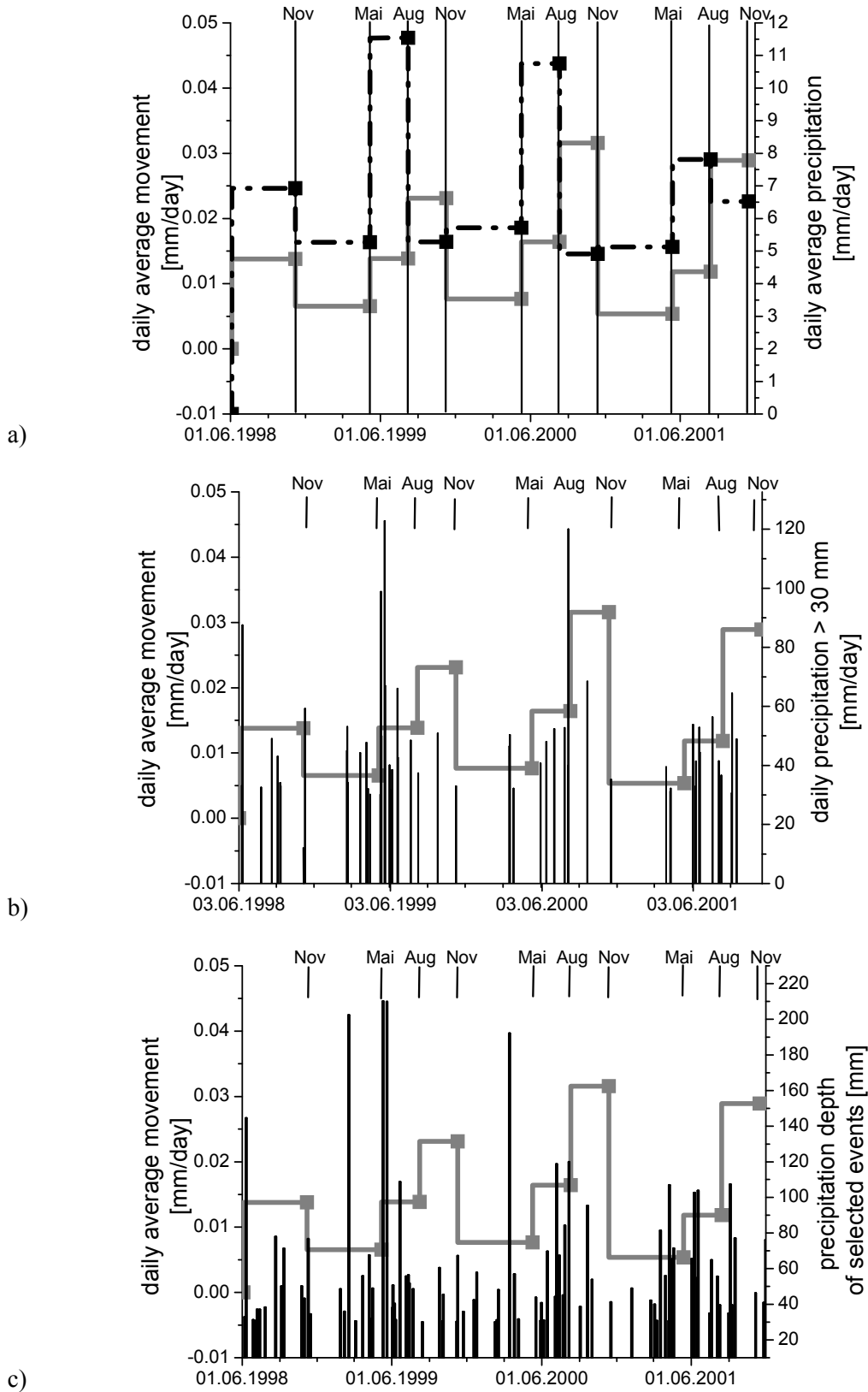
Figure 7-6: Selected plots for the comparison of GPS movement of group 2 with precipitation proxies, see also Appendix F-2. a) daily average movement with daily average precipitation, b) daily average movement with daily precipitation larger than 30 mm, c) daily average movement with precipitation depth of selected events which show that long lasting events do not correspond to movement rates.

8   A physically-based model to underpin major findings

The application of a physically-based hydrological model as CATFLOW (Maurer, 1997; Zehe *et al.*, 2001) is useful to better understand and visualise dominating hydrological processes on the Heumös slope. More conceptual modelling approaches would have two major shortcomings: the mass conservation included in CATFLOW gives a better basis for closing the calculated water balances. Secondly as most conceptual hydrological models are fitted on discharge time series, it is necessary to be able to rely on their good data quality. If this is not the case, a physically-based approach reduces the necessity of fitting a model and also, more output parameters can be used for validation. The advantage of CATFLOW is that the model can calculate major soil hydraulic processes on a time-continuous base, including an advanced soil-vegetation-atmosphere module (SVAT) for calculation of evapotranspiration.

Two dominant hydrological systems will be modelled representing dominant processes and structures of hydrotope #1 and #2. The results enhance the findings of the general hydrological behaviour of the hillslope body and the assumed pressure propagation from the southern slope. In hydrotope #1 the high inclination favours a surface runoff generation. Observations show, however, that preferential infiltration through macropores and shrinkage cracks dominate fast infiltration and lateral flow. Fast spring reactions suggest that the subsurface water dynamics are governed through fast processes. In this area the part of the surface runoff generation is less important than the amount of water that contributes to a groundwater level rise and, consequently, to a pressure rise. In contrast, generally high surface runoff production and low infiltration rates into the unsaturated zone of clay soils are found in hydrotope #2. With low conductivities and low subsurface fluxes, evapotranspiration seems to have significant influence on the water balance of the upper soils. The possibility for detailed discretisation of the catchment area and the subsurface, and the extensive SVAT module favour the use of CATFLOW in such an environment. The objective is to explore whether deep infiltration on the hillslope body influences the groundwater system.

1. The first presented model set-up will help to understand dominating processes on the hillslope body, represented by hydrotope #2, which is supposed to be dominated by surface runoff. The best runoff time series are from creek 3. The catchment is entirely located on hydrotope #2, and very steep slopes and rock scarps, which can produce high amount of debris in the creek, do not exist. The catchment model of creek 3 is introduced in chapter 8.2.

2. The second model set-up concentrates on the steep southern slope, namely hydrotope #1. The small 1128 m² subcatchment of the spring is used to simulate a likely concept of how the transition between the southern slope and the hillslope body might look like. The model is called the spring model (Chapter 8.3). One idea for the spring model set up is that preferential flow on the steep slopes leads to the filling of a subsurface storage, a pressure propagation is expected in the saturated subsurface towards the hillslope body. Hence, excess pressure cannot escape due to a confining cover. The pressure level rises and might reduce shear strength in the hillslope body. A single slope is the core of this model with a simplified set-up for the soil structure. The objective is to explore how the subsurface water contributes to pressure build-up and how stress release is conducted.

Two limitations in the concept of CATFLOW should be noted: 1) the complex issue of volume changing shrink- and swell processes in the soil. These processes change the matrix porosity and can produce preferential flow in shrinkage cracks in relation to soil moisture states. An applicable conceptual approach for catchment scale modelling of this kind of preferential infiltration has not been found yet (Bronswijk,

1988; Chertkov, 2003b; Greco, 2002). The problem is how to implement high flow rates in dry conditions and low flow rates in wet conditions in dependency of the actual soil moisture state. 2) a missing snow module reduces the performance in winter; an adequate snow accumulation and melt process needs to be implemented in CATFLOW yet. A simple conceptual snow model like a temperature-index approach would not meet the necessities of a physically-based model. An snow model with an energy balance approach (Blöschl & Kirnbauer, 1991) would be suitable but requires additional parameters to validate the model which were not measured on the Heumös slope.

8.1 The physically-based hydrological model CATFLOW

The physically-based model CATFLOW was developed and expanded in the hydrology section at the Universität Karlsruhe (TH) (Maurer, 1997; Zehe, 1999; Zehe *et al.*, 2001). The model was constructed and applied in the Weiherbach catchment (Plate, 1992; Zehe, 1999). The model has been applied successfully at the Weiherbach catchment (Maurer, 1997; Zehe, 1999; Zehe *et al.*, 2001) for a continuous calculation of three years in a silty soil (Loess) of the Kraichgau Region in Baden-Württemberg. It was also applied in a forested sandstone catchment in the Black Forest in Baden-Württemberg, the Duerreych creek catchment (Casper, 2002), for a clay soil catchment in northern Baden-Württemberg (Lindenmaier *et al.*, 2006), in the Schäfertal catchment in the mid German Harz mountains (Gräff, 2004), on forested hillslopes (Bott, 2002) and on agricultural hillslopes which were used for irrigation experiments (Sauer *et al.*, 2006).

The basic model philosophy of CATFLOW (Zehe *et al.*, 2001) is to subdivide a catchment into a number of hillslopes that are interconnected via a drainage network. Each hillslope is discretised along the main slope line into a 2-dimensional vertical grid using curvilinear orthogonal coordinates. Each model element, as defined by the grid, extends over the width of the hillslope. The widths of the elements can vary from the top to the toe of the hillslope. Surface runoff is routed on the hillslopes, fed into the channel network and routed to the catchment outlet. It is based on the convection diffusion approximation of the 1-dimensional Saint-Venant-Equation (Maurer, 1997). The hillslope module can simulate infiltration excess runoff, saturation excess runoff and return flow. Evapotranspiration is represented using an advanced SVAT model based on the Penman-Monteith approach that accounts for plant growth, soil albedo as a function of soil moisture and the impact of local topography on wind speed and radiation (Kolle & Fiedler, 1996). Soil water dynamics at each individual hillslope is assumed to be independent to adjacent slopes and is modelled using Richards Equation (Richards, 1931) in the pressure based form. The soil hydraulic functions are parameterised with the equations of van Genuchten (1980) and Mualem (1976). Preferential flow is represented using a simplified threshold approach to switch to a higher hydraulic conductivity when soil saturation exceeds field capacity; a validation for this approach was derived from field experiments (Zehe & Flühler, 2001a,b).

8.2 Set-up for the creek 3 catchment model

The essential prerequisite for a highly distributed physically-based model is an exhaustive data set both for the spatial distribution of hydraulic parameters as well as for the temporal resolution of necessary time series. It is not possible to provide all these information in sufficient quality and extent for each catchment study so that some data has been taken from the original set up from Maurer (1997) like the SVAT parameters. In the following, the basic structure of the model set-up is explained. Some parameters are more sensitive than others in the model. In addition, some parameters or data sets are readily available, whereas others are of minor quality or not available for the study site, thus in this case an

intense discussion of input data is needed. Quite a few parameters are also used in the spring-model so that they are not discussed in chapter 8.3 again.

To improve the sparsely available information about the pre-processing, a manual was written to document the pre-processing steps (Lindenmaier & Zehe, 2002). An advanced pre-processing wizard for the spatial data using ArcGis Visual Basic language was written with the help of this documentation by Reusser (2005).

8.2.1 Subdivision of hillslopes and channel network

The digital elevation model (DEM) is composed of 10 m topolines digitised out of the topographic map 1:50.000. In addition, 600 GPS measurement points taken in forest-free areas are implemented into the digitised topolines to add additional small-scale topography (Chapter 4.1). The composed topolines were used to generate a 5x5 m² grid, which was remodelled in several intervals including the integration of digitised depth contours like creek gullies.
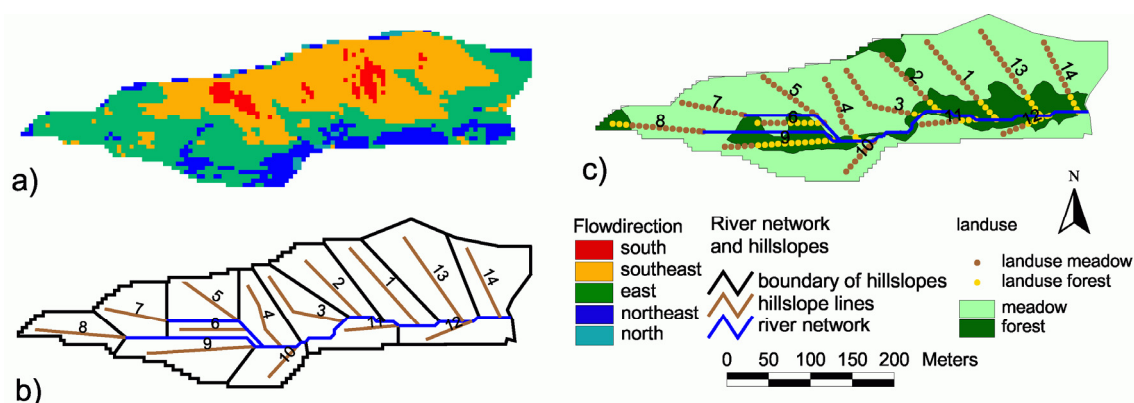
Figure 8-1: a) Flow direction calculated from the DEM; b) river network (blue), hillslopes (black border) and hillslope lines (brown) which represent the hillslope on the surface and are used for discretisation into depth; c) forest–meadow distribution which was used to implement landuse-specific parameters for the calculation of evapotranspiration.

With the help of ArcInfo routines and the graphical interface ArcTools, the DEM is prepared for delineating the catchment into hillslopes, connected with a channel network representing creek 3. The model catchment's shape is elongated in a west to east direction. The total height difference is 140 m, the uppermost grid cell lies at 1212 m and the weir is located at 1072 m a A. The total size of the catchment model is 65.300 m² which is slightly smaller than the catchment size calculated from the new DEM, which results in 67.330 m². Figure 8-1a shows the flow direction of each grid cell of the model catchment. Each black-bordered hillslope in figure 8-1b is supposed to represent a sub-catchment or sub unit of the total catchment comprising similar properties. A line is digitised in the middle of each hillslope in flow direction so that characteristic subsurface parameters are represented. The asymmetric shape of the catchment with long areas exposed to the south and short areas exposed to the north is visible in figure 8-1, according to the flow direction (compare orange with blue fields). This means that many flow cells are directed to the east, which complicates hillslope line placement. A hillslope line should represent the major flow direction of its particular hillslope. This kind of discretisation suggests that CATFLOW can be called a 2-½ dimensional model. The model catchment is parted in a total of 14 hillslopes with sizes of 2003 m² to 8824 m². Each hillslope line is parted into an equal amount of surface nodes. These

nodes represent the hillslope in terms of landuse, soil hydraulic parameters and border conditions, the 14 hillslope lines have lengths from 50 to 130 m.

Creek 3 is parted into two channels according to the DEM. The length of these discretised channels account to 619 m, which connect in the upper half of the catchment. Only one dominant and observable channel exists in the field but is surrounded by numerous smaller channels. Specific geometric parameters as well as roughness parameters (Strickler, 1923) are assigned to each channel node. Hillslopes, hillslope sizes or additional paved surfaces are assigned to the channel nodes as well. According to Maurer (1997) the channel cross section is represented as a trapezoid for each Strahler-order of the river network (Strahler, 1956). In mountain streams, roughness parameters are generally lower than in lowland streams (Furrer, 2001). According to the Strahler-order and specifications of Maurer (1997) roughness factors of 10 and 20 are chosen for the simulations. Model studies on an event base were used to approximate the Strickler roughness coefficient. Lower roughness indices are plausible because the channel bottom of creek 3 is very rough but this yields delayed and restrained runoff reactions in contradiction to observations.

8.2.2 Hillslope discretisation

The discretisation of the 2-dimensional vertical hillslope lines is conducted using a curvilinear orthogonal coordinate system (Maurer, 1997). This has the advantage that the border of a hillslope line can be represented continuously and without steps in contrast to Cartesian coordinates. The second advantage is that the discrete form of the 2-dimensional Richards equation for unsaturated subsurface flow is applicable in an orthogonal grid and so the numerical solution is more advanced (Maurer, 1997). The disadvantage is a more complicated pre-processing to achieve the curvilinear orthogonal coordinates.
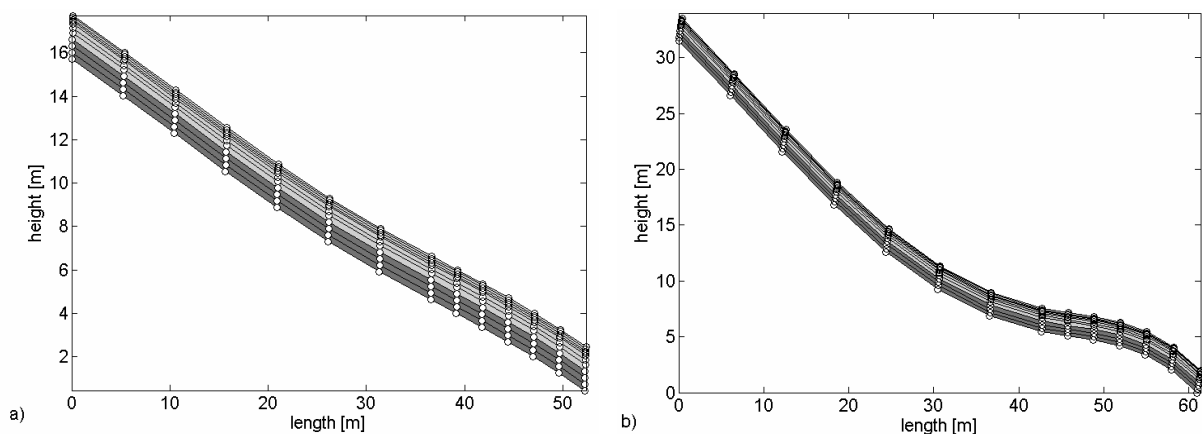
Figure 8-2: Two hillslopes of the model set up a) hillslope 12, b) hillslope 14. Dark grey represents the silty clay with a conductivity of 3.5*10^{-7} m/s, light grey represents the same soil type parameters but with a conductivity of 6.4*10^{7} m/s. The white points represent the nodes for calculation.

The hillslope lines are split into points with even distances by an AML-Routine in the GIS environment, favourable into a length which is slightly larger than the diagonal of a grid of the DEM. The hillslope line points need a monotonous slope for further processing. Nevertheless, sinks on the surface are allowed. This points are intersected with the DEM to derive three-dimensional coordinates. For each hillslope point an adjacent area from the hillslope is calculated with the Thiessen polygon method (Maurer, 1997) to achieve the size and width of the represented area to make up the balance for the calculated fluxes. These data is transferred from the ArcInfo environment to a MATLAB environment to refine the

structures to a desired amount of nodes (Figure 8-2). Each node can be assigned to several parameters depending on its location like landuse or soil hydraulic function parameters for the encountered soil type. Boundary conditions have to be assigned to border points. The creek 3 catchment model hillslopes are discretised into 10 nodes in vertical and 14 nodes in lateral direction.

8.2.3   Soil types and soil hydraulic parameters

The dominating soil of the creek 3 catchment is a stagnic gleysol. The investigated soil cores show similar soil properties, especially concerning hydraulic parameters. A catena is not distinguishable, the soil type is rather oriented at small scale movement structures as soil creeps or rotational slides. One soil type clearly dominates the soil cores, a silty clay. Soil hydraulic parameters are taken from Carsel and Parrish (1988) in (Maurer, 1997). To present a stagnic condition and to follow field observation, the model soil is set up with two layers. Both layers have the same parameters but different saturated hydraulic conductivities (Table 8-1).

Table 8-1: Parameters of the pedotransfer functions of the used soil types (Mualem, 1976; van Genuchten, 1980). The first two soils are the upper and lower horizon for the creek 3 catchment model. The other three soil types are designated for the spring model.

Taxonomy Soil Survey Division Staff (1993)	Soil type classification in the field after AG Boden (1999)	Saturated hydraulic conductivity Ksat [m/s]	Saturated soil moisture θ_s [ ]	Residual soil moisture θ_s [ ]	Reciprocal air entry point α [1/m]	Quantity characterising the pore size distribution n [ ]
SiC upper	Tu3	$6.40*10^{-07}$	0.36 or 0.6	0.07	0.5	1.09
SiC lower	Tu3	$1.70*10^{-07}$	0.36 or 0.6	0.07	0.5	1.09
SL	-	$1.23*10^{-05}$	0.41	0.06	7.5	1.89
L	-	$2.89*10^{-06}$	0.43	0.07	3.6	1.56
SiCL	-	$1.97*10^{-07}$	0.43	0.08	1.0	1.23

The soil hydraulic conductivity for model input is chosen according to results of local estimation from field tests and laboratory tests, please compare chapter 5.3 and 7.2. A hydraulic conductivity of $6.4*10^{-7}$ m/s is assigned to the upper horizon. This is the median of the field measurements in a depth of 20 cm on the meadow (Chapter 5.3). Stagnic properties are represented in the model soil through lower conductivities in the lower horizon, $3.5*10^{-7}$ m/s respectively. This value is derived from the hydraulic conductivity values of both the 50 cm constant head permeameter measurements on the meadow as well as from laboratory hydraulic conductivities of lower horizons (Figure 8-3a).

Macropores are abundant in the creek 3 catchment but the process representation in CATFLOW is different to the observations of Zehe *et al.* (2004; 2001a) in the Weiherbach catchment. Macropores in Loess soils are threshold governed which means that flow in a macropore does not occur before a certain soil moisture state of the matrix is reached. When this specific soil moisture state is reached the saturated hydraulic conductivity of a soil is multiplied by a defined factor in the model, i.e. the actual unsaturated hydraulic conductivity is calculated with a new global hydraulic conductivity. This gave good results in the Weiherbach catchment (Maurer, 1997; Zehe *et al.*, 2001). In soils with a high clay content, the factors need to be extremely high to have any influence on the unsaturated hydraulics (Sauer *et al.*, 2006). Initiation of macropore flow is considered to be different (Lindenmaier *et al.*, 2006), too. Shrinkage cracks dominate subsurface hydraulics in clay-rich soils. They are hydraulically active when the soil moisture state is rather dry. Such an initiation has yet to be implemented into CATFLOW. Clay soils show a complex behaviour through shrinking and swelling: Porosity and crack apertures change in relation to the water content (Figure 8-3). This is the reason why small macropore factors and a high

initiation threshold were taken for the model set-up. This enables to cut maximum discharge values but generally does not influence unsaturated soil water dynamics in the slope.

A high soil porosity was found on the Heumös slope (Chapter 5.2.2), differing from porosity values of the soil hydraulic functions for clay soil which was reported by Carsel & Parrish (1988). Their values probably refer to effective pore spaces but neglect the total pore space as it occurs in clay-rich soils. The model set-up was run with the reported porosity values which yielded good results for runoff and water balances. Though soil moisture values are too low. For this the set-up was changed to the measured total pore space values (Figure 8-3) to get values which are comparable with the TDR measurements.
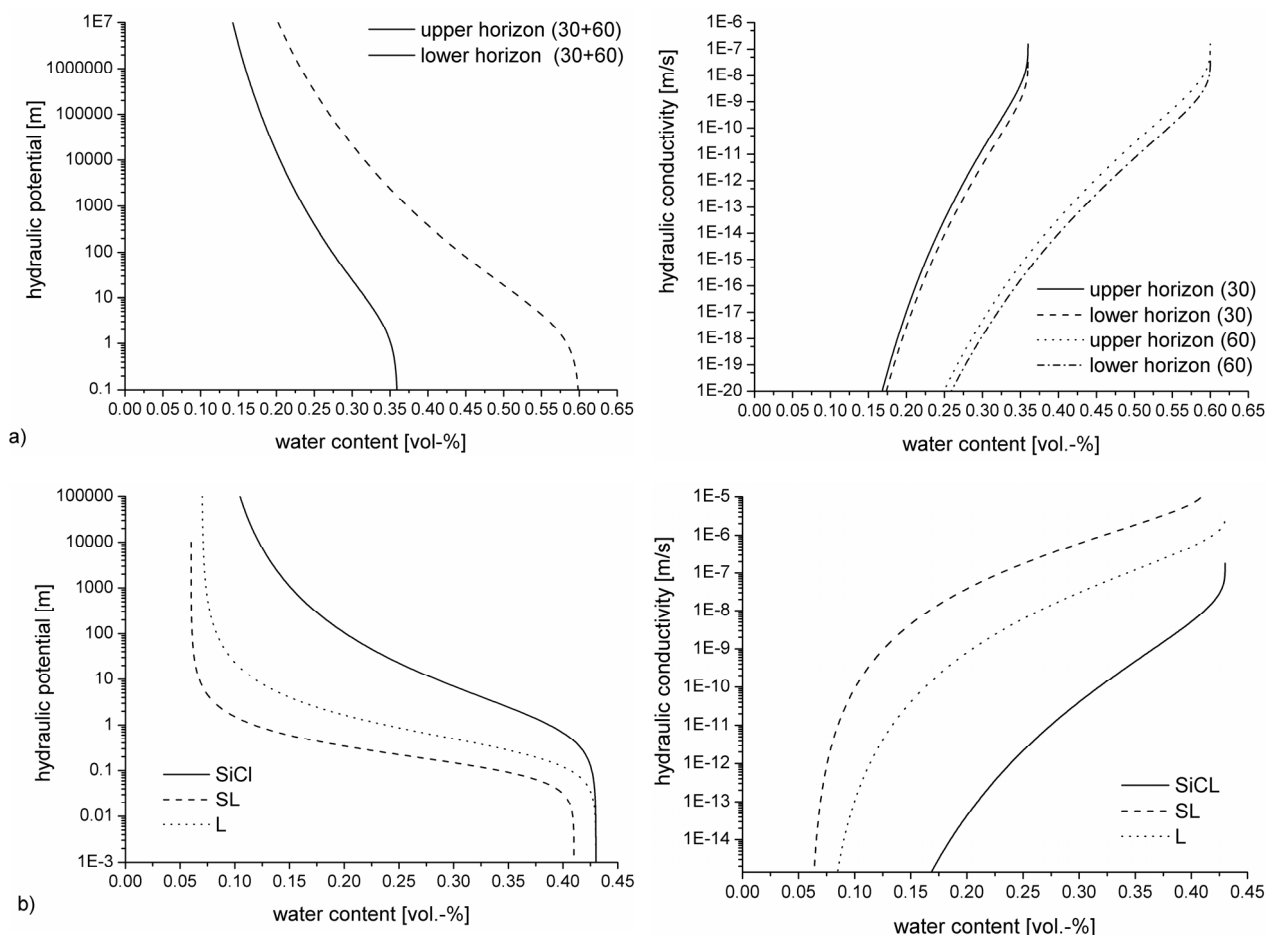
Figure 8-3: Pedotransfer functions and hydraulic conductivity – water content relation for the soil types used in the model: a) Heumös creek catchment model b) spring model

8.2.4   Landuse parameters

An alder and spruce forest in narrow strips alongside the creek and at its northern borders cover the creek 3 catchment. The remaining area is covered by a meadow used for cattle grazing and hay production. Figure 8-1c shows the distribution of landuse and how it is represented in the model structure. Parameters for the evapotranspiration module are root depth, plant coverage, plant height, specific albedo of the plant type, stomata resistance, specific plant type macropore parameters and leaf area index (Maurer, 1997). A definition of the surface roughness is needed for the surface runoff module. All parameters are taken from the literature (Kolle & Fiedler, 1996; Maurer, 1997).

8.2.5   Climate and precipitation time series

A sequence of periods is used for the model calculation, each representing a hydrological year on the Heumös slope. Calculations start on October 1st and run until September 31st of the following year. The hydrological years 1999, 2002, 2003, 2004 are used for calculation. The year 1999 was very wet and therefore is interesting for calculation. No climatological data is available for this year, this is why the climatological time series of the year 2004 are used instead. All other years have almost complete time series, despite small gaps. The gaps were filled with similar periods from either the previous or following years. Gaps and their replacements are listed in table 8-2. A comparison of runoff observation with calculated time series is conducted for selected time spans where good runoff data is available, e.g. the gravel-free periods of the summers 1999, 2002 and 2004. Periods with snow accumulation and melt are excluded from evaluation. Good observation of discharge exists for the calculation of the summer of 2002, especially for the 10/08/2002 event. Unfortunately, the climate station was not working from July to September. The hydrological years of 2002 and 2004 are considered to be normal in respect to precipitation, whereas the year 2003 was dry.

Precipitation time series are either from digitised Ebnit church I paper strips or from the new digital device of the same location. Heumös slope precipitation data has too many data gaps to be of good use. The year 2001 features a large data gap for the Ebnit church I gauge so that this year was excluded from calculations.

Table 8-2: Periods used for the calculation combined with different sets of the lower boundary condition. Data gaps were filled with equivalent time spans of preceding or following years.

Year	Period	Lower boundary condition	Remarks
1998	1.10.1998 – 31.12.1998	no flow	Only for spring model simulation, climate data is taken from 2004 time series.
1999	01.10.1998 – 30.09.1999	no flow gravity flow	No climate data available so that the 2004 climatological time series was taken Precipitation from digitised data
2002	01.10.2001 – 27.07.2002 27.07.2002 – 30.09.2002	no flow gravity flow	Original climate data only up to 27.07.2002; following climate data taken from 2004
2003	17.10.2002 – 29.09.2003	no flow gravity flow	Data set complete
2004	01.10.2003 – 29.09.2004	no flow gravity flow	20.01.2004 – 12.02.2004 missing climate data replaced by equivalent 2005 data
2004	01.10.2003 – 29.09.2004	no flow gravity flow	20.01.2004 – 12.02.2004 missing climate data replaced by equivalent 2005 data; models were run with high porosity values

## 8.2.6   Boundary- and initial conditions

Two hillslope margins have a fixed boundary condition in most cases: an atmospheric boundary condition for the surface nodes of each hillslope and a no-flow boundary condition for the left margin. Either a gravity-flow or a seepage boundary condition can be assigned to the right margin. The seepage boundary condition lead to very high calculation times for a model run so that it was discarded from further calculations. A cause for this are the soil hydraulic parameters of the silty clays. Either a no-flow boundary condition or a gravity-flow boundary condition is assigned to the lower margin. Both boundary conditions were tested for each model run.

Due to a lack of actual soil moisture information for the whole simulated catchment area, an initial moisture content for each calculation node has to be found. Measured soil moisture is near saturation on the Heumös slope so that initial condition was set to a very high value: 90 % of relative saturation was

selected for the beginning of calculation in October of each calculated year. This proved to be an appropriate value so that tuning of the soil moisture was not necessary.

8.3   Set-up of the spring model

The model set-up for the spring model is based on a single hillslope. It is supposed to represent the surficial catchment of spring 1 on the southern slope, the transition towards the hillslope body and parts of the hillslope body. Figure 8-4 sketches the principal set up of the hillslope. The set-up is based on the hypothesis of a lateral pressure propagation from the southern slope towards the hillslope body (Chapter 7.3): a confined and saturated zone in the hillslope body is influenced through changing soil moisture states in the adjacent steep southern slope. A release of pressure is only possible through gravity flow at the right boundary and seeping at the hillslope surface. The simulation has been conducted for 1998 because it is the only year with groundwater table time series. The calculated hydraulic potential cannot be directly equated with the measured groundwater table changes in borehole KB 3. The hydraulic potential output from CATFLOW is a node-wise value, which presents the vertical hydraulic potential at each node. The measured groundwater table changes represent hydraulic pressure levels of a three dimensional system. Nevertheless, a similar behaviour of the calculated time series of a certain node, which is in similar position as the piezometer device, and the groundwater table time series might show that stress build up and release in the model resemble field processes.
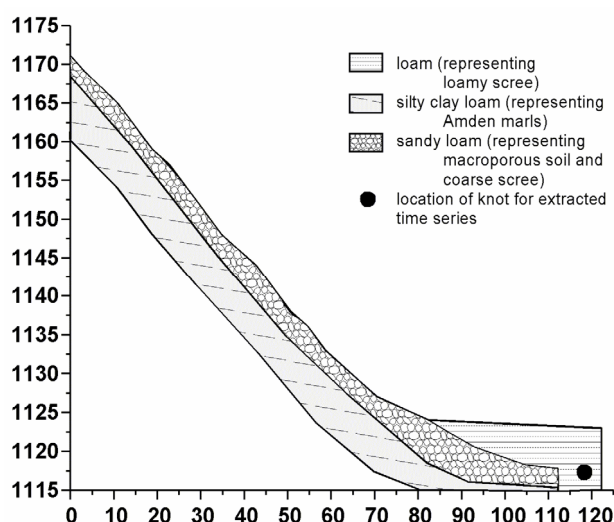
Figure 8-4: A sketch of the spring model set-up. A high conductivity layer represents the fast reacting soil column as well as a coarse scree cone. This cone is underlain by low conductivity material representing a transition to the Amden marlstones as the impermeable lower boundary condition. The soil column capping the coarse scree cone is represented by a silty loam. The depth of the layers is not to scale.

It should be noted that the mathematical core of CATFLOW is not designed to calculate water flow in saturated aquifers. Additionally, the material characteristics of a swell-shrinkable leptosol encountered on the southern slope cannot be represented accordingly with pedotransfer functions (Figure 8-3). It is helpful though that the generalised Richards equation is calculated on a pressure-based form so that saturated conditions are approximately right. Preferential infiltration into the leptosol on top of the southern slope is represented through a loamy sand. The same soil type is used for the scree material suggested to exist in a scree cone at the southern slope – hillslope body transition. The loamy sand is a material with fairly high conductivities and a low water storage capacity due to its high porosity (Figure

8-4). A loam is used with low hydraulic conductivities for the representation of the bedrock and some parts of the hillslope body (Table 8-1). A part of the scree cone cover is represented by a less conductive material as well, a silty clay loam. Grass was used as landuse parameter set instead of forest to reduce calculation time. The boundary conditions are 'no-flow' for the bottom, representing impermeable marlstones and gravity-flow at the right, lower side. The spring model set-up results are thought to be compared with piezometric data, so precipitation data from 1998 was used as well as "artificial" climatic time series (Table 8-2). Measured climatic data as well as runoff or discharge time series were not available for this period.

The same hillslope, exposed to the north, was used to calculate evapotranspiration depths for chapter 6.1.3 with yearly time series for climate and precipitation of 2002, 2003 and 2004. Data gaps were closed according to table 8-2.

8.4 Model results for creek 3 catchment simulation

The known restrictions of the discharge data complicate the validation of the model runs (Chapter 6.2). On the other hand, the high feasible discretisation and the physical based concept of CATFLOW has several advantages compared to models with more conceptual approaches (Bonomi & Cavallin, 1999; Malet *et al.*, 2005). Models based on physical equations do not need calibration of parameters. Parameters are derived by measurements; when the model concept represents the dominating processes of a catchment, the performance should be close to the observations. A failure of the model for certain climate conditions might mean that the process representation is not met in the model. Another advantage is that more state variables than discharge can be used to validate the model output, e.g. soil moisture or hydraulic potential. This is useful to narrow down errors from time series observation.

Table 8-3: Average precipitation depths per day for the period of May to August. a) Average precipitation depth for the WMO standard period from 1960-1990. b) Average precipitation depth for the observed summers.

a) May-August of WMO standard period 1960-1990	Precipitation [mm/day]		b) May-August	Precipitation [mm/day]
Minimum	6.30		1998	5.49
Maximum	11.30		1999	10.35
Average	7.92		2000	8.44
Median	7.54		2002	8.74
			2003	4.48
			2004	6.97

There are some restrictions of the measured discharge time series that should be kept in mind while reading through this chapter: the time series digitised from paper strips might have been not placed or arranged exactly and the rating curve often changed due to gravel deposition in the weir. Both the resolution in time as well as in discharge volume might differ from event to event. A good representation of processes in the simulations show results which better close the water balance for certain time spans. The winter period performance is not comparable to the measured time series without a snow module. This is why the focus will be on summer periods, preferably those with gravel-free times. Sometimes, the creek 1 time series performed better than the ones of creek 3 so that they are plotted for comparison. To characterise the chosen summer periods which exhibit differing time spans, they are listed with their average precipitation per day value and are compared to the average precipitation values of the WMO standard period (Table 8-3). The summer period of 1999 is wetter compared to the average, the summer

of 2003 is one of the driest recorded summers. The summer of 2002 and of 2004 are close to the average of the WMO period, though 2004 is still influenced by the dry winter of 2003-2004.

8.4.1   Event-based model performance

Like in chapter 6.5 a closer look is taken on some of the extreme events considering duration and precipitation depth as well as on short high-intensity rainstorms. All figures include the course of the specific event (precipitation, discharge and calculated relative saturation) as well as cumulative graphs, including the calculated evapotranspiration. The long lasting events in May 1999 and August 2002, which exhibit intensities of up to 3 mm/10min are plotted in figure 8-5. Both events show that an initially high relative saturation of $S \cong 0.9$ leads to an almost total recovery of precipitation in the discharge curve. The volume balance of measured and calculated discharge is nearly 1. This means that the model performs very well for water balance calculations, though recession is underestimated slightly. Processes enhancing the retention need to be improved in the model. This could either be done by implementing a better representation of the uppermost, highly conductive layer as described in chapter 7.2 or the surface roughness could be altered. Maximum peaks are underestimated in the event of May 1999 and overestimated in the event of August 2002 (Figure 8-5). Under- and overestimation of peaks is closely linked to the precipitation intensity and a strong link between precipitation intensity and peak runoff is observed (Chapter 6.2).
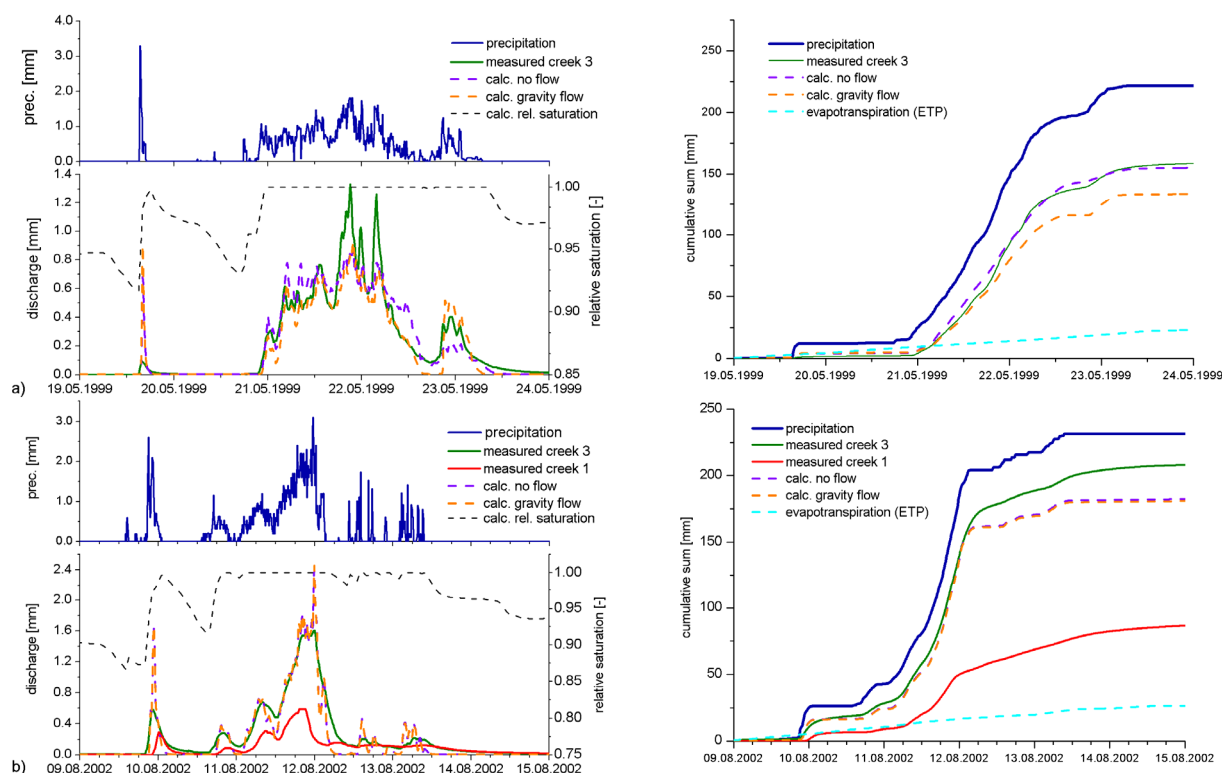
Figure 8-5: Simulation results for two long lasting precipitation events cut out of the yearly simulation periods. a) displays the second extreme event in May 1999 with 210 mm of precipitation in 74 h. b) displays the event of August 2002 with 205 mm of precipitation in 68 h. Precipitation and discharge in 10 min time-steps; relative saturation is extracted in 20 cm depth; evapotranspiration in hourly time-steps.

To validate the model the point of interest has to be directed to the idea of dominating surface runoff generation and inhibited deep infiltration and whether this is met with the model set-up. The cumulative

sums show that the no-flow boundary simulation performs well, if compared to the measured depth (Figure 8-5). In contrast, the gravity flow simulation features a higher loss. It is stated that the model set-up with a no-flow boundary allows a very good performance for these long lasting precipitation events. The more saturated the soil moisture condition is before an event, the better the model performs.

The selected high-intensity summer events are characterised by drier antecedent conditions with a relative saturation of $S \cong 0.75\text{-}0.8$ (Figure 8-6). In comparison to the long lasting events this means that the actual unsaturated hydraulic conductivity is more than one to two orders of magnitude smaller (Figure 8-3). See also chapter 6.5.2 for more information for these events. The simulation output distinctly overestimates discharge peaks. Especially for the event of August 2004 (Figure 8-6). A reason for the overestimated peaks is the clay soil behaviour: shrinkage cracks lead to a higher infiltrability and initial water loss during dry soil moisture states than the model can simulate. On the study site, preferential infiltration dominates over matrix infiltration at this soil moisture state. The high precipitation intensities (e.g. 7 mm in 10 min in figure 8-6a) are too high for the silty clay to take up and infiltration excess runoff is generated in the model.
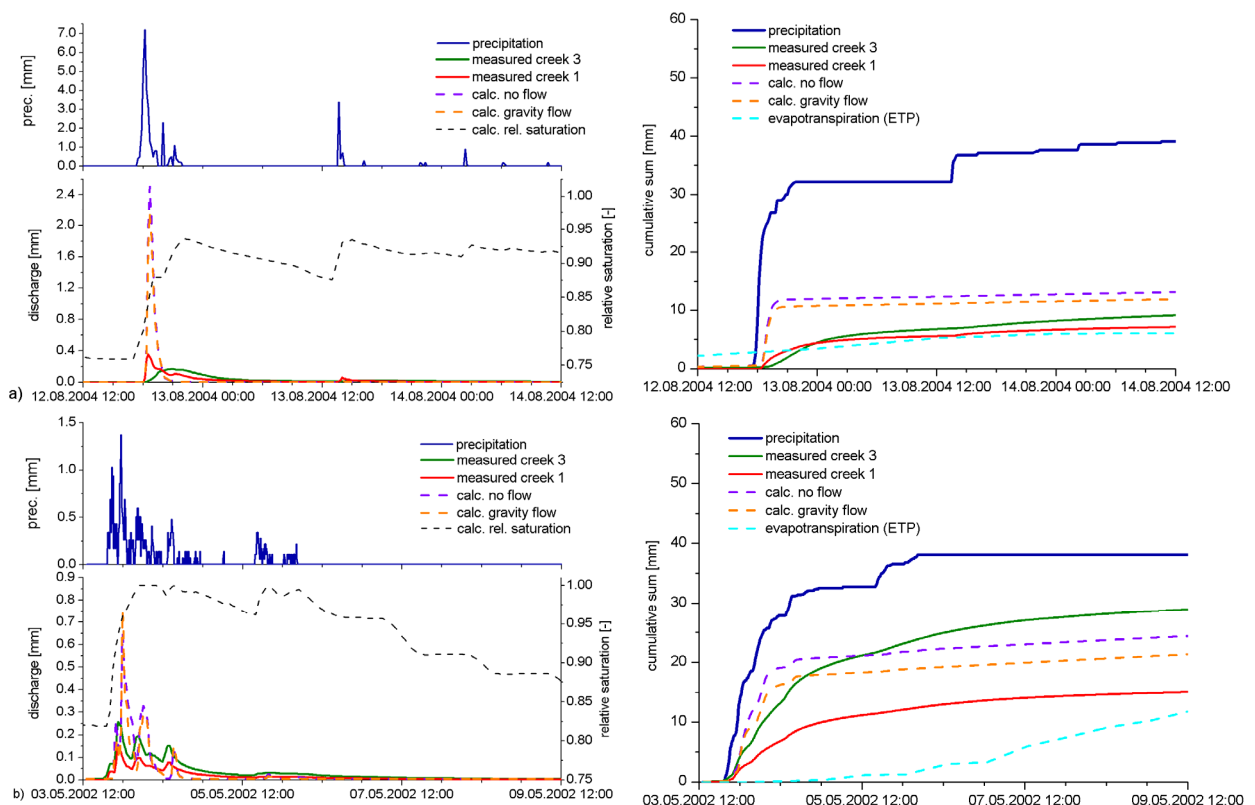
Figure 8-6: Overestimation of runoff peaks for a high-intensity rainstorm and a very small rainstorm: the low matrix hydraulic conductivity of the soil type hinders water to infiltrate; hence the peak surface runoff is overestimated. a) The event of August 2004: dry initial conditions and a high precipitation intensity leads to gross peak overestimation. b) early May 2002 after snowmelt, high initial moisture, low intensity, yet peak overestimation is observable. Precipitation and discharge is in 10 min time-steps, relative saturation is in 20 cm depth and evapotranspiration in hourly time-steps.

Several model runs have been undertaken to check the sensitivity of the model in this respect. Higher macropore parameters or shallow uppermost soil layers with higher conductivities or higher porosity values did not yield considerably better results for high-intensity events but yielded less good results for long lasting events. Nevertheless, calculated discharge depths of the no-flow boundary simulation is still

in better accordance to observations than the gravity flow boundary results. This means that deep infiltration would reduce the water balance too much and is not a feasible process during dry soil moisture conditions. Despite an overestimation of peaks and missing tailing in the recession, CATFLOW does well in distributing water into the right compounds. Small, high-intensity events show a high portion of surface runoff generation, other parts of the precipitated water are used up to increase soil moisture in the soil column, deep infiltration is negligible.

Shrinkage crack development is a soil moisture dependent process. A possible conceptual approach for catchment scale modelling could use an antecedent evapotranspiration factor to control shrinkage crack aperture to define a bypass flow.

8.4.2   Long term model performance in means of discharge volume

A closer look is taken on long-term performance with the event-based model performance in mind. Three summer periods is selected, the very wet summer of 1999, the very dry summer of 2003 and the „average" summer of 2004. Evaluation began after snowmelt had ceded so that different beginning times were featured. All periods finis on August 31st. Evapotranspiration shows a feasible value for 2003 and 2004 but not for 1999, as it has an artificial input of climate time series. Still, Figure 8-8 shows that the correlation coefficients and Nash-Sutcliffe efficiency are better, the wetter the hydrological year and the summer, respectively, was.

Dry periods perform worse in terms of the correlation and Nash-Sutcliffe efficiency. This is due to the more frequent occurrence of high intensity events in relation to periods with high precipitation depths. The overestimated calculated peak reduces the performance of the correlation coefficient. The more frequent occurrence of time-steps with low flows reduces the performance of the Nash-Sutcliffe efficiency. However, the total recovered volume is of more importance. The amount of recovery of precipitated water in the discharge shows that the lower the conductivity of the lower boundary, the better the volume balance. This means that performance on a long-term base is better for the 'no-flow' model set-up than the 'gravity-flow' model set-up. It is stated that the precipitation reaction on the hillslope body is dominated by surface runoff, on a long-term temporal scale. Deep infiltration has no influence and governing hydrological process in the soil column is a quick lateral interflow.

8.4.3   Comparison of measured and calculated average soil moisture values

The evapotranspiration-driven soil moisture state of the upper soil column is worth a second look. CATFLOW provides an output which enables to compare the distributed calculated soil moisture states to the measured TDR-signals. The weather station is located at the upper end of slope 12 at the border of a small forest patch alongside of the creek. The average calculated soil moisture is taken for the uppermost 30 cm but over the complete hillslope length. The land use of hillslope 12 is forest for 57 % of the surface nodes and 43 % of grass for the rest. In figure 8-8, average calculated soil moisture is plotted against the measured time series of the 35 cm TDR-rod in 2004. In summer, accordance of the time series is good. In winter, the observation shows a constant lower value than the calculation indicates. This is due to temperature dependent measurements of the TDR-rods (Chapter 4.2.2). Performance of the model for soil moisture values is better in the upper horizons, a less good agreement from measured time series to calculated time series for deeper horizons indicates that soil water movement in the matrix is even lower than the selected hydraulic conductivity in the model exhibits.
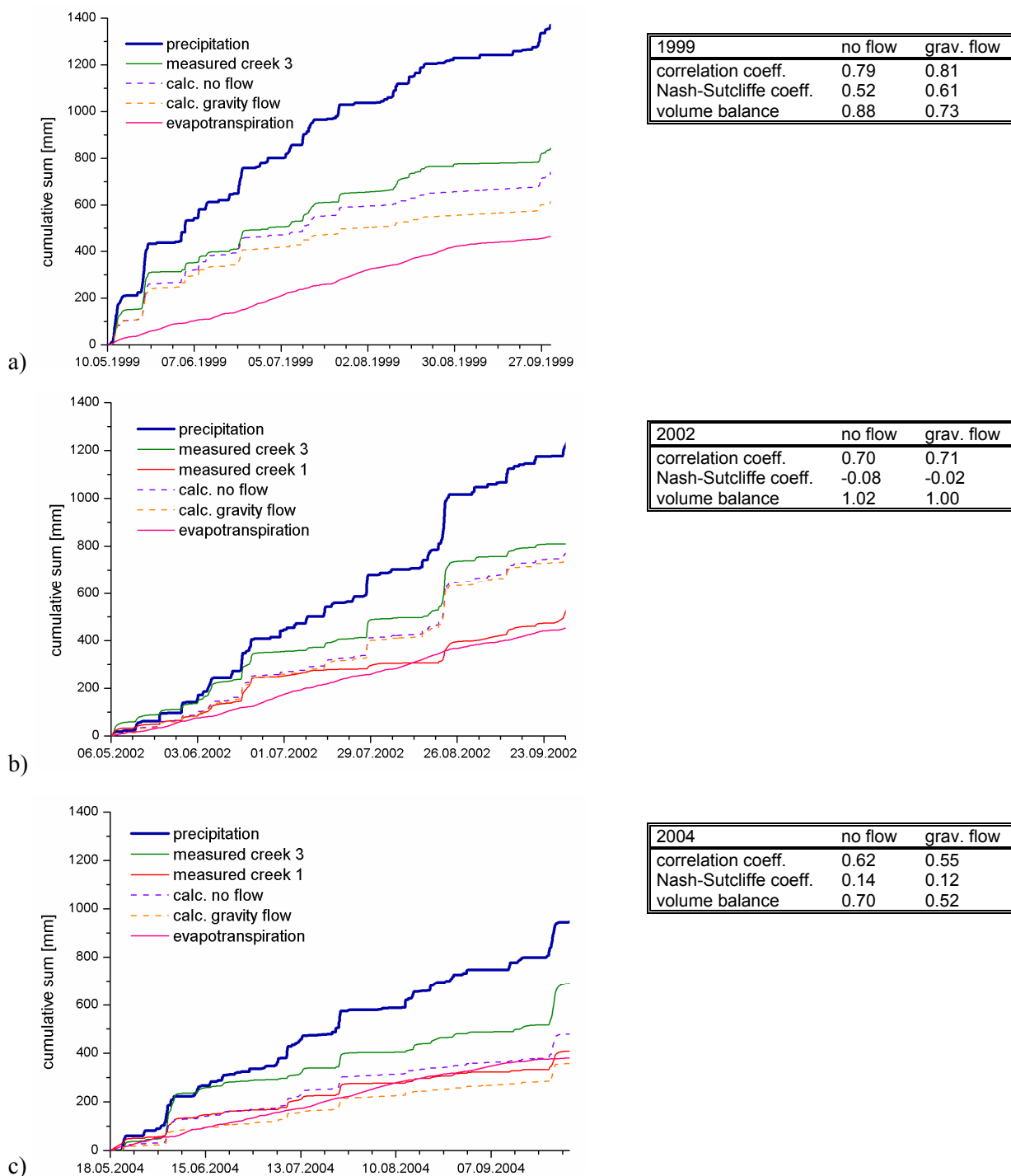
Figure 8-7: Cumulative measured and calculated time series for summer periods of 1999 (a), 2003 (b) and 2004 (c) as explained in the text. The tables show the correlation coefficient, the Nash-Sutcliffe coefficient and the volume balance (Chapter 4.3). The wetter the summer, the better the correlation coefficient and Nash-Sutcliffe coefficient. However, model performance is better tested with the volume balance, because it gives the quality of the simulation in accordance to the goals.
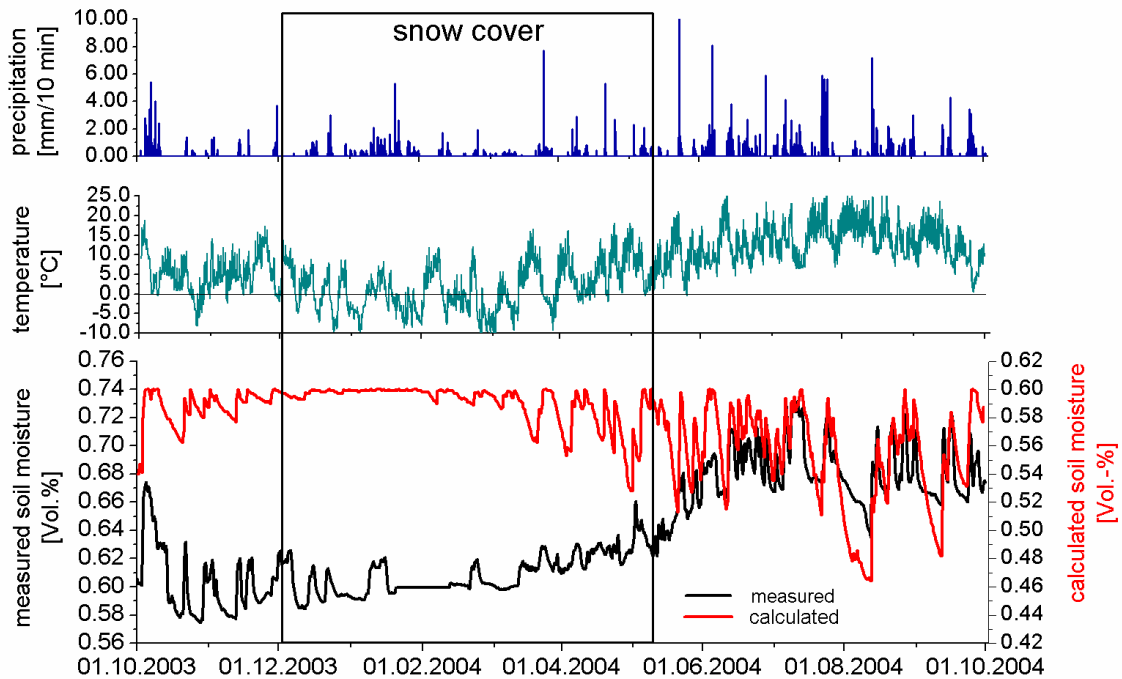
Figure 8-8: Soil moisture time series for 2004. From top to bottom: precipitation in 10 min intervals. The average daily temperature is plotted to estimate temperature-influenced measured soil moisture. The soil moisture values differ for the measured and calculated time series, which is a matter of chosen maximum porosity for the calculated time series and possible influence of charged clay minerals on the measured signal.

In figure 8-9 the spatial distribution of the soil moisture state is plotted for the driest period in 2004 which is August 11th. The August 12th event brought 32 mm of rainfall (Chapter 6.5.3). The calculated relative saturation is high near the creek and on the upper hillslopes where inclination is less. One hillslope represents wet conditions on August 11th. Low inclination characterises this area and observations show that this area is usually very moist.
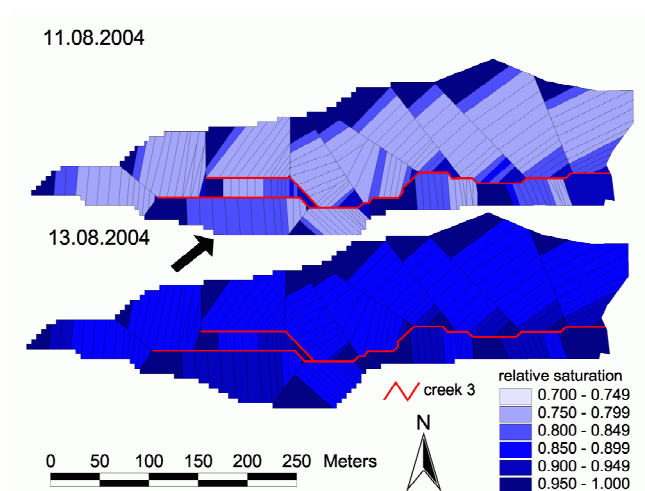
Figure 8-9: The spatial distribution of calculated relative saturation before and after the 12/08/2004 event with 32 mm of precipitation. The driest time of the year was the 11/08/2004 according to the TDR-signals, yet the moisture is typically high (Figure 6-14). The moister regions are at the upper slope areas with less inclination as well as at near-creek regions. The arrow indicates a relatively flat hillslope which features more moist conditions even in an overall dry moisture state.

8.5   Hydraulic potential of spring model hillslope in 1998

In figure 8-10 the groundwater table changes of the KB 3 piezometer device in a depth of 5.5 m is displayed together with the precipitation and the hydraulic potential time series of the spring model hillslope. The hydraulic potential line is taken from a single calculation node which lies in the lower right corner of the model hillslope, please compare figure 8-4.

The hydraulic potential in the deep soil column of the model hillslope is dominated by saturated soil moisture conditions. The changes of hydraulic potential are governed through changing levels of saturated conditions in the sandy loam above and through the gravity flow boundary condition at the right border. The progression of the hydraulic potential shows a seasonal behaviour similar to the observed groundwater table changes (Chapter 6.4.1). A high groundwater table is observed in the winter and spring is influenced by a long recession. The summer is dominated by calculated low hydraulic potential levels but shows similar quick rises as does the piezometer observations. The event correlation is not matched but this was not expected considering the restriction in the model set-up and the process representation (Chapter 8.3). Certain soil moisture states and antecedent conditions as well as specific precipitation events seem to trigger hydraulic potential reactions in the model. This is comparable to field observations and measurements.
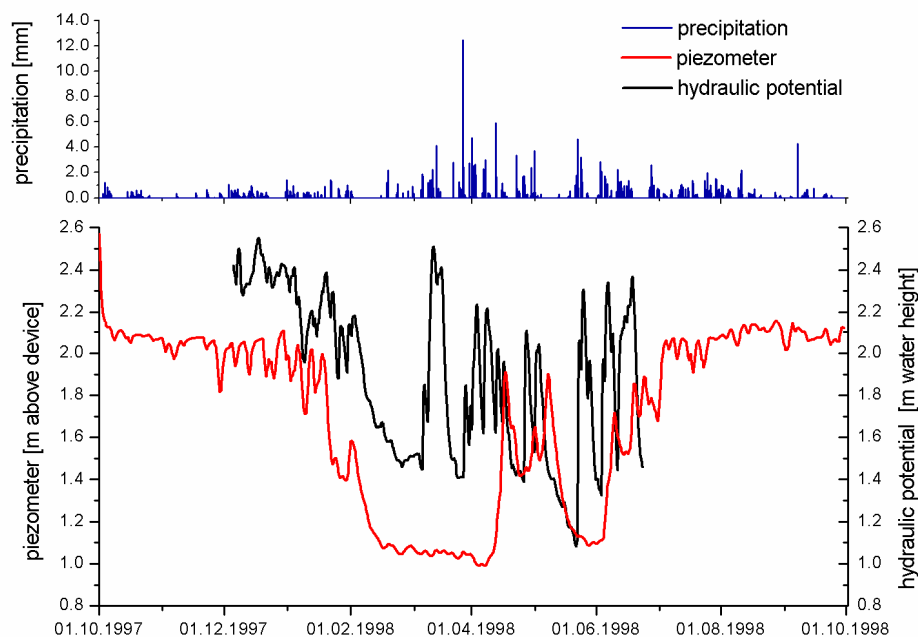
Figure 8-10: The piezometer time series compared to the hydraulic potential of the spring model set-up calculation in 1998. The climate time series are artificial so that small-scale fluctuations might not reflect real situations. This is why the calculated hydraulic potential has been smoothed. Note the yearly cycle with a low pressure stand in summer but higher variability as in winter.

113

9   Discussion and conclusions

This thesis wants to give a process-based view on hydrological mechanisms of unstable hillslopes which are prone to failure. The case study of the Heumös slope shows the importance of the identification of dominating processes and structures on different time and spatial, or structural scales. On the one hand, the initial observation scale of movement measurement seems to be chosen in time intervals which are too coarse. On the other hand, the detailed investigation and identification of processes and structures reveals and backs the hypothesis of a lateral pressure propagation. This would not have been possible without the synopsis and detailed investigations on different time and spatial scales and in different scientific disciplines. In the following, the major hydrological mechanisms will be discussed, then geological, pedological and hydrological aspects will be combined within the proposed structural and process scales.

Runoff generation and soil hydraulic processes

The most interesting identified hydrological process is fast preferential flow through macropores, soil pipes and especially a network of shrinkage cracks on the Heumös slope. There is a strong connection of water flow through preferential flow paths and soil moisture which again is dependent from a specific time and location. Very steep areas like the northern and southern slopes but also steep patches on the moving hillslope body are mostly influenced by water flow through preferential flow paths. Soil moisture changes are pronounced here which is also seen by the specific vegetation distribution of plants favouring periodically wet conditions. The high clay content of the soils leads to changes of their volume even in wet conditions. Many soil patches are often in an almost saturated condition, yet due to the specific behaviour of the plate-like clay minerals even small changes of moisture lead to a shrinkage and consequently to the opening of cracks. This means that shrinkage behaviour is a hydrologically relevant process even in wet clay soils in alpine environments.

The second dominating hydrological process encountered on the Heumös slope is saturation excess overland flow. Many patches, especially the ones with less steep topography are in a dominant wet to very wet soil moisture condition. These patches enlarge quickly during precipitation events which is due to the high initial soil moisture conditions and low matrix hydraulic conductivity. These flat patches contribute fast and readily to saturation excess runoff production during precipitation events and so govern channel discharge. The ecological moisture and hence the vegetation distribution show that hydrological processes on the hillslope body are dominated by surface runoff generation after all. The hydrographs show fast reactions after the onset of precipitation and fast rises of maximum discharge after maximum precipitation. So it can be concluded that the Heumös slope is a system with very fast response times. Recession of discharge is fast as well which indicates that retention is low. The shrinkage cracks and preferential flow paths through the unsaturated zone do not dominate catchment response during precipitation.

Groundwater system

Observations with the piezometer devices show relatively fast and high reactions of groundwater level changes at precipitation events. The geological profile indicates coarse sediments at the postglacial sediment – subglacial till transition. Finer postglacial sediments above this layer lead to the conclusion that a confined aquifer is encountered on the hillslope body. This is supported by the simulations with CATFLOW which show that deep seepage is not a favoured process on the hillslope body. The water budget of the creek 3 model catchment is better balanced with a no-flow boundary condition at the

bottom. A connectivity between the gleysols on top and the confined aquifer is not given and so there is no influence of deep seepage to groundwater table changes of the confined aquifer. The hypothesis that groundwater table changes are governed by groundwater level rises in debris cones at the southern hillslope – hillslope body transition and that these influence the confined aquifer in the hillslope body through a lateral pressure propagation. The recession analysis shows that the reaction of the observed spring 1 is very similar to the groundwater table changes seen in the piezometer in 5.5 m depth of borehole KB 3. It is possible to use spring 1 as a proxy for groundwater table changes in the confined aquifer of the hillslope body. With this, a reliable proxy for changes of load at the shear zone is available. Upcoming observation results in newly installed piezometers, in combination with the spring discharge, will help to calculate loading changes in the confined aquifer which can result in movement.

Combination of hydrological processes and movement

Hydrological processes influence the stability of hillslopes. Water content changes leads to changes in sediment stability, especially in clay-rich sediments. Groundwater table changes influence the balance of buoyancy forces of the confined aquifer and the sediment load. Water level changes on a long term temporal base are usually considered to affect the stability of a hillslope. On the Heumös slope, no long term changes were observable on an annual time scale. There are periodic movement and precipitation signals but these are on a shifted periodicity. The precipitation signals are followed by higher movement one observation interval later. But the question is, whether the chosen observation scale of the movement behaviour is wrong or rather indicates a derived quantity of movement. For example, maximum average movement can be a combination of successive single movement events which happen during a period of maximum groundwater table changes. There is the strong belief that the wrong observation scale is chosen here and that is why it is especially important to rethink process- and observation scales in landslide hydrology. The reason for this is the fast precipitation event related changes of the groundwater table. These infer that movement is coupled to a succession of events and not to long term creep. This is backed through observations with nanoseismic technology by Walter (2006). He could detect small scale rupture events near the location of the shear zone in the hillslope body during precipitation events. The identification of dominating processes both of hydrological, hydraulical and geomechanical origin in combination with structure identification is of vast importance for succeeding in the identification of the trigger mechanism and the state of stability of landslides.

Scaling in landslide hydrology

The theory of scaling is not commonly used in landslide research. It is e.g. a measure that process-based hydrological sciences use to cope with large space dimensions and different time scales of hydrometeorological processes. In the theory of landscape ecology, scales and scaling is the core idea of how to cope with the vast varieties of processes and patterns that evolve in a landscape. Measurements are often made on small scales but problem solving has to be done on large scales. This is also a fact for landslide research. Moving through different time and spatial scales is common in geology, maybe sometimes it is too common to even be recognised any more. Hence, it is useful to reflect scaling approaches in landslide research, especially when such a vast range of processes and structures are encountered which are usually covered scientifically by a lot of different disciplines. As the literature study in chapter 2 shows, deficits in hydrological descriptions and modelling still are abundant in landslide research. How can small material changes or the slow evolution of stability of a hillslope (several tens of thousand years) until failure be brought together with fast processes like precipitation, infiltration or surface runoff generation? The proposed approach to define scales in landslide research

which has a different look at hydrological and geomechanical patterns is useful to define dominating trigger mechanisms on landslides. Especially the map of ecological moisture helped to understand the hydrological control mechanisms. The dominating structures and processes on the Heumös slope will be discussed in the frame of geological and hydrological scales:

The deposition of marlstones as well as the tectonic uplift and folding of these rocks are the prerequisite for mass movement development in the Dornbirn Ache valley on the macro-scale. The high susceptibility to the weathering of marlstones is the key factor to mass movement development in this area. The glaciation times enhanced the vulnerability for the failure of hillslopes. Ablation and over-steepening of the mountain flanks as well as the deposition of subglacial till, which has a broad grain size distribution, lead to sediments prone to failure.

On the meso-scale, the history of post-glacial sedimentation governs the deposition of either coarse or loamy scree as well as the influence of weathering forces. This and the removal of sediments through erosional forces gives the necessary prerequisites for the Heumös slope to develop a critical condition for movement. The removal of sediments at the hillslope toe is an important external force that influences the stability. A second important force certainly is the climate regime with an extreme precipitation environment. Water influences the cohesion of the clay-rich material and additionally adds to the loading of the hillslope body. The infiltration of water into the subsurface influences both the shallow stability of the uppermost soil layers as well as the build-up of pressure forces in greater depths as has been recorded by the piezometer devices. From a hydrological point of view it is of utmost importance to understand the dominating hydrological processes and to close the water balance. The hydrological process identification precisely defines the movement of water on the surface and in the subsurface, the unsaturated and saturated soil zone respectively. Here, the micro scale dominates the identification of spatial patterns that lead to specific hydrological processes. Zones with dominating surface runoff generation or shallow subsurface flow can be separated from zones with fast infiltration and deeper subsurface storm flow. This process then governs groundwater table changes.

Wet to very wet contributing areas are defined with the help of the ecological moisture index map on the hillslope body. Here, stagnic gleysols dominate the runoff generation and low hydraulic conductivities inhibit deep infiltration of water. The water balance is best closed when all precipitation is either considered to evaporate or to be transformed into direct discharge, as observations suggest. Hence, the system is dominated by fast surface runoff and the huge amount of precipitation is directly removed in the creeks.

This is different for the southern slope adjacent to the hillslope body: Vegetation associations suggest a drier ecological moisture regime for this area. Detailed investigation on the micro-scale show that the southern slope is dominated by a network of interconnected shrinkage cracks. These govern the fast infiltration in the clay-rich leptosols. Shrinkage capacities are up to 35 vol.-% in soil moisture states, feasible for temperate climates, as a model for calculation of the soil shrinkage characteristic curve suggests. This means that volume change of the clay soils can govern the infiltration through shrinkage cracks even for a generally wet hydrological environment. The fast infiltration and flow in the subsurface is best observed in the spring 1 discharge reaction: after precipitation started a fast rise of the spring discharge considers fast subsurface storm flow in the adjacent slope. A long tailing of the discharge in spring 1 after an precipitation event indicates that a filled subsurface storage is only depleted slowly. A similar reactions is also observed at the borehole on the hillslope body, in 280 m distances. The similar reactions indicate that a lateral pressure propagation from the southern slope influences the groundwater

system of the hillslope body. Hence, a reactive hydrological system governed by micro-scale processes on the southern slope governs the deep subsurface water balance of the moving hillslope body which is on the meso-scale.

The point scale is represented by the specific clay behaviour which both influences hydrological processes and stability. Pore volume change and coupled water flow as well as cohesion need to be further integrated into landslide research.

Besides local, shallow surface movement on the hillslope body, the deep seated shear zone in 7.5-8.5 m depth can be influenced by these groundwater level changes. A direct relation of the subsurface hydraulic system with the movement could not be established yet. Surface movement observation showed that the hillslope body moves by about 10 cm a year towards the east (Depenthal & Schmitt, 2003). According to the specific inclination and location of the hillslope, different movement rates and directions are observed. The shear zone in 7.5-8.5 m depth moves with less than 1 cm per year (Schneider, 1999). Both movement observations could not be established with a high temporal resolution. The three to six month time-steps mean that the movement signals indicate a continuous creep. In the case of surface movement this even seems to work on a periodic time scale. A continuous periodic creep is not likely the major movement for the observed hillslope as long term hydrological signals do not correspond to this. It is rather suggested that a series of small scale jerky movements lead to the displacements of the hillslope as has been observed by Walter (2006). Specific climatological and hydrological conditions lead to these jerky movements. For the surface movements the period of highest movement rates is in midsummer. This corresponds with a time span of maximum evapotranspiration – one of the major factors for the release of water from the soils, and the time of most intense and variable precipitation, which means that in midsummer short high-intensity events with considerable precipitation sums govern the hydrological system.

The interrelation of dominating processes on the Heumös slope are difficult to grasp as a complex three dimensional system is encountered. Hence, physically-based modelling is needed to help identifying these processes. The application of CATFLOW shows that to identify dominating processes in the field are indeed representable in the model. The model application helps to understand the hydrological system of the Heumös slope and it is helpful to identify critical hydrological states that might lead to movement.

As discussed in the literature overview in chapter 2, many studies lack a profound identification of dominating hydrological processes in landslide research. In model application, which often is on a conceptual basis, important processes are not taken into account, inhibiting the closing of the water balance. Detailed process identification and recording still hampers determination of the closed water balances, e.g. as erosional forces reduce the discharge observation quality. On the other hand, models based on physical state laws can simulate observed processes in a better way than conceptual models can. The systematic approach of first identifying of spatial patterns and secondly a close up look at the dominating processes improved the understanding of the control mechanisms of the Heumös slope. The model application enhanced the findings of the perceptional idea and stimulated field research. This study proves that detailed hydrological studies are needed in landslide research to better understand fast processes in the case of landslides.

Ongoing research of the DFG funded research group For 581 will further enhance the understanding of dominating processes on the Heumös slope and advances hydrological and hydraulic model application for landslides.

References

AG Boden, 1996. Bodenkundliche Kartieranleitung. E. Schweizerbart' sche Verlagsbuchhandlung, Hannover. 392 pp.

Allaire-Leung, S.E., Gupta, S.C. and Moncriel, J.F., 1999. Dye adsorption in a loamy soil as influenced by Potassium Bromide. Journal of Environmental Quality, 28(6): 1831-1837.

Amoozegar, A., 1989. A compact constant-head permeameter for measuring saturated hydraulic conductivity of the vadose zone. Soil Science Society of America Journal, 53: 1356-1361.

Anderson, M.G. and Burt, T.P., 1990. Process Studies in Hillslope Hydrology: an overview. In: Anderson, M.G. and Burt, T.P. (Editors), Process Studies in Hillslope Hydrology. John Wiley & Sons, Chichester, 0-471-92714-7. pp. 1-8.

Anderson, M.G. and Lloyd, D.M., 1991. Using a combined slope hydrology-stability model to develop cut slope design charts. Proceedings of the Institut of Civil Engineers, 91: 705-718.

Angeli, M.-G., Buma, J., Gasparetto, P. and Pasuto, A. (Editors), 1998. A combined hydrology/stability model for low gradient clay slopes in the Italian Dolomites. Engineering geology, 49. 1-13 pp.

Angeli, M.-G., Pasuto, A. and Silvano, S., 1999. Towards the definition of slope instability behaviour in the Alverà mudslide (Cortina d'Ampezzo, Italy). Geomorphology, 30: 201-211.

Antoine, P., Giraud, A., Meunier, M. and Van Asch, T.W.J., 1995. Geological and geotechnical properties of the "Terres Noires" in southeastern France: Weathering properties, erosion solid transport and instability. Engineering geology, 40: 223-234.

Aquitronic Umweltmesstechnik GmbH, Germany. Kerner Strasse 3, D-73230 Kirchheim / Teck, http://www.aquitronik.de/.

Attenberger, E., 1989. Discharge and output of nutrients at the tile drain outflow of a drained area in the Tertiär Hügelland in South Bavaria. Zeitschrift für Kulturtechnik und Landentwicklung (30): 132-137.

Bates, R.L. and Jackson, J.A., 1984. Dictionary of geological terms. Anchor Books, Doubleday, 0-385-18101-9. 571 pp.

Baum, R.L. and Johnson, A.M., 1993. Steady movement of landslides in fine-grained soils - A model for sliding over an irregular slip surface. U.S. Geological Survey Bulletin, 1842(D): 28.

Becker, R., 2004. Spatial time domain reflectometry for monitoring transient soil moisture profiles, University of Karlsruhe. 230 pp.

Bell, F.G., 2003. Geological hazards - Their assessment, avoidance and mitigation. Spon Press, London, New York, 0-415-31851-3. 648 pp.

Beven, K., 2004. Robert E. Horton's perceptual model of infiltration processes. Hydrological Processes, 18: 3447-3460.

Beven, K. and Germann, K., 1982. Macropores and water flow in soils. Water resources research, 18(5): 1311-1325.

Biermann, W., 1991. Nur wer sich ändert.

Blonquist, J.M., Jones, S.B., Lebron, I. and Robinson, D.A., 2006. Microstructural and phase configurational effects determining water content: Dielectric relationships of aggregated porous media. Water Resources Research, 42(5).

Blonquist, J.M., Jones, S.B. and Robinson, D.A., 2005. Standardizing characterization of electromagnetic water content sensors: Part 2. Evaluation of seven sensing systems. Vadose Zone Journal, 4(4): 1059-1069.

Blöschl, G., 1996. Scale and scaling in hydrology. Wiener Mitteilungen; Wasser - Abwasser - Gewässer, 132. Wiener Mitteilungen, Wien. 346 pp.

Blöschl, G. and Kirnbauer, R., 1991. Point snowmelt models with different degrees of complexity - internal processes. Hydrology, 229: 127-147.

Blöschl, G. and Sivapalan, M., 1995. Scale issues in hydrological modelling: a review. Hydrological Processes, 9: 251-290.

Bonomi, T. and Cavallin, A., 1999. Three-dimensional hydrogeological modelling application to the Alverà mudslide (Cortina D'Ampezzo, Italy). Geomorphology, 30: 189-199.

Boogard, T., 2001. Analysis of hydrological processes in unstable clayey slopes. Nederlandse Geografische Studies, 287, Utrecht, 0169-4839.

Boogard, T. and van Asch, T.W.J., 2002. The role of the soil moisture balance in the unsaturated zone on movement and stability of the Beline landslide, France. Earth Surface Processes and Landforms, 27: 1177-1188.

Boogard, T.A., Antoine, P., Desvarreux, P., Giraud, A. and van Asch, T.W.J., 2002. The slope movements within the Mondorès graben (Drôme, France): The interaction between geology, hydrology and typology. Engineering Geology, 55: 297-312.

Bott, W., 2002. Prozessorientierte Modellierung des Wassertransports zur Bewertung von Hochwasserschutzmaßnahmen in bewaldeten Entstehungsgebieten, Johannes Gutenberg Universität, Mainz. 114 pp.

Bouma, J. and Dekker, L.W., 1981. A method for measuring the vertical and horizontal Ksat of clay soils with macropores. Soil Science Society of America Journal, 45: 662-663.

Bouwer, H., 1989. The Bouwer and Rice Slug Test - An Update. Ground Water, 27(3): 304-309.

Braudeau, E., Costantini, J.M., Bellier, G. and Colleuille, H., 1999. New device and method for soil shrinkage curve measurements and characterization. Soil Science Society of America Journal, 63: 525-535.

Bronswijk, J.J.B., 1988. Modeling of water balance, cracking and subsidence of clay soils. Journal of Hydrology, 97: 199-212.

Brunsden, D., 1999. Some geomorphological considerations for the future development of landslide models. Geomorphology, 30: 13-24.

BS 5930, 1999. Code of practice for site investigations. In: Engineering, B.S.C.f.B.a.C. (Editor).

Bundesamt für Eich- und Vermessungswesen, Austria. Schiffamtsgasse 1-3, A-1025 Wien, http://www.bev.gv.at/.

Butler, J.J., 1998. The design, performance and analysis of slug tests. Lewis Publishers, Boca Raton, 1-56670-230-5. 251 pp.

Carsel, R.F. and Parrish, R.S., 1988. Development of joint probability distributions of soil water retention characteristics. Water Resources Research, 24: 755-796.

Casale, R., Fantechi, R. and Flageollet, J.-C., (eds.), 1994. Temporal Occurrence and Forecasting of Landslides in the European Community, Final Report, Commission of the European Community Programme EPOCH. Bruxelles.

Casper, M., 2002. Die Identifikation hydrologischer Prozesse im Einzugsgebiet des Dürreychbaches (Nordschwarzwald). Mitteilungen des Instituts für Wasserwirtschaft und Kulturtechnik der Universität Karlsruhe (TH), 210. 169 pp.

Chertkov, V.Y., 2000. Modeling the pore structure and shrinkage curve of soil clay matrix. Geoderma, 95: 215-246.

Chertkov, V.Y., 2003a. Modeling the shrinkage curve of soil clay pastes. Geoderma, 112: 71-95.

Chertkov, V.Y., 2003b. A physically based model for the water retention curve of clay pastes. Journal of Hydrology, 286: 203-226.

Cho, S.E. and Lee, S.R., 2001. Instability of unsaturated soil slopes due to infiltration. Computers and Geotechnics, 28: 185-208.

City of Dornbirn Authorities, Austria. Abteilung Tiefbau, Rathausplatz 2, 6850 Dornbirn, http://dornbirn.at.

Collison, A.J.C. and Anderson, M.G., 1996. Using a combined slope hydrology / stability model to identify suitable conditions for landslide prevention by vegetation in the humid tropic. Earth Surface Processes and Landforms, 21: 737-747.

Crosta, G., 2004. Introduction to the special issue on rainfall-triggered landslides and debris flows. Engineering geology, 73: 191-192.

Davis, J.D., 2002. Statistics and data analysis in geology. John Wiley & Sons, New York, 0-471-17275-8. 638 pp.

Delmonaco, G. and Margottini, C., 2004. Meteorological factores influencing slope stability. Natural disasters and sustainable development: [lectures given at the European Comissions Advanced Study Course on "Natural disasters and sustainable development", held in Orvieto, Italy in Sept. 1998]. Springer Verlag, Berlin, 3-540-421998. 19-35 pp.

Depenthal, C. and Schmitt, G., 2002. Hydrologische und kinematische Prozesse bei Großhangbewegungen in bindigen Sedimenten - Endbericht zum Teilprojekt: Geodätische Erfassung der Kinematik einer Großhangbewegung. In: Geodätisches Institut, U.K.T. (Editor).

Depenthal, C. and Schmitt, G., 2003. Monitoring of a landslide in Vorarlberg / Austria. In: Stiros, S., Pytharouli, S. (Editor), Proceedings 11th International FIG Symposium on Deformation Measurements, May 25-28 2003, Santorini (Thera) Island, Greece, pp. 289-295.

Diamond, S., 1970. Pore size distribution in clays. Clays and Clay Minerals, 18(1): 7-23.

Dikau, R., Brundsen, D., Schrott, L. and Ibsen, M., 1996. Landslide recognition - Identification, movement and causes. Wiley & Sons, Chichester.

Dikau, R. and Schrott, L., 1999. The temporal stability and activity of landslides in Europe with respect to climatic change (TESLEC): main objectives and results. Geomorphology, 30: 1-12.

DIN 4022-1, 1987. Baugrund und Grundwasser; Benennen und Beschreiben von Boden und Fels - Schichtenverzeichnis für Bohrungen ohne durchgehende Gewinnung von gekernten Proben im Boden und im Fels. DIN Deutsches Institut für Normung e.V., Berlin.

DIN 4220, 1998. Bodenkundliche Standortbeurteilung: Kennzeichnung, Klassifzizierung und Anleitung von Bodenkennwerten (normative und nominale Skalierungen). DIN Deutsches Institut für Normung e.V., Berlin.

References

DIN 10381-4, 2004. Bodenbeschaffenheit - Probennahme - Teil 4: Anleitung für das Vorgehen bei der Untersuchung von natürlichen, naturnahen und Kulturstandorten (ISO 10381-4:2003). DIN Deutsches Institut für Normung e.V., Berlin.

DIN 18121-1, 1998. Baugrund, Untersuchung von Bodenproben- Wassergehalt Teil 1: Bestimmung durch Ofentrocknung. DIN Deutsches Institut für Normung e.V., Berlin.

DIN 18122-1, 1997. Baugrund, Untersuchung von Bodenproben- Zustandsgrenzen Teil 1: Bestimmung der Fließ- und Ausrollgrenze. DIN Deutsches Institut für Normung e.V., Berlin.

DIN 18122-2, 2000. Baugrund, Untersuchung von Bodenproben- Zustandsgrenzen Teil 1: Bestimmung der Schrumpfgrenze. DIN Deutsches Institut für Normung e.V., Berlin.

DIN 18124, 1997. Baugrund, Untersuchung von Bodenproben - Bestimmung der Korndichte: Kapillarpyknometer- Weithalspyknometer. DIN Deutsches Institut für Normung e.V., Berlin.

DIN 18125-1, 1997. Baugrund, Untersuchung von Bodenproben- Bestimmung der Dichte des Bodens Teil 1: Laborversuche. DIN Deutsches Institut für Normung e.V., Berlin.

DIN 18130-2, 2003. Baugrund, Untersuchung von Bodenproben- Bestimmung des Wasserdurchlässigkeitsbeiwerts Teil 2: Feldversuche. DIN Deutsches Institut für Normung e.V., Berlin.

DIN ISO 11277, 2002. Bestimmung der Partikelgrößenverteilung in Mineralböden: Verfahren mittels Siebung und Sedimentation. DIN Deutsches Institut für Normung e.V., Berlin.

Dittfurth, A., 2002. Abschätzung des Infiltrationsverhaltens auf Grundlage boden- und vegetationskundlicher sowie morphologischer Untersuchungen am Heumöser Hang in Ebnit / Vorarlberg, Universität Heidelberg. 95 pp.

Dunne, T. and Black, R.D., 1970. An experimental investigation of runoff production in permeable soils. Water resources research, 6: 478-490.

Dyck, S. and Peschke, G., 1995. Grundlagen der Hydrologie. Verlag für Bauwesen, Berlin. 536 pp.

Eberhardt, E., Thuro, K. and Luigenbuehl, M., 2005. Slope instability mechanisms in dipping interbedded conglomerates and weathered marls - the 1999 Rufi landslide, Switzerland. Engineering geology, 77: 35-56.

Eijkelkamp, The Netherlands. Nijverheidsstraat 30, 6987 EM Giesbeek, www.eijkelkamp.com.

Ellenberg, H., 1992. Zeigerwerte von Pflanzen in Mitteleuropa, Göttingen.

Ellenberg, H., 1996. Vegetation Mitteleuropas mit den Alpen - in ökologischer, dynamischer und historischer Sicht, Stuttgart.

Fam, M.A. and Dusseault, M.B., 1999. Determination of the reactivity of clay - fluid systems using liquid limit data. Canadian Geotechnical Journal, 36: 161-165.

Flageollet, J.-C., Maquaire, O., Martin, B. and Weber, D., 1999. Landslides and climatic conditions in the Barcelonnette and Vars basins (Southern French Alps, France). Geomorphology, 30: 65-78.

Flury, M. and Flühler, H., 1995. Tracer characteristics of brilliant blue FCF. Soil Science Society of America Journal, 59(1): 22-57.

Flury, M., Flühler, H., Leuenberger, J. and Jury, W.A., 1994. Susceptibility of soils to preferential flow of water: a field study. Water resources research, 30(7): 1945-1954.

Frydman, S., Talesnick, M., Greffen, S. and Shvarzman, A., 2007. Landslides and residual strength in marl profiles in Israel. Engineering geology, 89: 36-46.

Furrer, C.e., 2001. Rauheiten in ausgesuchten schweizerischen Fliessgewässern. Berichte des BWG, Serie Wasser, 1. Bundesamt für Wasser und Geologie, Schweiz.

Geologische Bundesanstalt, Austria. Neulinggasse 38, A-1030 Wien, http://www.geologie.ac.at/.

Geologisches Landesamt Baden-Württemberg, 1995. Symbolschlüssel Geologie (Teil 1) und Bodenkunde Baden-Württemberg, Freiburg.

Geonics Ltd., Canada. 1745 Meyerside Dr., Unit 8, Mississauga, Ontario, L5T 1C6, http://www.geonics.com/.

Gräff, T., 2004. Untersuchung des bodeninneren Abflusses in einer Mittelgebirgsregion beispielhaft vorgestellt am Schäfertal, Universität Potsdam, Potsdam. 132 pp.

Gräff, T., Zehe, E., Reusser, D., Lück, E. and Bronstert, A., 2007. Process identification through rejection of model structures in a mid mountainous rural catchment: observations of rainfall-runoff response and geophysical conditions. submitted to Hydrological Processes.

Grayson, R. and Blöschl, G.E., 2001. Spatial patterns in catchment hydrology - observations and modelling, Cambridge University Press, New York, 0-521-63316-8. 404 pp.

Greco, R., 2002. Preferential flow in macroporous swelling soil with internal catchment: model development and applications. Journal of Hydrology, 269(150-168).

Haneberg, W.C., 1995. Groundwater flow and the stability of heterogenous infinite slopes underlain by impervious strata. In: Haneberg, W.C. and Anderson, S.A. (Editors), Clay and shale slope instability. pp. 63-77.

Hannich, D., 2001. Kurzbericht über die geophysikalischen Untersuchungen in Ebnit, 02 - 04. Juli 2001, Angewandte Geologie Karlsruhe.

Hardenbicker, U. and Crozier, M.J., 2002. Soil pipes and slope stability. In: Rybár, J., Stemberk, J. and Wagner, P. (Editors), Landslides, pp. 565-569.

Harvey, A.M., 1971. Seasonal flood behaviour in a clay catchment. Journal of Hydrology, 12(2): 129-144.

Haude, W., 1955. Zur Bestimmung der Verdunstung auf möglichst einfache Weise. 11, Deutscher Wetterdienst. Offenbach.

Henry, J.-B., Malet, J.-P., Maquaire, O. and Grussenmeyer, P., 2002. The use of small-format and low-altitude aerial photos for the realization of high-resolution DEMs in mountainous areas: Application to the Super-Sauze earthflow (Alpes-De-Haute-Provences, France). Earth Surface Processes and Landforms, 27: 1339-1350.

Hicks, M.A. and Samy, K., 2002. Influence of heterogeneity on undrained clay slope stability. Quarterly Journal of Engineering Geology and Hydrogeology, 35: 41-49.

Hill, M.O., Mountford, J.O., Roy, D.B. and Bunce, R.G.H., 1999. Ellenberg's indicator values for British plants. In: Centre for Ecology and Hydrology (Editor), Huntington, UK, 1 870393 48 1, http://www.ceh.ac.uk/. pp. 46.

Hinkelmann, R. and Zehe, E., 2007. Kopplung von Strömungs- und Transportprozessen für die Modellierung von Großhangbewegungen. Hydrologie und Wasserbewirtschaftung(1): 51-54.

Hong, Y., Hiura, H., Shino, K., Sassa, K., Suemine, A., Fukuoka, H. and Wang, G., 2005. The influence of intense rainfall on the activity of large-sacle crystallline shist landslides in Shikoku Island, Japan. Landslides, 2: 97-105.

Honisch, M., Hellmeier, C. and Weiss, K., 2002. Response of surface and subsurface water quality to land use changes. Geoderma, 105(3-4): 277-298.

Horton, R.E., 1933. The role of infiltration in the hydrological cycle. Transaction American Geophysical Union, 14: 446-460.

Howind, J. and Schmitt, G., 1999. Hydrologische und kinematische Prozesse bei Großhangbewegungen in bindigen Sedimenten - Zwischenbericht zum Teilprojekt: Geodätische Erfassung der Kinematik einer Großhangbewegung. In: Geodätisches Institut, U.K.T. (Editor), pp. 32.

Hydrographischer Dienst Vorarlberg, Austria. Landhaus, A-6901 Bregenz, http://vorarlberg.at.

Ihringer, J., 2005. Softwarepaket zur Zeitreihenanalyse. Institut für Wasser und Gewässerentwicklung, Universität Karlsruhe, Karlsruhe.

IMKO GmbH, Germany. IMKO Micromodultechnik GmbH, Im Stöck 2, D-76275 Ettlingen, http://www.imko.de/.

IRIS Instruments, France. 1 avenue buffon BP 16007, 45060 Orleans Cedex 2, http://www.iris-instruments.com.

Iverson, N.R., 2000. Landslide triggering by rain infiltration. Water resources research, 36(7): 1897-1910.

Iverson, R.M., Reid, M.E., Iverson, N.R., LaHusen, R.G., Logan, M., Mann, J.E. and Brien, D.L., 2000. Acute sensitivity of landslide rates to initial soil porosity. Science, 290: 513-516.

Jahns, R.H., 1978. Geophysical predictions. Landslides: Analysis and control. Transportation Research Board, Special Report 176, National Academy of Sciences, Washington. 58-65 pp.

Jones, S.B., Blonquist, J.M., Robinson, D.A., Rasmussen, V.P. and Or, D., 2005. Standardizing characterization of electromagnetic water content sensors: Part 1. Methodology. Vadose Zone Journal, 4(4): 1048-1058.

Kanonier, J., Gasser, M., Sivetz, R. and Pfefferkorn, A., 2005. Das Starkregen- und Hochwasserereignis des August 2005 in Vorarlberg. Feldkirch.

Kariuki, P.C. and Van der Meer, F., 2004. A unified swelling potential index for expansive soils. Engineering geology, 72: 1-8.

Keusen, H.R., 2000. Die Rutschung Gryfenbach (Lauterbrunnen, BE) - Ihre dramatische Entwicklung im Jahr 1999. Bulletin für angewandte Geologie, 5(1): 73-83.

Kim, D.J., Jaramillo, R.A., Vauclin, M., Feyen, J. and Choi, S.I., 1999. Modeling of soil deformation and water flow in a swelling soil. Geoderma, 92: 217-238.

Kirnbauer, R., Blöschl, G., Haas, P., Müller, G. and Merz, B., 2001. Space-time patterns of runoff generation in the Löhnersbach catchment. Freiburger Schriften zur Hydrologie - Runoff generation and implications for river basin modelling, 13. Institut für Hydrologie, Universität Freiburg, Freiburg.

Knoedel, P., Young, R., Howard, A. and Farrar, J.A., 1998. Earth Manual Part 1. U.S Department of the Interior - Bureau of Reclamation, Denver. 313 pp.

Kohler, A., Abbaspour, K.C., Fritsch, M., van Genuchten, M.T. and Schulin, R., 2001. Simulating unsaturated flow and transport in a macroporous soil to tile drains subject to an entrance head: model development and preliminary evaluation. Journal of Hydrology, 254: 67-81.

Kolle, O. and Fiedler, F., 1996. Messung und numerische Simulation der Energie- und Feuchtebilanz der Bodenoberfläche. Zwischenbericht 1996 Weiherbachprojekt. Institut für Hydrologie und Wasserwirtschaft, Universität Karlsruhe. 15 - 40 pp.

Krause, P., Boyle, D.P. and Bäse, F., 2005. Comparison of different efficiency criteria for hydrological model assessment. Advances in Geosciences, 5: 89-97.

Ksat Inc., USA. P.O. Box 30813, Raleigh, North Carolina 27622, http://ksatinc.com.

Kuntze, H., Roeschmann, G. and Schwerdtfeger, G., 1994. Bodenkunde. Eugen Ulmer, Stuttgart, 3-8252-8076-4. 424 pp.

Landesvermessungsamt Baden-Württemberg, Germany. Büchsenstraße 54, 70174 Stuttgart, http://www.lv-bw.de/lvshop2/.

Legates, D.R. and McCabe Jr., G.J., 1999. Evaluating the use of "goodness-of-fit" measures in hydrologic and hydroclimatic model validation. Water Resources Research, 35(1): 233-241.

Lin, H., Bouma, J., Pachepsky, Y., Western, A., Thompson, J., van Genuchten, R., Vogel, H.-J. and Lilly, A., 2006. Hydropedology: Synergistic integration of pedology and hydrology. Water resources research, 42: W05301, doi: 10.1029/2005WR004085.

Lindenmaier, F. and Zehe, E., 2002. Preprocessing for the hydrological process model CATFLOW, internal report. Institut für Wasser und Gewässerentwicklung, Universität Karlsruhe (TH), pp. 11.

Lindenmaier, F., Zehe, E., Dittfurth, A. and Ihringer, J., 2005. Process identification on a slow moving landslide. Hydrological Processes, 19: 1635-1651.

Lindenmaier, F., Zehe, E., Helms, M., Evdakov, O. and Ihringer, J., 2006. Effect of soil shrinkage on runoff generation in micro and mesoscale catchments. Predictions in Ungauged Basins: Promise and Progress (Proceedings of symposium S7 held during the Seventh IAHS Scientific Assembly at Foz do Iguaçu, Brazil, April 2005), 303. 305-317 pp.

Löpmeier, F.J., 2001. Berechnung der Bodenfeuchte und Verdunstung mittels agrarmeteorologischer Modelle. Zeitschrift für Bewässerungswirtschaft, 29: 156-167.

Malet, J.-P., Auzet, A.-V., Maquaire, O., Ambroise, B., Descroix, L., Esteves, M., Vandervaere, J.-P. and Truchet, E., 2003. Soil surface characteristics influence on infiltration in black marls: Application to the Super-Sauze earthflow (Southern Alps, France). Earth Surface Processes and Landforms, 28: 547-564.

Malet, J.-P., van Asch, T.W.J., van Beck, R. and Maquaire, O., 2005. Forecasting the behaviour of complex landslides with a spatially distributed hydrological model. Natural Hazards and Earth System Sciences, 5: 71-85.

Maquaire, O., Malet, J.-P., Remaître, A., Locat, J., Klotz, S. and Guillon, J., 2003. Instability conditions of marly hillslopes: towards landsliding or gullying? The case of the Barcelonnette Basin, South East France. Engineering geology, 70: 109-130.

Markart, G., Kohl, B., Sotier, B., Schauer, T., Bunza, G. and Stern, R., 2006. Geländeanleitung zur Abschätzung des Oberflächenabflussbeiwertes bei Starkregen - Grundzüge und erste Erfahrungen. In: Gutknecht, D. (Editor), Wiener Mitteilungen: Methoden der hydrologischen Regionalisierung, 3-85234-088-8. pp. 159-178.

Maurer, T., 1997. Physikalisch begründete, zeitkontinuierliche Modellierung des Wassertransports in kleinen ländlichen Einzugsgebieten. Mitteilungen Institut für Hydrologie und Wasserwirtschaft, 61, Karlsruhe. 238 pp.

McGarry, D. and Malafant K.W.J., 1987. The analysis of volume change in unconfined units of soil. Soil Science Society of America Journal, 51: 290-297.

Meisina, C., 2004. Swelling-shrinking properties of weatherd clayey soils associated with shallow landslides. Quarterly Journal of Engineering Geology and Hydrogeology, 37: 77-94.

MeteoSchweiz, 2006. Starkniederschlagsereignis August 2005, Arbeitsberichte der MeteoSchweiz, 211. 63 pp.

Mierlo, J. and Illner, M., 1998. Statistische Grundlagen und Modelle für die Weiterverarbeitung von GPS-Ergebnissen. Mitteilungen des DVW-Landesvereins Baden-Württemberg, 2: 84-108.

Millington, R.J. and Quirk, J.P., 1959. Permeability of porous media. Nature, 183: 387-388.

Molkenthin, F., Hinkelmann, R., Lindenmaier, F. and Zehe, E., 2006. Web-baseed information system for multi-scale physical state variables, 7th International Conference on Hydroinformatics HIC, Nice, France.

Mualem, Y., 1976. A new model for predicting the hydraulic conductivity of unsaturated porous media. Water Resources Research, 12: 513-522.

Munsell Soil Colour Chart, 2000. Torso Verlag, EAN-Nr.: 4250193400781.

Nash, J.E. and Sutcliffe, J.V., 1970. River flow forecasting through conceptual models, Part I - A discussion of principles. Journal of Hydrology, 10: 282-290.

Návar, J., Mendez, J., Bryan, R.B. and Kuhn, N.J., 2002. The contribution of shrinkage cracks to infiltration in Vertisols of Northeastern Mexico. Canadian Journal of Soil Sciences, 82: 65-74.

Novák, V., Šimůnek, J. and van Genuchten, M.T., 2000. Infiltration of water into soil with cracks. Journal of Irrigation and Drainage Engineering, 126(1): 41-47.

Oberhauser, R., 1998. Erläuterungen zur Geologisch-Tektonischen Übersichtskarte von Vorarlberg, 1:200000. In: Österreich, G.B. (Editor), Wien.

Oberhauser, R., Draxler, I., Krieg, W. and Resch, W., 1991. Erläuterungen zu Blatt 110 St. Gallen Süd und 111 Dornbirn Süd, Geologische Karte der Republik Österreich 1: 25000. Geologische Bundesanstalt, Wien.

Olsen, P.A. and Haugen, L.E., 1998. A new model of the shrinkage characteristic applied to some Norwegian soils. Geoderma, 83: 67-81.

Ott Messtechnik GmbH & Co. Kg, Germany. Ludwigstr. 16, 87437 Kempten, www.ott-hydrometry.de.

Peng, X. and Horn, R., 2005. Modeling soil shrinkage curve across a wide range of soil types. Soil Science Society of America Journal, 69: 584-592.

Plate, E., (ed.), 1992. Weiherbach -Projekt: Prognosemodell für die Gewässerbelastung durch Stofftransport aus einem kleinem ländlichen Einzugsgebiet. Schlussbericht zur 1. Projektphase des BMFT-Verbundprojekts. Mitteilungen des Instituts für Hydrologie und Wasserwirtschaft, Universität Karlsruhe, 43, Karlsruhe.

Pret, K., 2001. Untersuchung der Einsatzmöglichkeiten des Programmmoduls Auto Terrain zur Erstellung eines digitalen Geländemodells am Beispiel des Heumöser Hangs in Ebnit (Vorarlberg), Universität Karlsruhe.

Rahardjo, H., Aung, K.K., Leong, E.C. and Rezaur, R.B., 2004. Characteristics of residual soils in Singapore as formed by weathering. Engineering geology, 73: 157-169.

Rahardjo, H., Lee, T.T., Leong, E.C. and Rezaur, R.B., 2005. Response of a residual soil slope to rainfall. Canadian Geotechnical Journal, 42: 340-351.

Reid, M.E., 1997. Slope instability caused by small variations in hydraulic conductivity. Journal of Geotechnical and Geoenvironmental Engineering: 717-725.

Remaître, A., Malet, J.-P. and Maquaire, O., 2005. Morphology and sedimentology of a complex debris flow in a clay shale basin. Earth Surface Processes and Landforms, 30: 339-348.

Remaître, A., Malet, J.-P., Maquaire, O., Ancey, C. and Locat, J., 2005. Flow behaviour and runout modelling of a complex debris flow in a clay shale basin. Earth Surface Processes and Landforms, 30: 479-488.

Reusser, D. and Zehe, E., 2005. CATFLOW Wizard, internal report. Universität Potsdam, Institut für Geoökologie.

Reynolds, J.M., 2005. An introduction to applied and environmental geophysics. John Wiley & Sons Inc., Chichester, 10 0471 96802 1. 778 pp.

Richards, L.A., 1931. Capillary conduction of liquids through porous media. Physics(1): 318-333.

Ruff, M., 2005. GIS-Gestützte Risikoanalyse für Rutschungen und Felsstürze in den Ostalpen (Vorarlberg, Österreich). Universitätsverlag Karlsruhe, Karlsruhe, 3-937300-46-5. 135 pp.

Ruff, M. and Czurda, K., 2007. Landslide Susceptibility Analysis with a Heuristic Approach at the Eastern Alps (Vorarlberg, Austria). Geomorphology, In Press, Available online 14 June 2007.

Rupp, D.E., Owens, J.M., Warren, K.L. and Selker, J.S., 2004. Analytical method for estimating saturated hydraulic conductivity in a tile drained field. Journal of Hydrology, 289: 111-127.

Sauer, T., Kreiter, T., Schobel, S., Casper, M. and Müller, C., 2006. Möglichkeiten und Grenzen der Modellierbarkeit bodenhydrologischer Prozesse auf unterschiedlichen Skalen am Beispiel der Tieflockerung. In: Casper, M. and Herbst, M. (Editors), Niederschlag - Abfluss - Modellierung, Beiträge zum RIMAX-Workshop am 10./11. April 2006, Trier, pp. 55-70.

Scheffer, F. and Schachtschabel, P., 1998. Lehrbuch der Bodenkunde, Stuttgart.

Schneider, U., 1999. Untersuchungen zur Kinematik von Massenbewegungen im Modellgebiet Ebnit (Vorarlberger Helvetikum), Universität Karlsruhe (TH), Karlsruhe, 0933-2510. 153 pp.

Schneider, U., pers. communication.

Schulz, K., Seppelt, R., Zehe, E., Vogel, H.-J. and Attinger, S., 2006. Importance of spatial structures in advancing hydrological sciences. Water resources research, 42(W03S03, doi: 10.1029/2005WR004301).

Schuster, R.L. and Wieczorek, G.F., 2002. Landslide triggers and types. In: Rybár, J., Stemberk, J. and Wagner, P. (Editors), Landslides. Proceedings of the first european confernce on landslides, Prague, Czech Republic, June 24-26, 2002. Balkema Publishers, 90-5809-393 X. pp. 734.

Schütz, B., 2000. Großhangrutschung Sibratsgfäll-Rindberg und Umgebung, Universität Karlsruhe (TH), Karlsruhe. 133 pp.

Schwenk, M., 1999. Geologische, ingenieurgeologische und hydrologische Untersuchungen der Massenbewegung am Heumöser Hang in Ebnit (Gemeinde Dornbirn) Vorarlberg, Österreich, Universität Karlsruhe (TH), Karlsruhe. 128 pp.

SEBA Hydrometrie GmbH, Germany. Gewerbestr. 61a, D-87600 Kaufbeuren, http://www.seba.de.

Sherman, L.K., 1932. Streamflow from rainfall by the unit hydrograph method. Engineering News Record, 180: 501-505.

Šimůnek, J., Jarvis, N.J., van Genuchten, M.T. and Gärdenäs, A., 2003. Review and Comparison of models for describing non-equilibrium and preferential flow and transport in the vadose zone. Journal of Hydrology, 272: 14-35.

Smit Sibinga-Lokker, C., 1965. Beiträge zur Geomorphologie und Glazialgeologie des Einzugsgebietes der Dornbirner Ache (Vorarlberg, Österreich), Universität Amsterdam, Amsterdam. 127 pp.

Soil Survey Division Staff, 1993. Soil Survey Manual, 18, Washington, http://soils.usda.gov/technical/manual/.

Sommer Messtechnik, Austria. Straßenhäuser 27, A-6842 Koblach, http://www.sommer.at.

Squarzoni, C., Delacourt, C. and Allemand, P., 2003. Nine years of spatial and temporal evolution of the La Valette landslide observed by SAR interferometry. Engineering geology, 68: 53-66.

References

Stamm, C., Sermet, R., Leuenberger, J., Wunderli, H., Wydler, H., Fluehler, H. and Gehre, M., 2002. Multiple tracing of fast solute transport in a drained grassland soil. Geoderma, 109(3-4): 245-268.

Stinnesbeck, W., Schulte, P., Lindenmaier, F., Adatte, T., Affolter, M., Schilli, L., Keller, G., Stuben, D., Berner, Z., Kramar, U., Burns, S.J. and Lopez-Oliva, J.G., 2001. Late Maastrichtian age of spherule deposits in northeastern Mexico: implication for Chicxulub scenario. Canadian Journal Of Earth Sciences, 38(2): 229-238.

Strahler, A.N., 1956. Hypsometric (area-altitude) analyis of erosional topography. Geological Society of America Bulletin, 63: 1117-1142.

Strickler, A., 1923. Beiträge zur Frage der Geschwindigkeitsformel und der Rauhigkeitszahl für Ströme, Kanäle und geschlossene Leitungen. Bern.

Tallaksen, L.M., 1995. A review of baseflow recession analysis. Journal of Hydrology, 165: 349-370.

Terlien, M.T.J., 1998. The determination of statistical and deterministic hydrological landslide-triggering tresholds. Environmental Geology, 35(2-3): 124-130.

Therzaghi, K., 1950. Mechanism of landslides. Applications of geology to engineering practice. Berkey Volume, American Geological Society. 83-123 pp.

Troch, P., De Troch, F.P. and Brutsaert, W., 1993. Effective water table depth to describe initial conditions prior to storm rainfall in humid regions. Water resources research, 29(2): 427-434.

Tsaparas, I., Rahardjo, H., Toll, D.G. and Leong, E.C., 2002. Controlling parameters for rainfall induced landslides. Computers and Geotechnics: 1-27.

Uchida, T., Kosugi, K. and Mitzuyama, T., 2001. Effects of pipeflow on hydrological process and its relation to landslide: a review of pipeflow studies in forested headwater catchments. Hydrological Processes, 15: 2151-2174.

UGT, Germany. Eberswalder Str. 84a, 15374 Müncheberg, www.ugt-online.de.

Uhlenbrook, S. and Leibundgut, C., 2002. Process-oriented catchment modelling and multi-response validation. Hydrological Processes, 16: 423-440.

van Asch, T.W.J., 2005. Modelling the hysteresis in the velocity pattern of slow-moving earth flows: the role of excess pore pressure. Earth Surface Processes and Landforms, 30: 403-411.

van Asch, T.W.J. and Buma, J., 1997. Modelling groundwater fluctuations and the frequency of movement of a landslide in the Terres Noires Region of Barcelonnette (France). Earth Surface Processes and Landforms, 22: 131-141.

van Asch, T.W.J., Buma, J. and van Beek, L.P.H., 1999. A view on some hydrological triggering systems in landslides. Geomorphology, 30: 25-32.

van Asch, T.W.J., Hendriks, M.R., Hessel, R. and Rappange, F.E., 1996. Hydrological triggering conditons of landslides in varved clays in the French Alps. Engineering geology, 42: 239-251.

van den Ham, G., 2006. Numerical simulation and engineering-geological assessment of a creeping slope in the Alps, Universität Karlsruhe (TH). 100 pp.

van den Ham, G. and Czurda, K., 2002. Numerical modelling of a slowly deforming slope in the Vorarlbergian Alps, Austria, Geophysical Research Abstracts. European Geophysical Society 27th General Assembly.

van Genuchten, M.T., 1980. A closed-form equation for predicting the hydraulic conductivity of unsaturated soils. Soil Science Society of America Journal, 44: 892-898.

Vorarlberger Kraftwerke AG, Austria. Weidachstraße 6, 6900 Bregenz, http://www.vkw.at/inhalt/at/2376.htm.

Waldenmeyer, G., 2000. Boden- und vegetationskundliche Voruntersuchungen am Heumöser Hang (Ebnit, Vorarlberg/Österreich). Institut für Geoökologie, Universität Karlsruhe (TH), pp. 10.

Walter, M., 2006. Seismische Untersuchungen von Massenbewegungen am Heumöser Hang in Ebnit (Vorarlberg) mittels Nanoseismic Monitoring, Universität Stuttgart, Stuttgart. 80 pp.

Werner, R. and Auer, I., 2001. Klima von Vorarlberg - Eine anwendungsorientierte Klimatographie. Amt der Vorarlberger Landesregierung, 3-901487-28-X, 3-901487-29-8.

Wienhöfer, J., pers. communication.

Wilding, L.P. and Tessier, D., 1988. Genesis of vertisols: shrink-swell phenomena. In: Wilding, L.P. and Puentes, R. (Editors), Vertisols: their distribution, properties, classification and management. Soil Management Support Services, College Station, Texas 77843., Texas A&M University Printing Center. pp. 55-81.

Wilkinson, P.L., Brooks, S.M. and Anderson, M.G., 2000. Design and application of an automated non-circular slip surface search within a combined hydrology and stability model (CHASM). Hydrological Processes, 14: 2003-2017.

Wilmanns, O., 1993. Ökologische Pflanzensoziologie: Eine Einführung in die Vegetation Mitteleuropas, Heidelberg.

Wooding, R.W., 1968. Steady infiltraion from a shallow circular pond. Water resources research, 4: 1259-1273.

Wraith, J.M. and Or, D., 1999. Temperature effects on soil bulk dielectric permittivity measured by time domain reflectometry: Experimental evidence and hypothesis development. Water resources research, 35(2): 361-369.

Wunderlich, T.A., 1995. Die geodätische Überwachung von Massenbewegungen. Felsbau, 13(6): 414-419.

Wust-Bloch, G.H. and Joswig, M., 2006. Pre-collapse identification of sinkholes in unconsolidated media at Dead Sea area by 'nanoseismic monitoring' (graphical jacknife location of weak sources by few. low-SNR records). Geophysical Journal International, 167: 1220-1232.

Wyssling, G., 1986. Der frühkretazische Schelf in Vorarlberg und im Allgäu. Stratigraphie, Sedimentologie und Paläogeographie. Jahrbuch der Geologischen Bundesanstalt, Wien. 129 pp.

Xiang, W., 1997. Der Einfluß der Kationenbelegung auf die bodenmechanischen und rheologischen Eigenschaften von Tonen am Beispiel einer ostalpinen Großhangbewegung. Schriftenreihe Angewandte Geologie Karlsruhe, 48, Karlsruhe. 190 pp.

Zehe, E., 1999. Stofftransport in der ungesättigten Bodenzone auf verschiedenen Skalen. Institut für Hydrologie und Wasserwirtschaft, 64. Mitteilungen des Instituts für Hydrologie und Wasserwirtschaft, Universität Karlsruhe (TH), Karlsruhe. 227 pp.

Zehe, E. and Blöschl, G., 2004. Predictability of hydrologic response at the plot and catchment scales: the role of initial conditions. Water resources research, 40(10): W10202, doi: 10.1029/ 2003WR002869.

Zehe, E., Elsenbeer, H., Lindenmaier, F., Schulz, K. and Blöschl, G., 2007. Patterns of predictability in hydrological threshold systems. Water resources research, 43(W07434).

Zehe, E. and Flühler, H., 2001a. Preferential transport of isoproturon at a plot scale and a field scale tile-drained site. Journal of Hydrology, 247: 100-115.

Zehe, E. and Flühler, H., 2001b. Slope scale variation of flow patterns in soil profiles. Journal of Hydrology, 247: 116-132.

Zehe, E., Maurer, T., Ihringer, J. and Plate, E., 2001. Modelling water flow and mass transport in a Loess catchment. Physics & Chemistry of the Earth, Part B, 26: 487 - 507.

Zimmermann, B., Elsenbeer, H. and De Moraes, J.M., 2006. The influence of land-use changes on soil hydraulic properties: Implications for runoff generation. Forest Ecology and Management, 222: 29-38.

Zohdy, A.A.R., 1989. A new method for the automatic interpretation of Schlumberger Wenner sounding curves. Geophysics, 54(2): 245-253.

List of figures

List of tables

Appendix

A. Complement to Chertkov´s model for the soil shrinkage characteristic curve

Chertkov´s model (2000; 2003a) is an approximation for calculating the soil shrinkage characteristic curve. Factor $\bar{a}$ is needed to calculate the specific clay volume between the shrinkage limit and the air entry point. The variable $\bar{a}$ is defined as

$$\bar{a} = \frac{1}{4(v_z / v_s - 1)\rho_w(\rho_w / \rho_s)(1 - F_z)}$$

F_z is the pore volume fraction occupied by water at the shrinkage limit. F_z could be derived of the specific clay pore geometry, also called microparameters. For example, it is possible to measure a pore dimension distribution with the mercury intrusion method (Diamond, 1970). This was not possible for the case of these samples so that an estimated value for F_z was taken from Chertkov (2000). Microparameters of clay particles can be estimated through geometric considerations. The clay mineral has a highly ordered structure and specific platelike shapes; hence a culmination of clay particles should also have specific pore shapes. Chertkov´s model does not include changes of clay mineral charge due to changing ion concentration in the pore fluid.

B. Properties of geological material

Appendix B-1: Mineral content derived from semi-quantitative X-ray diffractometer analysis, extracted from Schneider (1999).

	quartz	swellable clay minerals	illite kaolinite	carbonate	feldspar	organic
Amden marlstone	35	10	10	41	2	2
subglacial till	37	10.5	8	40	0	4.5
glacial endlake sediment	29	10	15	40	1	5
postglacial sediment	28	51	10	5	2	4
postglacial sediment	32	15	10	30	3	10

Appendix B-2: Carbonate content of samples from borehole KB 3, extracted from Schneider (1999).

depth sample taken	carbonate content
m	%
0.0	27.5
2.0	29.3
4.8	42.5
8.0	47.5
9.5	36.6
14.9	53.9
18.8	54.2

Appendix B-3: Laboratory analysis of soil samples from Schneider (1999) and Schwenk (1999).

sample name	rock type	longitude	latitude	depth sample taken [cm]	consistency limit				water uptake %	carbonate content %	grain size distribution				organic content	
					water content weight-%	liquid limit weight-%	plasticity limit weight-%	consistency number			clay weight-%	silt weight-%	sand weight-%	gravel weight-%	weight-%	weight-%
H2	post-glacial sediment	-44511.1	5245034.8	40-60	59.6	53.4	30.3	0.22	100.5	5.4	30.4	69.6	0.0		10.8	15.3
H3	post-glacial sediment	-44411.4	5245290.4	30	60.1	61.9	31.2	0.06		7.6	31.5	53.4	15.1		4.9	7.6
H4	post-glacial sediment	-44216.9	5245247.4	40	48.2	63.4	29.4	0.11		36.6	38.8	60.5	0.7		1.9	3.6
TDR 30	post-glacial sediment	-44763.4	5245324.9	30	61.1	63.7	26.6	0.49	95.5	12.1	29.9	53.6	16.5		4.3	5.1
TDR 90	post-glacial sediment	-44763.4	5245324.9	90	30.6					40.3					3.1	4.6
AV5	weathered Amden marlstone	-45008.3	5245148.8	20	40.5	61.7	29.7	0.66	70.3	5.1					2.3	4.1
S7	glacial endlake sediment	-43770.6	5245429.3	20-40	22.6	25.5	18.7	0.43	62.8	47.8	6.5	48.7	44.7		0.9	1.1
M9	subglacial till	-43841.6	5245145.6	50	29.6	39.4	23.1	0.60	55.4	32.8					1.1	2.7
M10	subglacial till	-43637.3	5245324.7	20-40	32.4					49.3	6.8	6.9	24.3	58.7	1.3	1.7
W1	Wang marlstone			surface						73.4						
A6	Amden marlstone			surface						44.4						
L8	Leimern marlstone			surface						66.3						

C.   Relative movement rates of measurement points and reference systems

The GPS movement data has been kindly ceded from co-worker Claudia Depenthal from the Institut für Geodäsie, Universität Karlsruhe (Depenthal & Schmitt, 2002; Depenthal & Schmitt, 2003; Howind & Schmitt, 1999) of the first research effort. Measurements were conducted from 1998-2001. Electronic source for the projection systems is http://www.geocities.com/mapref/mapref.html.

Appendix C-1: Relative movement rates of boreholes in lateral direction

	04.06.1998	06.11.1998	07.05.1999	08.08.1999	09.11.1999	10.05.2000
KB1	0	0.7	3.7	8.2	13.5	11.5
KB2	0	1.7	16.2	14.5	8.3	8.1
KB3	0	0.9	0.7	0.3	1.0	1.9

grey coloured fields indicate movement rates which are below the detection limit

Appendix C-2: Relative movement rates of object points measured with the Global Positioning System in lateral direction on the Heumös slope. Measurement periods without significant movement are in grey.

	reference date 04.06.1998	04.06.1998-06.11.1998	06.11.1998-07.05.1999	07.05.1999-08.08.1999	08.08.1999-09.11.1999	09.11.1999-10.05.2000	10.05.2000-11.08.2000	11.08.2000-12.11.2000	12.11.2000-13.05.2001	13.05.2001-14.08.2001	14.08.2001-15.11.2001
days of measurement period	0	155	182	93	93	183	93	93	182	93	93
GPS 1	0	0.7	0.7	0.8	0.9	0.8	0.3	1.8	0.7	1.8	2.1
GPS 2	0	0.4	0.9	1.4	0.3	0.6	1.0	1.0	0.1	1.2	2.0
GPS 3	0	1.4	2.1	0.4	1.3	0.5	1.3	2.5	1.8	1.8	3.0
GPS 4	0	0.8	0.9	0.5	0.5	0.5	1.3	0.8	0.8	1.4	2.7
GPS 5	0	1.2	0.7	1.6	2.8	2.3	3.2	5.3	4.1	4.6	6.9
GPS 6	0	2.0	4.2	4.7	6.2	8.1	9.7	12.7	12.4	14.3	16.2
GPS 7	0	2.1	3.6	4.4	7.5	9.7	11.2	13.4	15.4	16.1	18.4
GPS 8	0	2.4	5.0	6.4	9.2	12.2	13.2	16.7	18.7	19.9	23.2
GPS 9	0	2.5	4.1	6.8	8.6	11.8	12.0	15.7	18.2	19.7	22.5
GPS 10	0	2.1	5.6	9.6	13.2	19.0	20.5	23.2	30.2	33.3	37.0
GPS 11	0	0.7	0.8	5.1	6.0	7.0	11.7	13.9	24.7	28.9	31.4
GPS 50	0	1.3	1.4	1.0	0.5	1.5	0.9	1.7	0.3	6.0	6.8
GPS 51	0	2.9	4.6	6.1	9.4	12.0	14.2	17.0	18.2	19.5	21.9
GPS 52	0	2.4	1.5	2.1	2.8	1.3	2.3	1.3	1.5	0.5	1.6
GPS 53	0	1.6	2.2	0.9	2.2	0.8	0.8	3.0	1.7	2.8	4.1
GPS 54	0	0.5	1.3	1.6	0.4	1.6	1.2	1.9	0.8	1.4	1.4
GPS 55	0	3.1	1.9	3.6	4.2	2.1	2.2	4.7	2.5	7.2	6.4
GPS 56	0	1.2	0.8	1.8	4.1	4.4	5.7	8.4	9.1	10.8	11.1
GPS 57	0	1.3	3.8	8.9	8.7	12.5	14.6				
GPS 58	0	0.2	1.4	0.9	0.3	2.0	1.3	0.7	0.8	2.0	1.0
GPS 59	0	3.0	4.9	8.7	9.7	12.2	13.7	16.2	17.0	17.4	18.5
GPS 60	0	2.8	2.9	4.4	6.4	6.5	9.0	12.0	13.8	14.8	19.1
GPS 61	0	1.2	1.5	2.5	4.0	2.7	5.0	8.2	8.0	8.7	10.9
GPS 62	0	0.8	2.2	0.2	0.9	0.4	0.5	1.3	1.4	0.6	4.0

grey coloured fields indicate movement rates which are below the detection limit

Appendix C-3: Relative movement rates of traverse points in lateral direction on the Heumös slope. Measurement periods without significant movement are in grey.

	referen ce date 04.06. 1998	04.06.-05.08. 1998	05.08.-06.11. 1998	06.11.-07.05. 1999	07.05.-08.08. 1999	08.08.-09.11. 1999	09.11.-10.05. 2000	10.05.-11.08. 2000	11.08.-12.11. 2000	12.11.-13.05. 2001	13.05.-14.08. 2001
days of measurem ent period	0	62	93	182	93	93	183	93	93	182	93
PP1	0	0.8	0.5	2.9	1.2	1.5	0.6	0.5	1.1	1.1	0.4
PP2	0	2.7	0.4	2.1	0.5	2.7	0.4	0.2	1.2	1.2	0.4
PP3	0	3.3	0.8	3.0	0.9	4.1	1.5	0.6	1.4	1.4	0.4
PP4	0	4.5	2.3	4.1	1.2	5.1	5.0	1.2	3.5	3.5	1.3
PP5	0	5.6	3.1	5.8	1.7	5.6	8.1	2.0	4.5	4.5	1.7
PP6	0	6.2	4.1	5.7	1.9	6.0	8.1	2.7	4.9	4.9	1.9
PP7	0	7.6	5.4	7.4	2.0	6.7	10.7	3.3	6.2	6.2	2.7
PP8	0	9.5	6.4	9.8	3.4	6.8	15.0	3.7	6.9	6.9	3.3
PP9	0	10.8	6.3	10.5	2.9	7.1	15.1	4.3	7.2	7.2	3.8
PP10	0	12.9	7.0	11.0	3.3	7.2	16.6	4.9	7.6	7.6	4.1
PP11	0	15.3	8.5	13.8	4.8	7.8	19.8	5.9	8.7	8.7	5.1
PP12	0	16.8	9.1	14.3	4.9	8.0	19.7	6.1	8.8	8.8	5.6
PP13	0	19.0	9.8	12.3	5.7	8.4	15.8	7.6	7.5	7.5	7.1
PP14	0	21.1	13.7	11.5	5.5	11.4	18.7	7.1	9.2	9.2	10.4
PP15	0	26.3	17.5	11.7	7.4	14.4	19.0	9.8	9.9	9.9	14.0

grey coloured fields indicate movement rates which are below the detection limit

Appendix C-4: Reference systems for Austria for the projection of GIS data, as has been used by the author.

Position:
Militärgeographisches Institut (MGI)
Ellipsoid: Bessel 1841
Map Projection: Gauß-Krüger (3 Zones)
Central Point/Datum: Hermannskogel
Height: meters above Adria (m a A)

Zone M28	
Projection	TRANSVERSE
Zunits	NO
Units	METERS
Spheroid	BESSEL
Xshift	0.0000000000
Yshift	0.0000000000
Parameters	
1.00000	/* scale factor at central meridian
10 20 00	/* longitude of central meridian
00 00 00	/* latitude of origin
150000.0000	/* false easting (meters)*
0.00000	/* false northing (meters)

* some CATFLOW operations inhibited negative coordinates, this is why a transformation of some GIS data with an offset of 150000 has been conducted.

Appendix C-5: Reference systems for Baden-Württemberg, Germany for the projection of GIS data, as has been used by the Institut für Geodäsie, Universität Karlsruhe.

Position:
Rauenberg - DHDN (Potsdam Datum)
Ellipsoid: Bessel 1841
Map Projection: Gauß-Krüger
Central Point/Datum: Rauenberg (Substitute: Potsdam Helmertturm)
Height: Normal Null (NN)
Reference Level: Amsterdamer Pegel

Projection	TRANSVERSE
Zunits	NO
Units	METERS
Spheroid	BESSEL
Xshift	0.0000000000
Yshift	0.0000000000
Parameters	
1.00000	/* scale factor at central meridian
09 00 00	/* longitude of central meridian
00 00 00	/* latitude of origin
3500000.0000	/* false easting (meters)
0.00000	/* false northing (meters)

D. Information of soil and vegetation characteristic parameters

Appendix D-1: Translation of German Ellenberg indicator ranges to English expressions.

4.5-5.4	fresh to moist	frisch und mäßig frisch
5.5-6.4	moist to damp	mäßig feucht und wechselfeucht
6.5-7.4	damp	feucht
7.5-8.4	damp to wet	naß
8.4-9.4	wet	offenes Wasser

Appendix D-2: Selected vegetation associations from Dittfurth (2002) for each ecological moisture class.

Profile G1: fresh to moist	F	R	N
Briza media	x	x	2
Carex flacca	6	8	4
Carex hostiana	9	6	2
Cirsium palustre	8	4	3
Dactylorhiza fuchsii	?	?	?
Festuca rubra trichophylla	7	x7	x2
Hippocrepis comosa	3	7	2
Leontodon hispidus	5	7	x6
Lotus corniculatus	4	7	3
Molinia caerula	7	x	2
Phyteuma orbiculare orbiculare	x5	8	3
Picea abies	x	x	x
Plantago lanceolata	x	x	x
Plantago media	4	7	3
Poa pratensis angustifolia	x	x	3
Polygala vulgaris	4	3	2
Potentilla erecta	x	x	2
Primula farinosa	x8	9	2
Tofielda calyculata	x8	8	2
Trifolium montanum	3	8	2
Trifolium pratense	5	x	x
Trollius europaeus	7	6	5
median	**5.5**	**6.8**	**2.6**
average	**5.0**	**7.0**	**2.0**

Profile 152: moist to damp	F	R	N
Cirsium oleraceum	7	7	5
Equisetum telmateia	8	8	5
Leontodon hispidus	5	7	x6
Leucanthemum vulgare	4	x	3
Lotus corniculatus	4	7	3
Molinia caerula	7	x	2
Petasitis paradoxus	6	8	3
Phyteuma orbiculare orbiculare	x5	8	3
median	**5.9**	**7.5**	**3.4**
average	**6.0**	**7.5**	**3.0**

Profile 554 damp	F	R	N
Anthoxanthum odorathum	x	5	x
Carex distans	6	8	x
Carex flava	9	8	2
Cynosurus cristatus	5	x	4
Dactylorhiza fuchsii	?	?	?
Dactylorhiza majalis	8	7	3
Equisetum palustre	8	x	3
Filipendula ulmaria	8	x	5
Lotus corniculatus	4	7	3
Trollius europaeus	7	6	5
median	**6.9**	**6.8**	**3.6**
average	**7.5**	**7.0**	**3.0**

Profile 454: damp to wet	F	R	N
Caltha palustris	9	x	x6
Carex paniculata	9	x6	5
Cirsium oleraceum	7	7	5
Crepis paludosa	8	8	6
Equisetum palustre	8	x	3
Juncus inflexus	7	8	4
Lathyrus pratensis	6	7	6
Mentha longifolia	x	x	x
Scirpus sylvaticus	8	4	4
Valeriana dioica	8	x5	2
median	**7.8**	**6.8**	**4.4**
average	**8.0**	**7.0**	**4.5**

Profile 555: wet	F	R	N
Caltha palustris	9	x	x6
Equisetum palustre	8	x	3
Filipendula ulmaria	9	x	6
Geum rivale	9	x	5
Mentha longifolia	x	x	x6
Ranunculus aconitifolius	8	5	6
median	**8.6**	**5.0**	**5.0**
average	**9.0**	**5.0**	**5.5**

x: indicator was not used for average and median calculation due to anthropogenic influence
?: no existing indicator value
F: moisture indicator
R: reaction indicator
N: nitrate indicator

Appendix D-3: Geoelectrical profiles GEP 2 and 3 and the perpendicular profile GEP 4. Location of profiles as sketched in figure 4-1, GPS refers to object points which lie on the profile.

138
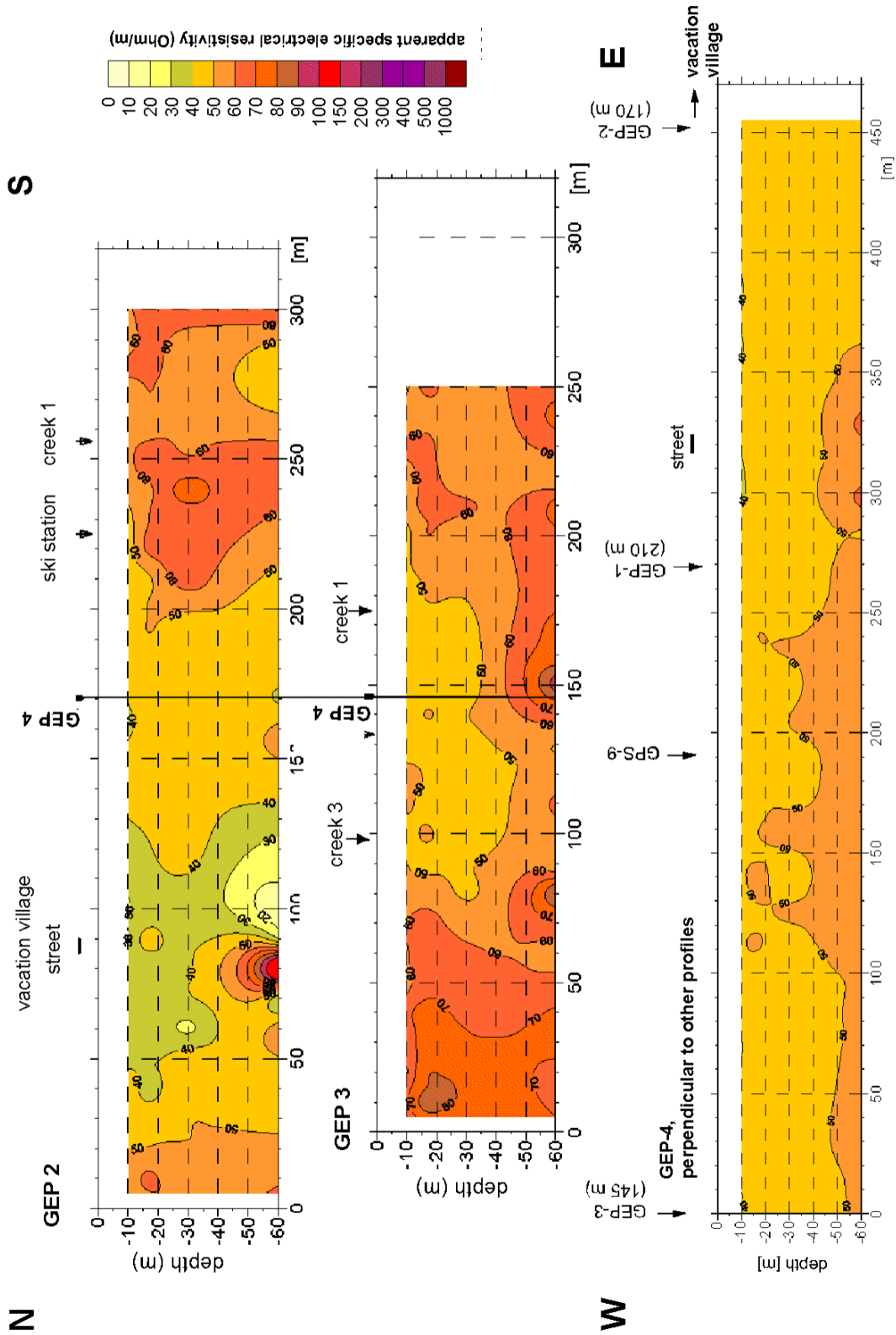
Appendix D-4: Gravimetric water content of hollow core sampler logs (RKS 1- RKS11), related to field observation of consistency.

sample	depth [m]	water content [weight-%]	material	consistency classification in the field
RKS 1-1	1.30	8.2	G, tU	moist
RKS 2-1	2.30	29.2	uT,G	very soft
RKS 2-2	3.20	9.4	uT,G	very soft - soft
RKS 2-3	4.00	33.6	uT,G	soft - firm
RKS 4-1	0.50	4.5	uT,G	hard
RKS 4-2	2.90	7.9	uT,G	stiff-hard
RKS 5-1	1.40	14.2	uT,G	firm
RKS 5-2	2.90	8.3	G,u	moist
RKS 6-1	0.80	4.4	uT,G	firm-stiff
RKS 7-1	1.20	15.5	tU,G	soft
RKS 7-2	2.20	14.4	tU,G	soft
RKS 7-3	2.75	29.1	tU,G	very soft - soft
RKS 10-1	1.00	47.6	uT	very soft - soft
RKS 10-2	2.95	28.3	uT	firm
RKS 10-3	5.10	12.5	G	dry
RKS 11-1	0.60	29.5	uT	soft - firm
RKS 11-2	1.15	47.0	ut,G	soft - firm

Appendix D-5: Liquid, plastic and shrinkage limit of some samples, BB samples are from the stained profile on the southern slope, NHU and NHO are upper and lower northern slope, *spring* is a sample from a wetland near the spring 1. NHU sample is highly organic, which is the reason for abnormal values.

sample	water content [weight-%]	liquid limit [weight-%]	plasticity limit [weight-%]	shrinkage limit [weight-%]	liquid limit volume [cm³]	shrinkage volume [cm³]	grain density [g/cm³]	wet density [g/cm³]	consistency value $Ic = w_{ll}-w_{pl}$
BB-1	0.29	0.87	0.49	0.24	56.6	31.6	-	-	0.38
BB-2	0.31	0.79	0.43	0.24	59.6		-	-	0.36
NHU-3	0.52	1.53	0.75	0.34	56.6	24.6	-	-	0.77
NHO-4	0.31	0.79	0.36	0.25	59.6	28.6	-	-	0.42
Spring	0.60	0.63	0.28	0.22	54.3	32.6	2.25	1.60	0.35

Appendix D-6: Grain size classification for four soil profiles from Dittfurth (2002).

horizon	sample depth	skeletal content	sand [%]			silt [%]			clay [%]	grain size class after AG Boden (1996)	combined grain size classes [%]		
	cm	>2mm	(gS) >630µm	(mS) >200µm	(fS) >63µm	(gU) >20µm	(mU) >6,3µm	(fU) >2µm	(T) <2µm		sand	silt	clay
G1 Ah	0.05	0.05	0.40	1.10	5.80	10.30	17.20	25.30	39.80	Tu3	7.3	52.8	39.8
G1 Sd	0.22	-	0.00	0.50	4.70	10.10	26.00	15.40	43.20	Tu3	5.2	51.5	43.2
G1 Sw	0.50	-	0.00	0.30	3.80	8.10	24.20	21.10	42.50	Tu3	4.1	53.4	42.5
G1 eCv	0.73	2.72	1.20	2.00	5.60	23.40	12.50	20.50	34.80	Tu3	8.8	56.4	34.8
G2 Ah	0.14	-	0.50	1.00	12.10	16.50	13.60	15.40	41.00	Lt3	13.6	45.5	41.0
G2 Srw	0.25	0.06	0.40	1.20	5.30	15.60	21.20	17.00	39.30	Tu3	6.9	53.8	39.3
G2 Srw-eCv	0.80	8.58	1.60	5.40	9.70	22.50	14.60	22.40	23.80	Lu	16.7	59.5	23.8
G3 Ah	0.12	-	0.30	2.20	4.30	10.70	12.50	29.10	41.00	Tu3	6.8	52.3	41.0
G3 Ah-Srw	0.40	-	0.30	1.30	3.00	7.10	18.80	18.50	51.00	Tu2	4.6	44.4	51.0
G3 Srw	0.70	-	0.10	0.70	3.10	7.80	12.60	22.50	53.10	Tu2	3.9	42.9	53.1
G3 eCv	1.25	8.91	1.60	3.00	10.60	27.20	12.70	21.50	23.50	Lu	15.2	61.4	23.5
G4 Ah	0.08	0.10	1.70	3.40	4.00	10.60	10.00	32.20	38.10	Tu3	9.1	52.8	38.1
G4 Ah-Sd	0.24	0.15	0.80	1.70	5.00	9.20	17.50	10.10	55.50	Tu2	7.5	36.8	55.5
G4 Sew	0.40	0.03	0.10	0.40	3.00	7.10	17.70	21.60	50.00	Tu2	3.5	46.4	50.0
G4 eCv-Sew	0.55	14.01	2.50	5.30	12.30	29.10	12.10	20.30	18.50	Lu	20.1	61.5	18.5
G4 eCv	1.00	45.18	5.10	8.10	13.10	20.90	31.10	10.80	10.80	Uls	26.3	62.8	10.8

Appendix D-7: field measurements of soil hydraulic conductivity (K_{sat}) with constant head permeameter in the forest (a) and on the meadow (b) hood infiltrometer measurements on the meadow (c) and laboratory hydraulic conductivity measurements in undisturbed soil cores (e) and results from slug tests (f).

a) meadow

sample name	depth [cm]	K_{sat} [m/s]
1ES	13.5	5.00E-08
2ES	12.5	1.28E-07
B1	12.5	2.61E-07
4	12.5	3.61E-07
2	13.0	6.03E-07
A1	12.5	6.39E-07
1	12.5	6.67E-07
3	13.0	1.58E-06
2a	12.5	1.93E-06
1a	12.0	2.97E-06
1	13.0	1.17E-05
2	20.5	3.89E-08
A2	20.0	2.03E-07
B2	22.0	2.56E-07
1b	20.0	3.17E-07
2	20.0	3.33E-07
2b	20.8	3.47E-06
3	21.0	2.51E-05
5	20.0	5.07E-05
1	21.0	5.95E-05
1	20.0	8.55E-05
A3	50.0	1.22E-07
6	50.0	2.25E-07
3	60.0	1.49E-05

b) forest

sample name	depth [cm]	K_{sat} [m/s]
2	12.5	8.61E-08
1	14.0	2.58E-07
1	12.5	1.10E-05
5	13.0	1.31E-05
1	13.5	2.48E-05
6	13.0	3.22E-05
1	12.5	3.49E-05
2	13.0	5.06E-05
3	12.5	5.35E-05
4	12.5	too large
2	13.0	too large
4	13.0	too large
5	20.0	2.58E-08
2	36.0	5.00E-08
1	20.0	8.33E-08
6ES	20.0	8.28E-07
2	21.0	6.61E-06
7	20.0	2.71E-05
3a	20.0	2.76E-05
4ES	20.0	3.10E-05
3ES	20.0	3.19E-05
2	20.0	4.75E-05
2907_A	20.0	1.00E-03
2907_B	20.0	2.86E-05
2907_C	20.0	1.00E-03
2907_D	20.0	4.50E-06
2907_E	20.0	9.54E-06
2907_F	20.0	3.06E-05
2907_G	20.0	1.47E-05
2907_H	20.0	1.00E-03
2907_I	20.0	1.32E-05
2907_J	20.0	3.70E-05
0408_A	20.0	5.64E-06
0408_B	20.0	1.00E-03
0408_C	20.0	7.03E-07
0408_D	20.0	1.76E-05
0508_A	20.0	2.79E-06
0508_B	20.0	6.13E-06
0508_C	20.0	1.33E-05
0508_D	20.0	8.58E-07
0508_E	20.0	1.38E-05
0508_F	20.0	1.16E-05
0508_G	20.0	5.17E-05
5ES	50.0	5.28E-08
3b	52.0	1.78E-07
3	50.0	2.06E-07

c) hood infiltrometer measurements

sample name	infiltrability [m/s]
H-1	2.71E-04
H-2	9.65E-05
H-3	3.65E-05
H-4	1.77E-04
H-5	8.61E-05
H-6	8.61E-05
H-7	5.74E-05
H-8	1.04E-04
H-1	6.25E-06
H-2	8.34E-05
H-3	6.02E-04
H-4	5.87E-04
H-1	2.35E-04
H-2	7.04E-05
H-3	2.23E-04
H-4	5.87E-05
H-1	2.82E-04
H-2	3.55E-04
H-3	2.40E-04

e) laboratory K_{sat} measurement of undisturbed soil cores

location soil profile and soil horizon	sample name	Ksat [m/s]	soil type	remark
1-1	U 1	6.2E-06	SIC	
	U 2	1.5E-05	SIC	
	U 3	macropore	SIC	
	U 4	2.6E-04	SIC	crack
1-2	U 5	no reaction	SIC	
	U 6	2.0E-07	SIC	crack
	U 7	4.5E-08	SIC	crack
	U 8	no reaction	SIC	
1-3	U 9	no reaction	SIC	
	U 10	no reaction	SIC	
	U 11	2.5E-06	SIC	
	U 12	no reaction	SIC	
2-1	U 13	9.6E-07	SIC	
	U 14	macropore	SIC	
	U 15	1.0E-05	SIC	
	U 16	4.5E-05	SIC	
2-2	U 17	1.6E-07	SIL	
	U 18	9.3E-06	SIL	
	U 19	2.8E-05	SIL	
	U 20	4.5E-05	SIL	
3-1	U 21	1.9E-04	SICL	roots
	U 22	macropore	SICL	
	U 23	1.6E-05	SICL	aggregates
	U 24	5.8E-05	SICL	
3-2	U 25	3.0E-04	SICL	
	U 26	2.0E-04	SICL	roots
	U 27	5.6E-07	SICL	
	U 28	3.7E-07	SICL	
3-3	U 29	macropore	SIL	
	U 30	1.6E-07	SIL	
	U 31	5.8E-06	SIL	
	U 32	8.8E-05	SIL	

f) slug test

name	Ksat [m/s]	filter position [m]
RKS 1	1.26E-08	2.3-3.2
RKS 3	1.68E-09	1.1-2.0
RKS 6	5.47E-09	0.7-1.6
RKS 9	4.99E-09	1.1-2.0

E. Set-up of measurement network and devices

Excerpts from the web-based information database Turtle (Molkenthin *et al.*, 2006), the database is located on http://www.grosshang.de and is available for internal users. The excerpts contain information about the location of instruments, data gaps and special information, a link to instrument types, a raw data base and a tensor data base, as well as the range an unit of measured values.

Appendix E-1: Report for Grosshang DornbirnStadt digital – RawData. This data has been provided by the (City of Dornbirn Authorities, Austria). This data set is also called *Ebnit church II* data set.

Measurement Files: 4
Last modified at: 23.02.2007 21:09
Start Time: 08.10.2003 00:00
End Time: 07.12.2006 07:00
Remarks: readme.html   Range

Name	Instruments	Tensor	Label	Unit	From	To
Matthies_Grund	DBInstrument0	Db_Water_Level_MG	Db_Pegel_MG	cm	-5	20
	DBInstrument1	Db_Battery_Voltage_MG	Db_Voltage	V	0	15
Alte_Post	DBInstrument2	Db_Water_Level_AP	Db_Pegel_AP	cm	-5	20
	DBInstrument3	Db_Water_Temperature_AP	Db_W_Temp_AP	°C	-20	50
	DBInstrument4	Db_Electric_Conductance_AP	Db_Leitf.	µS	0	500
	DBInstrument5	Db_Battery_Voltage_AP	Db_Voltage	V	0	15
Sportplatz	DBInstrument6	Db_Water_Level_SP	Db_Pegel_SP	cm	-5	20
	DBInstrument7	Db_Wind_Direction_SP	Db_Direction_SP	°	0	360
	DBInstrument8	Db_Wind_Gust_SP	Db_Gust_SP	m/s	0	30
	DBInstrument9	Db_Wind_Speed_SP	Db_Speed_SP	m/s	0	30
Ebnit_Kirche	DBInstrument10	Db_Air_Temperature_Ebnit	Db_AirTemp-Dorf	°C	-20	50
	DBInstrument11	Db_Humidity_Ebnit	Db_F-Dorf	%F	0	100
	DBInstrument12	Db_Precipitation_Ebnit	Db_Precipitation	mm	0	30
Heumoes_Hang	Pegelsensor_UPM-8	Db_Water_Level_H_Creek1	Db_Pegel_H_Creek1	cm	-20	100
	Snowsensor_USH-8	Db_Snow_Height_H	Db_SnowHeight	m	0	3
	DBInstrument15	Db_Air_Temperature_H	Db_AirTemp-Heum	°C	-20	50
	DBInstrument16	Db_Battery_Voltage_H	Db_Voltage	V	0	15
	Pegelsensor_UPM-8	Db_Water_Level_UPM_Creek1	Db_Pegel_USH_Creek1	cm	0	50

Appendix E-2: Report for Grosshang HeumoesStation – RawData. This data set is also called *Heumös slope*.

Measurement Files: 96
Last modified at: 24.02.2007 11:06
Start Time: 17.08.2001 14:48
End Time: 24.11.2006 13:39
Remarks: readme.html

Name	Instruments	Tensor	Label	Unit	Range	
Station_Karlsruhe	HH_Imko6410-a	Hh_Air_Temperature	Hh_AirTemp	°C	-30	50
	HH_Imko6410-b	Hh_Air_Humidity	Hh_AirHumidity	%	0	100
	HH_Imko7382	Hh_Soil_Moisture_20	Hh_Bodenfeuchte20	%	20	100
	HH_Imko7600	Hh_Soil_Moisture_30	Hh_Bodenfeuchte30	%	20	100
	HH_Imko7603	Hh_Soil_Moisture_50	Hh_Bodenfeuchte50	%	20	100
	HH_Imko7401	Hh_Soil_Moisture_80	Hh_Bodenfeucht80	%	20	100
	HH_Imko7626	Hh_Precipitation	Hh_Precipitation	mm	0	30
	HH_Imko7628	Hh_Global_Radiation	Hh_GlobalRadiation	W/m²	0	1500
	HH_Imko7627	Hh_Wind_Speed	Hh_Speed	m/s	0	10
	HH_Imko3532	Hh_Wind_Direction	Hh_Direction	°	0	360

Appendix E-3: Report for Grosshang EbnitChurch historic – RawData. This data set has been provided by the (Hydrographischer Dienst Vorarlberg, Austria). It consists of digitized paper strips and digital data. This data set is also called *Ebnit church I*.

Measurement Files: 5
Last modified at: 22.02.2007 20:47
Start Time: 01.01.1998 00:00
End Time: 05.06.2004 07:00
Remarks: readme.html
Station Overview   Range

Name	Instruments	Tensor	Label	Unit	From	To
Ebnit_church	EKInstrument0	Ek_Precipitation	Ek_Precipitation	mm	0	30

Appendix E-4: Report for Grosshang HeumoesBach digital – RawData.

Measurement Files: 4
Last modified at: 22.02.2007 20:39
Start Time: 12.01.2005 21:40
End Time: 10.06.2006 08:50
Remarks: readme.html   Range

Name	Instruments	Tensor	Label	Unit	From	To
HeumoesBach_Quelle	ATP15-1WL	Hb_Water_Level_Spring	Hb_Pegel_Spring	m	0	0.4
	ATP15-1T	Hb_Water_Temperature_Spring	Hb_Temperature_Spring	°C	-20	50
HeumoesBach_Pegel	ATP15-2WL	Hb_Water_Level_Creek3	Hb_Pegel_C3	m	0	1
	ATP15-2T	Hb_Water_Temperature_Creek3	Hb_Temperature_C3	°C	-20	50

Appendix E-5: Report for Grosshang HeumoesBach historic – RawData; this database has not been established yet.

Measurement Files: 96
Last modified at: 24.02.2007 11:06
Start Time: 17.08.2001 14:48
End Time: 24.11.2006 13:39
Remarks: readme.html

Name	Instruments	Tensor	Label	Unit	Range	
KB_2	Piezometer_5.5	Not implemented yet	GWL_KB_2_5.5m	m	-3.0	-5.0
	Piezometer_10	Not implemented yet	GWL_KB_2_10m	m	-3.5	-5.0
	Piezometer_13	Not implemented yet	GWL_KB_2_13m	m	-3.0	-5.0
	Temperatur	Not implemented yet	Temp_KB_2	°C	6.0	9.0
KB_3	Piezometer_5.5	Not implemented yet	GWL_KB_2_5.5m	m	-2.0	-4.5
	Piezometer_12	Not implemented yet	GWL_KB_2_12m	m	-9.0	-10.0
E_B1	Ott_B1	Not implemented yet	Hb_Creek1_hist	cm	-20	80
E_B2	Ott_B2	Not implemented yet	Hb_Creek2_hist	cm	-20	80
E_B3	Ott_B3	Not implemented yet	Hb_Creek3_hist	cm	-20	80
Quelle_1	Seba	Not implemented yet	Hb_Spring1_hist	cm	-20	80

Appendix E-6: Overview of data from Hochälpele station, data will not be implemented into the database.

Measurement Files: 1
Start Time: 01.01.2000 00:00
End Time: 05.12.2001 12:50

Name	Unit	Range	
Wind_Speed	m/s	0.0	13.9
Air_Temperature	°C	-15.0	30.0
Radiation_90_degrees	W/m²	0	1150
Radiation_60_degrees	W/m²	0	1260
Precipitation	mm	0	30

Appendix E-7: Overview of data from Breitenberg station, data will not be implemented into the database.

Measurement Files: 1
Start Time: 01.01.2000 00:00
End Time: 05.12.2001 12:50

Name	Unit	Range	
Air temperature	C	-15.0	30.0
Air humidity	%rF	0	100
Wind direction	°	0	360
Wind Gust	m/s	0	30
Precipitation	mm	0	30
Wind Speed	m/s	0	30
TB -250	C	-15.0	30.0
TB - 50	C	-15.0	30.0
TB 0	C	-15.0	30.0
TS + 20	C	-15.0	30.0
TS + 50	C	-15.0	30.0

Appendix E-8: Overview of data from additional pluviographs, data will not be implemented into the database.

Type	Instrument	Unit	Range	
Pluviograph 2	Seba	mm	0	30
Pluviograph 5	Seba	mm	0	30

Appendix E-9: a) Measured values of water stage-discharge relation for the creek gauges (Schwenk, 1999) and the spring gauge as measured in 2006. b) Equations with the best fit for water stage-discharge relation calculation.

a)

creek discharge		spring discharge	
water stage	discharge	water stage	discharge
[m]	[l/s]	[cm]	[l/s]
0.050	0.8	4.0	0.022
0.055	1.0	4.7	0.024
0.060	1.3	12.1	0.025
0.065	1.5	12.7	0.039
0.070	1.8	13.2	0.040
0.075	2.2	15.1	0.042
0.080	2.6	16.1	0.044
0.085	3.0	17.1	0.055
0.090	3.4	17.2	0.062
0.095	3.9	17.4	0.066
0.100	4.4	17.5	0.071
0.110	5.6	17.6	0.078
0.120	6.9	19.6	0.125
0.130	8.5	19.1	0.142
0.140	10.2	20.0	0.155
0.150	12.1	20.3	0.194
0.160	14.2	21.5	0.204
0.170	16.5		
0.180	19.0		
0.190	21.7		
0.200	24.7		
0.225	33.2		
0.250	43.2		
0.275	54.8		
0.300	68.1		
0.325	83.2		
0.350	100.2		
0.375	119.1		

b)

creek 1+ 3 water stage-discharge relation: q1+ q2
creek 2   water stage-discharge relation: q1

$$q_1 = 1380 \cdot w^{2.5} \qquad\qquad 0.00\,m - 0.50\,m$$

$$q_2 = q_1(0.5) + 1838 \cdot (2.4 - 0.2 \cdot w)^{1.5} \quad 0.50\,m - 0.85\,m$$

spring 1 water stage-discharge relation

$$q_1 = 0.0036764 \cdot w \qquad\qquad 0.00\,cm - 14.00\,cm$$

$$q_2 = 0.0843330 \cdot w \qquad\qquad 14.00\,cm - 15.50\,cm$$

$$q_3 = 0.0600000 \cdot w \qquad\qquad 15.75\,cm - 22.00\,cm$$

q = discharge in [l/s]
w = water level in [m] or [cm]

F. Rainfall-runoff investigation

Appendix F-1: Selected precipitation – discharge events from summer periods of 1999, 2002, 2003 and 2004. Events were selected according to the quality of discharge time series and in respect of gravel content in weirs.

event date	length [h]	precipitation depth [mm]	depth >1mm [mm]	discharge creek 1 [mm]	discharge creek 2 [mm]	discharge creek 3 [mm]	max. discharge creek 1 [l/s]	max. discharge creek 2 [l/s]	max. discharge creek 3 [l/s]	runoff coefficient creek 1 [mm]	runoff coefficient creek 2 [mm]	runoff coefficient creek 3 [mm]
10.05.1999*	109.90	209.71	124.03			146.08			165.35			0.70
19.05.1999*	60.60	209.16	97.84			155.71			151.49			0.71
03.05.2002	28.56	32.50	9.78	9.65	15.53	12.74	50.57	27.23	22.50	0.30	0.48	0.39
11.05.2002	16.49	32.55	24.58	9.23	11.85	11.86	140.56	93.78	89.45	0.28	0.36	0.36
18.05.2002	14.28	42.42	23.10	14.18	20.13	14.64	65.77	41.02	26.73	0.33	0.48	0.35
23.05.2002	14.96	30.57	4.41	8.88	19.00	9.76	63.14	51.03	36.47	0.29	0.62	0.32
25.05.2002	16.66	15.02	1.17	4.35	9.67	6.89	44.15	31.43	22.50	0.29	0.64	0.46
26.05.2002	53.04	56.22	1.23	23.06	47.43	38.56	78.00	61.04	43.00	0.41	0.84	0.69
03.06.2002	14.45	27.13	12.19	3.23	6.04	3.00	55.82	51.26	26.56	0.12	0.22	0.11
06.06.2002	13.60	73.67	69.36	debris filled	43.29	61.00	debris filled	111.32	133.14	debris filled	0.59	0.83
08.06.2002	0.68	6.41	5.31	"	1.23	0.80	"	18.02	6.96	"	0.19	0.12
09.06.2002	19.38	46.45	40.50	"	45.07	32.04	"	127.42	76.52	"	0.97	0.69
19.06.2002	2.38	25.40	24.46	"	4.09	1.30	"	83.12	19.60	"	0.16	0.05
20.06.2002	0.51	6.20	5.26	"	0.30		"	4.06		"	0.05	
24.06.2002	17.68	17.42	14.99	"	2.45	0.66	"	7.65	1.83	"	0.14	0.04
27.06.2002	16.83	27.93	14.53	"	11.58	6.97	"	25.89	15.36	"	0.42	0.25
03.07.2002	19.04	40.90	35.20	"	18.49	13.59	"	80.38	50.80	"	0.45	0.33
13.07.2002	12.92	19.05	2.32	"	2.59		"	10.20		"	0.14	
17.07.2002	26.01	89.50	82.00	"	71.76	62.15	"	153.73	122.51	"	0.80	0.69
25.07.2002	6.63	8.74	3.84	"	1.58	0.88	"	9.77	2.36	"	0.18	0.10
04.08.2002	8.16	29.49	28.26	"	5.37	3.00	"	20.81	9.34	"	0.18	0.10
06.08.2002	40.12	41.75	27.10	"	23.79	15.88	"	23.68	16.51	"	0.57	0.38
09.08.2002	93.33	231.40	220.20	"	239.25	171.34	"	243.26	160.45	"	1.03	0.74
27.05.2004	31.11	22.80	14.00	4.35		6.47	19.85		11.63	0.19		0.28
01.06.2004	18.53	13.80	0.00	2.71		5.53	17.02		12.10	0.20		0.40
01.06.2004	107.27	132.20	113.10	70.10		179.49	199.78		131.91	0.53		1.36
02.06.2004	32.81	82.20	75.00	43.03		92.98	199.78		131.91	0.52		1.13
04.06.2004	27.37	36.10	33.10	16.90		50.14	62.88		55.79	0.47		1.39
27.06.2004	1.70	10.20	8.40	1.94		2.29	10.96		7.72	0.19		0.23
05.07.2004	15.98	28.20	20.30	6.01		4.07	113.17		9.26	0.21		0.14
08.07.2004	11.05	48.50	37.40	22.41		9.71	245.11		25.89	0.46		0.20
22.07.2004	0.68	9.30	7.70	0.15		0.25	3.90		0.70	0.02		0.03
23.07.2004	2.38	15.30	14.60	4.06		3.63	197.65		16.51	0.27		0.24
24.07.2004	14.62	68.20	64.50	39.72		52.72	292.31		98.44	0.58		0.77

Appendix F-1, continued: Selected precipitation – discharge events from summer periods of 1999, 2002, 2003 and 2004. Events were selected according to the quality of discharge time series and in respect of gravel content in weirs.

event date	length [h]	precipitation depth [mm]	depth >1mm [mm]	discharge creek 1 [mm]	discharge creek 2 [mm]	discharge creek 3 [mm]	max. discharge creek 1 l/s	max. discharge creek 2 l/s	max. discharge creek 3 l/s	runoff coefficient creek 1 mm	runoff coefficient creek 2 mm	runoff coefficient creek 3 mm
29.07.2006	6.80	16.80	9.80	0.79		0.70	25.05		4.43	0.05		0.04
31.07.2006	2.55	4.10	2.30	0.02		0.04	38.25		14.90	0.00		0.01
31.07.2006	13.26	21.30	15.20	2.15		2.20	0.96		1.30	0.10		0.10
31.07.2006	57.12	43.00	41.20	7.43		8.75	24.72		7.42	0.17		0.20
01.08.2006	30.43	17.00	16.20	3.82		5.29	38.25		14.90	0.23		0.31
03.08.2006	115.43	143.00	111.30	146.94		106.42	384.02		184.91	0.74		0.74
09.08.2006	183.26	55.30	40.60	15.05		30.18	39.44		17.77	0.27		0.55
18.08.2006	4.42	7.50	1.30	0.35		0.42	2.17		1.70	0.05		0.06
19.08.2006	21.59	20.50	12.70	4.20		7.20	22.35		19.58	0.21		0.35
24.08.2006	5.61	12.70	10.40	1.78		3.18	202.96		9.86	0.14		0.25
26.08.2006	104.38	107.90	105.90	47.02		82.32	49.89		95.78	0.44		0.76
07.09.2006	7.82	35.10	29.00	11.15		16.20	312.77		147.01	0.32		0.46
16.09.2006	65.28	98.60	92.90	44.05		70.99	232.13		99.85	0.45		0.72
25.09.2006	45.22	36.70	3.60	11.79			83.13			0.32		

Blank cells: time series have a gap for specific event or data does give no plausible result
Debris filled: gauge is debris filled and so calculation might be disturbed
* 1999 events: water height is set too low so that discharge is too low, too. Runoff coefficients are supposed to be nearly one.

Appendix F-2: Plot of precpitation sum, precipitation duration and average intensity of 656 events between January 1998 and September 2006, extracted with the automated event selection method (Chapter 4.3.3). Data from digitised paper strips and digital data is separated.
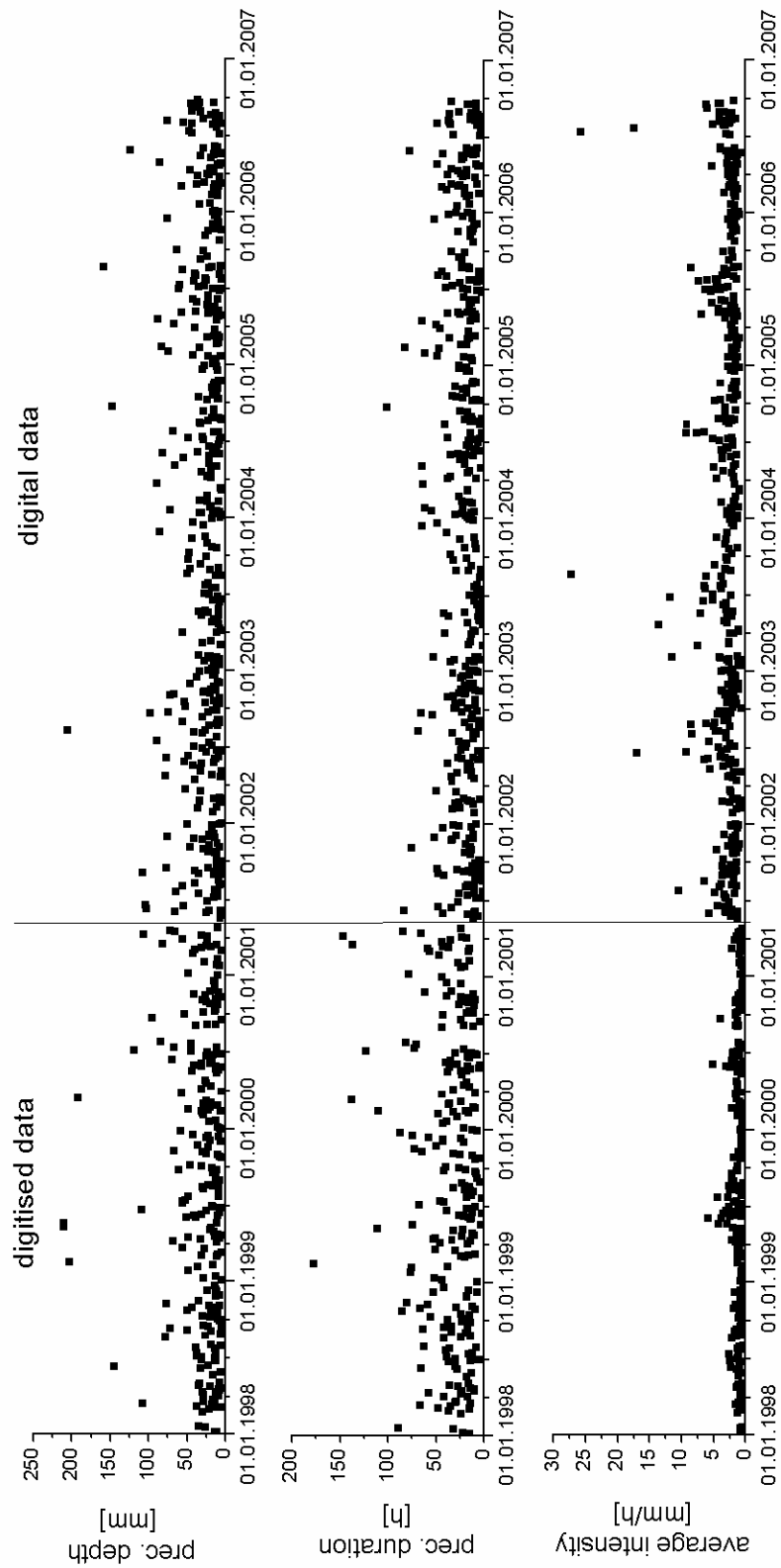
Appendix F-3a: Plots for comparison of GPS movement with precipitation proxies for group 1.

a) precipitation sum per GPS measurement period
b) monthly cumulative precipitation
c) selected daily cumulative precipitation > 30 mm
d) precipitation sum of selected events
e) average precipitation rate
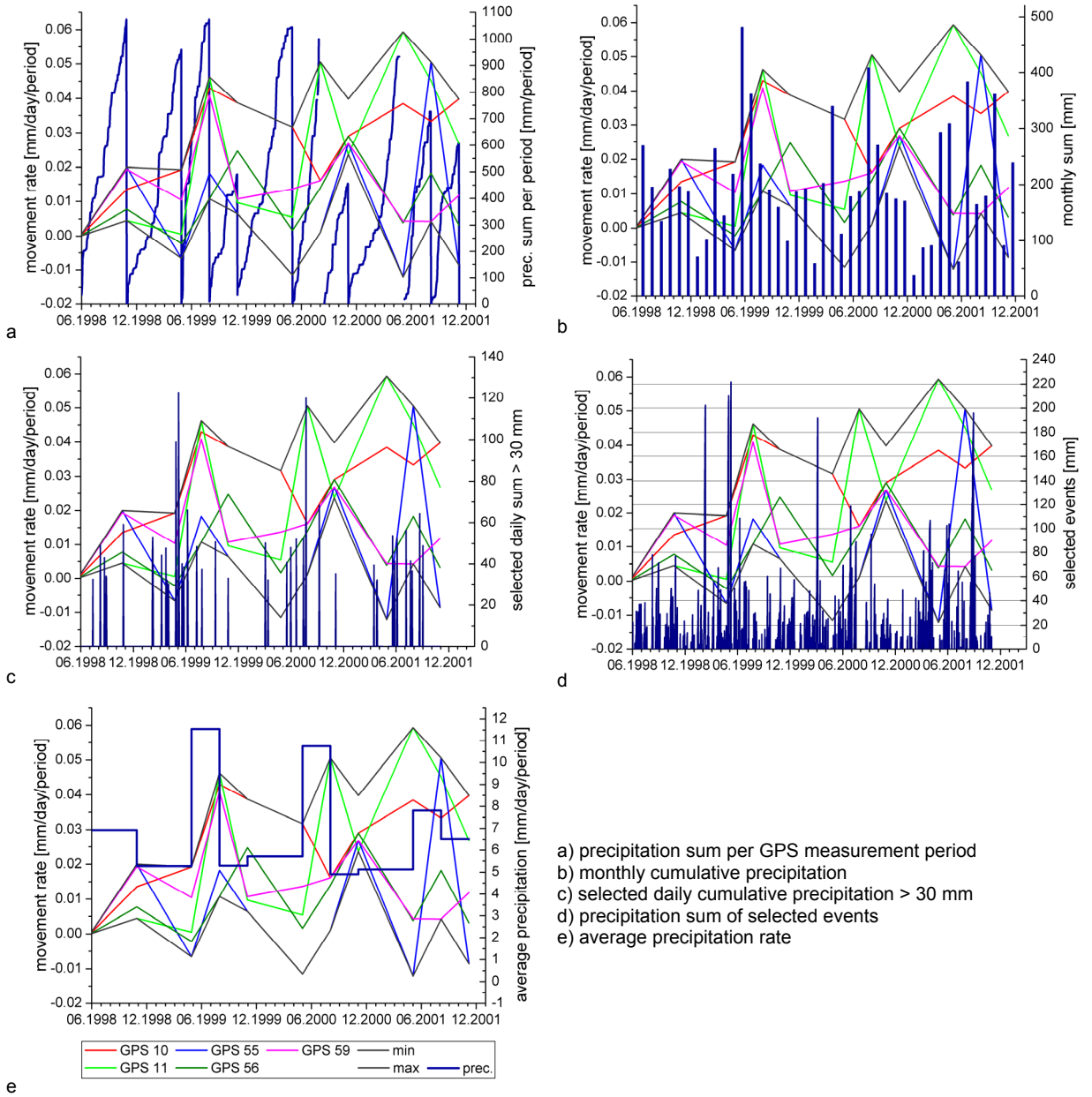
Appendix F-4a: Plots for comparison of GPS movement with precipitation proxies for group 1.

a) precipitation sum per GPS measurement period
b) monthly cumulative precipitation
c) selected daily cumulative precipitation > 30 mm
d) precipitation sum of selected events
e) average precipitation rate

150
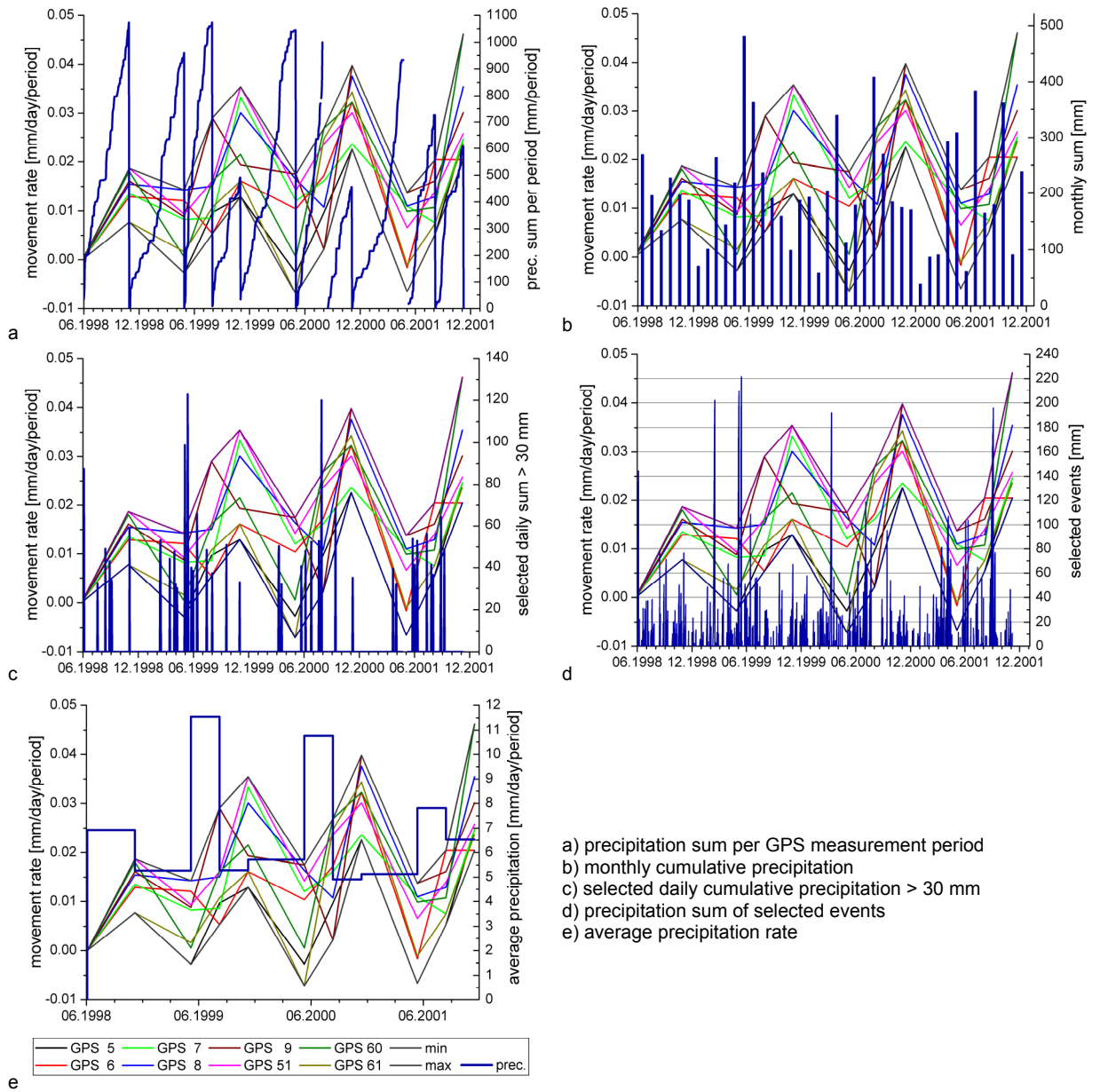
Appendix F-5a: Plots for comparison of GPS movement with precipitation proxies for group 1.
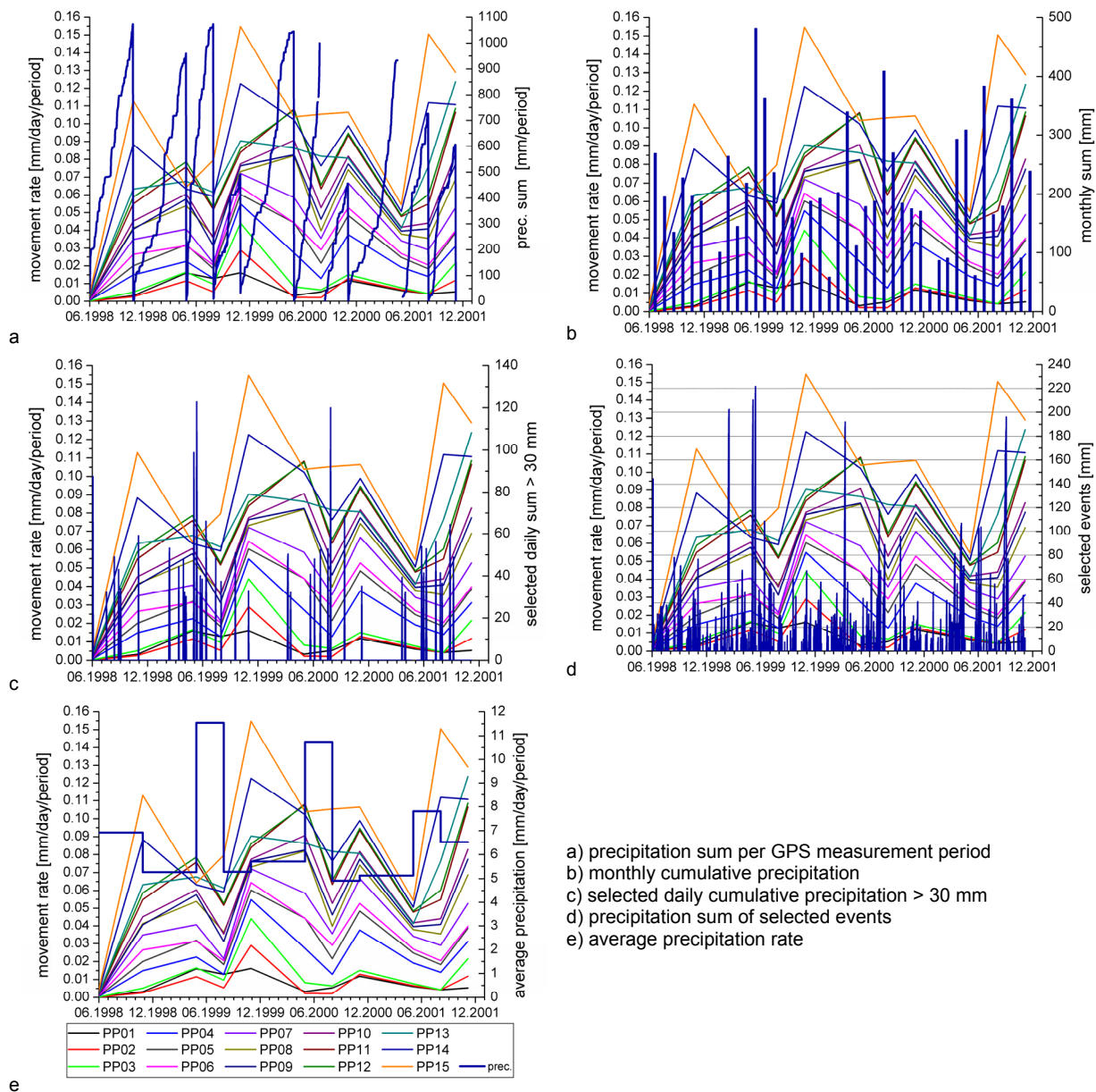
a) precipitation sum per GPS measurement period
b) monthly cumulative precipitation
c) selected daily cumulative precipitation > 30 mm
d) precipitation sum of selected events
e) average precipitation rate

151

G.   Catflow input data

Major CATFLOW input data for the model runs of creek 3 catchmen model and spring 1 model. In Catflow, both global and hillslope specific files are defined. The order of items is according to the specific input file.

Soil parameters:

Soil type	Saturated hydraulic conductivity K_{sat} [m/s]	Saturated soil moisture θs [ ]	Residual soil moisture θs [ ]	Reciprocal air entry point α [1/m]	Quantity, characterising the pore size distribution n [ ]
Creek 3 model set-up					
SiC 1	$6.40*10^{-07}$	0.36 or 0.6	0.07	0.5	1.09
SiC 2	$1.70*10^{-07}$	0.36 or 0.6	0.07	0.5	1.09
Spring 1 model set-up					
SL	$1.23*10^{-05}$	0.41	0.06	7.5	1.89
L	$2.89*10^{-06}$	0.43	0.07	3.6	1.56
SiCL	$1.97*10^{-07}$	0.43	0.08	1.0	1.23

Time series:

Begin and end of model input of precipitation time series
Creek 3 catchment

      01.10.1998 00:00 - 30.09.1999 00:00
      09.11.2001 13:00 - 30.09.2002 00:00
      01.10.2002 00:00 - 30.09.2003 00:00
      01.10.2003 00:00 - 30.09.2004 00:00
      16.10.2005 19:00 - 03.07.2006 14:00

Spring model

      01.01.1998 00:00 - 31.12.1998 00:00

Begin and end of mode input of climate time series with replaced time spans

Creek 3 catchment	Substitution
01.10.1998 00:00 - 30.09.1999 00:00	Complete data from 01.10.2003 00:00 - 30.09.2004 00:00
09.11.2001 13:00 - 30.09.2002 00:00	27.07.2002 00:00 - 30.09.2002 00:00 from 2004
01.10.2002 00:00 - 30.09.2003 00:00	
01.10.2003 00:00 - 30.09.2004 00:00	20.01.2004 00:00 - 12.02.2004 00:00 from 2005
16.10.2005 19:00 - 03.07.2006 14:00	
Spring model	
01.01.1998 00:00 - 31.12.1998 00:00	Complete data from 01.01.2004 00:00 - 31.12.2004 00:00

Landuse types

Needle forest

DAY	KST	MAK	BFI	BBG	TWU	PFH	PALB	RSTMIN	WP_BFW	F_BFW		
0	3	1	4	1	0.5	0.4	1	1	1	1	DAY	time
											KST	roughness coefficient of vegetation
1	4	1	0.5	1	0.6	0.33	0.2	200	0.05	30	MAK	specific vegetation macropore factor
75	4	1	0.5	1	0.6	0.42	0.2	200	0.05	30	BFI	leaf area index
105	2	1	0.78	1	0.6	0.66	0.2	200	0.05	30	BBG	plant coverage
135	2	1	0.85	1	0.6	0.83	0.2	200	0.05	30	TWU	root depth
165	1	1	1	1	0.6	0.92	0.2	200	0.05	30	PFH	plant height
195	2	1	0.95	1	0.6	1	0.2	200	0.05	30	PALB	plant specific albedo
225	2	1	0.88	1	0.6	1	0.2	200	0.05	30	RSTMIN	minimum stomata resistance
255	2	1	0.8	1	0.6	0.66	0.2	200	0.05	30	WP_BFW	wilting point
285	3	1	0.75	1	0.6	0.5	0.2	200	0.05	30	F_BFW	wilting point
315	4	1	0.5	1	0.6	0.33	0.2	200	0.05	30		
366	4	1	0.5	1	0.6	0.33	0.2	200	0.05	30		

meadow

DAY	KST	MAK	BFI	BBG	TWU	PFH	PALB	RSTMIN	WP_BFW	F_BFW
0	3	1	14	0.8	1.5	10	1	1	1	1
1	2	1	0.9	0.75	1	1	0.2	100	0.05	30
75	2	1	0.9	0.75	1	1	0.2	100	0.05	30
105	2	1	0.95	0.75	1	1	0.2	100	0.05	30
135	2	1	1	0.81	1	1	0.2	100	0.05	30
165	2	1	1	0.94	1	1	0.2	100	0.05	30
195	2	1	1	1	1	1	0.2	100	0.05	30
225	2	1	1	1	1	1	0.2	100	0.05	30
255	2	1	0.95	1	1	1	0.2	100	0.05	30
285	2	1	0.9	1	1	1	0.2	100	0.05	30
315	2	1	0.9	0.94	1	1	0.2	100	0.05	30
366	2	1	0.9	0.75	1	1	0.2	100	0.05	30

River network: 32 nodes with trapezoid channel geometry accordint to Maurer (1997):

	1st Strahler order	2nd Strahler order
Bottom width	1.2	1.25
Slope of channel banks	0.5	0.5
Roughness coefficient	10	20

Hillslope specific files: 14 hillslopes with 11 nodes in vertical and 14 nodes in lateral direction.

hillslope number	area [m^2]	width [m]	length [m]
1	6068.0	64.7	93.8
2	8823.9	70.5	125.2
3	5766.3	45.5	126.7
4	5332.8	54.9	97.2
5	4573.1	40.5	113.0
6	3911.2	45.0	86.9
7	4679.2	59.0	79.3
8	2003.2	24.5	81.9
9	4585.3	59.0	77.7
10	3675.9	33.2	110.8
11	5832.4	44.5	131.2
12	3319.0	63.6	52.2
13	2997.2	45.1	66.5
14	3713.3	60.9	61.0

Soil type assignment to hillslope nodes and node spacing for catchment model set-up; 1 refers to soiltype SiC 1; 2 refers to soiltype SiC 2; eta refers to vertical direction, xsi to lateral direction form lower left node.

eta

	0.00	0.10	0.20	0.30	0.40	0.50	0.60	0.70	0.75	0.80	0.85	0.90	0.95	1.00
1.00	1	1	1	1	1	1	1	1	1	1	1	1	1	1
0.95	1	1	1	1	1	1	1	1	1	1	1	1	1	1
0.90	1	1	1	1	1	1	1	1	1	1	1	1	1	1
0.85	1	1	1	1	1	1	1	1	1	1	1	1	1	1
0.80	1	1	1	1	1	1	1	1	1	1	1	1	1	1
0.70	1	1	1	1	1	1	1	1	1	1	1	1	1	1
0.60	1	1	1	1	1	1	1	1	1	1	1	1	1	1
0.45	2	2	2	2	2	2	2	2	2	2	2	2	2	2
0.30	2	2	2	2	2	2	2	2	2	2	2	2	2	2
0.15	2	2	2	2	2	2	2	2	2	2	2	2	2	2
0.00	2	2	2	2	2	2	2	2	2	2	2	2	2	2

xsi

Soil type assignment to hillslope nodes and node spacing for springmodel set-up; 1 refers to soiltype SL; 2 refers to soiltype L; 3 refers to soiltype SiCl eta refers to vertical direction, xsi to lateral direction form lower left node.

```
eta
1.00 1 1 1 1 1 1 1 1 1 1 1 1 1 1 1 2 2 2 2 2 2 2 2 2 2 2 2 2 2 2 2 2 3 3 3 3 3 3 3 3
0.95 1 1 1 1 1 1 1 1 1 1 1 1 1 1 1 1 1 2 2 2 2 2 2 2 2 2 2 2 2 2 2 3 3 3 3 3 3 3 3 3
0.90 1 1 1 1 1 1 1 1 1 1 1 1 1 1 1 1 1 1 1 1 1 1 1 1 2 2 2 2 2 2 2 3 3 3 3 3 3 3 3 3
0.85 1 1 1 1 1 1 1 1 1 1 1 1 1 1 1 1 1 1 1 1 1 1 1 1 1 2 2 2 2 2 2 2 3 3 3 3 3 3 3 3
0.80 1 1 1 1 1 1 1 1 1 1 1 1 1 1 1 1 1 1 1 1 1 1 1 1 1 1 2 2 2 2 2 2 3 3 3 3 3 3 3 3
0.75 1 1 1 1 1 1 1 1 1 1 1 1 1 1 1 1 1 1 1 1 1 1 1 1 1 1 1 2 2 2 2 2 3 3 3 3 3 3 3 3
0.70 1 1 1 1 1 1 1 1 1 1 1 1 1 1 1 1 1 1 1 1 1 1 1 1 1 1 1 1 2 2 2 2 3 3 3 3 3 3 3 3
0.65 1 1 1 1 1 1 1 1 1 1 1 1 1 1 1 1 1 1 1 1 1 1 1 1 1 1 1 1 2 2 2 2 3 3 3 3 3 3 3 3
0.60 1 1 1 1 1 1 1 1 1 1 1 1 1 1 1 1 1 1 1 1 1 1 1 1 1 1 1 1 1 2 2 2 3 3 3 3 3 3 3 3
0.55 3 3 3 3 3 3 3 3 3 3 3 3 3 3 3 3 3 3 3 3 3 3 3 1 1 1 1 2 2 2 2 2 3 3 3 3 3 3 3 3
0.50 3 3 3 3 3 3 3 3 3 3 3 3 3 3 3 3 3 3 3 3 3 3 3 1 1 1 1 1 1 2 2 2 3 3 3 3 3 3 3 3
0.45 3 3 3 3 3 3 3 3 3 3 3 3 3 3 3 3 3 3 3 3 3 3 3 1 1 1 1 1 1 2 2 2 3 3 3 3 3 3 3 3
0.40 3 3 3 3 3 3 3 3 3 3 3 3 3 3 3 3 3 3 3 3 3 3 3 1 1 1 1 1 1 2 2 3 3 3 3 3 3 3 3 3
0.35 3 3 3 3 3 3 3 3 3 3 3 3 3 3 3 3 3 3 3 3 3 3 3 3 3 1 1 1 1 1 1 1 3 3 3 3 3 3 3 3
0.30 3 3 3 3 3 3 3 3 3 3 3 3 3 3 3 3 3 3 3 3 3 3 3 3 3 1 1 1 1 1 1 1 3 3 3 3 3 3 3 3
0.25 3 3 3 3 3 3 3 3 3 3 3 3 3 3 3 3 3 3 3 3 3 3 3 1 1 1 1 1 1 1 1 1 3 3 3 3 3 3 3 3
0.20 3 3 3 3 3 3 3 3 3 3 3 3 3 3 3 3 3 3 3 3 3 3 1 1 1 1 1 1 1 1 1 3 3 3 3 3 3 3 3 3
0.15 3 3 3 3 3 3 3 3 3 3 3 3 3 3 3 3 3 3 3 3 3 3 3 3 3 3 3 3 3 3 3 3 3 3 3 3 3 3 3 3
0.10 3 3 3 3 3 3 3 3 3 3 3 3 3 3 3 3 3 3 3 3 3 3 3 3 3 3 3 3 3 3 3 3 3 3 3 3 3 3 3 3
0.05 3 3 3 3 3 3 3 3 3 3 3 3 3 3 3 3 3 3 3 3 3 3 3 3 3 3 3 3 3 3 3 3 3 3 3 3 3 3 3 3
0.00 3 3 3 3 3 3 3 3 3 3 3 3 3 3 3 3 3 3 3 3 3 3 3 3 3 3 3 3 3 3 3 3 3 3 3 3 3 3 3 3

xsi  0.000 0.025 0.050 0.075 0.100 0.125 0.150 0.175 0.200 0.225 0.250 0.275 0.300 0.325 0.350 0.375 0.400 0.425 0.450 0.475 0.500 0.525 0.550 0.575 0.600 0.625 0.650 0.675 0.700 0.725 0.750 0.775 0.800 0.825 0.850 0.875 0.900 0.925 0.950 0.975
```

Macropores assigned to each hillslope: From 0.50 to 1.00 of all nodes in eta direction and from 0.0 to 1.0 for xsi direction: factor 10. Initiation of Macropores: relative saturation $S = 0.8$.

Initial relative saturation for all nodes: $S = 0.95$.

Boundary conditions:

boundary	No flow model set-up	Gravitation flow model set-up		Possible boundaries
L left	0	0	0	No-flow
R right	-3	-3	-3	Gravitation flow
O upper	-99	-99	-10	Channel seep
U lower	0	-3	-99	atmosphere